

**CHARACTERIZATION OF PROTEIN-LIGAND
INTERACTIONS: THE ROLE OF THERMODYNAMIC
AND STRUCTURAL DATA IN THE DRUG DISCOVERY
PROCESS**

DISSERTATION

zur Erlangung des Grades
des Doktors der Naturwissenschaften
der Naturwissenschaftlich-Technischen Fakultät III
Chemie, Pharmazie, Bio- und Werkstoffwissenschaften
der Universität des Saarlandes

von

Tobias Klein

Saarbrücken

2012

Tag des Kolloquiums:	14. September 2012
Dekan:	Prof. Dr. Wilhelm F. Maier
Vorsitzender:	Prof. Dr. Claus-Michael Lehr
Berichterstatter:	Prof. Dr. Rolf W. Hartmann Prof. Dr. Dr. h.c. Hans H. Maurer Prof. Dr. Ulrike Holzgrabe
Akad. Mitarbeiter:	Dr. Britta Diesel

Die vorliegende Arbeit wurde von Januar 2009 bis Mai 2012 unter Anleitung von Herrn Prof. Dr. Rolf W. Hartmann in der Fachrichtung 8.2 Pharmazeutische und Medizinische Chemie der Naturwissenschaftlich-Technischen Fakultät III der Universität des Saarlandes angefertigt.

**I DON'T KNOW ANYTHING,
BUT I DO KNOW THAT EVERYTHING IS INTERESTING
IF YOU GO INTO IT DEEPLY ENOUGH.**

RICHARD P. FEYNMAN

THANK JU!

SUMMARY

Comparing biological activities and thermodynamic profiles obtained for one compound toward proteins, differing only in few residues is a promising strategy to increase the knowledge of protein-ligand interactions and active site topologies thereby enabling rational drug design.

For this purpose, wild type proteins and their mutants carrying a set of point mutations can be used. Such an approach was applied in the present study to guide the development of small-molecule antagonists targeting PqsR, a novel target to limit *Pseudomonas aeruginosa* pathogenicity. It resulted in two chemically diverse fragments with antagonistic activity and provided insights into their binding modes. The latter can be used to assist fragment optimization and therefore the identified PqsR antagonists are promising scaffolds for further drug design efforts against this important pathogen.

Alternatively, proteins from various species, which are highly conserved in sequence and differ only in few residues, might be considered. This line of attack was also utilized employing human and marmoset monkey 17 β -HSD1, a promising target for the treatment of estrogen-dependent diseases. By means of *in silico* methods a better understanding of 17 β -HSD1 active site topologies and inhibitor binding modes was achieved that guided the elaboration of a lead compound.

The described strategy was successfully applied for hit identification and lead optimization reflecting its benefit in drug design.

ZUSAMMENFASSUNG

Die möglichst genaue Kenntnis der räumlichen Gestalt der Ligand Bindungsstelle und der damit verbundenen Protein-Ligand-Wechselwirkungen ist eine Voraussetzung für rationales Wirkstoffdesign. Eine aussichtsreiche Strategie um diese Informationen zu erhalten, ist es biologische/biophysikalische Daten einer Verbindung gegenüber Proteinen zu vergleichen, die sich nur in wenigen Aminosäuren unterscheiden.

Einerseits können dazu Wildtyp und Mutanten genutzt werden, was in dieser Studie zur Entwicklung von PqsR Antagonisten geführt hat. PqsR ist ein neues Target zur Limitierung der *Pseudomonas aeruginosa* Pathogenität. Zwei chemisch verschiedene, antagonistische Fragmente wurden entdeckt und Aufschlüsse über deren Bindungsmodi erhalten, die zur weiteren Optimierung genutzt werden können. Somit stellen die entdeckten Liganden vielversprechende Grundgerüste zur weiteren Wirkstoffentwicklung gegen dieses relevante Pathogen dar.

Alternativ können hochkonservierte Proteine verschiedener Spezies in Betracht gezogen werden. Unter Verwendung von humaner und marmoset 17 β -HSD1, einem erfolgversprechenden Target zur Behandlung estrogenabhängiger Erkrankungen, wurden durch *in silico* Methoden das aktive Zentrum der 17 β -HSD1 sowie Bindungsmodi ausgewählter Hemmstoffe untersucht. Anhand der erstellten Modelle wurde eine Leitverbindung weiterentwickelt.

Diese Strategie wurde erfolgreich für das Wirkstoffdesign bei der Hit Identifizierung sowie der Lead Optimierung angewendet.

PAPERS INCLUDED IN THIS THESIS

This thesis is divided into four publications, which are referred to in the text by their Roman numerals.

I Identification of Small-Molecule Antagonists of the *Pseudomonas aeruginosa* Transcriptional Regulator PqsR: Biophysically Guided Hit Discovery and Optimization

Tobias Klein, Claudia Henn, Johannes C. de Jong, Christina Zimmer, Benjamin Kirsch, Christine K. Maurer, Dominik Pistorius, Rolf Müller, Anke Steinbach, and Rolf W. Hartmann

ACS Chem. Biol. **2012**, DOI: 10.1021/cb300208g.

II A Guidepost for Hit Selection and Optimization Targeting the *Pseudomonas aeruginosa* Transcriptional Regulator PqsR: Combination of Thermodynamic Analysis and Site-Directed Mutagenesis

Tobias Klein, Michael Zender, Christina Zimmer, Anke Steinbach, and Rolf W. Hartmann

Parts of this manuscript will be submitted to a peer-reviewed journal for publication.

III Structural Basis for Species Specific Inhibition of 17 β -Hydroxysteroid Dehydrogenase Type 1 (17 β -HSD1): Computational Study and Biological Validation

Tobias Klein, Claudia Henn, Matthias Negri, and Martin Frotscher

PLoS ONE **2011**, *6*, e22990.

IV Bicyclic Substituted Hydroxyphenylmethanone Type Inhibitors of 17 β -Hydroxysteroid Dehydrogenase Type 1 (17 β -HSD1): The Role of the Bicyclic Moiety

Alexander Oster, Tobias Klein, Claudia Henn, Ruth Werth, Sandrine Marchais-Oberwinkler, Martin Frotscher, and Rolf W. Hartmann

ChemMedChem **2011**, *6*, 476-487.

CONTRIBUTION REPORT

The author wishes to clarify his contributions to the publications **I–IV** in the thesis.

- I** The author significantly contributed to the rational ligand design concept. In addition, the author performed the heterologous expression and purification of PqsR^{C87} and planned and generated the site-directed mutants. The author planned, executed, measured, and analyzed the ITC experiments. Further, the author significantly contributed to the interpretation of the results and conceived and wrote the manuscript.
- II** The author performed the heterologous expression and purification of PqsR^{C87} and planned and generated the site-directed mutants. In addition, the author planned, executed, measured, and analyzed the ITC experiments. The author significantly contributed to the ligand design concept. Further, the author significantly contributed to the interpretation of the results and conceived and wrote the manuscript.
- III** The author significantly contributed to the design of the study. Further, the author conceived and performed the computational experiments and analyzed the data. In addition, the author significantly contributed to the interpretation of the results and conceived and wrote the manuscript.
- IV** The author conceived and performed the computational experiments and analyzed the data. Further, the author significantly contributed to the inhibitor design concept. The author significantly contributed to the interpretation of the results and conceived and wrote the manuscript.

ABBREVIATIONS

17 β -HSD	17 β -Hydroxysteroid dehydrogenase
3 β -HSD	3 β -Hydroxysteroid dehydrogenase
3D	Three-dimensional
ACTH	Adrenocorticotrophic hormone
ADH	Antidiuretic hormone
ADMET	Absorption, distribution, metabolism, excretion, and toxicology
AHL	N-acylhomoserine lactone
AI	Autoinducer
AKR	Aldo-ketoreductases
BEI	Binding efficiency index
CAAD	Computer-aided drug design
CF	Cystic fibrosis
CFTR	Cystic fibrosis transmembrane conductance regulator
Clint	Intrinsic metabolic clearance
CoA	Coenzyme A
COF	Cofactor binding site
CoMFA	Comparative molecular field analysis
COX	Cyclooxygenase
CYP	Cytochrome P450
CYP11A1	Cholesterol desmolase
CYP11B1	11 β -Hydroxylase
CYP11B2	11 β /18-Hydroxylase
CYP17	17 α -Hydroxylase-17,20-lyase
CYP19	Aromatase
CYP21A	21-Hydroxylase
DHEA	Dehydroepiandrosteron
DHT	Dihydrotestosterone
E1	Estrone
E2	Estradiol
E3	Estriol
EDD	Estrogen-dependent disease
EE	Enthalpy efficiency
ER	Estrogen receptor
FSH	Follicle-stimulating hormone
GALS	Genetic algorithm local search
GBSA	Generalized born surface area
GnRH	Gonadotropin-releasing hormone
GPCR	G-protein coupled receptors
HAQ	Hydroxy-alkyl-quinolone
HHQ	2-Heptyl-4(1 <i>H</i>)-quinolone
HSL	Homoserine lactone
HTH	Helix-turn-helix
<i>i</i> Bu	Isobutyl
IC ₅₀	Concentration required for 50 % inhibition
<i>i</i> Pr	Isopropyl
ITC	Isothermal titration calorimetry
IUPAC	International union of pure and applied chemistry

K_A	Association constant
K_D	Dissociation constant
LBD	Ligand binding domain
LE	Ligand efficiency
LH	Luteinizing hormone
LogP	Octanol-water partition coefficient
LPS	Lipopolysaccharide
LTTR	LysR-type transcriptional regulator
MD	Molecular dynamics
MEP	Molecular electrostatic potential
mM	Millimolar
MM	Molecular mechanics
Mvfr	Multiple virulence factor regulator
NAD ⁺	Nicotinamide adenine dinucleotide
NADH	Nicotinamide adenine dinucleotide (reduced form)
NADP ⁺	Nicotinamide adenine dinucleotide phosphate
NADPH	Nicotinamide adenine dinucleotide phosphate (reduced form)
nM	Nanomolar
NMR	Nuclear magnetic resonance
NSAID	Non-steroidal antiinflammatory drugs
PBSA	Poisson Boltzmann surface area
PDB	Protein data bank
PGE ₂	Prostaglandin E2
PLS	Partial-least-squares
PQS	<i>Pseudomonas</i> quinolone signal
QS	<i>Quorum sensing</i>
QSAR	Quantitative structure-activity relationships
QSPR	Quantitative structure-property relationships
RBA	Relative binding affinity
RMSD	Root-mean-square deviation
RNA	Ribonucleic acid
S5AR	5 α -Reductase
SAR	Structure-activity relationships
SBD	Substrate binding domain
SD	Standard deviation
SDR	Short-chain dehydrogenase/reductase
SERM	Selective estrogen receptor modulator
SF	Selectivity factor
SPR	Surface plasmon resonance
SUMO	Small ubiquitin-like modifier
T3	Triiodothyronine
T4	Thyroxine
<i>t</i> Bu	<i>Tert</i> -butyl
TCS	Two-component regulatory system
TSH	Thyroid-stimulating hormone
μ M	Micromolar

INHALTSVERZEICHNIS

1	Introduction	1
1.1	Rational Drug Design	1
1.1.1	Isothermal titration calorimetry in drug design	1
1.1.2	Computational techniques in drug design.....	3
1.2	<i>Pseudomonas</i> Quinolone Signaling as Drug Target.....	7
1.2.1	<i>Pseudomonas aeruginosa</i> : an important opportunistic pathogen.....	7
1.2.2	The <i>Pseudomonas aeruginosa</i> quorum sensing network	9
1.2.3	Jamming <i>pqs</i> quorum sensing as a new approach for the treatment of <i>Pseudomonas aeruginosa</i> infections	13
1.3	17 β -Hydroxysteroid Dehydrogenase Type 1 as Drug Target.....	15
1.3.1	Biochemical communication in eukaryotes: hormones as signal transmitter.....	15
1.3.2	Estrogen-dependent diseases	22
1.3.3	17 β -HSD1 as promising target for the treatment of estrogen-dependent diseases	25
2	Aim of the Thesis	28
3	Results.....	30
3.1	Identification of Small-Molecule Antagonists of the <i>Pseudomonas aeruginosa</i> Transcriptional Regulator PqsR: Biophysically Guided Hit Discovery and Optimization	30
3.2	A Guidepost for Hit Selection and Optimization Targeting the <i>Pseudomonas aeruginosa</i> Transcriptional Regulator PqsR: Combination of Thermodynamic Analysis and Site-Directed Mutagenesis.....	50
3.3	Structural Basis for Species Specific Inhibition of 17 β -HSD1: Computational Study and Biological Validation	65
3.4	Bicyclic Substituted Hydroxyphenylmethanone Type Inhibitors of 17 β -Hydroxysteroid Dehydrogenase Type 1 (17 β -HSD1): The Role of the Bicyclic Moiety	91
4	Final Discussion	118
5	References.....	132
6	Acknowledgements	142
7	Appendix.....	143
7.1	Curriculum Vitae	143
7.2	Publications	144
7.3	Oral Presentations.....	145
7.4	Poster Presentations	145

1 Introduction

1.1 Rational Drug Design

Besides cardiovascular and infectious diseases, cancer is the leading cause of death worldwide (WHO, 2008). As those diseases constantly threaten human life, new drugs are always in great demand for prevention and treatment. However, it is generally acknowledged that drug discovery and development are time (Myers and Baker, 2001) and resources (DiMasi et al., 2003) consuming processes.

From early on, the discovery of new drugs involved a trial-and-error approach on naturally derived materials and substances. This was expanded by systematic pharmacological evaluations of both natural and synthetic compounds in the first half of the twentieth century. However, most new drugs until the 1970s were discovered by serendipity (Kaul, 1998; Rester, 2008). Over the past 30 years the route of drug discovery has been changed. With advances in computational techniques and molecular biology as well as with the development of biophysical methods, that is, mainly X-ray crystallography, nuclear magnetic resonance (NMR) spectroscopy, isothermal titration calorimetry (ITC) and surface plasmon resonance (SPR) spectroscopy, it became possible to place drug discovery on a rational basis (Mavromoustakos et al., 2011). The use of complementary experimental and computational techniques provides a lot of information on the system under study. This knowledge can be utilized in a positive way to streamline drug discovery, which is characteristic for a rational drug design approach. The latter has the potential to increase the chances of success in many stages of the discovery process, from the identification of novel targets and elucidation of their function to the discovery and development of lead compounds with desired properties (Bajorath, 2001).

1.1.1 Isothermal titration calorimetry in drug design

Isothermal titration calorimetry (ITC) provides a rapid route to a full thermodynamic characterization of a molecular interaction – for example, a protein and a small-molecule ligand. A single ITC experiment provides the changes in free energy (ΔG), enthalpy (ΔH) and entropy (ΔS) as well as the stoichiometry N of the reaction. While ΔH , N , and the association constant K_A are directly measured (Figure 1), ΔG and ΔS are calculated from Eq. (1)

$$\Delta G = \Delta H - T\Delta S = RT\ln K_A = -RT\ln K_D \quad (1)$$

Determination of the thermodynamic parameters offers detailed information on a molecular interaction: ΔG reports on the affinity, ΔH is the heat associated with the number and the

strength of non-covalent bonds, ΔS reports on the overall change in the degrees of freedom of the system (Ladbury, 2010).

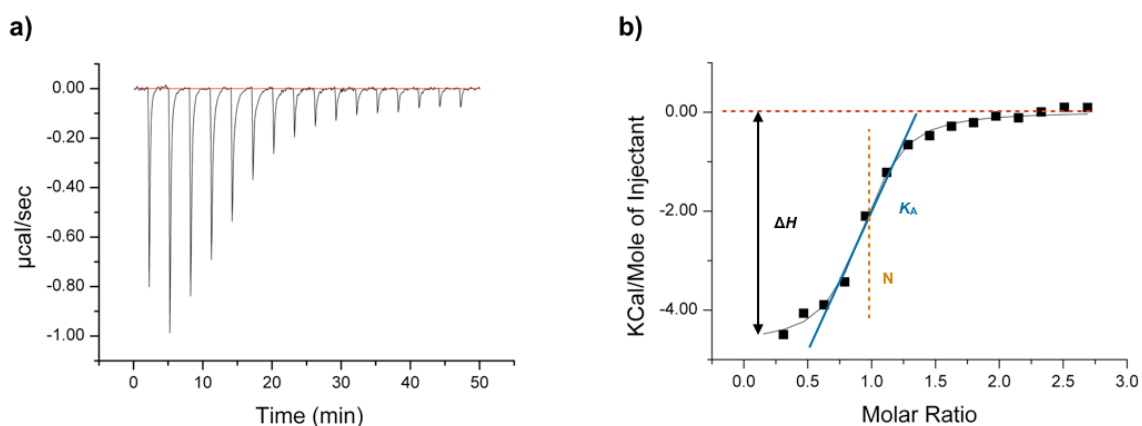


Figure 1. Typical titration data. **a)** raw data. **b)** binding isotherm created by plotting the integrated heat peaks against the molar ratio of the ligand.

In the drug discovery process, affinity (ΔG , K_D) can be used as criteria for hit or lead identification. But as in the optimization process, increasing affinity of a candidate is usually accompanied by an increase in molecular mass (Lipinski, 2000) screening for affinity alone can result in compounds with lower molecular mass being discarded. In order to deal with this problem, efficiency indices should be used as guideposts (Abad-Zapatero and Metz, 2005). This is a way of normalizing the affinity and molecular size of a compound to provide a useful comparison between compounds with a range of molecular weight and affinity. A measure that includes affinity is the ligand efficiency (LE). It is calculated as the binding energy of the ligand ΔG per heavy atom (Hopkins et al., 2004). However, to account for heteroatoms the binding efficiency index (BEI), which engages the total molecular weight instead of the number of non-hydrogen atoms is superior (Abad-Zapatero and Metz, 2005).

Favorable ΔH values indicate a good non-covalent bond complementary between proteins and small molecules and compounds with more favorable ΔH values make additional or stronger interactions (Figure 2). Therefore ΔH provides also a viable measure with which medicinal chemists can rank compounds, in particular using the accordant efficiency index, the enthalpy efficiency (EE; $EE = \Delta H / \text{number of non-hydrogen atoms}$; Ladbury et al., 2010).

The ΔS value is constituted by the solvation entropy change and the conformational entropy change. The solvation entropy change is favorable and originates from the release of water molecules as the drug and the binding cavity undergo complete or partial desolvation upon binding. The conformational entropy change, by contrast, is almost always unfavorable as the binding process involves the loss of conformational degrees of freedom of both the drug molecule and the protein (Figure 2). During the drug design process the loss in conformational

entropy can be minimized by introducing conformational constraints in the drug molecule such that fewer conformational degrees of freedom are lost upon binding (Freire, 2004).

In summary, thermodynamic parameters can aid decision making in hit or lead selection and particularly in combination with structural data it can streamline the optimization process and provides new insights into the energetic characteristics of protein-ligand interactions. Accordingly, integrating calorimetric data delivers a valuable tool in the drug discovery process.

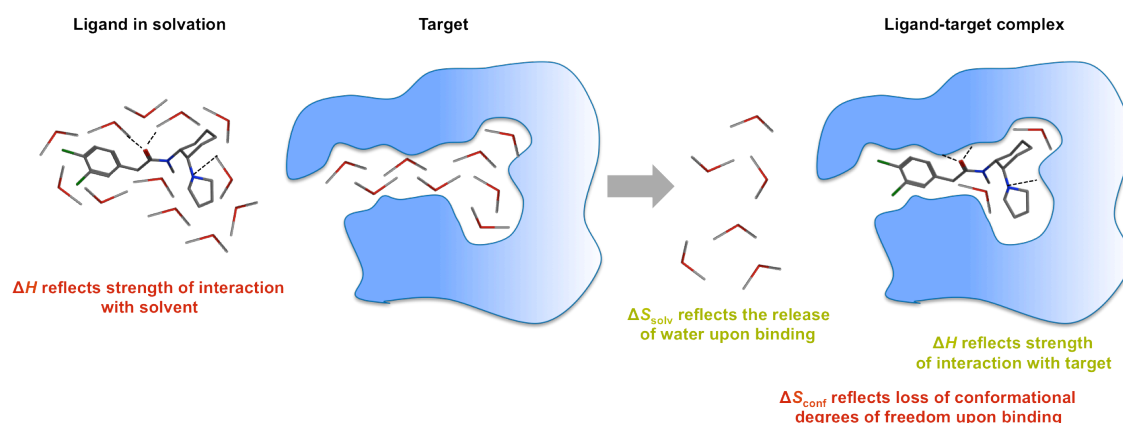


Figure 2. The binding affinity of a small molecule to its target (blue) is determined by the balance of the magnitude of its interactions with the target and those with the solvent water as well as the solvation and conformational entropy changes. H-bonds are indicated as dashed lines; modified from Freire (2004).

1.1.2 Computational techniques in drug design

Computer-aided drug design (CADD) involves all computer-assisted techniques used to discover, design and optimize biologically active compounds with a putative use as drugs (Wermuth et al., 1998). These *in silico* methods are being utilized in many steps of the drug discovery process including hit identification, hit-to-lead selection, lead optimization, and ADMET (absorption, distribution, metabolism, excretion, and toxicology) prediction. Commonly used computational approaches comprise statistical mathematical methods that are based on structural properties (quantitative structure-activity/property relationships) as well as those techniques, which employ the three-dimensional (3D) structure of either ligands (ligand-based drug design) or the biological target (structure-based drug design; Wermuth et al., 1998).

1.1.2.1 Statistical methods

Quantitative structure-activity relationship (QSAR) models are quantitative regression methods that attempt to correlate physicochemical properties (descriptors) of chemical substances with their biological activity to obtain a reliable statistical model for prediction of the activities of new compounds within a series (Hansch, 1969). The term quantitative structure-property relationship (QSPR) is used when instead of the biological activity other properties like

solubility, permeability or toxicology are concerned as dependent variables (Bradbury, 1994). Given that the descriptors characterizing steric, topological, electronic, and hydrophobic properties of molecules (Taft et al., 2008) could efficiently be determined by experimental or computational means, QSAR can decrease the number of compounds to be synthesized by facilitating the selection of the most promising candidates. Beyond the prediction capacity, QSAR models assist drug discovery by leveraging existing structure-activity data, providing insights into mechanism or identifying an alternative mechanism of action, recognizing important structural characteristics, and suggesting new design strategies (Perkins et al., 2003).

1.1.2.2 Ligand-based drug design

Ligand-based drug design is a popular approach for drug discovery, which is applied in the absence of the 3D structure of the macromolecular target. It is based on analyzing known molecules that bind to the drug target thereby highlighting those chemical features responsible for the biological activity (Kurogi and Güner, 2001). Pharmacophore modeling and 3D QSAR are the most important and widely used tools in ligand-based drug design.

According to the definition by IUPAC (Wermuth et al., 1998), a pharmacophore model is an ensemble of steric and electronic features that is necessary to ensure the optimal supramolecular interactions with a specific biological target and to trigger (or block) its biological response. Pharmacophore modelling from multiple ligands involves two main steps: (1) creating the conformational space for each ligand to represent conformational flexibility and aligning the multiple ligands; (2) determination of the essential common chemical features. In ligand-based pharmacophore modeling handling conformational flexibility of ligands and conducting molecular alignment represent the key techniques and also the main difficulties (Yang, 2010). Once a pharmacophore model is generated it is mostly used for querying 3D chemical databases to search for potential ligands, which is the so-called pharmacophore-based virtual screening or for incremental construction of completely novel candidate structures that conform to the requirements of a given pharmacophore, which is termed as *de novo* design (Wermuth et al., 1998; Yang, 2010).

3D QSAR has emerged as a natural extension to the classical QSAR models and as the name suggests, it employs descriptors derived from the spatial representation of the ligands to predict their biological activities (Wermuth et al., 1998). The Comparative Molecular Field Analysis (CoMFA; Cramer et al., 1988) has become a prototype of 3D QSAR methods (Podlogar and Ferguson, 2000). The idea underlying this methodology is that differences in biological activity are often related to differences in the magnitudes of molecular fields surrounding the investigated ligands. Close to pharmacophore modeling, the selected ligand molecules are first aligned in 3D space and subsequently placed in a 3D grid box. The values of steric and electrostatic potential energies are calculated with different probe groups at each grid

point. Finally, the 3D QSAR model is generated by partial-least-squares (PLS) analysis of the resulting interaction field values and allows identifying the quantitative influence of specific molecular features on the biological activity (Verma et al., 2010).

Clearly, ligand-based drug design is an effective method that can provide both predictive models suitable for compound optimization and crucial insights into the nature of the interactions between drug targets and ligand molecules.

1.1.2.3 Structure-based drug design

The knowledge of the 3D structure of the macromolecular target is a prerequisite to carry out a structure-based drug design strategy (Wermuth et al., 1998). The structural information is generally obtained by X-ray crystallography or NMR. However, in the case of targets with no experimentally determined structures, homology modeling is the most reliable alternative to predict the target structure (Kalyaanamoorthy and Chen, 2011). Structure-based design approaches aim at evaluating the complementarities and predicting the possible binding modes and affinities between small molecules and their targets (Zhang, 2011) in order to develop compounds that perfectly match the binding site and simultaneously incur energetically favorable interactions. Besides homology modeling that enables structure-based drug design against protein targets with unknown structures commonly used computational techniques are molecular docking, pharmacophore modeling, and *de novo* design.

Homology modeling is based on the general observation that evolutionarily related sequences have similar 3D structures (Chothia and Lesk, 1986). As a consequence, the 3D structure of a given protein sequence (target) can be built employing one or more proteins of known structure (templates) that share statistically significant sequence similarity. The 3D structure prediction process involves several consecutive steps: template identification, target-template alignment, model building, and model refinement and evaluation (Martí-Renom et al., 2000). Although each step can introduce errors that affect the modeled structure, optimal use of structural information from available templates and correctness of sequence-to-structure alignment are the most significant determinants of final model quality (Ginalska, 2006).

Molecular docking is a process of predicting the ligand conformation and its orientation inside the target structure (Kalyaanamoorthy and Chen, 2011). It is carried out in two parts starting with the determination whether a given conformation and orientation of a ligand fits the active site, which is so-called posing. In the second step an energy-based score is provided to order the poses (Kitchen et al., 2004). These scoring functions are features that aid in investigating the interactions between the small molecule and the biological target, thereby providing information about biological activity (Kalyaanamoorthy and Chen, 2011). Docking is applied at different stages of the drug discovery process for three main purposes: (1) predicting the binding mode of a known active ligand; (2) identifying new ligands using virtual screening;

(3) predicting the binding affinities of related compounds from a known active series. Of these three challenges, successful prediction of a ligand binding mode is the area where most success has been achieved but accurate prediction of binding affinities for a set of molecules turns out to be genuinely difficult (Leach et al., 2006). The latter is mainly due to the major drawbacks of molecular docking that are the lack or poor flexibility of the protein, which is not permitted to adjust its conformation upon ligand binding, and the absence of a unique and widely applicable scoring function, which precisely calculates solvation energies (Alonso et al., 2006; Leach et al., 2006). A strategy to deal with this problem is combining molecular docking with molecular dynamics (MD) simulations. MD simulations are a computational approach in which Newton's equations of motions are solved for an atomistic representation of a molecular system to obtain information about its time-dependent properties. They can treat both ligand and protein in a flexible way, allowing for an induced fit of the binding site around the newly introduced ligand. In addition, the effect of explicit water molecules can be studied directly, and very accurate binding free energies can be obtained. Further MD simulations can be used during the preparation of the experimental or homology modeling derived 3D structure before docking, to optimize it and account for protein flexibility (Alonso et al., 2006).

The 3D structure of a macromolecular target or a macromolecule-ligand complex can also be used to build a pharmacophore model. So termed structure-based pharmacophore modeling involves an analysis of the complementary chemical features of the active site and their spatial relationships, and a subsequent pharmacophore model assembly with selected features. As described for the ligand-based pharmacophore model, a structure-based pharmacophore model can be used for virtual screening and *de novo* design (Yang, 2010).

In addition to employing a pharmacophore model, small fragments can also be placed by docking in the target binding site. Such a target-based *de novo* design can be carried out by fragment linking or growing techniques. In the linking process different small fragments are added simultaneously to different active site residues of the target and connected to a final single compound whereas in the growing technique a single fragment is placed in the active site and grown well complementarily against the binding site (Kalyaanamoorthy and Chen, 2011).

In summary, the role of computational models is to increase prediction based on existing knowledge. *In silico* methods are very useful tools in rational drug design to minimize the time for identification, characterization and structure-optimization for novel drug candidates.

1.2 *Pseudomonas* Quinolone Signaling as Drug Target

1.2.1 *Pseudomonas aeruginosa*: an important opportunistic pathogen

Pseudomonas aeruginosa is a ubiquitous Gram-negative bacterium capable of surviving in a broad range of natural environments and known to infect a wide range of animal and plant hosts (Rahme et al., 1995). In humans, the opportunistic pathogen is the most common bacterium found in nosocomial infections. It is responsible for 16% of nosocomial pneumonia cases, 12% hospital acquired urinary tract infections, 8% of surgical wound infections (van Delden and Iglewski, 1998), and 10% of bloodstream infections (Gordon et al., 1998). Further, it causes life-threatening infections in immunocompromised persons, such as patients with AIDS, where *P. aeruginosa* bacteremia is associated with 50% of deaths (Mendelson et al., 1994).

Beyond this, *P. aeruginosa* plays an important role in cystic fibrosis (CF) patients. The latter are characteristically susceptible to chronic infection by *P. aeruginosa*, which is responsible for high rates of illness and death in this population (Govan and Deretic, 1996). CF results from a mutation in the cystic fibrosis transmembrane conductance regulator (CFTR) gene, which encodes a chloride channel involved in the transport of electrolytes across epithelial and other cell membranes (Riordan, 2008). The defect leads to highly viscous mucus and a failure in the airway mucociliary clearance mechanisms. Hence, the normally sterile lower airways are compromised by the accumulation of mucous and trapped bacteria (Hart and Winstanley, 2002).

The major reason for the persistence of *P. aeruginosa*, which is rarely eradicated despite even intensified antibiotic therapy, is the ability of forming biofilm structures. A biofilm is a structured consortium of bacteria, embedded in a biopolymer matrix consisting of polysaccharides, extracellular DNA and other macromolecular components such as proteins, lipids and biosurfactants. The pattern of biofilm development involves initial attachment to a solid surface, the formation of microcolonies, and finally differentiation of microcolonies into mature biofilms (Costerton et al., 1999; Figure 3).

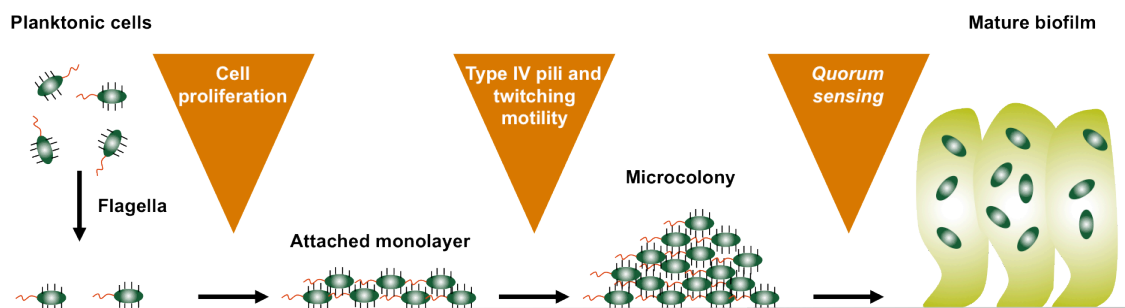


Figure 3. Model of the development of a mature *P. aeruginosa* biofilm from planktonic cells. Flagella (red) are involved in attachment, and Type IV pili (black) are required for twitching motility on a surface and the formation of microcolonies in the attached monolayer. *Quorum sensing* serves as a maturation signal leading to the formation of differentiated, thick mature biofilm structures; modified from Costerton et al. (1999).

Characteristically, gradients of nutrients and oxygen exist from the top to the bottom of biofilms and these gradients are associated with decreased bacterial metabolic activity and increased doubling times of the bacterial cells. It is these more or less dormant cells that are responsible for some of the tolerance to antibiotics (Høiby et al., 2010). Further, the mutation frequency of biofilm-growing bacteria is significantly increased compared to planktonically growing isogenic bacteria (Driffield et al., 2008) and there is increased horizontal gene transmission in biofilms (Molin and Tolker-Nielsen, 2003). Thus, bacterial cells in biofilms may simultaneously produce enzymes that degrade antibiotics, have antibiotic targets of low affinity and overexpress efflux pumps that have a broad range of substrates. Besides the ability of a biofilm to work as a protection shield against antibiotics and adverse conditions, be they phage or amoeba in nature or biocides in industrial settings (Costerton et al., 1999), it counterworks the human immune response (Bjarnsholt et al., 2010).

Moreover, the capacity of *P. aeruginosa* to produce such diverse, often overwhelming infections is due to the exceptional adaptability to variable and frequently adverse environmental conditions (Vasil, 1986) as well as the aptitude to express an arsenal of virulence factors. The latter includes both cell-associated and extracellular products, which play an important pathological role in the colonization, the survival of the bacteria, and the invasion of tissues (Bjarnsholt et al., 2010; Figure 4).

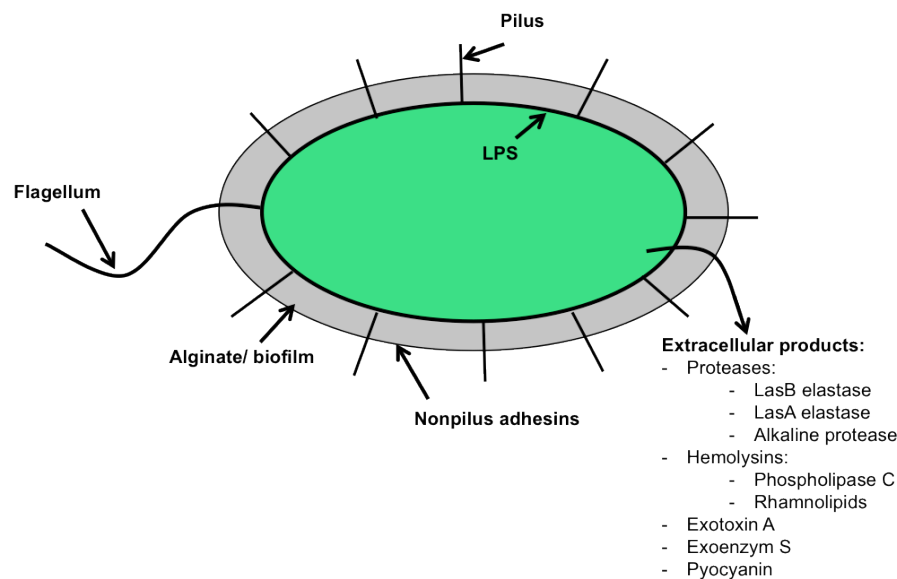


Figure 4. *P. aeruginosa* virulence factors. *P. aeruginosa* has both cell-associated (flagellum, pilus, nonpilus adhesins, alginate/ biofilm, lipopolysaccharide (LPS)) and extracellular virulence factors (proteases, hemolysins, exotoxin A, exoenzyme S, pyocyanin); modified from van Delden et al. (1998).

The coordinated production and secretion of these virulence factors as well as the biofilm formation (Figure 3) are controlled by a complex cell density dependent cell-to-cell communication system known as *quorum sensing* (QS; Swift et al., 2001).

1.2.2 The *Pseudomonas aeruginosa* quorum sensing network

Until recently, bacteria were considered autonomous single-cell organisms with little capacity for collective behaviours. However, now it is appreciated that bacterial cells are highly communicative and possess an extraordinary capacity for social behaviors. Termed as *quorum sensing* (QS; Fuqua et al., 1994), bacterial cell-to-cell communication involves producing, releasing, detecting, and responding to small hormone-like molecules (Swift et al., 2001). The latter are referred to as autoinducers as they induce their own synthesis. The signal molecules increase in concentration as a function of cell density and activate or repress corresponding transcriptional regulators (Gram-negative bacteria) or sensor kinases (Gram-positive bacteria) after a threshold concentration has been reached (Miller and Bassler, 2001; Waters and Bassler, 2005).

Thereby, QS allows bacteria to monitor the environment for other bacteria and to alter behavior on a population-wide scale in response to changes in the number and/or species present in a community. Most QS-controlled processes are unproductive when undertaken by individual bacteria acting alone but become beneficial when carried out simultaneously by a large number of cells. Thus, QS confuses the distinction between prokaryotes and eukaryotes because it enables bacteria to act as multicellular organisms (Waters and Bassler, 2005).

The first described QS system is that of the bioluminescent marine bacterium *Vibrio fischeri* that colonizes the light organ of the Hawaiian squid *Euprymna scolopes* (Nealson and Hastings, 1979). LuxI is the signal synthase, which produces the *N*-acylhomoserine lactone (AHL) autoinducer *N*-(3-oxo-hexanoyl)-L-homoserine lactone (3-oxo-C6-HSL). After a critical threshold concentration has been reached, the latter interacts with the transcriptional regulator LuxR and activates the transcription of the luciferase operon (Engebrecht and Silverman, 1984). Importantly, as *luxI* is encoded in the luciferase operon its expression is also induced creating a positive feedback loop (Stevens et al., 1994). In Gram-negative bacteria, most QS systems consist of a LuxR-type transcriptional regulator (R) and an acylated homoserine lactone autoinducer (AI) by what LuxRI QS systems are considered as the paradigm for QS in Gram-negative bacteria (Fuqua et al., 1996; Figure 5).

P. aeruginosa employs the *las* and *rhl* communication systems, which use AHL autoinducers. Both systems consist of two pairs of LuxRI homologs, LasRI and RhlRI, respectively. In the *las* system, the *lasI* gene product directs the synthesis of *N*-(3-oxo-dodecanoyl)-L-homoserine lactone (3-oxo-C12-HSL), which interacts with the transcriptional regulator LasR and activates target promoters (Gambello and Iglewski, 1991; Passador et al., 1993).

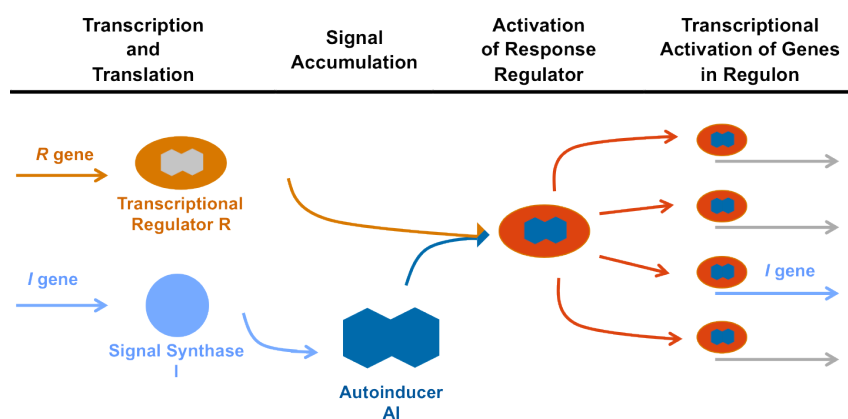


Figure 5. Generalized model for QS in Gram-negative bacteria. The key components of any QS module are the transcriptional regulator R, the signal synthase I, and the autoinducer molecule AI. The R and I proteins are expressed from their respective *R* and *I* genes; modified from Swift et al. (2001).

In the *rhl* system, *rhlI* directs the synthesis of *N*-(butanoyl)-L-homoserine lactone (C4-HSL), which interacts with the cognate regulator RhlR and stimulates the transcription of target genes (Ochsner et al., 1994; Ochsner and Reiser, 1995; Figure 6).

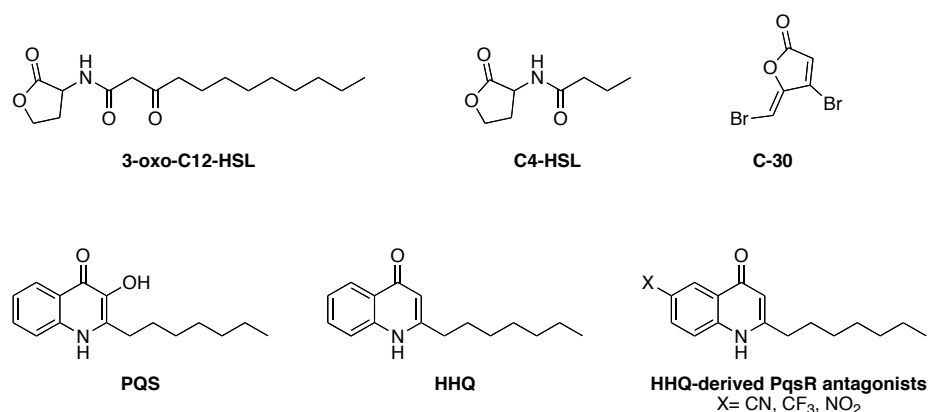


Figure 6. Structures of the *P. aeruginosa* QS signal molecules 3-oxo-C12-HSL, C4-HSL, PQS, HHQ, the QS inhibitor C-30, and the HHQ-derived PqsR antagonists.

The *las* and *rhl* systems are organized as a hierarchy placing the *las* system above the *rhl* system (Latifi et al., 1996). Further, they have been found to regulate the timing and production of multiple virulence factors including elastase, alkaline protease, exotoxin A, rhamnolipids, pyocyanin, lectins, superoxide dismutases and biofilm formation (Smith and Iglewski, 2003; Figure 7).

While both AHL-mediated QS systems are widespread among Gram-negative bacteria, the occurrence of a third *pqs* QS system (Pesci et al., 1999) is rather unique and restricted to particular *Pseudomonas* and *Burkholderia* strains (Diggle et al., 2006). It functions via the 4-hydroxy-2-alkylquinolone (HAQ) signal molecules PQS (*Pseudomonas* quinolone signal; 2-

heptyl-3-hydroxy-4(1*H*)-quinolone) and its precursor HHQ (2-heptyl-4(1*H*)-quinolone; Figure 6). Both interact with their receptor PqsR, also known as multiple virulence factor regulator (MvfR), which is essential for full *P. aeruginosa* pathogenicity (Cao et al., 2001; Xiao et al., 2006; Figure 7). In common with the AHL-dependent QS systems, the *pqs* system is involved in the regulation of *P. aeruginosa* virulence including pyocyanin biosynthesis (Dubern and Diggle, 2008), biofilm formation and maturation (Allesen-Holm et al., 2006), the production of exoproducts like elastase, alkaline proteases, rhamnolipids, and hydrogen cyanide (Déziel et al., 2005), and the expression of efflux pumps (Diggle et al., 2003). Further, PQS itself can downregulate the host innate immune response (Kim et al., 2010).

The biosynthesis of HHQ involves the condensation of anthraniloyl-coenzyme A (CoA) with a β -ketodecanoyl moiety and requires the *pqsABCD* gene products (Gallagher et al., 2002; Pistorius et al., 2011). PqsA was identified as an anthranilate-CoA ligase involved in anthranilate activation (Coleman et al., 2008), while PqsB, PqsC, and PqsD show similarities with β -keto-acyl-acyl carrier protein synthetases (Dubern and Diggle, 2008). PqsD catalyzes the decarboxylative Claisen condensation of the β -keto fatty acid and the activated anthraniloyl-CoA, followed by heterocycle formation via intramolecular condensation under elimination of water. Based on the fact, that PqsB and PqsC are absolutely required for HHQ biosynthesis, these two enzymes probably produce an activated form of the β -ketodecanoic acid, which exhibits a higher affinity to PqsD (Pistorius et al., 2011).

HHQ is already active as a signaling molecule (Xiao et al., 2006) but it can be converted intracellularly into PQS through the action of PqsH. The latter is a probable FAD-dependent monooxygenase, which is located outside of the *pqsABCDE* operon and under control of the *las* system. Thereby it provides a link between AHL- and HAQ-signaling (Gallagher et al., 2002) while the *pqs* system is placed in between the *las-rhl* hierarchy (McKnight et al., 2000; Figure 7). Along with HHQ and PQS, *P. aeruginosa* produces more than 50 different HAQs that vary in the substitution at position 3 and the length and saturation of their alkyl side chain, and most are present only in small amounts (Lépine et al., 2004).

In addition to the biosynthetic enzymes PqsA-D, the *pqs* operon contains a fifth gene, *pqsE* (Gallagher et al., 2002), which does not take part in the biosynthesis of PQS. The function of the *pqsE* gene is not known, but it is required for the production of multiple PQS-controlled virulence factors (Farrow et al., 2008; Rampioni et al., 2010; Figure 7).

The regulation of the HAQ biosynthetic genes including the *phnAB* (encodes the anthranilate synthases) and *pqsABCDE* operons occurs through PqsR, a LysR-type transcriptional regulator (LTTR; Cao et al., 2001) that is encoded slightly downstream of the *pqs* operon. It is positively controlled by LasR and negatively regulated by RhlR (Wade et al., 2005). PqsR was predicted to be membrane associated and it binds the promoter of *pqsABCDE*. This binding increases dramatically in the presence of PQS and HHQ (Xiao et al., 2006),

thereby the latter trigger their own biosynthesis and function similar to other AI molecules (Figure 7).

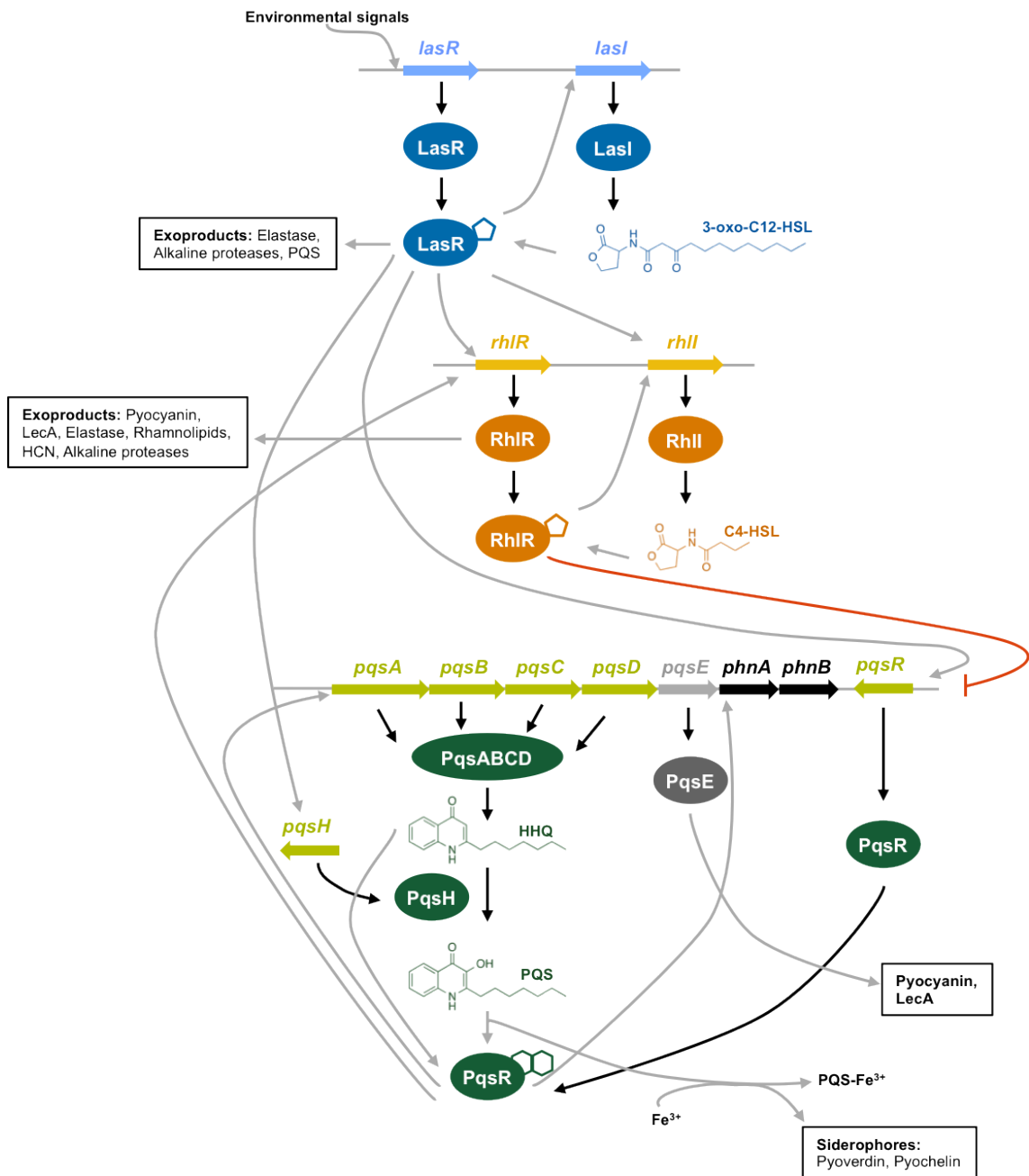


Figure 7. *P. aeruginosa* cell-to-cell signaling. HAQ and AHL-dependant quorum sensing are intimately linked since LasR/3-oxo-C12-HSL is required for full expression of *pqsH*. The transcription of *pqsR* is positively regulated by LasR and negatively regulated by RhIR. HHQ is produced via *pqsA-D* itself regulated by *pqsR*. Both PQS and HHQ induce the expression of *pqsA-E* in a PqsR-dependant manner. The production of lectin and pyocyanin also require PqsE. Furthermore, PQS released from the cell is capable of binding iron, forming a PQS- Fe^{3+} complex. The removal of iron from the extra-cellular environment by PQS induces expression of genes involved in siderophores production in an independent manner from cell-to-cell signaling. Grey arrows represent positive regulation; red lines represent negative regulation; modified from Dubern & Diggle (2008).

1.2.3 Jamming *pqs* quorum sensing as a new approach for the treatment of *Pseudomonas aeruginosa* infections

Since the introduction of antibiotics in clinical therapy, the deployment of any novel antibiotic has been followed by the evolution of clinically significant resistance to that antibiotic in as little as a few years (Palumbi, 2001). This has led to the appearance and spread of bacteria that are resistant to practically all antimicrobial drugs available on the market, so-called *superbugs*. *P. aeruginosa* has joined the ranks of *superbugs* due to its enormous capacity to engender resistance (Breidenstein et al., 2011). Yet the development of new classes of therapeutics to treat *P. aeruginosa* infections has lagged far behind the growing need for such drugs.

Traditional antibiotics work by either inhibiting bacterial growth (bacteriostatic) or killing the cell (bacteriocidal; Figure 8). However, these modes of action impose selective pressure that fosters the selection of antibiotic-resistant strains. Therefore, we must consider developing antimicrobials that have novel modes of action and exhibit less evolutionary pressure.

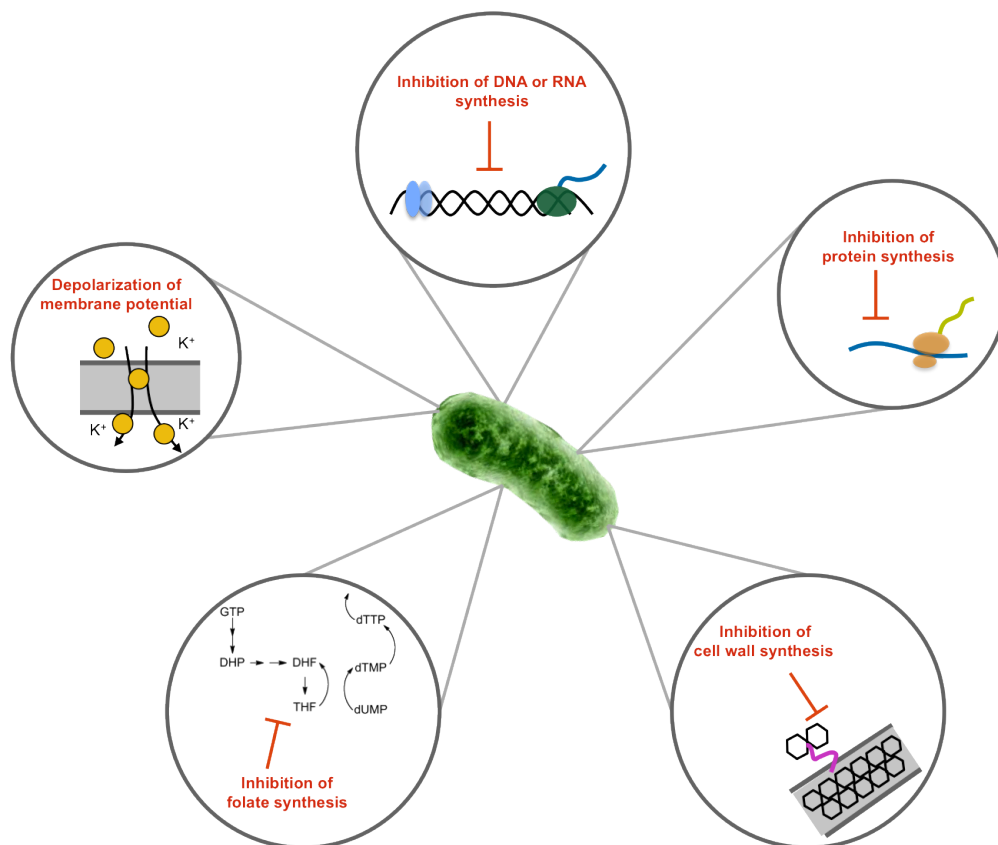


Figure 8. Traditional targets of antibacterial compounds. Traditional antibiotics function by inhibiting DNA or RNA synthesis, inhibiting protein synthesis, inhibiting cell wall synthesis, inhibiting folate synthesis, or depolarizing membrane potential.

Alternatives are disrupting the interaction between the host and the pathogen or the specific attenuation of bacterial virulence, which can be attained by targeting key regulatory systems that

mediate the expression of virulence factors (Clatworthy et al., 2007; Klein et al., 2010). One of the target regulatory systems, currently being discussed as drug target, is *quorum sensing* (Rasmussen and Givskov, 2006; Bjarnsholt and Givskov, 2007). Given that QS does not affect bacterial growth, jamming bacterial communication is generally believed to be unlikely to pose harsh selective pressure, thus minimizing the risk of resistance development (Defoirdt et al., 2010).

Over the last decade disruption of AHL-dependent QS came up as a novel target aiming at the reduction of bacterial virulence (Hentzer et al., 2002). Recently, it was shown that combination treatment of C-30, a synthetic furanone, which interferes with AHL-dependent QS (Hentzer et al., 2003; Figure 6), and tobramycin resulted in an increased clearance of *P. aeruginosa* in a infection mouse model (Christensen et al., 2012). However, AHL-dependent QS systems are widespread among Gram-negative bacteria, thereby precluding the selective disruption of cell-to-cell communication in a single species. In addition, *P. aeruginosa lasR* mutants emerged in the airway of a CF patient and resulted in increased fitness under certain growth conditions (Heurlier et al., 2005; Sandoz et al., 2007; Wilder et al., 2009). The relative prevalence of *lasR* mutants in the CF airway is likely to influence the efficacy of new drugs targeting AHL-dependent QS.

Therefore, we consider the *pqs* system that is characteristic for *P. aeruginosa* as a highly attractive target for drug development to interfere with *P. aeruginosa* pathogenicity and biofilm formation. The general validity of this approach is supported by the fact that *pqsR*, *pqsA*, *pqsH*, and *pqsE* mutants display attenuated virulence in mice (Cao et al., 2001; Déziel et al., 2005; Xiao et al., 2006). Further, *pqsA* mutants formed flat, altered biofilms that were more susceptible to treatment with the biocide sodium dodecyl sulphate than the *P. aeruginosa* wild-type biofilms (Allesen-Holm et al., 2006). A reduced pathogenicity was also observed in a mouse infection model when animals infected with the wild-type strain were treated with halogenated anthranilic acid derivatives that inhibit PQS biosynthesis. This treatment led to a significant increase in survival in comparison to the control group (Lesic et al., 2007). Based on the fact that PQS is produced in high amounts in the sputum of the CF patients (Palmer et al., 2005), it can be assumed that blocking the *pqs* QS system should make the *P. aeruginosa* lung infection in CF patients better treatable.

Two options to target *pqs* QS are: (1) inhibition of PqsD, a key enzyme in the biosynthesis of the signal molecules HHQ and PQS or (2) antagonizing PqsR, thereby avoiding the transcription of PqsR controlled genes. So far no PqsD inhibitors are reported in literature while the first PqsR antagonists were recently derived from the natural effector HHQ (Lu et al, 2012; Figure 6).

1.3 17 β -Hydroxysteroid Dehydrogenase Type 1 as Drug Target

1.3.1 Biochemical communication in eukaryotes: hormones as signal transmitter

Chemical communication between cells ensures coordination of behaviour and activities. As described above, in prokaryotes cell to cell signaling results from autoinducers and is usually referred to as *quorum sensing*. Intercellular communication in eukaryotes is also based on diffusible chemical signals, in fact neurotransmitters and hormones (Voet and Voet, 1994). In the classical view, hormones are chemical substances, which are synthesized by specialized glands for release into the general blood circulation and transport to distant target tissues, where they unfold their effects. Hormones are essential for nearly all functions of the human body like regulation of metabolism, stimulation or inhibition of growth, control of the reproductive cycle, regulation of the blood pressure, or preparation of the body for mating, fighting, fleeing and other activity. In order to exert these effects in the target cells, hormones interact with specific receptors involving ion channels, G-protein coupled receptors (GPCRs), transcription factors, and receptors with independent or associated enzyme activity, i.e. receptor-tyrosin-kinases.

Hormone production, release, and effect interact with each other and for many hormones this process is regulated by a hierarchical three-step system: the hypothalamic-pituitary axis (Figure 9).

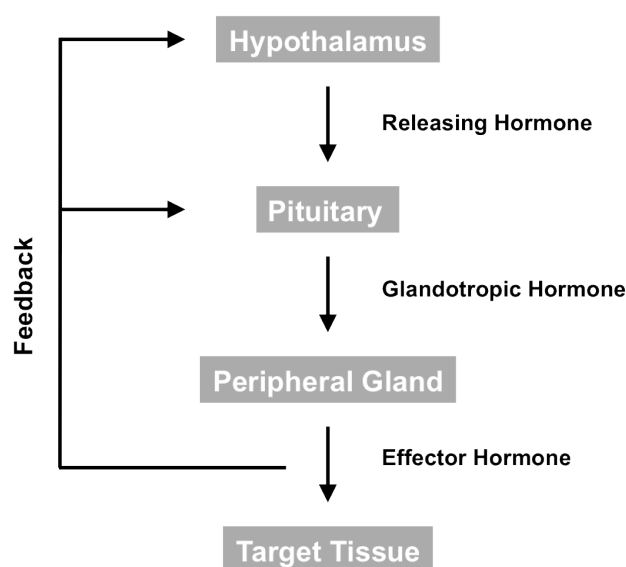


Figure 9. Negative feedback regulation. The secretory activity of the hypothalamic-pituitary axis is dependent on the concentration of the accordant effector hormone.

The hypothalamus is the central regulator, which delivers a releasing hormone thereby stimulating the production of a glandotropic hormone in the pituitary. The latter induces the

formation of an effector hormone in a peripheral gland that is finally responsible for the cellular effect. The concentration of the effector hormone in the blood circulation is detected by the hypothalamus and accordingly it regulates the distribution of the releasing hormone. Increasing hormone concentration results in a reduced and decreasing hormone concentration in an enhanced disposal of the releasing hormone constituting a negative feedback regulation (Mutschler, 2001; Aktories et al., 2011).

Considering their chemical nature hormones can be divided into steroid hormones (i.a. sex hormones and adrenal corticoids), hormones that are derived from amino acids (i.a. adrenaline, dopamine, thyroxine (T4), and triiodothyronine (T3)), and peptide hormones (i.a. insuline, antidiuretic hormone (ADH), and adrenocorticotrophic hormone (ACTH)) including glycoproteins, which bear additional carbohydrate side-chains (i.a. luteinizing hormone (LH), follicle-stimulating hormone (FSH), and thyroid-stimulating hormone (TSH; Aktories et al., 2011). Given that hormones function across different distances various types of signal transmission can be distinguished (Labrie, 1991; Voet and Voet, 1994; Figure 10):

- endocrine function matches the classical definition of hormones
- paracrine hormones are released from one cell and influence neighbouring cells
- autocrine hormones exert an action on the producing cell
- intracrine activity describes the formation of active hormones which perform their action in the same cells without release into the pericellular compartment

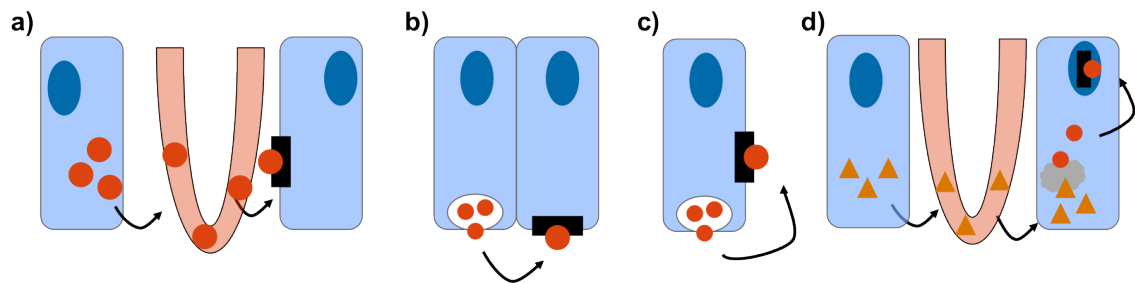


Figure 10. Schematic representation of **a)** endocrine, **b)** paracrine, **c)** autocrine, and **d)** intracrine secretion; modified from Labrie et al. (1991).

Besides the well known endocrine, paracrine, and autocrine modes of signal transmission the term of intracrine activity was first coined in 1988 (Labrie et al.) for describing the fact that “locally produced androgens and/or estrogens exert their action in the cells where synthesis took place, without release in the extracellular space”. In classical endocrine systems only a small amount of the secreted hormones is utilized in the target tissues or exerts their effects while the great majority is actually degraded. In contrast, an intracrine system requires minimal amounts of biologically active hormones to carry out their maximum hormonal effects since the hormones act at the same place as they are produced. Therefore, the intracrine system is considered a markedly efficient mode of hormone action. Converting inactive precursor

hormones to their corresponding active forms and *vice versa* provides autonomous control to target tissues which are thus able to adjust the formation and metabolism of sex steroids according to local requirements (Labrie, 1991).

1.3.1.1 Signaling by estrogens: a class of sex steroid hormones

Together with the adrenal corticosteroids the sex steroids are grouped as steroid hormones, which are sterane derivatives. The biosynthesis of steroid hormones starts from cholesterol as a common precursor and employs dehydrogenases and cytochrome P450 (CYP) enzymes (Figure 11). The corticosteroids can be divided in mineralocorticoids (e.g. aldosterone) and glucocorticoids (e.g. cortisol) that regulate the electrolyte and fluid homeostasis and glucose levels, respectively. Further, the glucocorticoids typically exert anti-inflammatory, immunomodulating as well as bone-catabolizing functions (Schäcke et al., 2002).

The group of sex steroids comprises androgens, gestagens, and estrogens. Androgens, the male sex steroids, are responsible for sexual differentiation and development in men, as well as the maintenance and support of sexual tissues in adults (Dehm and Tindall, 2007). The naturally occurring androgens are C₁₉-steroids that are generally synthesized in the testis but also in the adrenals and in the ovaries. The predominantly circulating androgen in men is testosterone that is converted to the most potent androgen 5 α -dihydrotestosterone (DHT) in target tissues. Androstendione and dehydroepiandrosterone (DHEA), however, are the most important androgens, which are produced in ovaries.

The female sex steroids include gestagens and estrogens that regulate essential biological processes in the organism i.a. development of the female sex organs and secondary sex characteristics, the regulation of the menstrual cycle and reproduction (Travis and Key, 2003). Gestagens are C₂₁-steroids based on a pregnane core with progesterone being the physiologically occurring gestagene that is mainly produced in the ovary. In premenopausal women the latter is also the main source of the biologically appearing estrogens estrone (E1), estradiol (E2), and estriol (E3; Sasano et al., 1989) that are C₁₈-steroids. Though, in postmenopausal women, the estrogen production moves to peripheral tissues such as adipose tissue or skin (Bulun et al., 2001) and almost all of the sex steroids are synthesized from precursors of adrenal origin (Jansson, 2009).

In general, the synthesis of the most potent estrogen E2 from androstendione involves 17 β -hydroxysteroid dehydrogenase (17 β -HSD) and aromatase (CYP19) and can follow two pathways: (1) reversible reduction of androstendione to testosterone (17 β -HSD3) succeeded by irreversible aromatization of the steroidal A-ring; (2) aromatization of the A-ring and subsequent reduction of E1 to E2 (17 β -HSD1; Figure 11). Interestingly, the principal substrate for extra-ovarian aromatase activity in women is androstenedione (Bulun et al., 2000). In the target tissue 17 β -HSD1 catalyzes the activation of E1 to the highly potent E2 (Gangloff et

al., 2001), thus in the context of intracrinology it constitutes the molecular switch that allows pre-receptor modulation.

Steroid hormones act *via* intracellular receptors that function as transcriptional regulators and alter the transcription of specific target genes. Accordingly, estrogenic effects are mediated by steroid hormone receptors: the estrogen receptors (ER) ER α (Walter et al., 1985) and ER β (Kuiper et al., 1996) that show considerable sequence similarity (96 % in the DNA-binding domain and 53 % in the hormone-binding domain) and share the common structure of steroid hormone nuclear receptors (Mendelsohn and Karas, 1999). Estrogens have widespread effects on both genital and extragenital systems. Genital target tissues are the uterus, the cervix, the vagina, and the mamma where estrogens are responsible for i.a. proliferation of the endometrium and development of endometrial glands, production and physical properties of the cervical mucus as well as maintenance of gravidity (Aktories et al., 2011). Further estrogens influence bone formation (Turner et al., 1994), cause vasodilatation, and induce water retention (Mendelsohn and Karas, 1999), to name but a few extragenital effects. Besides its physiological functions the most potent estrogen E2 is involved in the development of diseases such as breast cancer, endometriosis and endometrial hyperplasia. Increased E2/E1 ratios as well as high levels of 17 β -HSD1 mRNA in diseased tissues point out the pivotal role of 17 β -HSD1, which catalyzes the activation of E1 to E2.

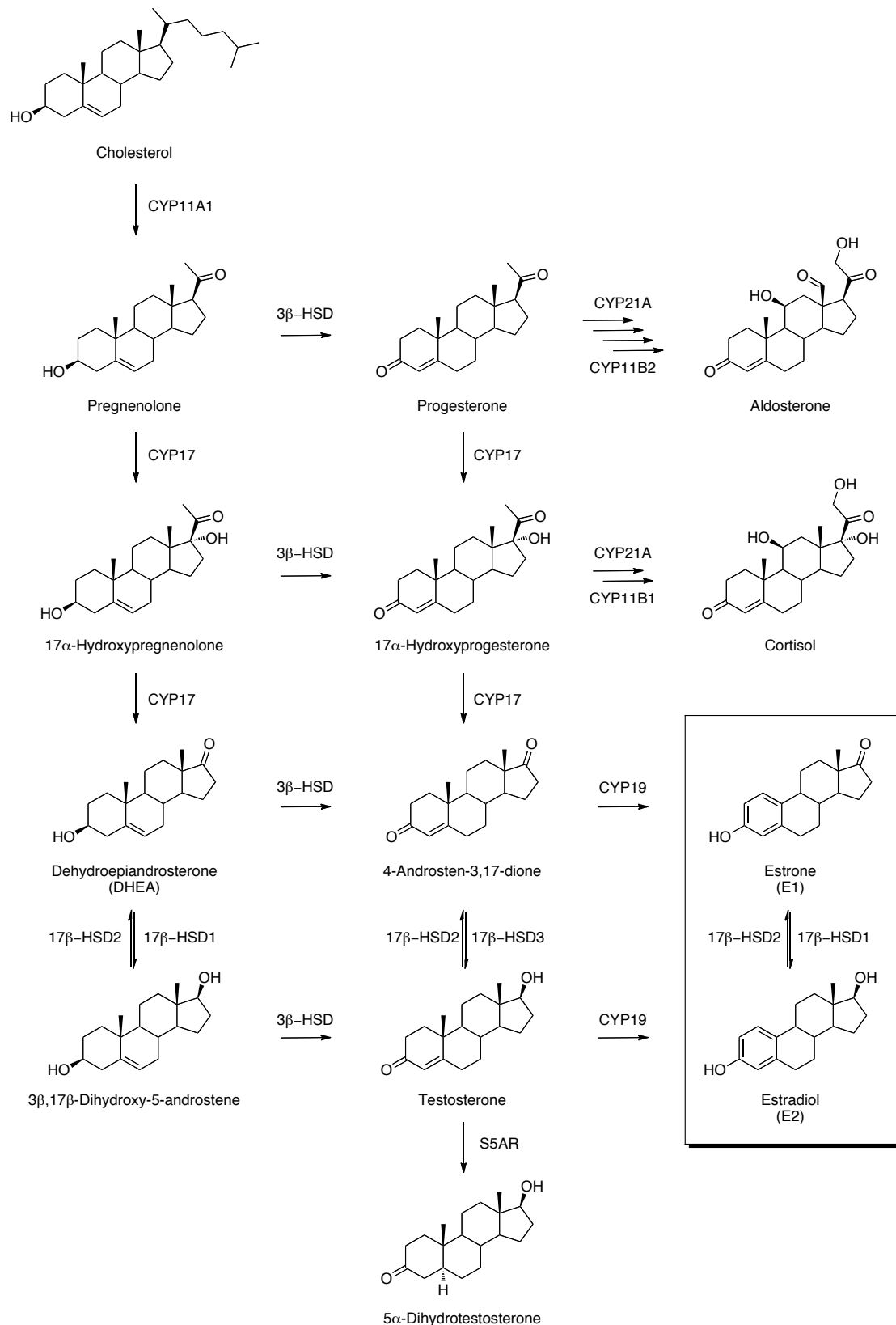


Figure 11. Biosynthetic pathway of steroid hormones. CYP11A1: cholesterol desmolase; CYP17: 17 α -hydroxylase/17,20-lyase; 3 β -HSD: 3 β -hydroxysteroid dehydrogenase/ Δ 5- Δ 4 isomerase; CYP21A: 21-hydroxylase; CYP11B1: 11 β -hydroxylase; CYP11B2: 11 β /18-hydroxylase; CYP19: aromatase; 17 β -HSD: 17 β -hydroxysteroid dehydrogenase; S5AR: 5 α -reductase.

1.3.1.2 17 β -Hydroxysteroid Dehydrogenase Type 1: a key player in estradiol biosynthesis

17 β -HSD1 is a cytosolic enzyme that belongs to the short-chain dehydrogenases/reductases (SDRs) protein family (Jornvall et al., 1995) as most of the fourteen identified 17 β -HSDs (Luu-The, 2001; Moeller and Adamski, 2009; Prehn et al., 2009). The only exception known so far is 17 β -HSD5, which belongs to the aldo-ketoreductases (AKR; Persson et al., 2009). 17 β -HSD1 consists of 327 amino acid residues (34.9 kDa) and the active form exists as homodimer (Peltoketo et al., 1988). To date 22 crystal structures of 17 β -HSD1 are available in the protein data bank (PDB) as: apoform (1bhs), holoform (1fdv, 1qyv), binary complex with E2, androgens or inhibitors (1fds, 1fdw, 1dht, 3dhe, 1jtv, 1iol, 3dey, 1i5r, 3hb4, 3klm, 3klp) and ternary complex with cofactor and E2, androstenediol or inhibitors (1fdt, 1equ, 1fdu, 1a27, 1qyw, 1qyx, 3hb5, 3km0). Remarkably, no crystal structure with the substrate E1 exists. All crystals reveal an overall identical tertiary structure: a seven-stranded parallel β -sheet (β A to β G), surrounded by six parallel α -helices (α B to α G), three on each side of the β -sheet. The basic fold of the segment β A to β F is a doubly wound α/β motif, with alternating β -strands and α -helices. Whereas the β A to β F segment is the classic 'Rossmann fold', associated with nicotinamide adenine dinucleotide binding, the β D to β G segment, in addition to being partly in the Rossmann fold, forms the substrate binding domain (SBD; Figure 12a; Ghosh et al., 1995). The latter is described as a hydrophobic tunnel with polar residues at each end: His221/Glu282 on the C-terminal side, and Ser142/ Tyr155 on the other side. E2 is stabilized by hydrogen bonds between the O3 and His221/Glu282, as well as between the O17 and Tyr155/Ser142. The apolar residues of Leu149, Val225, Phe226, and Phe259 are also involved in steroid binding by forming hydrophobic contacts (Azzi et al., 1996). Apart from this, Leu149 with its forke-like structure controls substrate specificity of 17 β -HSD1 by C₁₈/C₁₉-steroid discrimination (Han et al., 2000; Gangloff et al., 2003; Figure 12b).

Major differences in the crystal structures have been identified only for the highly flexible β F α G'-loop. It is not resolved in ten crystal structures, while the remaining twelve showed high b-factor values for this area, which is an additional hint for the flexibility of the β F α G'-loop. The latter can occupy three possible orientations, dependent on the presence of cofactor and ligands: an opened, a semi-opened and a closed enzyme conformation (Negri et al., 2010). Given that the β F α G'-loop is located at the interface between the cofactor binding site (COF) and the SBD it delimits the shape and volume of both cavities (Figure 12a).

In human 17 β -HSD1 the amino acid residues Asn114, Ser142, Tyr155 and Lys159 form the catalytic tetrad that is present in the majority of the SDR enzymes. Together with a conserved water molecule, which is stabilized by a H-bond with Asn114 it plays a critical role for the

enzymatic reaction of 17 β -HSD1 (Filling et al., 2002): a reversible hydride transfer from NADPH to E1, which is attended by a proton shift for charge equalization.

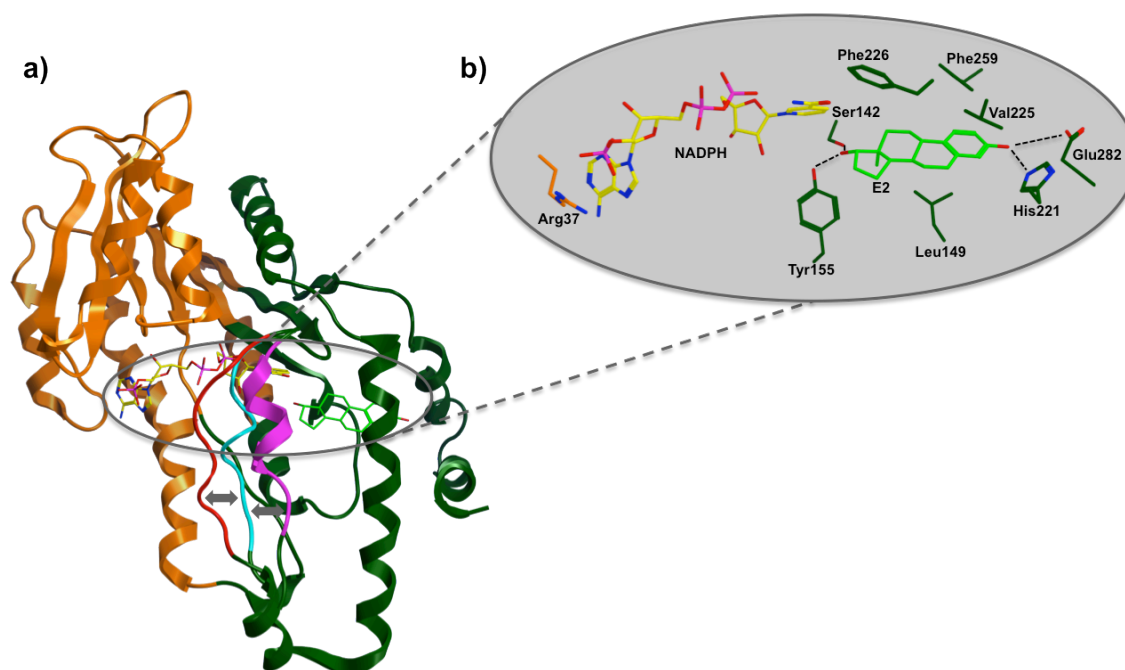


Figure 12. Structural insights into human 17 β -HSD1. **a)** Tertiary structure of 17 β -HSD1 (PDB entry 1a27); the COF is coloured in orange, the SBD in green, and the β F α G'-loop in cyan (closed conformation); the β F α G'-loop in the opened conformation (PDB entry 1iol) is coloured in magenta and in the semi-opened conformation (PDB entry 1i5r) in red. **b)** Binding modes of E2 (light green) and NADPH (yellow) in the SBD and the COF, respectively; H-bonds are drawn as black dashed lines.

Three catalytic mechanisms are proposed for 17 β -HSD1 (Penning, 1997; Ghosh and Vihko, 2001) including one concerted (simultaneous transfer of hydride and proton) and two stepwise mechanisms (Figure 13). The latter differ in the intermediate presence of either an oxyanion or a carbocation. Despite the availability of numerous structural data, it has not yet been clarified which mechanism is the most likely one (Marchais-Oberwinkler et al., 2010).

In vitro 17 β -HSD1 is able to catalyze both the reduction and oxidation depending on which redox state of cofactor is added. However, under *in vivo* conditions, such as in living cells, the catalysis is unidirectional due to distinct affinities of 17 β -HSD1 for nicotinamide cofactors and existing cofactor gradients. Structural and mutagenesis studies revealed that in the Rossmann fold of 17 β -HSD1 the positively charged side-chain of Arg37 forms a salt bridge with the 2'-phosphate group of NADP(H) (Figure 12b; Huang, 2001) that consequently led to a favored binding of the phosphorylated cofactors. Further NADP⁺ is preferably abundant in its reduced form (NADPH/NADP⁺ > 500), whereas NAD⁺ is mainly present in its oxidized form (NAD⁺/NADH > 700) and these ratios are homeostatically maintained by glucose metabolism and O₂ supply (Sherbet et al., 2007; 2009).

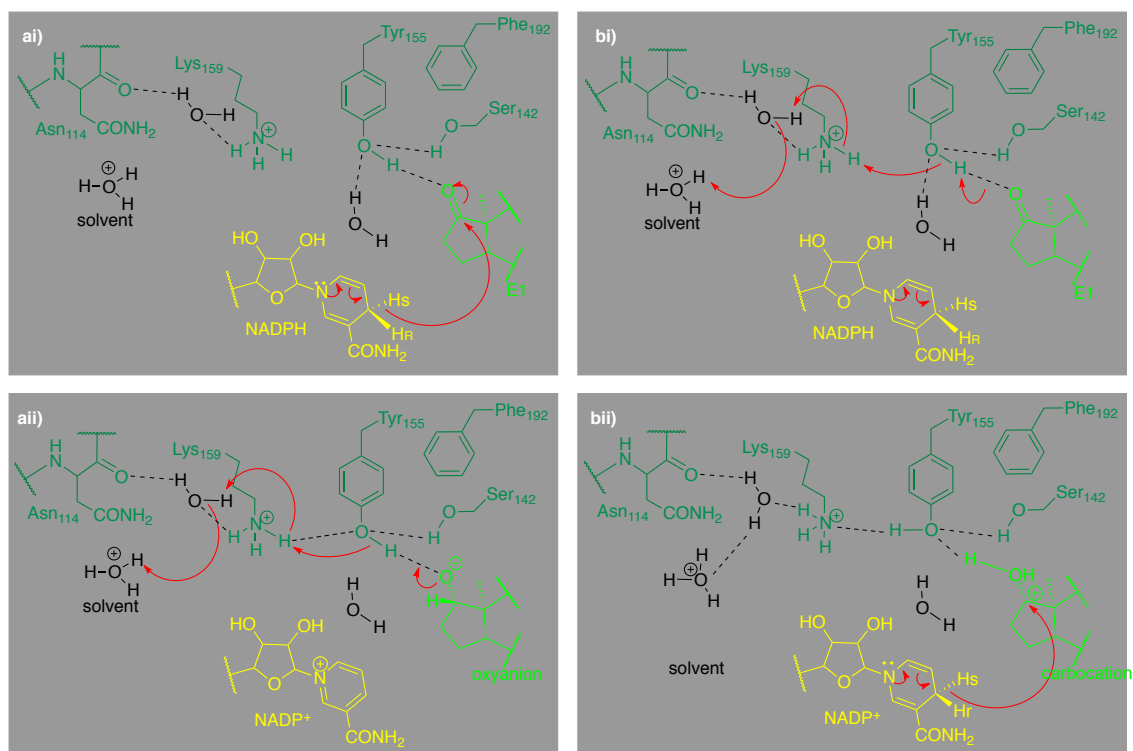


Figure 13. Two possible stepwise catalytic mechanisms of 17 β -HSD1. **a)** In the first step the pro-S hydride of NADPH is transferred to the β -face of E1 at the planar C17 carbon (ai), resulting in an energetically favorable aromatic system; subsequently the resultant oxyanion is protonated by the acidic OH group of Tyr155 (a ii). **b)** In the first step the keto oxygen of E1 is protonated by the acidic OH of Tyr155 (bi); then the resultant carbocation accepts the pro-S hydride of NADPH at the β -face (b ii). The proton relay is facilitated by a H-bond network involving Lys159, two water molecules and Asn114, an electrostatic interaction between the protonated side chain of Lys159 and the phenyl ring of Tyr155 (Ghosh and Vihko, 2001) as well as T-stacking between Phe192 and Tyr155 (Negri et al., 2010). Hydrogen bonds are represented in dashed lines; modified from Marchais-Oberwinkler et al. (2010).

1.3.2 Estrogen-dependent diseases

Estrogens influence many physiological processes in mammals such as reproduction, cardiovascular health, or bone integrity to name but a few. Given this widespread role for estrogens in human physiology, it is not surprising that estrogens are also implicated in the development and progression of numerous diseases, which include but are not limited to breast cancer, endometriosis, and endometrial hyperplasia (Deroo and Korach, 2006).

1.3.2.1 Breast cancer

Breast cancer is a type of cancer originating from the epithelial cells that line the terminal duct lobular unit. Cancer cells that remain within the basement membrane of the elements of the terminal duct lobular unit are classified as non-invasive. An invasive breast cancer is one in which there is dissemination of cancer cells outside the basement membrane of the ducts and lobules into the surrounding adjacent normal tissue (Sainsbury et al., 2000). It is by far the most

frequent cancer among women with an estimated 1.38 million new cancer cases diagnosed in 2008 (23% of all cancers), and ranks second in both sexes (10.9% of all cancers) after lung cancer (12.7% of all cancers; Ferlay et al., 2010). Data from both clinical and animal studies demonstrated that estrogens, particularly E2, are implicated in the etiology of human breast cancer. Among the most widely accepted risk factors for breast cancer are early menarche, late menopause, post-menopausal obesity, and hormone replacement therapy, which can be thought as measures of the cumulative ‘dose’ of estrogens that the breast epithelium is exposed to over time (Henderson and Feigelson, 2000). However, the responsible mechanism by which E2 contributes to the development of mammary cancer remains incompletely understood. The generally accepted hypothesis is that estrogens bind to ER α or ER β and stimulate the transcription of genes encoding growth factors. Cell proliferation is essential for carcinogenesis because cell division increases the risk of errors during DNA replication, which if not corrected, can lead to cancer (Yue et al., 2005). In this context the expression pattern of ER α or ER β plays an important role. ERs are present in extremely low quantities in normal breast epithelial cells. In contrast, 30% of premenopausal and 60% of postmenopausal breast cancers have measurable ERs and are determined as estrogen receptor positive (ER+; Cotterchio et al., 2003).

The estrogen-dependent proliferation and progress of breast cancer is further enhanced by the increased E2/E1 ratio. This is due to increased expression of 17 β -HSD1 in breast tumors compared to normal breast epithelium (Jansson, 2009). On the other hand, the expression of 17 β -HSD2, which catalyzes the reverse reaction (oxidation of E2 to E1), is not increased (Vihko et al., 2004), in some cases it is even reduced (Sasano et al., 2000).

1.3.2.2 Endometriosis

Endometriosis is a chronic estrogen dependent gynecological condition that is defined as the presence of endometrial glands and stroma outside of the uterine cavity. It affects at least 3.6% of women (Ferrero et al., 2010) and causes pain symptoms, including dysmenorrhea, deep dyspareunia, and chronic pelvic pains, as well as infertility. Endometriosis is pathohistologically a benign disease. However, it is characterized by a malignant tumor-like nature in that it grows, infiltrates and adheres to the surrounding tissues (Kitawaki et al., 2002). Although its exact etiology and pathogenesis are unclear, the most widely accepted theory for the pathogenesis has been proposed by Sampson (1927) and assumes that metastatic implantation occurs after the reflux of endometrial cells through the fallopian tubes. Given that endometriosis is highly estrogen dependent the aberrant expression of aromatase, the overexpression of 17 β -HSD1, and the deficiency in 17 β -HSD2 in endometriotic tissues may result in accumulation of E2 and thus promote the formation and growth of endometriosis (Tsai et al., 2001). Further, in endometric lesions the highly potent E2 favours its own formation by establishing a positive feedback loop: E2 induces cyclooxygenase-2 (COX-2) giving rise to elevated concentrations of prostaglandin

E₂ (PGE₂; Bulun et al., 2000); PGE₂ in turn, is the most potent known stimulator of aromatase in endometriotic stromal cells (Noble et al., 1997).

1.3.2.3 Therapeutic options

The mainstay for breast cancer treatment is surgery. Depending on the stage of the cancer it can be an excision of the tumour with surrounding normal breast tissue (breast conservation surgery) or removal of the entire breast (mastectomy; Sainsbury et al., 2000). In general, after surgery patients receive radiotherapy to reduce the risk of recurrence (Maughan et al., 2010). In the post-operative treatment, also termed as adjuvant therapy (Liu et al., 2010), also chemotherapy is a component that decreases cancer recurrence and disease-specific death (Maughan et al., 2010). Further chemotherapy is an integral part of preoperative (neoadjuvant) systemic therapy to convert inoperable cancers into candidates for surgical resection or to reduce the size of the tumor in relation to the breast to make breast conservation surgical therapy feasible (Liu et al., 2010).

An alternative therapeutical approach is settled on the endocrine level. Endocrine therapies aim at inhibiting estrogen production or blocking estrogen receptor action, thereby preventing stimulation of an estrogen-sensitive tumor (Maughan et al., 2010). In the adjuvant treatment of pre- and postmenopausal women with ER+ breast cancer endocrine therapy is an inherent part (Stuart-Harris and Davis, 2010) and it is increasingly being employed in the neoadjuvant therapy of postmenopausal women with ER+ mammary carcinoma to improve surgical options. However, for premenopausal women, neoadjuvant endocrine therapy remains investigational (Chia et al., 2010).

The biosynthesis of estrogens can be inhibited by gonadotropin-releasing hormone (GnRH) analogs, which interfere with the hypothalamic-pituitary-gonadal axis. Both GnRH agonists (e.g. busereline) and antagonists (e.g. cetrorelix) can be used and lead to a suppression of ovarian estrogen production, a state called reversible medical castration. A continuous application of GnRH agonists leads to the down-regulation of pituitary gonadotropin secretion by establishing a negative feedback mechanism (Figure 9; Emons et al., 2003). GnRH antagonists compete with natural GnRH for binding to the GnRH receptors and in contrast to GnRH agonists they avoid an initial stimulation of the gonadotropin secretion (Aktories et al., 2011).

Another strategy to interfere with estrogen biosynthesis is inhibiting aromatase that catalyzes the conversion of androgens to estrogens (Figure 11). Currently, aromatase inhibitors of the third generation are available including both steroidal (e.g. formestane) and nonsteroidal (e.g. anastrozole; Aktories et al., 2011).

Selective estrogen receptor modulators (SERMs) are synthetic molecules which bind to ER and can modulate its transcriptional capabilities in different ways in diverse estrogen target

tissues (Peng et al., 2009). In other words they can both act as agonists and antagonists. For example, tamoxifen, one of the first generation SERMs, inhibits the growth of breast cancer cells while it stimulates the proliferation of the endometrium.

Pure ER antagonists completely inhibit the estrogen dependent gene transcription and compared to SERMs no agonistic activity is observed. Fluvestrant is on the market for the treatment of tamoxifen-resistant ER+ breast cancer in postmenopausal woman (Aktories et al., 2011).

Surgical treatment of endometriosis is widely done and can be performed using laparoscopy. But considering the regression aspect of the lesions, ovariectomy is the most effective therapy (Kitawaki et al., 2002). Nonselective non-steroidal antiinflammatory drugs (NSAIDs) inhibit the synthesis of prostaglandins at both the COX-1 and COX-2 sites, and their use for the treatment of endometriosis has been largely studied, even though it is associated with various side effects. In the mild stage of endometriosis some NSAIDs acting on the pain symptomatology are used for long-term treatment (Cobellis et al., 2004). The selective inhibition of COX-2 is an effective therapeutic approach to endometriosis-associated pelvic pain (Cobellis et al., 2004), however due to side effects and the actual state of clinical data it can only be recommended for patients with severe endometriosis under clearly defined conditions (Ebert et al., 2005).

Further medical treatments for endometriosis focus on the hormonal alteration of the menstrual cycle attempting to produce a pseudo-pregnancy or pseudo-menopause. In this context GnRH analoga, oral contraceptives, and androgens are employed (Olive and Pritts, 2001). So far aromatase inhibitors and SERMs are not integrated into the therapeutic concept to treat endometriosis but recent studies showed promising results (Racine et al., 2010; Kulak et al., 2011).

1.3.3 17 β -HSD1 as promising target for the treatment of estrogen-dependent diseases

Estrogen-dependent diseases (EDDs) such as breast cancer or endometriosis are a severe threat for women (Ferlay et al., 2010; Ferrero et al., 2010). Consequently the treatment of these diseases is a major therapeutic challenge. Besides surgery and chemotherapy suppression of the estrogenic effects is a major therapeutic approach to accomplish this task. However, the endocrine therapies that are currently used in the clinic such as GnRH analoga, SERMs or aromatase inhibitors cause unwanted side effects. Strong reduction of estrogen levels in the whole body or blockade of estrogen action lead to adverse events largely mimicking menopausal symptoms, including hot flashes, losses in bone mineral density, gynecologic symptoms, and arthralgias (Abdulhaq and Geyer, 2008). Due to their tissue specific functionality, SERMs carry the risk to induce cancer in different tissues such as the endometrium, where they act as ER agonists (Angela DeMichele, 2008). Another drawback of

the presently applied endocrine therapies is the development of resistance that is observed for both antiestrogens and aromatase inhibitors (Urruticoechea, 2007). Further, the applicability of the latter is limited to postmenopausal women. In women with functioning ovaries suppression of estrogen synthesis can trigger a reflex increase in gonadotropins, which in turn causes an increase in ovarian production of aromatase and estrogens (Figure 9), as well as stimulation of estrogen-dependent tumor cells (Ortmann et al., 2009).

Therefore, we must consider developing novel therapeutical strategies for the treatment of estrogen-dependent diseases that predominantly affect intracellular E2 production in the diseased tissues. Such an intracrine approach has already been proved successful for the treatment of androgen dependent diseases such as benign prostatic hyperplasia and alopecia by using 5 α -reductase (5 α AR) inhibitors (Picard et al., 2002; Aggarwal et al., 2009). A promising target to locally reduce E2 levels in diseased tissues is 17 β -HSD1 that catalyzes the intracellular activation of E1 into E2. Both hormone-dependent breast cancer and endometriosis are estrogen-dependent diseases, with an increase in the ratio of 17 β -HSD1 to 17 β -HSD2 (Sasano et al., 2000; Tsai et al., 2001; Jansson, 2009) expression resulting in an increased E2/E1 ratio. Therefore inhibition of 17 β -HSD1 has the potential to balance the increased E2/E1 ratio thereby reducing the E2 dependent proliferating effect. Further, this strategy is not expected to cause the unwanted effects that are characteristic for the endocrine therapies, as it does not interfere with the E1 biosynthesis. Hence, E1 is able to unfold its weak estrogenic activity.

Different animal models support the general validity of this approach. In immunodeficient mice that were inoculated with T-47D breast cancer cells stably expressing human 17 β -HSD1 and 17 β -HSD2 a decrease of tumor growth could be demonstrated by application of a steroidal 17 β -HSD1 inhibitor (Day et al., 2008). Further, endometrial hyperplasia of transgenic mice ubiquitously expressing high levels of human 17 β -HSD1 could be reversed using of a steroidal 17 β -HSD1 inhibitor (Saloniemi et al., 2010).

In the past ten years a great deal of work was invested in the development of 17 β -HSD1 inhibitors. Most of the inhibitors of 17 β -HSD1 reported are based on the steroid scaffold including E1 and E2 derivatives. There are also hybrid inhibitors that consist of a steroidal scaffold linked to an adenosine moiety to cover both the SBD and COF (Poirier, 2003; 2009; Day et al., 2010; Marchais-Oberwinkler et al., 2010). However, as the steroidal inhibitors are close to the natural ER ligands E1 and E2 it cannot be excluded that steroidal inhibitors show affinity to human ERs or other steroid receptors. In order to reduce the risk of undesired side effects caused by interaction with steroid receptors the development of non-steroidal inhibitors has come into focus. Several classes of non-steroidal inhibitors have been discovered including gossypol derivatives (Brown et al., 2003), phytoestrogens (Poirier, 2003), thiophenopyrimidinones (Messinger et al., 2006; Karkola et al., 2008; Lilienkampf et al., 2009), and biphenyl ethanones (Allan et al., 2008). In the effort to identify a lead structure, that can be

optimized as selective 17 β -HSD1 inhibitor for the treatment of estrogen-dependent diseases the group of Prof. Hartmann has made an important contribution to the field of non-steroidal 17 β -HSD1 inhibitors. So far five different classes of potent and selective non-steroidal 17 β -HSD1 inhibitors have been identified: the (hydroxyphenyl)naphthols (Frotscher et al., 2008; Marchais-Oberwinkler et al., 2008; 2009; 2011; Henn et al., 2012), the bis(hydroxyphenyl) substituted arenes (Bey et al., 2008a; 2008b; 2009), the heterocyclic substituted biphenylols (Oster et al., 2010b), the bicyclic substituted hydroxyphenylmethanones (Oster et al., 2010a), and the hydroxybenzothiazoles (Spadaro et al., 2012a; 2012b; Figure 14).

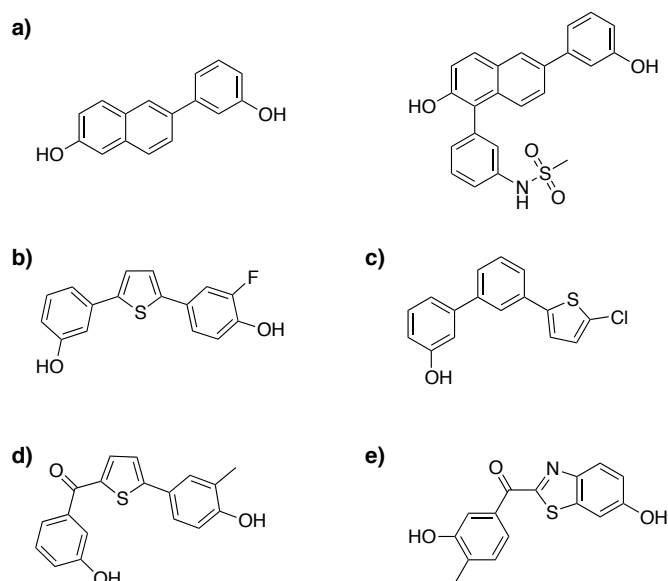


Figure 14. Representative structures of non-steroidal 17 β -HSD1 inhibitor classes. **a)** (hydroxyphenyl)naphthols; **b)** bis(hydroxyphenyl) substituted arenes; **c)** heterocyclic substituted biphenylols; **d)** bicyclic substituted hydroxyphenylmethanones; **e)** hydroxybenzothiazoles.

2 Aim of the Thesis

Corpora non agunt nisi fixata (drugs do not act unless they are bound) – in 1913, it was Paul Ehrlich who first proposed the concept of highly specific interactions between drugs and their macromolecular targets, which usually are proteins. A detailed knowledge of the specific protein-ligand interactions is essential to understand physiological processes on a molecular level and to modulate pathophysiological states. Very importantly it enables rational drug design. The latter has the potential to increase the chances of success in many stages of the drug discovery process, from the identification of novel targets and elucidation of their function to the design and development of lead compounds with desired properties. Therefore, this thesis is aimed at increasing the body of knowledge of protein-ligand interactions and active site topologies as well as understanding structure-activity relationships (SAR) by thermodynamic and structural profiling to aid the drug discovery process. In doing so, the comparison of affinities, inhibitory potencies, and thermodynamic signatures obtained for one compound toward proteins, differing only in few amino acid residues is a promising strategy. For this purpose, wild type proteins and their mutants carrying a set of point mutations can be used. Alternatively, ortholog, highly conserved proteins from various species might be considered. In the present study, both approaches were applied to investigate in particular the *P. aeruginosa* transcriptional regulator PqsR and human 17 β -HSD1 that are promising targets for limiting *P. aeruginosa* pathogenicity and the treatment of estrogen-dependent diseases, respectively. Given that infectious and estrogen-dependent diseases are a constant threat for humans not least due to the development of resistances or unsatisfying current therapies there is an urgent need for drugs with novel modes of action.

We consider antagonizing PqsR as a novel, promising strategy to attenuate PqsR-dependent virulence of *P. aeruginosa* without affecting bacterial viability. Thus, we believe that this approach is unlikely to pose harsh selective pressure thereby minimizing the risk of resistance development. In 6-position substituted HHQ derivatives constitute a class of potent PqsR antagonists. However, an important drawback of the HHQ-derived antagonists is the insufficient physicochemical properties. Hence, one major goal of this thesis was the identification of small, druglike molecules targeting the QS key player PqsR. To achieve this goal, we followed a rational design strategy combined with a fragment screening approach. Thermodynamic profiling of ligands binding to wild-type PqsR and site-directed mutants was applied as guidepost for hit selection and optimization. This approach is particularly suitable as it provides insights into ligand binding modes and the energetic characteristics of protein-ligand interactions.

17 β -HSD1 catalyzes the activation of E1 to the most potent estrogen E2, which is known to have a crucial role in the development and proliferation of estrogen-dependent diseases.

Consequently, inhibition of 17 β -HSD1 is considered as a valuable therapeutic approach for their treatment. In the past, several steroidal and non-steroidal inhibitors of 17 β -HSD1 have been described but so far none of the candidates has entered clinical trials. Furthermore, there is no cocrystal structure of a non-steroidal inhibitor in complex with 17 β -HSD1 indicating a lack of understanding the underlying protein-ligand interactions. Therefore, the present study is targeted at increasing the knowledge of active site topologies and protein-ligand interactions in order to facilitate structure-based drug design and optimization. To achieve this goal, inhibitory potencies of selected non-steroidal inhibitors toward human and marmoset 17 β -HSD1, which are highly conserved in sequence, were determined, compared and rationalized on a structural basis employing a set of computational methods. The obtained binding mode models were used to assist the design and synthesis of novel 17 β -HSD1 inhibitors.

3 Results

3.1 Identification of Small-Molecule Antagonists of the *Pseudomonas aeruginosa* Transcriptional Regulator PqsR: Biophysically Guided Hit Discovery and Optimization

Tobias Klein, Claudia Henn, Johannes C. de Jong, Christina Zimmer, Benjamin Kirsch, Christine K. Maurer, Dominik Pistorius, Rolf Müller, Anke Steinbach, and Rolf W. Hartmann

Reprinted with permission from *ACS Chemical Biology* **2012**, DOI: 10.1021/cb300208g.
Copyright: © 2012 American Chemical Society.

Publication I

Abstract: The Gram-negative opportunistic pathogen *Pseudomonas aeruginosa* produces an intercellular alkyl quinolone signaling molecule, the *Pseudomonas* quinolone signal. The *pqs* quorum sensing communication system that is characteristic for *P. aeruginosa* regulates the production of virulence factors. Therefore, we consider the *pqs* system a novel target to limit *P. aeruginosa* pathogenicity. Here, we present small molecules targeting a key player of the *pqs* system, PqsR. A rational design strategy in combination with surface plasmon resonance biosensor analysis led to the identification of PqsR binders including four top candidates with good ligand efficiencies. Determination of thermodynamic binding signatures using isothermal titration calorimetry and functional characterization in a heterologous reporter gene assay in *E. coli* guided the optimization of the best hit that resulted in the potent hydroxamic acid-derived PqsR antagonist **11** ($IC_{50} = 12.5 \mu\text{M}$). This compound showed a K_D value of $4.1 \mu\text{M}$, displayed a similar potency in *P. aeruginosa* ($IC_{50} = 23.6 \mu\text{M}$) and reduced the production of the virulence factor pyocyanin. Beyond this, site-directed mutagenesis together with thermodynamic analysis provided insights into the energetic characteristics of protein-ligand interactions suggesting the presence of hydrogen bonds and CH/ π interactions. Thus the identified PqsR antagonists are promising scaffolds for further drug design efforts against this important pathogen.

Introduction

Pseudomonas aeruginosa is an environmental highly adaptable opportunistic pathogen that is one of the leading causes for nosocomial infections¹ and is responsible for chronic lung infections in the majority of cystic fibrosis patients.² It coordinates group behaviours via a cell density dependent cell-to-cell communication system known as *quorum sensing* (QS).³ Beside the *las*^{4, 5} and the *rhl*^{6, 7} communication systems, which use *N*-acyl homoserine lactones as autoinducers, *P. aeruginosa* employs a characteristic *pqs* QS system.⁸ It functions via the signal molecules PQS (2-heptyl-3-hydroxy-4-quinolone) and its precursor HHQ (2-heptyl-4-quinolone) that interact with their receptor PqsR to control the production of a number of virulence factors such as pyocyanin and biofilm formation.⁹⁻¹¹ Due to growing antibiotic resistance there is an urgent need for therapeutics with novel modes of action. Targeting bacterial virulence or disrupting the interaction between the host and the pathogen are attractive options that are increasingly being explored.¹² Therefore we consider PqsR a novel, promising target to disrupt PqsR-dependent gene expression thereby limiting *P. aeruginosa* pathogenicity without affecting bacterial viability.¹³ Recently, we reported on the discovery of the first PqsR antagonists.¹⁴ However, as their structures are derived from the natural effector HHQ they have insufficient physicochemical properties to be used as a drug. Here, we describe the discovery and optimization of small molecules targeting the transcriptional regulator PqsR using a rational design strategy guided by biophysical methods. Combination of site-directed mutagenesis and thermodynamic analysis enabled us to study protein-ligand interactions in detail.

Results and Discussion

The κ -opioid receptor agonist (\pm)-*trans*-U50488 (**1**) was recently found to stimulate the transcription of *pqsABCDE* in *P. aeruginosa* PAO1 indicating that it could act via PqsR.¹⁵ Employing surface plasmon resonance (SPR) biosensor analysis and isothermal titration calorimetry (ITC) we confirmed that **1** binds to PqsR (Figure 1; Supplementary Figures S1 and S2) thereby providing a promising starting point for the identification of small-molecule PqsR ligands.

We applied a rational design strategy that involves the simplification of **1** into smaller fragments and analogues. In the context of antibacterial drug discovery, fragment-based design is a promising strategy since it allows to address the key issues namely insufficient physicochemical properties and lack of chemical diversity.^{16, 17} The derived in house library included (i) *N*-heteroaromatic substituted benzamides, (ii) substituted benzyl- and benzamides, and (iii) *N*-phenyl substituted isonicotin- and nicotinamides (Figure 1).

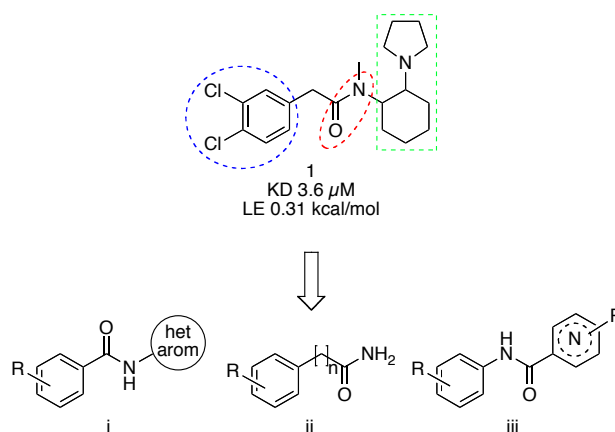


Figure 1. Ligand-based design strategy. Structure of the PqsR ligand (\pm)-*trans*-U50488 **1** (top) and general structures **i-iii** of the derived focused library (below). K_D value and ligand efficiency (LE) were determined using ITC.

Screening of the focussed library (106 compounds) in a SPR biosensor assay monitoring the affinity toward PqsR (biotinylated PqsR was immobilized on a streptavidin coated sensorchip) revealed binders including four top candidates with outstanding ligand efficiencies (LE, Figure 2).

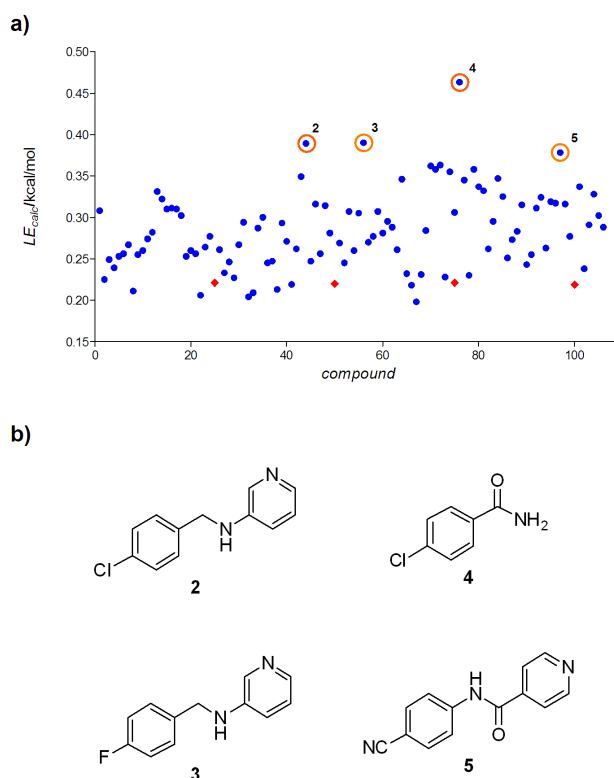
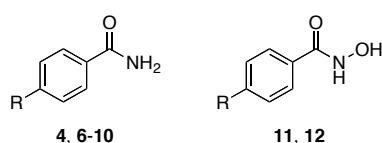


Figure 2. SPR screening data analysis. **a)** Compound data overlay for binding, referenced for blanks, DMSO calibration and streptavidin reference flow cell; blue dots represent calculated LE for compounds; red squares represent calculated LE for positive control **1** (referring surface stability); orange circles represent screening hits. Compounds were injected at $100\mu\text{M}$. **b)** Chemical structures of the top four hits.

The major drawback of screening small simple molecules is that the binding affinity is usually low.¹⁷ Therefore, LE, which is calculated as the binding energy of the ligand per heavy atom thereby normalizing the affinity and molecular size of a compound, was used for effective hit selection.¹⁸ To account for heteroatoms the binding efficiency index (BEI), that engages the total molecular weight instead of the number of non-hydrogen atoms¹⁹ is superior but here the ranking did not change. To verify and further characterize the best hit **4**, we carried out a thermodynamic analysis and evaluated its agonistic and antagonistic activity (Table 1).

Table 1. Thermodynamic parameters of ligands **1**, **4**, and **6-12** binding to PqsR and their agonistic and antagonistic activities.



Ligand	R	K_D [μM]	ΔG [kcal mol ⁻¹]	ΔH [kcal mol ⁻¹]	$-T\Delta S$ [kcal mol ⁻¹]	LE [kcal mol ⁻¹]	Agonistic activity [%]	Antagonistic activity [%]
1		3.6±0.4	-7.4±0.1	-4.7±0.1	-2.7±0.1	0.31	n.a.	18±3*
4	Cl	25.5±2.5	-6.3±0.1	-4.1±0.2	-2.1±0.2	0.63	n.a.	53±7*
6	Me	31.2±3.4	-6.1±0.1	-2.2±0.1	-3.9±0.1	0.62	33±2*	n.i.
7	Et	7.3±0.6	-7.0±0.1	-4.6±0.3	-2.4±0.3	0.64	122±13*	n.i.
8	<i>i</i> Pr	3.0±0.4	-7.5±0.1	-6.3±0.3	-1.3±0.4	0.63	111±10*	n.i.
9	<i>t</i> Bu	0.9±0	-8.3±0	-9.7±0.3	1.5±0.3	0.63	43±3*	48±1*
10	<i>i</i> Bu	5.7±0.9	-7.2±0.2	-7.9±0.4	0.7±0.1	0.55	32±3*	45±8*
11	<i>t</i> Bu	4.1±0.6	-7.4±0.1	-8.9±0.2	1.5±0.3	0.53	n.a.	78±12*
12	Et	19.7±1.2	-6.4±0	-4.8±0.2	-1.6±0.2	0.54	n.a.	50±9*

ITC titrations were performed at 298 K. Data represent mean ± SD from at least three independent experiments. Agonistic activity was determined by measuring the PqsR stimulation induced by 100 μM of the test compound compared to 50 nM PQS (= 100%); n.a. = no agonism (agonistic activity ≤ 10%). Antagonistic activity was determined by measuring the inhibition of the PqsR stimulation induced by 50 nM PQS in the presence of 100 μM test compound (full inhibition = 100%); n.i. = no inhibition (antagonistic activity ≤ 10%). Mean value of at least two independent experiments with $n = 4$, standard deviation less than 25%. Significance: For the agonist test, induction compared to the basal value; for the antagonist test, decrease of the PQS-induced induction. * $p < 0.003$; * $p < 0.05$.

Using ITC a dissociation constant (K_D) of 25.5 μM was determined for **4** binding to PqsR and the LE of 0.63 kcal/mol confirmed the high potential of **4** as starting point for optimization. Further, we examined the PqsR-mediated transcriptional effect in a reporter gene assay by measuring the β -galactosidase activity in *E. coli* harbouring the pEAL08-2 plasmid containing the *tac_P-pqsR* and *pqsA_P-lacZ* fusion genes.²⁰ *E. coli* was used as it provides a system to characterize the functionality of PqsR ligands independent of the entire *pqs* system present in *P. aeruginosa*.²¹ Remarkably, in the *E. coli* reporter gene assay **1** did not stimulate the transcription of *pqsABCDE* as described,¹⁵ rather it acts as a weak PqsR antagonist.

More important, for ligand **4** a significant reduction of the PqsR stimulation was observed. Considering the promising LE and the antagonistic activity compound **4** was chosen as starting point for structural modifications.

Variation of the length of the alkyl chain in PQS^{21, 22} as well as in HHQ and its derivatives¹⁴ had demonstrated a chain length dependency of agonistic and antagonistic activities revealing the alkyl chain as a key feature. Therefore, alkyl chains varying from C1 to C4 were introduced in the *para*-position of the benzamide core that led to compounds **6-10** (Table 1; Figure 3).

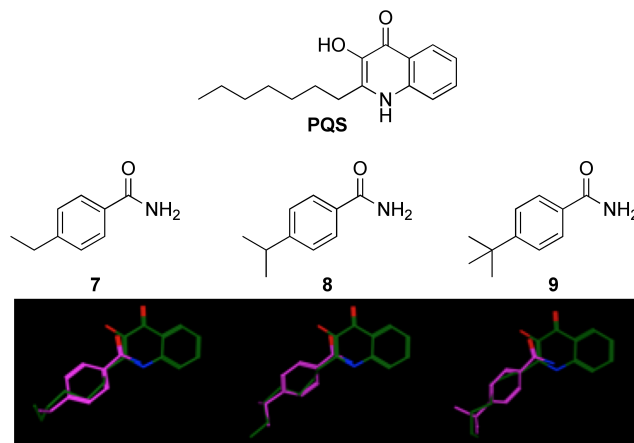


Figure 3. Flexible alignment of **7**, **8**, and **9** (magenta) with the natural ligand PQS (green). Alignment was done using the flexible alignment utility of MOE2010.10 (Chemical Computing Group Inc., Montreal, Canada).

Compared to **4** ($K_D = 25.5 \mu\text{M}$) the *tert*-butyl substituted benzamide (**9**, $K_D = 0.9 \mu\text{M}$) showed a 29-fold increase in binding affinity and the LE remained constant at a value of 0.63 kcal/mol. However, changing the constitution from *tert*- to *iso*-butyl (compound **10**, $K_D = 5.7 \mu\text{M}$) reduced the affinity again. Analysis of the thermodynamic signatures revealed that ligands **7-10** are enthalpy driven binders indicating a good non-covalent bond complementary between the protein and the compounds.²³ However, with increasing enthalpic contribution in this series the entropic terms became more unfavorable, thereby partially compensating the enthalpic gain (Figure 4).

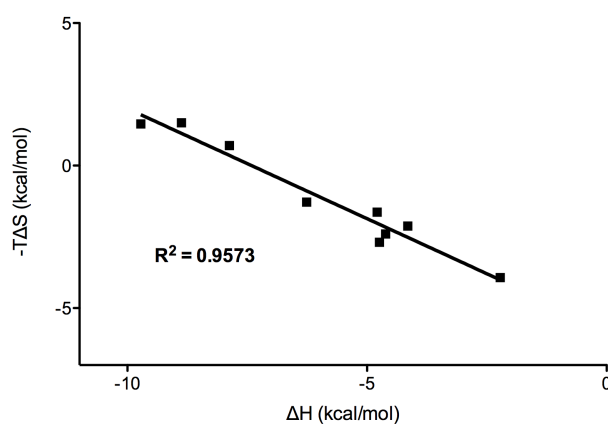


Figure 4. Plot of enthalpy (ΔH) vs entropy ($-T\Delta S$). ΔH and $-T\Delta S$ are highly correlated thereby clearly evidencing an enthalpy-entropy compensation effect in the protein-ligand complexes of the current study.

The replacement of the Cl-substituent in *para*-position of **4** by alkyl-residues (compounds **6-10**) inverted the functional properties from antagonistic (**4**) to agonistic activity (**6-10**). Interestingly, the ligands with the bulkiest substituents **9** and **10** showed in addition to their moderate agonistic activity a significant reduction of the PqsR stimulation. These findings demonstrate the impact of the alkyl moiety on binding affinity as well as on functional properties.

In order to elucidate the role of the amide function, we exchanged it by a hydroxamic acid in the ligand with the highest affinity and the most favorable enthalpic contribution (compound **9**). The resulting compound **11** ($K_D = 4.1 \mu\text{M}$) displayed a 4.6-fold reduced affinity compared to **9** that is due to a decrease in ΔH . Interestingly, the antagonistic potency was improved and the agonistic activity was completely lost. To investigate whether in the alkyl-substituted series the replacement of the amide by a hydroxamic acid in general can turn agonists into antagonists the corresponding derivative of **7** (compound **12**) was synthesized. Indeed, **12** ($K_D = 19.7 \mu\text{M}$) is also a pure PqsR antagonist.

Combining ITC with site-directed mutagenesis provides a valuable thermodynamic tool to identify the effects of specific residues in interaction with ligands.²⁴ Gln194, the only polar residue in the PQS-binding pocket,^{25, 26} was mutated and the binding of **1**, **8**, **9**, and **11** to the resulting PqsR Q194A mutant was analyzed by ITC (Table 2).

Table 2. Effect of the Q194A mutation on the thermodynamic parameters of ligand binding.

Ligand	$\Delta\Delta G$ [kcal mol ⁻¹]	$\Delta\Delta H$ [kcal mol ⁻¹]	$-T\Delta\Delta S$ [kcal mol ⁻¹]
1	0.0±0.1	0.1±0.1	-0.1±0.1
8	-1.3±0.3*	-4.0±0.3*	2.7±0.4*
9	-1.3±0*	-4.4±0.3*	3.1±0.3*
11	-0.5±0.1*	-4.1±0.4*	3.6±0.4*

$\Delta\Delta G$, $\Delta\Delta H$, and $-T\Delta\Delta S$ are $\Delta G_{WT} - \Delta G_{mutant}$, $\Delta H_{WT} - \Delta H_{mutant}$, and $-T(\Delta S_{WT} - \Delta S_{mutant})$, respectively. Negative values indicate a loss; positive values, a gain compared to wild-type. Errors indicate SD calculated via Gaussian error propagation. Significance: effect of the Q194A mutation on the thermodynamic parameters of ligand binding compared to the wild-type. * $p < 0.003$.

While the point mutation of Gln194 to Ala did not affect the binding of **1**, the affinity of **8**, **9**, and **11** was significantly decreased. The latter reveals that Gln194 is only involved in the binding of **8**, **9**, and **11**, but ITC and SPR competition experiments though confirmed that **1** and **11** bind to the same binding site (Figure 5).

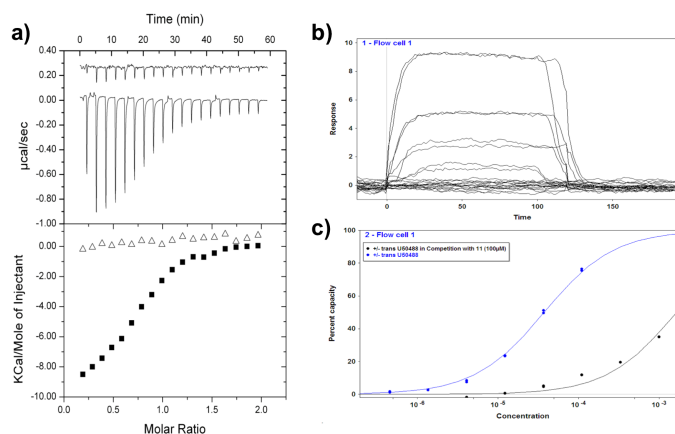


Figure 5. Competitive binding of ligands to PqsR^{C87} as measured by ITC and SPR. **a)** Raw ITC data (top) and integrated normalized data (bottom) for titrations of 94 μM H₆SUMO-PqsR^{C87} with 900 μM **11** (■) in the absence of **1** and in the presence of 1 mM compound **1** (Δ). **b)** Overlay of sensorgrams for compound **1** in competition with **11** to H₆SUMO-PqsR^{C87} measured in duplicates at 12°C; double referenced and DMSO calibrated. **c)** Blue line: Fit of the duplicate (\pm)-*trans*-U50488 equilibrium response data from the H₆SUMO-PqsR^{C87} surface to a 1:1 interaction; black line: Fit of the duplicate (\pm)-*trans*-U50488 equilibrium response data from the H₆SUMO-PqsR^{C87} surface to a 1:1 interaction in the presence of 100 μM of compound **11**.

Interestingly, for the interaction of **8**, **9**, and **11** with the Q194A mutant a comparable loss in ΔH was observed with values ranging from 4.0 to 4.4 kcal/mol. Considering that a well-placed H-bond can make a favorable enthalpic contribution in the order of -4 to -5 kcal/mol,²⁷ the results suggest that Gln194 forms H-bonds with **8**, **9**, and **11**. Further, the binding of the latter ligands to the Q194A mutant showed positive $-T\Delta\Delta S$ values relative to those of the wild-type. This might be due to the increased conformational flexibility both of the ligand and the protein in the absence of the H-bond.

As shown in Table 1, variation of the alkyl chain (compounds **6-10**) affects the enthalpy ΔH demonstrating that the alkyl chain is involved in the formation of non-covalent interactions like CH/ π hydrogen bonds. The latter have their origin in dispersion forces, which have an impact on the enthalpic term of free energy.²⁸ To probe for CH/ π interactions Phe221 that is lining the PQS-binding pocket^{25, 26} was mutated to Ala. Ligand **9**, which showed the highest affinity toward PqsR ($K_D = 0.9 \mu\text{M}$) was selected for analysis and the thermodynamic signatures for the binding of **9** to wild-type and F221A mutant PqsR are shown in Figure 6.

Indeed, the F221A point mutation affected the binding of **9** and with a deficit of 7.6 kcal/mol the enthalpic contribution was significantly reduced compared to the wild-type. A salient feature of the CH/ π hydrogen bond is that it works cooperatively and for cases involving aliphatic CH groups as the hydrogen donor, the energy of a CH/ π hydrogen bond is between -1.5 and -2.5 kcal/mol.²⁹

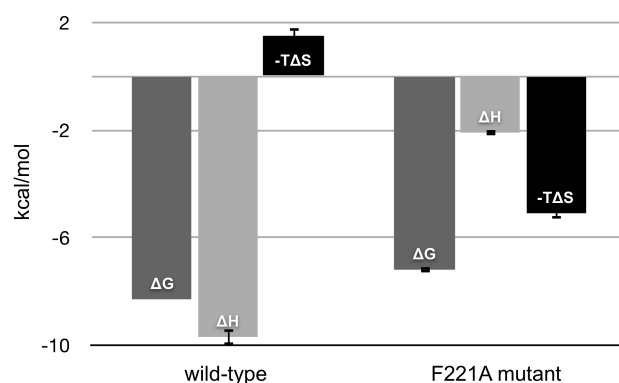


Figure 6. Thermodynamic profiles determined by ITC for the binding of ligand **9** to wild-type and F221A mutant PqsR. Data shown are mean \pm SD, $n = 3$.

This indicates that Phe221 might form three CH/ π bonds with the *t*Bu-moiety of **9** as described for the interaction of benzene with isobutane.³⁰

Given that *P. aeruginosa* is characterized by a synergy between drug efflux pumps with broad substrate specificity and low outer membrane permeability³¹ we examined whether the most potent antagonist **11** also shows an effect when tested in a *P. aeruginosa* background. Remarkably, the antagonistic activity could be confirmed (IC_{50} in *E. coli* = 12.5 μ M vs. IC_{50} in *P. aeruginosa* = 23.6 μ M; Figure 7).

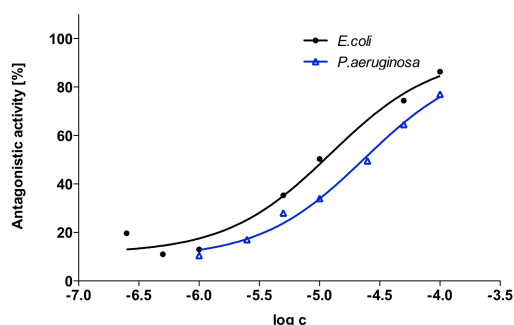


Figure 7. Determination of IC_{50} values in *E. coli* and *P. aeruginosa*. IC_{50} values were determined in the reporter gene assays. Compound **11** was tested at seven concentrations in competition with 50 nM PQS. IC_{50} value in *E. coli*: 12.5 μ M; mean value of three experiments. IC_{50} value in *P. aeruginosa*: 23.6 μ M; mean value of two experiments with $n = 4$. The log (inhibitor) vs. response model (Prism 5.0) was applied for nonlinear regression and determination of IC_{50} -values; the Hill slope was constrained equal to 1.0.

Two possible explanations for this encouraging finding might be that the penetration of the hydrophilic hydroxamic acid **11** ($\log P = 2.1$; calculated with MOE2010.10) across the outer membrane exceeds its efflux or that the antagonist **11** is no substrate of the efflux pumps. Additionally, **11** is able to reduce the production of the virulence factor pyocyanin in *P. aeruginosa* ($IC_{50} = 87.2 \mu$ M; Figure 8).

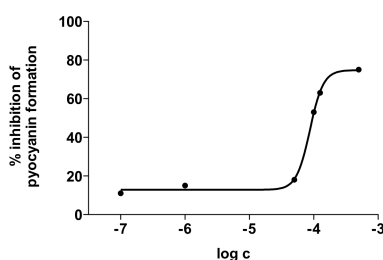


Figure 8. Effect of **11** on the pyocyanin production in *P. aeruginosa* PA14. For the determination of the IC_{50} value the pyocyanin levels in *P. aeruginosa* PA14 were spectrophotometrically determined at A_{520} nm in the presence of compound **11** at six concentrations. IC_{50} value in: 87.3 μ M; mean value of three experiments. The log (inhibitor) vs. response-variable slope model (Prism 5.0) was applied for nonlinear regression and determination of the IC_{50} -value.

Conclusion

In summary, through application of rational design and biophysical methods, we developed to the best of our knowledge the first small-molecule PqsR ligands. LEs and functional properties were used to guide the elaboration process that resulted in the potent hydroxamic acid-derived PqsR antagonist **11**. Compared to the recently described HHQ analogues¹⁴ compound **11** is a less potent antagonist but, as a consequence of its low molecular weight and its activity in *P. aeruginosa*, it has high potential for further optimization. Beyond this, site-directed mutagenesis together with thermodynamic analysis disclosed that Gln194 and Phe221 are involved in ligand binding, probably by making hydrogen bonds and CH/ π interactions, respectively. The rational simplification strategy in combination with biophysical methods, using LE as a primary filter, revealed promising hits. Accordingly, this approach is a valuable tool in drug design. Future experiments will address hit to lead optimization to open the door for antibiotics with novel modes of action for the treatment of *P. aeruginosa* infections.

Methods

Construction of pSUMO3_ck4_pqsR^{C87}. For generation of pSUMO3_ck4_pqsR^{C87} containing the truncated pqsR^{C87} gene of *P. aeruginosa* PA14, the pqsR gene from nucleotide 259 to the stop codon was PCR-amplified from genomic DNA using the forward primer 5'-TATGAGTACTAATCTCAACAAGGGTCCGCGC-3' and reverse primer 5'-TGTACAATTGCTACTCTGGTGCGGCGCGCT-3' (*ScaI*/*MfeI* sites underlined) and subsequently cloned into the *ScaI*/*MfeI* sites of the pSUMO3_ck4 vector in order to express it as a H₆SUMO-fusion protein. The construct was confirmed by DNA sequencing. This plasmid adds 104 amino acids to the N-terminus of the PqsR sequence starting at N87.

Preparation of pSUMO3_ck4_Q194ApqsR^{C87} and pSUMO3_ck4_F221ApqsR^{C87}. The Q194A and the F221A mutants was generated using the QuikChange Site-Directed Mutagenesis

Kit (Stratagene, La Jolla, CA) according to the manufacturer's instructions using the pSUMO3-ck4-pqsR^{C87} plasmid as a template. Briefly, the forward primer 5'-CTGGCCAATTACCGGGCGATCAGCCTCGGCAGC-3' (A194 underlined) and the reverse primer 5'-GCTGCCGAGGCTGATCGCCCGGTAATTGGCCAG-3' (A194 underlined) were used to amplify the Q194A gene through 16 cycles of PCR (35 s denaturation at 95 °C, 60 s annealing at 55 °C, and 6.5 min extension at 68 °C). The forward primer 5'-CTCTTCGTGGAAAACGCGGACGACATGCTGCGTCTG 3' (A221 underlined) and the reverse primer 5'-CAGACGCAGCATGTCGTCCGCGTTTTCCACGAAGAG 3' (A221 underlined) were used to amplify the F221A gene through 16 cycles of PCR using the same conditions as described above. After treatment with *DpnI*, the PCR product was transformed into *E. coli* strain XL1-Blue. Plasmid DNA was then purified from transformants using the GenElute™ HP Plasmid Miniprep Kit (Sigma-Aldrich, St. Louis, MO) and sequenced to confirm the Q194A and the F221A mutations.

Protein Expression and Purification. Wild-type, Q194A mutant, and F221A mutant H₆SUMO-PqsR^{C87} were expressed in *E. coli* and purified using a single affinity chromatography step. Briefly, *E. coli* BL21 (DE3) cells containing the pSUMO3_ck4_pqsR^{C87}, the pSUMO3_ck4_Q194ApqsR^{C87} or the the pSUMO3_ck4_F221ApqsR^{C87} plasmid were grown in LB medium containing 50 µg ml⁻¹ kanamycin at 37 °C to an OD₆₀₀ of approximately 0.8 and induced with 0.2 mM IPTG for 16 h at 16 °C. The cells were harvested by centrifugation (5000 rpm, 10 min, 4 °C) and the cell pellet was resuspended in 100 ml binding buffer (50 mM Tris-HCl, pH 7.8, 150 mM NaCl, 20 mM imidazole, 10% glycerol (v/v)) and lysed by sonication for a total process time of 2.5 min. Cell debris were removed by centrifugation (13000 rpm, 30 min) and the supernatant was filtered through a syringe filter (0.2 µm). The clarified lysate was immediately applied to a Ni-NTA column (GE Healthcare), washed with 50 mM Tris-HCl, pH 7.8, 150 mM NaCl, 20 mM imidazole, 10% glycerol (v/v), and eluted with 500 mM imidazole. The protein containing fractions were buffer-exchanged into 20 mM Tris, pH 7.4, 150 mM NaCl, 10% glycerol (v/v) for the wild-type and into 20 mM Tris, pH 7.8, 300 mM NaCl, 10% glycerol (v/v) for the Q194A and the F221A mutants, using a PD10 column (GE Healthcare) and judged pure by SDS-PAGE analysis. The H₆SUMO-tagged proteins were stored at -80 °C and used for biophysical studies.

Minimal biotinylation of H₆SUMO-PqsR^{C87}. Minimal biotinylation of the H₆SUMO-PqsR^{C87} was achieved by mixing 56 nmol of H₆SUMO-PqsR^{C87} (1 eq.) with 28 nmol of EZ-link sulfoNHS LC-LC-biotin (0.5 eq.; Thermofisher Scientific) that was freshly dissolved in water. Biotinylation reaction mixture was incubated on ice for 2 hours. To remove unreacted biotin reagent, the entire biotinylation mixture was subjected to size exclusion chromatography on a Superdex200 HR (16/600) column equilibrated in storage buffer (1x PBS, pH 7.4, 10% glycerol

(v/v)). A protein peak containing biotinylated H₆SUMO-PqsR^{C87} protein was collected (0.3 mg/ml), stored at -80 °C and used for SPR studies.

Surface Plasmon Resonance. SPR binding studies were performed using a Reichert SR7500DC instrument optical biosensor (Reichert Technologie, Depew, NY 14043 USA). SAD500 sensor chips from Xantec (Xantec Analytics, Düsseldorf) were used. Dimethyl sulfoxide (DMSO), biotin and (±)-*trans*-U50488 methanesulfonate were purchased from Sigma. Library collection consisted of 106 compounds with molecular weight range of 100 to 350 Da.

Immobilization of biotinylated H₆Sumo-PqsR^{C87}. Biotinylated H₆SUMO-PqsR^{C87} was immobilized on a SAD500 (Streptavidin coated) sensor chip at 25 °C. HEPES (50 mM HEPES, pH 7.4, 150 mM NaCl) was used as the running buffer. The streptavidin carboxymethyl dextran surface was preconditioned 30 min with running buffer until the baseline was stable. Biotinylated H₆SUMO-PqsR^{C87} was diluted into running buffer to a concentration of 100 µg/mL and coupled to the surface with a 2-min injection. Remaining streptavidin and the reference cell were blocked with a 3-min injection of biotin (3µg/mL). Biotinylated H₆SUMO-PqsR^{C87} (39494 Da) was immobilized at density of 2200 RU for the binding affinity experiment of (±)-*trans*-U50488 methanesulfonate and at a density of 5506 RU for the library screen.

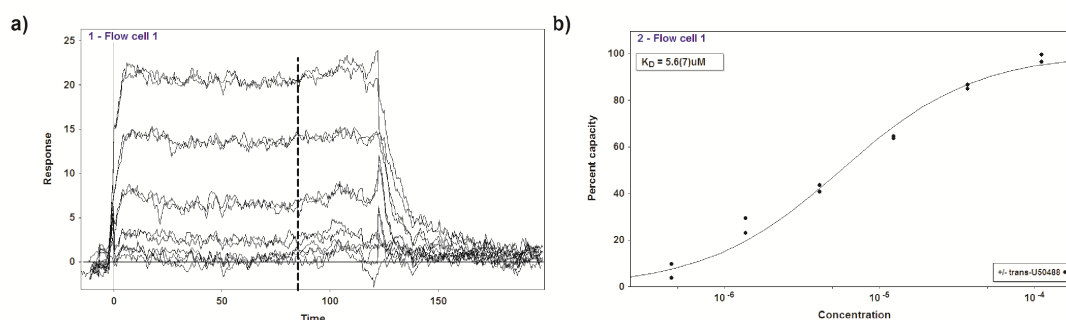


Figure S1. Binding affinity for (±)-*trans*-U50488. **a)** Overlay of sensorgrams for confirmed hit binding to H₆SUMO-PqsR^{C87} measured in duplicates at 12°C; double referenced. **b)** Fit of the duplicate (±)-*trans*-U50488 equilibrium response data from the H₆SUMO-PqsR^{C87} surface to a 1:1 interaction.

Binding affinity for (±)-*trans*-U50488 methanesulfonate. The binding experiment was performed at 12°C at a constant flow rate of 80 µl/min in instrument running buffer (50 mM HEPES, 150 mM NaCl, pH 7.4, 5% DMSO (v/v), 0.05% P20 (v/v)). A 10 mM stock of *trans*-U50488 methanesulfonate in running buffer was directly diluted to a concentration of 1 mM and then diluted in a 3-fold dilution series from 111 µM down to 457 nM. Before starting the experiments 12 warm-up blank injections were performed. Zero-buffer blank injections and DMSO calibrations were included for double referencing. Individual concentrations were injected in duplicates from lowest to highest concentrations for 120 s association and 5 min dissociation time. Scrubber software was used for processing and analysing data. Equilibrium

dissociation constant (K_D) was determined by locally fitting appropriate experimental data to a 1:1 model using fitting procedure available within Scrubber software. Overlay plot of sensorgrams and affinity plot in adequate logarithmic units for the concentrations³² are shown in Supplementary Figure S1.

Library Screening. Concentrations of ligand stock solutions in DMSO were determined by the weight of the compound. Compounds as 10 mM DMSO stocks were diluted in DMSO to 2 mM. Final ligand concentrations (100 μ M) were achieved by diluting 1:20 (v/v) in the experimental buffer (50 mM HEPES, pH 7.4, 150 mM NaCl, 0.05% P20 (v/v)) resulting in a final DMSO concentration of 5% (v/v). Binding experiments were performed at 12°C at a constant flow rate of 100 μ l/min in instrument running buffer (50 mM HEPES, pH 7.4, 150 mM NaCl, 5% DMSO (v/v), 0.05% P20 (v/v)). Each compound was injected for 26 s association - and 120 s dissociation time. Positive control ((\pm)-*trans*-U50488 methanesulfonate) was injected each 25th injection at 20 μ M to assess stability and reproducibility of the assay. 110 compounds were screened within 6 hours in 96 well plates. Data evaluation was performed using Scrubber (<http://www.biologic.com.au>) and Microsoft Excel software for data processing and analysis. Using Scrubber software, SPR signals in flow cell containing captured biotinylated protein were transformed, referenced against the blank surface (streptavidin) and further corrected for DMSO refractive index change (excluded volume effect). Compounds showing promiscuous binding response³³ were removed from the screening data. Report binding points, taken for each fragment injection after a contact interval of 19-s were analyzed. K_D values were estimated using Eq. (1) derived from the Langmuir adsorption isotherm.

$$K_D = (R_{\max} * C/R) - C \quad (1)$$

R_{\max} , R , and C correspond to the normalized saturation response of the compound, the normalized response of the test compound, and the concentration of the test solution, respectively. For the ranking of the best hits, the LE was calculated as previously described^{18, 34} from Eq. (2),

$$LE = -RT \ln K_D / (\text{heavy atom count}) \quad (2)$$

T is the absolute temperature, and $R = 1.98$ cal/mol/K.

Competition experiments for (\pm)-*trans*-U50488 methanesulfonate and compound 11.

The competition experiment was performed at 12°C at a constant flow rate of 25 μ l/min in instrument running buffer (50 mM HEPES, 150 mM NaCl, pH 7.4, 5% DMSO (v/v), 0.05% P20 (v/v), 100 μ M compound **11**). A 10 mM stock of *trans*-U50488 methanesulfonate in running buffer was directly diluted to a concentration of 1 mM and then diluted in a 3-fold dilution

series from 333 μM down to 4,57 μM . Before starting the experiments 12 warm-up blank injections were performed. Zero-buffer blank injections and DMSO calibrations were included for double referencing. Individual concentrations were injected in duplicates from lowest to highest concentrations for 120 s association and 5 min dissociation time. Scrubber software was used for processing and analysing data. Equilibrium dissociation constant (K_D) was determined by locally fitting appropriate experimental data to a 1:1 model using fitting procedure available within Scrubber software. Overlay plot of sensorgrams and affinity plot in adequate logarithmic units for the concentrations³² are shown in Figure 5.

Isothermal titration calorimetry. ITC experiments were carried out using an ITC₂₀₀ instrument (Microcal Inc., GE Healthcare). Concentrations of ligand stock solutions in DMSO were determined by the weight of the compound. Final ligand concentrations were achieved by diluting 1:20 (v/v) in the experimental buffer resulting in a final DMSO concentration of 5% (v/v). Protein concentration was determined by measuring the absorbance at 280 nm using a theoretical molarity extinction coefficient of 22,900 $\text{M}^{-1}\text{cm}^{-1}$. DMSO concentration in the protein solution was adjusted to 5% (v/v). ITC measurements were routinely performed at 25 °C in 20 mM Tris, pH 7.4, 150 mM NaCl, 10% glycerol (v/v), 5% DMSO (v/v) for the wild-type PqsR^{C87} and in 20 mM Tris, pH 7.4, 300 mM NaCl, 10% glycerol (v/v), 5% DMSO (v/v) for the Q194A and the F221A mutants, respectively. The titrations were performed on 66-200 μM H₆SUMO-PqsR^{C87}, H₆SUMO-Q194APqsR^{C87} or H₆SUMO-F221APqsR^{C87} in the 200 μl sample cell using 2-2.7 μl injections of 0.7-2.5 mM ligand solution every 180 s. The competition experiment was performed on 94 μM H₆SUMO-PqsR^{C87}, which was incubated with 1mM compound **1** for 30 min at 25 °C. Raw data were collected and the area under each peak was integrated. To correct for heats of dilution and mixing the final base line consisting of small peaks of the same size at the end of the experiment was subtracted. The experimental data were fitted to a theoretical titration curve (one site binding model) using MicroCal Origin 7 software, with ΔH (enthalpy change in kcal/mol), K_A (association constant in M^{-1}), and N (number of binding sites) as adjustable parameters. Thermodynamic parameters were calculated from Eq. (3),

$$\Delta G = \Delta H - T\Delta S = RT\ln K_A = -RT\ln K_D \quad (3)$$

where ΔG , ΔH , and ΔS are the changes in free energy, enthalpy, and entropy of binding, respectively, T is the absolute temperature, and $R = 1.98$ cal/mol/K. The LE for each compound was calculated from Eq. (4),

$$\text{LE} = -\Delta G/(\text{heavy atom count}) \quad (4)$$

where ΔG is the change in free energy and heavy atom count is the number of non-hydrogen atoms of the compound. For each ligand at least three independent experiments were performed. Representative ITC titrations of **1**, **8**, and **11** against H₆SUMO-PqsR^{C87} and H₆SUMO-Q194APqsR^{C87} are shown in Supplementary Figure S2. Representative ITC titrations of **9** against H₆SUMO-PqsR^{C87}, H₆SUMO-Q194APqsR^{C87}, and H₆SUMO-F221APqsR^{C87} are shown in Supplementary Figure S3. Representative ITC titrations of **4**, **6**, **7**, **10**, and **12** against H₆SUMO-PqsR^{C87} are shown in Supplementary Figure S4.

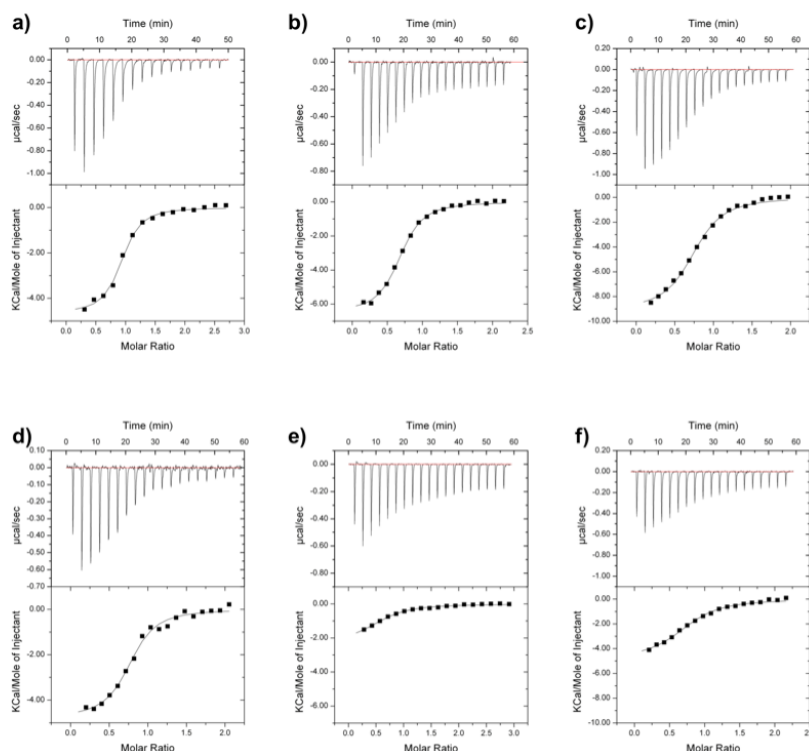


Figure S2. Representative ITC titrations. **a**) ITC titration of **1** (1.4 mM) against H₆SUMO-PqsR^{C87} (111 µM). **b**) ITC titration of **8** (900 µM) against H₆SUMO-PqsR^{C87} (83 µM). **c**) ITC titration of **11** (900 µM) against H₆SUMO-PqsR^{C87} (94 µM). **d**) ITC titration of **1** (1 mM) against H₆SUMO-Q194APqsR^{C87} (100 µM). **e**) ITC titration of **8** (2 mM) against H₆SUMO-Q194APqsR^{C87} (141 µM). **f**) ITC titration of **11** (1 mM) against H₆SUMO-Q194APqsR^{C87} (95 µM). The recorded change in heat is shown in units of µcal/sec as a function of time for successive injections of the ligand (upper row). Integrated heats (black squares) plotted against the molar ratio of the binding reaction. The continuous line represents the results of the non-linear least squares fitting of the data to a binding model (lower row).

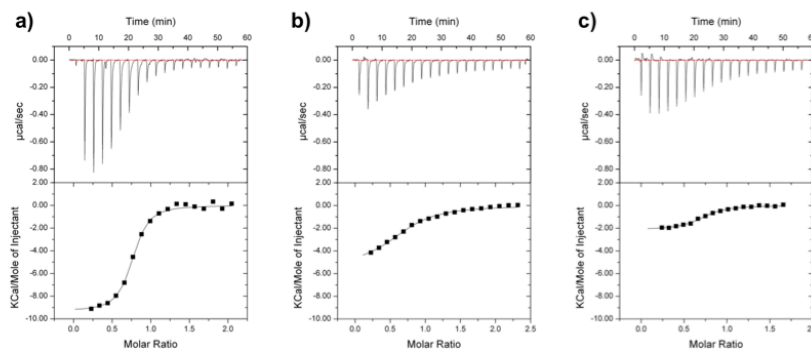


Figure S3. Representative ITC titrations. **a)** ITC titration of **9** (700 μM) against $\text{H}_6\text{SUMO-PqsR}^{\text{C87}}$ (67 μM). **b)** ITC titration of **9** (700 μM) against $\text{H}_6\text{SUMO-Q194APqsR}^{\text{C87}}$ (66 μM). **c)** ITC titration of **9** (1 mM) against $\text{H}_6\text{SUMO-F221APqsR}^{\text{C87}}$ (124 μM). The recorded change in heat is shown in units of $\mu\text{cal/sec}$ as a function of time for successive injections of the ligand (upper row). Integrated heats (black squares) plotted against the molar ratio of the binding reaction. The continuous line represents the results of the non-linear least squares fitting of the data to a binding model (lower row).

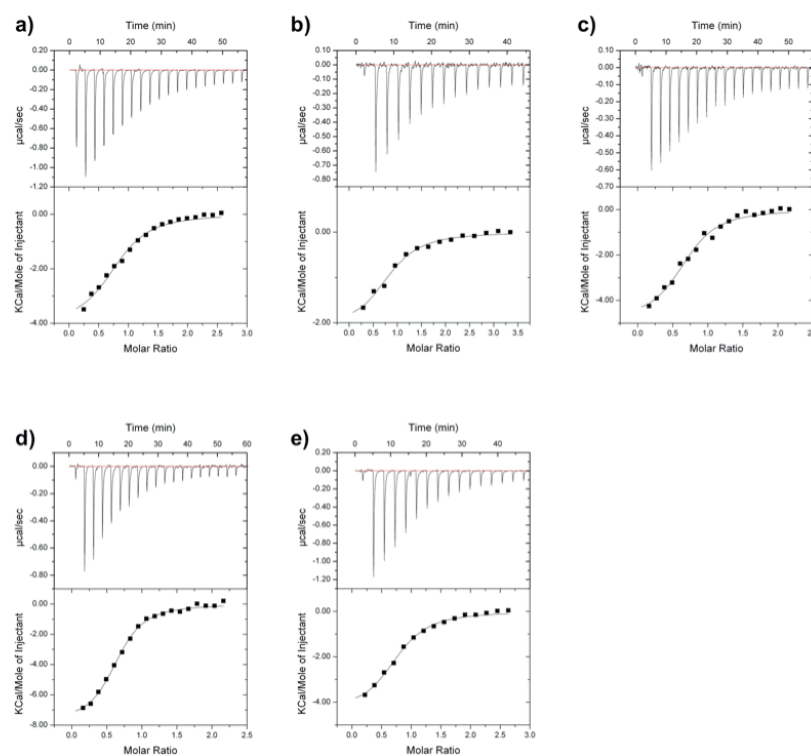


Figure S4. Representative ITC titrations. **a)** ITC titration of **4** (2.5 mM) against $\text{H}_6\text{SUMO-PqsR}^{\text{C87}}$ (200 μM). **b)** ITC titration of **6** (2.5 mM) against $\text{H}_6\text{SUMO-Q194APqsR}^{\text{C87}}$ (157 μM). **c)** ITC titration of **7** (900 μM) against $\text{H}_6\text{SUMO-PqsR}^{\text{C87}}$ (83 μM). **d)** ITC titration of **10** (900 μM) against $\text{H}_6\text{SUMO-Q194APqsR}^{\text{C87}}$ (83 μM). **e)** ITC titration of **12** (2 mM) against $\text{H}_6\text{SUMO-Q194APqsR}^{\text{C87}}$ (158 μM). The recorded change in heat is shown in units of $\mu\text{cal/sec}$ as a function of time for successive injections of the ligand (upper row). Integrated heats (black squares) plotted against the molar ratio of the binding reaction. The continuous line represents the results of the non-linear least squares fitting of the data to a binding model (lower row).

Reporter Gene Assay in *E. coli*. The ability of the compounds to either stimulate or antagonize the PqsR-dependent transcription was performed as previously described using a β -galactosidase reporter gene assay²⁰ in *E. coli* expressing PqsR with some modifications to enable a higher throughput³⁵. PQS and PqsR ligands were diluted in ethyl acetate, added to the wells of a 96 deep well plate and the solvent was evaporated. Overnight cultures of *E. coli* DH5 α cells containing the plasmid pEAL08-2 which encodes PqsR under the control of the *tac* promoter and the β -galactosidase reporter gene *lacZ* controlled by the *pqsA* promoter, were diluted 1:100 in Luria-Bertani medium with ampicillin (50 μ g/ml). The culture was incubated at 37 °C with shaking until it reached an OD₆₀₀ of 0.2. For the determination of agonistic activities, 1 ml aliquots were supplemented with either PQS (50 nM) or the test compound (100 μ M). Ethyl acetate was used as control. Antagonistic effects of the compounds (100 μ M) were evaluated in the presence of 50 nM PQS. The β -galactosidase activity was determined after a 2.5 h incubation period at 37 °C with shaking (150 rpm). OD₆₀₀, OD₄₂₀ and OD₅₅₀ were measured and the activity is expressed as ratio of the ethyl acetate control relative to the cultures that received either PQS, a test compound or both.

Reporter Gene Assay in *P. aeruginosa* PA14. The ability of the compounds to either stimulate or antagonize the PqsR-dependent transcription was performed as previously described using a β -galactosidase reporter gene assay²⁰ in *PA 14* Δ *pqsA*³⁵. PQS and PqsR ligands were diluted in ethyl acetate, added to the wells of a 96 deep well plate and the solvent was evaporated. Overnight cultures of *PA14* cells containing the plasmid pEAL08-2 which encodes PqsR under the control of the *tac* promoter and the β -galactosidase reporter gene *lacZ* controlled by the *pqsA* promoter, were diluted 1:100 in Luria-Bertani medium with carbenicillin (250 μ g/ml). The culture was incubated at 37 °C with shaking until it reached an OD₆₀₀ of 0.2. For the determination of agonistic activities, 1 ml aliquots were supplemented with either PQS (50 nM) or the test compound (100 μ M). Ethyl acetate was used as control. Antagonistic effects of the compounds (100 μ M) were evaluated in the presence of 50 nM PQS. The β -galactosidase activity was determined after a 2.5 h incubation period at 37 °C with shaking (150 rpm). After the incubation period the aliquots were shaken at least for 1 min (1000rpm). OD₆₀₀, OD₄₂₀ and OD₅₅₀ were measured and the activity is expressed as ratio of the ethyl acetate control relative to the cultures that received either PQS, a test compound or both.

Pyocyanin assay. Pyocyanin produced by *P. aeruginosa* PA14 was determined using the method of Essar et al.³⁶ with some modifications: Cultures were inoculated with a starting OD₆₀₀ = 0.02 in 24 well plates (Greiner, Cellstar) containing 1.5 ml PPGAS medium per well. PPGAS medium (20 mM NH₄Cl, 20 mM KCl, 1.6 mM MgSO₄, 120 mM Tris-HCl, pH 7.2, 0.5% (w/v) glucose, 1% (w/v) Bacto™ Tryptone)³⁷ was found to enhance pyocyanin production. DMSO as a control or DMSO solutions of inhibitors were added to the cultures to a final DMSO concentration of 1%. Plates were incubated at 37 °C, 200 rpm and a humidity of 75% for 16 hrs.

For pyocyanin determination, 900 μl of each culture were extracted with 900 μl of chloroform. The solution was centrifuged (14.000 rpm, 15 min) to separate the phases. 800 μl of the organic phase were mixed with 250 μl of 0.2 M HCl. After centrifugation (14.000 rpm, 15 min), 80 μl of the aqueous phase was transferred to 96 well plates (Nunc U96 MicroWell™) for measurement of OD₅₂₀ using FLUOstar Omega (BMG Labtech). For each sample, cultivation and extraction were performed in triplicates.

Chemical and Analytical Methods. ¹H and ¹³C NMR spectra were recorded on a Bruker DRX-500 instrument. Chemical shifts are given in parts per million (ppm), and tetramethylsilane (TMS) was used as internal standard for spectra obtained in CDCl₃, MeOH-*d*₄ and DMSO-*d*₆. Coupling constants (*J*) are given in hertz. Mass spectrometry (LC/MS) was performed on a MSQ[®] electro spray mass spectrometer (Thermo Fisher). The system was operated by the standard software Xcalibur[®]. A RP C18 NUCLEODUR[®] 100-5 (125 × 3 mm) column (Macherey-Nagel GmbH) was used as stationary phase with water/acetonitrile mixtures as eluents. All solvents were HPLC grade. Reagents were used as obtained from commercial suppliers without further purification. The reaction progress was determined by thin-layer chromatography (TLC) analyzes on silica gel 60, F₂₅₄ (Merck). Visualization was accomplished with UV light. Melting points were measured using melting point apparatus SMP3 (Stuart Scientific). The apparatus is uncorrected.

General procedure for the synthesis of amides.³⁸ **Synthesis of 4-ethylbenzamide**³⁹ (**7**). A solution of 4-ethylbenzoic acid (746 mg, 500 mmol), thionyl chloride (1 mL) and *N,N*-dimethylformamide (3 drops) was heated at 80 °C for 1 h. The reaction mixture was evaporated under reduced pressure. The residue was redissolved in toluene (10 mL). At 0 °C the mixture was added to concentrated ammonia (20 mL). After stirring for 30 minutes the precipitate was collected by suction filtration, washed with water and *n*-hexane, and dried under reduced pressure at 50 °C. Recrystallization from ethyl acetate afforded compound **7** (0.41 g, 55%). Mp: 164-165 °C. ¹H-NMR (500 MHz, CDCl₃): δ = 1.25 (t, *J* = 7.6 Hz, 3H), 2.69 (q, *J* = 7.6 Hz, 2H), 6.12 (bs, 2H), 7.26 (d, *J* = 8.2 Hz, 2H), 7.74 (d, *J* = 8.5 Hz, 2H). ¹³C-NMR (125 MHz, CDCl₃): δ = 15.2, 28.8, 127.4, 128.1, 130.8, 148.7, 169.5. LC/MS: *m/z* = 150.06 (M + H)⁺, 191.13 (M + H + CH₃CN)⁺, *t_R* = 8.77 min, 98.6% pure (UV).

Synthesis of 4-isopropylbenzamide⁴⁰ (**8**). Compound **8** was prepared from 4-isopropylbenzoic acid according to the general procedure (0.24 g, 49%). Mp: 150.5-151.5 °C. ¹H-NMR (500 MHz, DMSO-*d*₆): δ = 1.20 (d, *J* = 6.9 Hz, 6H), 2.92 (septet, *J* = 6.9 Hz, 1H), 7.26 (bs, 1H), 7.30 (d, *J* = 8.2 Hz, 2H), 7.80 (d, *J* = 8.2 Hz, 2H), 7.89 (bs, 1H). ¹³C-NMR (125 MHz, DMSO-*d*₆): δ = 23.6, 33.3, 126.1, 127.6, 131.9, 151.7, 167.8. LC/MS: *m/z* = 164.11 (M + H)⁺, 205.09 (M + H + CH₃CN)⁺, *t_R* = 8.54 min, >99% pure (UV).

Synthesis of 4-isobutylbenzamide⁴¹ (**10**). Compound **10** was prepared from 4-isobutylbenzoic acid according to the general procedure. The final product was crystallized

from ethyl acetate (0.45 g, 51%). Mp: 154-155 °C. ¹H-NMR (500 MHz, CDCl₃): δ = 0.89 (d, *J* = 6.6 Hz, 6H), 1.89 (nonet, *J* = 6.8 Hz, 1H), 2.52 (d, *J* = 7.2 Hz, 2H), 6.00 (bs, 2H), 7.21 (d, *J* = 8.5 Hz, 2H), 7.73 (d, *J* = 8.1 Hz, 2H). ¹³C-NMR (125 MHz, CDCl₃): δ = 15.2, 28.8, 127.4, 128.1, 130.8, 148.7, 169.5. LC/MS: *m/z* = 178.18 (M + H)⁺, 219.05 (M + H + CH₃CN)⁺, *t_R* = 10.72 min, 97.3% pure (UV).

General procedure for the synthesis of hydroxamic acids.⁴² **Synthesis of 4-(*tert*-butyl)-*N*-hydroxybenzamide (11).** *O*-(Tetrahydro-2-pyranyl)hydroxylamine (352 mg, 3.00 mmol) and sodium carbonate (159 mg, 1.50 mmol) were dissolved in a water-chloroform mixture (1:1, 10 mL). 4-*tert*-Butylbenzoyl chloride (590 mg, 3.00 mmol) was added and the solution was stirred for 30 minutes at room temperature. Both layers were separated and the water layer was extracted with chloroform. The combined organic layers were evaporated under reduced pressure leaving a foam. The solid was dissolved in methanol (20 mL). 0.1 N aqueous HCl (20 mL) was added and the solution was stirred overnight at room temperature. The solvent was removed under reduced pressure leaving compound **11** as a white solid (573 mg, 99%). Mp: 135.3-136.8 °C (lit. ⁴³ 141-144 °C). ¹H-NMR (500 MHz, MeOH-*d*₄): δ = 1.28 (s, 9H), 7.45 (d, *J* = 8.5 Hz, 2H), 7.69 (d, *J* = 8.5 Hz, 2H), 11.14 (bs, 1H). ¹³C-NMR (125 MHz, MeOH-*d*₄): δ = 31.6, 35.8, 126.5, 128.1, 131.3, 156.4, 169.8. LC/MS: 235.04 (M + H + CH₃CN)⁺, *t_R* = 8.32 min, 96.0% pure (UV).

Synthesis of 4-ethyl-*N*-hydroxybenzamide (12). Compound **12** was prepared from 4-ethylbenzoyl chloride according to the general procedure (258 mg, 52%). Mp: 103.0-104.8 °C (lit. ⁴⁴ 106.5-107 °C). ¹H-NMR (500 MHz, CDCl₃): δ = 1.17 (t, *J* = 7.6 Hz, 3H), 2.61 (q, *J* = 7.6 Hz, 2H), 7.17 (d, *J* = 7.9 Hz, 2H), 7.66 (d, *J* = 7.9 Hz, 2H), 8.56 (bs, 1H), 10.66 (bs, 1H). ¹³C-NMR (125 MHz, CDCl₃): δ = 15.1, 28.6, 126.9, 127.8, 128.7, 148.1, 165.7. LC/MS: *m/z* = 165.94 (M + H)⁺, 207.03 (M + H + CH₃CN)⁺, 330.81 (2M + H)⁺ *t_R* = 6.68 min, 95.0% pure (UV).

Acknowledgement

The authors thank S. Amann for her help in performing the reporter gene assay. We are very grateful to C. Cugini and D. Hogan (Dartmouth Medical School, Hanover, NH, USA) for kindly supplying the plasmid pEAL08-2. The *P. aeruginosa* PA14 strain was kindly provided by S. Häussler (Helmholtz Centre for Infection Research, Braunschweig, Germany).

References

- (1) Blanc, D. S., Petignat, C., Janin, B., Bille, J., and Francioli, P. (1998) Frequency and molecular diversity of *Pseudomonas aeruginosa* upon admission and during hospitalization: a prospective epidemiologic study. *Clin. Microbiol. Infect.* *4*, 242-247.
- (2) Koch, C., and Høiby, N. (1993) Pathogenesis of cystic fibrosis. *Lancet* *341*, 1065-1069.

- (3) Swift, S., Downie, J. A., Whitehead, N. A., Barnard, A. M., Salmond, G. P., and Williams, P. (2001) Quorum sensing as a population-density-dependent determinant of bacterial physiology. *Adv. Microb. Physiol.* *45*, 199-270.
- (4) Gambello, M. J., and Iglewski, B. H. (1991) Cloning and characterization of the *Pseudomonas aeruginosa* lasR gene, a transcriptional activator of elastase expression. *J. Bacteriol.* *173*, 3000-3009.
- (5) Passador, L., Cook, J. M., Gambello, M. J., Rust, L., and Iglewski, B. H. (1993) Expression of *Pseudomonas aeruginosa* virulence genes requires cell-to-cell communication. *Science* *260*, 1127-1130.
- (6) Ochsner, U. A., Koch, A. K., Fiechter, A., and Reiser, J. (1994) Isolation and characterization of a regulatory gene affecting rhamnolipid biosurfactant synthesis in *Pseudomonas aeruginosa*. *J. Bacteriol.* *176*, 2044-2054.
- (7) Ochsner, U. A., and Reiser, J. (1995) Autoinducer-mediated regulation of rhamnolipid biosurfactant synthesis in *Pseudomonas aeruginosa*. *Proc. Natl. Acad. Sci. USA* *92*, 6424-6428.
- (8) Pesci, E. C., Milbank, J. B., Pearson, J. P., McKnight, S., Kende, A. S., Greenberg, E. P., and Iglewski, B. H. (1999) Quinolone signaling in the cell-to-cell communication system of *Pseudomonas aeruginosa*. *Proc. Natl. Acad. Sci. USA* *96*, 11229-11234.
- (9) Allesen-Holm, M., Barken, K. B., Yang, L., Klausen, M., Webb, J. S., Kjelleberg, S., Molin, S., Givskov, M., and Tolker-Nielsen, T. (2006) A characterization of DNA release in *Pseudomonas aeruginosa* cultures and biofilms. *Mol. Microbiol.* *59*, 1114-1128.
- (10) Dubern, J.-F., and Diggle, S. P. (2008) Quorum sensing by 2-alkyl-4-quinolones in *Pseudomonas aeruginosa* and other bacterial species. *Mol. Biosyst.* *4*, 882-888.
- (11) Déziel, E., Gopalan, S., Tampakaki, A. P., Lépine, F., Padfield, K. E., Saucier, M., Xiao, G., and Rahme, L. G. (2005) The contribution of MvfR to *Pseudomonas aeruginosa* pathogenesis and quorum sensing circuitry regulation: multiple quorum sensing-regulated genes are modulated without affecting lasRI, rhlRI or the production of N-acyl-L-homoserine lactones. *Mol. Microbiol.* *55*, 998-1014.
- (12) Clatworthy, A. E., Pierson, E., and Hung, D. T. (2007) Targeting virulence: a new paradigm for antimicrobial therapy. *Nat. Chem. Biol.* *3*, 541-548.
- (13) Xiao, G., Déziel, E., He, J., Lépine, F., Lesic, B., Castonguay, M.-H., Milot, S., Tampakaki, A. P., Stachel, S. E., and Rahme, L. G. (2006) MvfR, a key *Pseudomonas aeruginosa* pathogenicity LTTR-class regulatory protein, has dual ligands. *Mol. Microbiol.* *62*, 1689-1699.
- (14) Lu, C., Kirsch, B., Zimmer, C., de Jong, J. C., Henn, C., Maurer, C. K., Müsken, M., Häussler, S., Steinbach, A., and Hartmann, R. W. (2012) Discovery of Antagonists of PqsR, a Key Player in 2-Alkyl-4-quinolone-Dependent Quorum Sensing in *Pseudomonas aeruginosa*. *Chem. Biol.* *19*, 381-390.
- (15) Zaborina, O., Lepine, F., Xiao, G., Valuckaite, V., and Chen, Y. (2007) Dynorphin activates quorum sensing quinolone signaling in *Pseudomonas aeruginosa*. *PLoS Pathog.*
- (16) Mochalkin, I., Miller, J. R., Narasimhan, L., Thanabal, V., Erdman, P., Cox, P. B., Prasad, J. V. N. V., Lightle, S., Huband, M. D., and Stover, C. K. (2009) Discovery of antibacterial biotin carboxylase inhibitors by virtual screening and fragment-based approaches. *ACS Chem. Biol.* *4*, 473-483.
- (17) Waldrop, G. L. (2009) Smaller is better for antibiotic discovery. *ACS Chem. Biol.* *4*, 397-399.
- (18) Hopkins, A. L., Groom, C. R., and Alex, A. (2004) Ligand efficiency: a useful metric for lead selection. *Drug Discov. Today* *9*, 430-431.
- (19) Abad-Zapatero, C., and Metz, J. T. (2005) Ligand efficiency indices as guideposts for drug discovery., In *Drug Discov. Today*, pp 464-469.
- (20) Cugini, C., Calfee, M. W., Farrow, J. M., Morales, D. K., Pesci, E. C., and Hogan, D. A. (2007) Farnesol, a common sesquiterpene, inhibits PQS production in *Pseudomonas aeruginosa*. *Mol. Microbiol.* *65*, 896-906.
- (21) Fletcher, M. P., Diggle, S. P., Crusz, S. A., Chhabra, S. R., Cámara, M., and Williams, P. (2007) A dual biosensor for 2-alkyl-4-quinolone quorum-sensing signal molecules. *Environ. Microbiol.* *9*, 2683-2693.
- (22) Hodgkinson, J., Bowden, S. D., Galloway, W. R. J. D., Spring, D. R., and Welch, M. (2010) Structure-activity analysis of the *Pseudomonas* quinolone signal molecule. *J. Bacteriol.* *192*, 3833-3837.
- (23) Ladbury, J. E., Klebe, G., and Freire, E. (2010) Adding calorimetric data to decision making in lead discovery: a hot tip. *Nat. Rev. Drug Discov.* *9*, 23-27.

- (24) Ciulli, A., Williams, G., Smith, A. G., Blundell, T. L., and Abell, C. (2006) Probing Hot Spots at Protein–Ligand Binding Sites: A Fragment-Based Approach Using Biophysical Methods. *J. Med. Chem.* *49*, 4992-5000.
- (25) de Bentzmann, S., and Plésiat, P. (2011) The *Pseudomonas aeruginosa* opportunistic pathogen and human infections. *Environ. Microbiol.* *13*, 1655-1665.
- (26) Williams, P. (2011) Book of Abstracts. *1st International HIPS Symposium, Saarbrücken, Germany*, June 16.
- (27) Freire, E. (2008) Do enthalpy and entropy distinguish first in class from best in class? *Drug Discov. Today* *13*, 869-874.
- (28) Ramírez-Gualito, K., Alonso-Ríos, R., Quiroz-García, B., Rojas-Aguilar, A., Díaz, D., Jiménez-Barbero, J., and Cuevas, G. (2009) Enthalpic nature of the CH/ π interaction involved in the recognition of carbohydrates by aromatic compounds, confirmed by a novel interplay of NMR, calorimetry, and theoretical calculations. *J. Am. Chem. Soc.* *131*, 18129-18138.
- (29) Nishio, M. (2011) The CH/ π hydrogen bond in chemistry. Conformation, supramolecules, optical resolution and interactions involving carbohydrates. *Phys. Chem. Chem. Phys.* *13*, 13873-13900.
- (30) Ran, J., and Wong, M. W. (2006) Saturated hydrocarbon-benzene complexes: theoretical study of cooperative CH/ π interactions. *J. Phys. Chem. A* *110*, 9702-9709.
- (31) Ma, D., Cook, D. N., Hearst, J. E., and Nikaïdo, H. (1994) Efflux pumps and drug resistance in gram-negative bacteria. *Trends Microbiol.* *2*, 489-493.
- (32) Rich, R. L., and Myszka, D. G. (2010) Grading the commercial optical biosensor literature—Class of 2008: ‘The Mighty Binders’. *J. Mol. Recognit.* *23*, 1-64.
- (33) Giannetti, A. M., Koch, B. D., and Browner, M. F. (2008) Surface plasmon resonance based assay for the detection and characterization of promiscuous inhibitors. *J. Med. Chem.* *51*, 574-580.
- (34) Navratilova, I., and Hopkins, A. L. (2010) Fragment screening by surface plasmon resonance. *ACS Med. Chem. Lett.* *1*, 44-48.
- (35) Griffith, K. L., and Wolf Jr, R. E. (2002) Measuring β -Galactosidase Activity in Bacteria: Cell Growth, Permeabilization, and Enzyme Assays in 96-Well Arrays. *Biochem. Biophys. Res. Commun.* *290*, 397-402.
- (36) Essar, D. W., Eberly, L., Hadero, A., and Crawford, I. P. (1990) Identification and characterization of genes for a second anthranilate synthase in *Pseudomonas aeruginosa*: interchangeability of the two anthranilate synthases and evolutionary implications. *J. Bacteriol.* *172*, 884-900.
- (37) Zhang, Y., and Miller, R. M. (1992) Enhanced octadecane dispersion and biodegradation by a *Pseudomonas rhamnolipid* surfactant (biosurfactant). *Appl. Environ. Microbiol.* *58*, 3276-3282.
- (38) Drescher, K., Haupt, A., Unger, L., Turner, S. C., Braje, W., and Grandel (Abbott GmbH & CO KG), R. (2006) *WO 2006/040179*.
- (39) Wagner, P. J., and Wang, L. (2006) Electronic Effects of Ring Substituents on Triplet Benzylic Biradicals. *Org. Lett.* *8*, 645-647.
- (40) Chill, S. T., and Mebane, R. C. (2010) Facile One-Pot Conversion of Aldehydes into Amides. *Synth. Commun.* *40*, 2014-2017.
- (41) Willard, M. L., and Maresh, C. (1940) Optical Constants of Benzamide, its Homologs, and Some Aliphatic Amides. *J. Am. Chem. Soc.* *62*, 1253-1257.
- (42) Kliegel, W., and Nanninga, D. (1983) Borchelate von N-substituierten Hydroxamsäuren. *Chem. Ber.* *116*, 2616-2629.
- (43) Singerman, G. M. (1975) *US 3994997*.
- (44) Berndt, D. C., Utrapiromsuk, N., and Conran, D. E. (1984) Substituent effects and mechanism in the micellar hydrolysis of hydroxamic acids. *J. Org. Chem.* *49*, 106-109.

3.2 A Guidepost for Hit Selection and Optimization Targeting the *Pseudomonas aeruginosa* Transcriptional Regulator PqsR: Combination of Thermodynamic Analysis and Site-Directed Mutagenesis

Tobias Klein, Michael Zender, Christina Zimmer, Anke Steinbach, and Rolf W. Hartmann

Parts of this manuscript will be submitted to a peer-reviewed journal for publication.

Publication II

Abstract: The Gram-negative pathogen *Pseudomonas aeruginosa* coordinates group behaviours via a cell density dependent cell-to-cell communication system known as *quorum sensing* (QS). *P. aeruginosa* employs a characteristic *pqs* QS system that functions via the signal molecules PQS and its precursor HHQ, which interact with their receptor PqsR thereby controlling the production of virulence factors and biofilm formation. Therefore, we consider the *pqs* system a novel target to limit *P. aeruginosa* pathogenicity. Here, we describe the thermodynamic and functional characterization of SPR screening hits as guidepost for candidate selection and optimization using isothermal titration calorimetry and a heterologous reporter gene assay in *E. coli*, respectively. Given its enthalpy driven binding affinity ($K_D = 1.3 \mu\text{M}$), good ligand efficiency ($LE = 0.50 \text{ kcal/mol}$), and antagonistic activity ($IC_{50} = 9.6 \mu\text{M}$) the oxadiazole derivative **2** was the most promising hit. Site-directed mutagenesis together with thermodynamic analysis disclosed that **2** and the former reported small-molecule PqsR ligands (**B**, **C**) bind competitively to PqsR but do not cover exactly the same space in the ligand-binding domain of PqsR. Beyond this, first structural modifications of **2** together with calorimetric evaluation disclosed the role of the amino- and the trifluoromethyl group of compound **2** for ligand binding. Thus, our findings can be used to assist fragment optimization and provide a promising starting point for fragment growing or merging strategies that will be applied in future experiments.

Introduction

Bacteria are routinely challenged by drastic changes in their extracellular environments¹ and the ability of bacterial pathogens to sense their immediate environment plays a significant role on their capacity to survive and cause diseases.² Therefore, bacteria have developed systems for constantly observing the environment to adapt their lifestyles by modulating the transcription of subsets of genes. Beside two-component regulatory systems (TCSs) that allow bacteria to couple external stimuli to adaptive response³ they have developed *quorum sensing* (QS) systems⁴ to monitor the environment for other bacteria and to alter behavior on a population-wide scale.⁵ The Gram-negative opportunistic pathogen *Pseudomonas aeruginosa* exists in various environmental habitats and is known to infect a wide range of animal and plant hosts.⁶ In humans, it is one of the leading causes for nosocomial infections⁷ and is responsible for chronic lung infections in the majority of cystic fibrosis (CF) patients.⁸ *P. aeruginosa* coordinates group behaviours employing three QS systems. The *las*^{9,10} and the *rhl*^{11,12} communication systems, which use *N*-acyl homoserine lactones as autoinducers are widespread among Gram-negative bacteria. Yet, the third QS system, the *pqs* system¹³ is rather unique and restricted to particular *Pseudomonas* and *Burkholderia* strains.¹⁴ It functions via the 4-hydroxy-alkylquinolone (HAQ) signal molecules PQS (*Pseudomonas* quinolone signal; 2-heptyl-3-hydroxy-4(1*H*)-quinolone) and its precursor HHQ (2-heptyl-4(1*H*)-quinolone; Figure1).

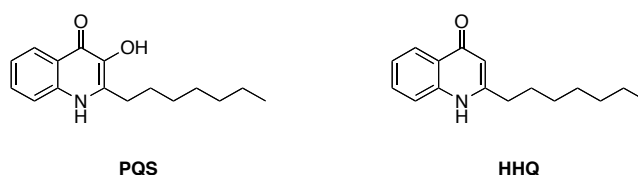


Figure 1. Structures of the *P. aeruginosa* QS signal molecules PQS and HHQ.

Both interact with their receptor PqsR^{15,16} to control the transcription of virulence genes such as pyocyanin,¹⁷ rhamnolipids, or hydrogen cyanide¹⁸ to name but a few and biofilm formation.¹⁹ PqsR, also known as multiple virulence factor regulator (MvfR), belongs to the family of LysR-type transcriptional regulators (LTTR). The latter are inactive prior to their binding to small molecules, termed as ligands or coinducers. LTTRs comprise approximately 330 amino acids and important structural regions remain highly conserved: at the C terminus is a ligand-binding domain (LBD) and at the N terminus is a helix–turn–helix (HTH) motif, which provides a means of binding to DNA.²⁰ PqsR consists of 332 amino acids and the C-terminal domain between amino acids 92–298 contains a predicted LBD.¹⁵

P. aeruginosa has joined the ranks of superbugs;²¹ bacteria that are resistant to practically all antimicrobial drugs available on the market. This is not only due to the high intrinsic resistance of *P. aeruginosa*²² but also to the application of bacteriostatic and bacteriocidal drugs, which impose selective pressure. Therefore, the development of antimicrobials that have novel modes

of action has come to the fore. In this context we consider PqsR a novel, promising target to disrupt PqsR-dependent gene expression thereby limiting *P. aeruginosa* pathogenicity without affecting bacterial viability.¹⁵ Recently, we reported on the discovery of two different classes of PqsR antagonists: derivatives of the natural effector HHQ (**A**)^{23,24} and hydroxamic acid (**B**)/benzamide (**C**)-derived fragments with low molecular weight (Figure 2).²⁵

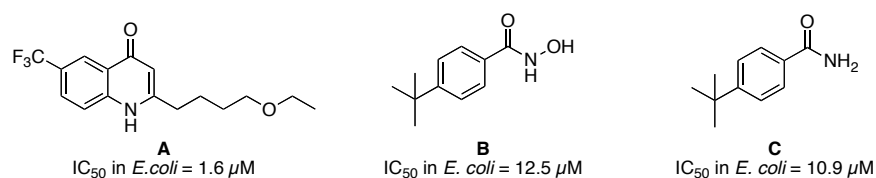


Figure 2. Representative structures of our two classes of PqsR antagonists: derivatives of the natural effector HHQ (**A**), and hydroxamic acid (**B**)/benzamide (**C**)-derived fragments.

Regarding antibacterial discovery, fragment-based design is a promising strategy since it allows to address the key issues namely insufficient physicochemical properties and the lack of chemical diversity.^{26,27} For the development of PqsR antagonists, this strategy has been proven successful by the hydrophilic hydroxamic-acid derived fragments. In contrast to the HHQ derivatives²⁴ they show a comparable potency in *E. coli* and *P. aeruginosa*,²⁵ which might be due to their ability to penetrate across the low permeable outer membrane of *P. aeruginosa*.²² In order to identify novel hits that increase chemical diversity and facilitate the application of fragment optimization strategies²⁸ the CSIRO fragment library has been screened against PqsR employing surface plasmon resonance (SPR) biosensor analysis and five promising hits were identified (Figure 3).²⁹

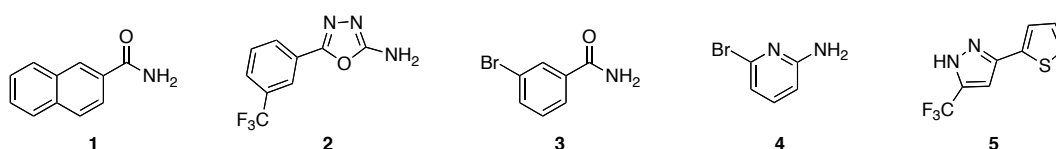


Figure 3. Chemical structures of the top five hits from the CSIRO fragment library screening.

Here, we describe the thermodynamic and functional characterization of the top five CSIRO-screening hits as guidepost for candidate selection and optimization. In combination with site-directed mutagenesis and first structural modifications the thermodynamic data enabled us to study protein-ligand interactions and to estimate the covered space in the LBD.

Results and Discussion

In the SPR screening K_D values were used as selection criteria, however, the evaluation of the compound affinity alone often does not provide a clear indication of which ligands to select for further progression. Therefore, the thermodynamic parameters, which provide a tool for understanding biomolecular interactions and an aid for decision making in drug discovery,^{30,31} were determined using isothermal titration calorimetry (ITC, Table 1).

Table 1. Thermodynamic parameters of ligands binding to PqsR.

Ligand	K_D (SPR) [μM]	K_D (ITC) [μM]	ΔG [kcal mol ⁻¹]	ΔH [kcal mol ⁻¹]	$-T\Delta S$ [kcal mol ⁻¹]	LE [kcal mol ⁻¹]
A		0.6 \pm 0	-8.5 \pm 0	-9.1 \pm 0.1	0.7 \pm 0.1	0.38
B		4.1 \pm 0.6	-7.4 \pm 0.1	-8.9 \pm 0.2	1.5 \pm 0.3	0.53
C		0.9 \pm 0	-8.3 \pm 0	-9.7 \pm 0.3	1.5 \pm 0.3	0.63
1	0.8 \pm 0.2	1.8 \pm 0.2	-7.9 \pm 0.1	-8.6 \pm 0.2	0.7 \pm 0.2	0.60
2	0.8 \pm 0.3	1.3 \pm 0.3	-8.0 \pm 0.1	-8.5 \pm 0.5	0.4 \pm 0.6	0.50
3	6.8 \pm 3.5	7.6 \pm 0.7	-7.0 \pm 0.1	-6.9 \pm 0.1	-0.1 \pm 0.1	0.35
4	6.8 \pm 3.8	10.0 \pm 1.3	-6.8 \pm 0.1	-9.3 \pm 0.4	2.5 \pm 0.4	0.85
5	10.7 \pm 6.5	8.5 \pm 0.7	-6.9 \pm 0	-8.6 \pm 0	1.6 \pm 0.1	0.49

ITC titrations were performed at 298 K. Data represent mean \pm SD from at least two independent experiments.

The measured data confirmed the top five hits as PqsR binder and showed that the different techniques SPR and ITC result in very comparable dissociation constants (K_D). Accordingly, naphthalene-2-carboxamide (**1**, $K_D = 1.8 \mu\text{M}$) and the oxadiazole derivative **2** ($K_D = 1.3 \mu\text{M}$) displayed the best affinities of the verified hits and bind only slightly weaker than the HHQ derivative **A** ($K_D = 0.6 \mu\text{M}$) and the benzamide **C** ($K_D = 0.9 \mu\text{M}$). The ratio of free binding affinity to molecular size is termed as ligand efficiency (LE), and allows to compare hits of widely differing structures and activities.³² LE values > 0.33 kcal/mol are desirable through the process of optimization.³³ Remarkably, compounds **1-5** showed LEs in the range of 0.35-0.85 kcal/mol and hence are above this threshold (Table 1). Analysis of the thermodynamic signatures revealed that the hits **1-5** are enthalpy driven binders (Table 1) indicating a good non-covalent bond complementary between the protein and the compounds.³¹ Given that it is harder to improve the ΔH contribution than to improve the ΔS contribution, enthalpy driven binders are rather taken on the next optimization level than entropy driven binders. Further, increasing the entropic contribution is accompanied by increasing hydrophobicity and therefore the improvement is limited by the compounds solubility.³¹ Taken together, these data emphasize the high potential of the previously identified hits.

In order to evaluate the agonistic and antagonistic activities of the PqsR ligands **1-5** we examined the PqsR-mediated transcriptional effect in a reporter gene assay by measuring the β -galactosidase activity in *E. coli* harbouring the pEAL08-2 plasmid containing the *tacP-pqsR* and *pqsAP-lacZ* fusion genes (Table 2).³⁴ *E. coli* was used as it provides a system to characterize the functionality of PqsR ligands independent of the entire *pqs* system present in *P. aeruginosa*.³⁵

Table 2. Functional activities of PqsR ligands.

Ligand	Agonistic activity [%]	Antagonistic activity [%]
A	n.a. ^a	68±2 ^{a*}
B	n.a.	78±12 [*]
C	43±3 [*]	48±1 [*]
1	53±14 [*]	46±9 [*]
2	n.a.	107±9 [*]
3	n.a.	n.i.
4	n.a.	22±12
5	n.a.	n.i.

Agonistic activity was determined by measuring the PqsR stimulation induced by 100 μM of the test compound compared to 50 nM PQS (= 100%); n.a. = no agonism (agonistic activity \leq 20%). Antagonistic activity was determined by measuring the inhibition of the PqsR stimulation induced by 50 nM PQS in the presence of 100 μM test compound (full inhibition = 100%); n.i. = no inhibition (antagonistic activity \leq 20%). Mean value of at least two independent experiments with $n = 4$, standard deviation less than 25%. Significance: For the agonist test, induction compared to the basal value; for the antagonist test, decrease of the PQS-induced induction. ^a)Agonistic and antagonistic activity were determined in the presence of 5 μM test compound. * $p < 0.003$; ^{*} $p < 0.05$.

None of the assessed screening hits displayed agonistic activity except for compound **1**. Interestingly, in addition to its moderate agonistic activity it significantly reduced the stimulation of PqsR. Such a mixed functional profile was recently observed for ligand **C**²⁵ indicating that this is a common feature of aromatic substituted carboxamides with high affinity toward PqsR. While **3-5** showed no or only a weak antagonistic activity the oxadiazole **2** was identified as a highly potent PqsR antagonist: 100 μM of **2** led to full inhibition of the PqsR stimulation induced by 50 nM PQS. Compared to the HHQ analogue **A** ($\text{IC}_{50} = 1.3 \mu\text{M}$) compound **2** ($\text{IC}_{50} = 9.6 \mu\text{M}$) is a less potent PqsR antagonist but it reveals the same potency as the hydroxamic acid-derived **B** ($\text{IC}_{50} = 12.5 \mu\text{M}$).

The recently measured thermodynamic data indicated that the *tert*-butyl substituted benzamide **C** interacts with Glu194 and Phe221 via H-bonds. Identification of further fragments, which cover additional or different space in the LBD will facilitate the application of optimization strategies such as fragment linking or growing. In this context, combining ITC with site-directed mutagenesis provides a valuable tool to analyze the identified fragments. Of the identified hits, compounds **1** and **2** looked the most promising with respect to K_D , LE, and functionality. Therefore, their binding to the Q194A and F221A PqsR mutants was evaluated by ITC (Table 3).

Table 3. Effect of point mutations on the thermodynamic parameters of PqsR ligands.

Ligand	Q194A			F221A		
	$\Delta\Delta G$ [kcal mol ⁻¹]	$\Delta\Delta H$ [kcal mol ⁻¹]	$-T\Delta\Delta S$ [kcal mol ⁻¹]	$\Delta\Delta G$ [kcal mol ⁻¹]	$\Delta\Delta H$ [kcal mol ⁻¹]	$-T\Delta\Delta S$ [kcal mol ⁻¹]
C	-1.3±0.3*	-4.4±0.3*	3.1±0.3*	-1.0±0.1*	-7.6±0.3*	6.6±0.4*
1	-1.1±0.1*	-3.2±0.2*	2.1±0.2*	-0.4±0.1*	-7.1±0.2*	6.7±0.2*
2	-0.6±0.1*	-0.3±0.6	-0.3±0.7	-0.6±0.1*	-7.1±0.5*	6.5±0.6*

$\Delta\Delta G$, $\Delta\Delta H$, and $-T\Delta\Delta S$ are $\Delta G_{WT} - \Delta G_{mutant}$, $\Delta H_{WT} - \Delta H_{mutant}$, and $-T(\Delta S_{WT} - \Delta S_{mutant})$, respectively. Negative values indicate a loss; positive values, a gain compared to wild-type. Errors indicate SD calculated via Gaussian error propagation. Significance: effect of the point mutation on the thermodynamic parameters of ligand binding compared to the wild-type. * $p < 0.003$; * $p < 0.05$.

Due to the structural similarity between naphthalene-2-carboxamide (compound **1**) and the PqsR ligand **C** it is not wondrous that Gln194 is also involved in the binding of **1**. Comparing the thermodynamic signatures of **1** binding to Q194A mutant and wild-type PqsR a loss in ΔH of 3.2 kcal/mol was observed. The latter suggests the presence of a weak H-bond between **1** and Gln194. Further, the binding of compound **1** to the Q194A mutant showed positive $-T\Delta\Delta S$ values relative to those of the wild-type. This is in accordance to what was found for compound **C** and might be due to the increased conformational flexibility both of the ligand and the protein in the absence of an H-bond. The F221A point mutation affected the binding of **1** and with a deficit of 7.1 kcal/mol the enthalpic contribution was significantly reduced compared to the wild-type. Probably, F221 might be involved in a π - π interaction with the naphthalene core of **1**. However, theoretical investigations revealed an interaction energy of -4.2 kcal/mol for the benzene-naphthalene complex in the parallel-displaced type.³⁶ The measured data suggest that **1** adopts the same binding mode as the hydroxamic-acid **B** and the benzamide **C**, respectively. Thus, compound **1** does not offer structural suggestions for the optimization of the former identified ligands.

Interestingly, for the oxadiazole **2** there was no significant difference in the enthalpic contribution observed when binding to Q194A mutant and wild-type PqsR. This revealed that Gln194 is not involved in the binding of **2** but competition experiments confirmed that **2** binds to the same binding site as **C** (Figure 4).

This is in agreement with the fact that the binding of **2** was affected by the F221A mutation. Compared to the wild-type the enthalpic contribution was reduced by 7.1 kcal/mol. Possibly, the phenyl moiety of **2** makes a π - π interaction with F221 that is favored by the presence of the electron withdrawing CF₃-substituent.³⁷ Given that **2** and **C** bind to the same binding site but do not interact with the same amino acids there is room for optimization by fragment growing. Accordingly, the oxadiazole derivative **2** is the most promising candidate of the identified hits not least due to its different molecular scaffold.

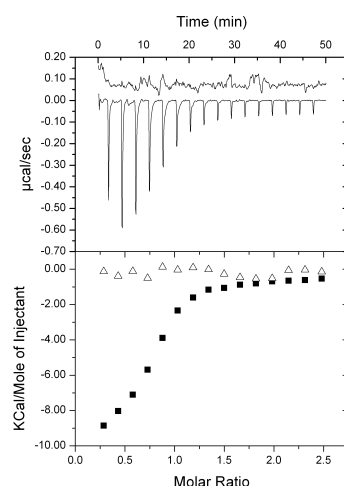


Figure 4. Competitive binding of ligands to PqsR as measured by ITC. Raw ITC data (top) and integrated normalized data (bottom) for titrations of 43 μM $\text{H}_6\text{SUMO-PqsR}^{\text{C87}}$ with 500 μM **2** (■) in the absence of **C** and in the presence of 500 μM compound **C** (Δ).

First structural modifications of **2** in combination with thermodynamic analysis were done to evaluate the relative contribution of the different functional groups. The CF_3 moiety was replaced by a methyl group and the thermodynamic signature of the resulting compound **6** was compared to that of **2** (Figure 5).

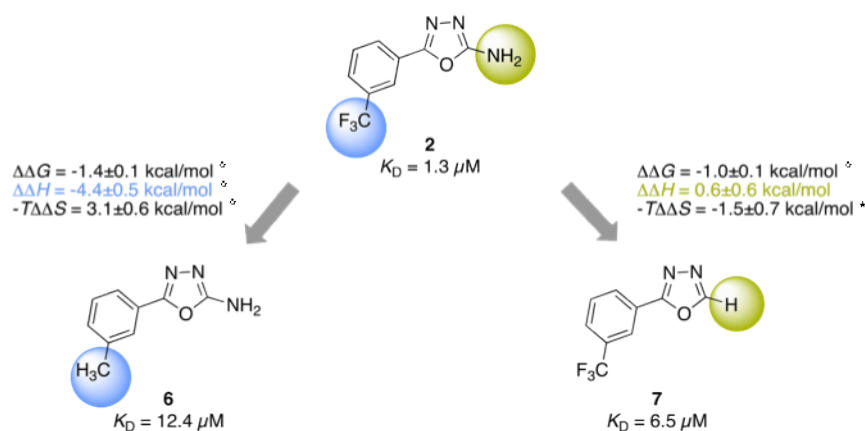


Figure 5. Relative thermodynamic contributions of functional groups to PqsR binding. $\Delta\Delta G$, $\Delta\Delta H$, and $-T\Delta\Delta S$ are $\Delta G_2 - \Delta G_{6/7}$, $\Delta H_2 - \Delta H_{6/7}$, and $-T(\Delta S_2 - \Delta S_{6/7})$, respectively. Negative values indicate a loss; positive values, a gain compared to compound **2**. Errors indicate SD calculated via Gaussian error propagation. Significance: thermodynamic contribution of the functional group on the binding of **2** to PqsR. $^{\circ} p < 0.003$; $^{\ast} p < 0.05$.

Indeed, ligand **6** showed reduced affinity toward PqsR (**6**, $K_D = 12.4 \mu\text{M}$ vs. **2**, $K_D = 1.3 \mu\text{M}$), which was due to a significant loss in ΔH of 4.4 kcal/mol. Considering the loss in enthalpy, that is caused by the F221A mutation (7.1 kcal/mol) and the loss in enthalpy that is due to the exchange of the CF_3 vs. CH_3 (4.4 kcal/mol) the enthalpic contribution of a possible π - π

interaction between **6** and Phe221 is 2.7 kcal/mol. Remarkably, this is consistent with the binding energy of the gas-phase benzene dimer ranging from 2.0 to 3.0 kcal/mol.³⁸

The thermodynamic profile of compound **2** binding to the Q194A mutant PqsR revealed that the amino group of **2** does not make an H-bond with the only polar residue in the LBD, Gln194.³⁹ Yet, to investigate whether the amino group is involved in the formation of a H-bond with polar backbone atoms of PqsR it was replaced by hydrogen. The binding affinity of the resulting ligand **7** ($K_D = 6.5 \mu\text{M}$) was lower in comparison to **2** ($K_D = 1.3 \mu\text{M}$) but even more interesting there was no significant difference in the enthalpic contributions (Figure 5). This finding allowed us to exclude that the amino group makes any H-bonds. Further, the PqsR-**7** complex is entropically more unfavorable than the PqsR-**2** complex and two possible explanations for this finding are (1) compound **7** with its smaller molecular size might release less water molecules from the LBD than **2**, (2) the binding of **2** might stabilize PqsR in a more disordered conformation compared to the binding of **7**.⁴⁰

In the benzamide class of PqsR ligands, the *tert*-butyl substituted **C** ($K_D = 0.9 \mu\text{M}$) showed a significantly increased affinity compared to the CF_3 substituted **8** ($K_D = 7.2 \mu\text{M}$) that was due to an enthalpic gain (Figure 6). In contrast, the introduction of an electron-donating group such as an alkyl moiety is predicted to induce an increasingly unfavorable effect on a π - π interaction due to repulsion of the increasingly negative electron densities forming on the aromatic centre.³⁷ These extremes can be explained by the assumption that the *tert*-butyl substituent of **C** directly interacts with the receptor and does not impact a probable π - π interaction formed by the phenyl ring of **C**. This hypothesis is further substantiated by the fact that variation of the alkyl chain in **C** affects the enthalpy ΔH .²⁵

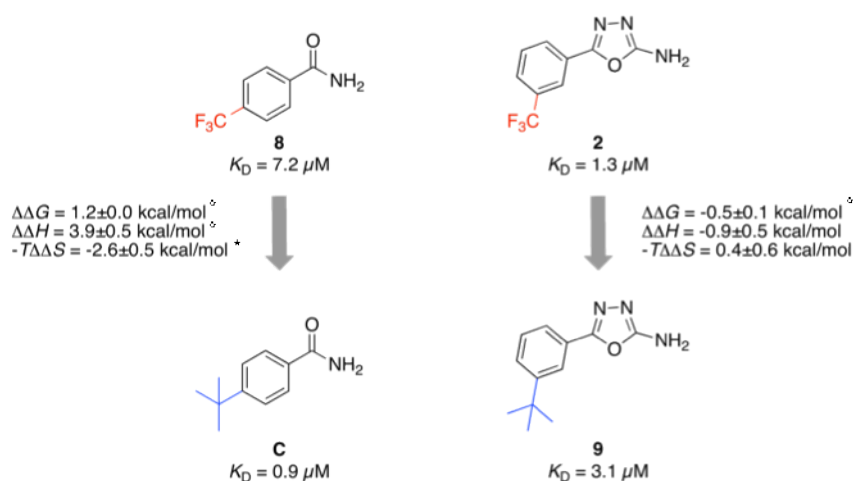


Figure 6. Effect of replacing a CF_3 group by a *t*Bu residue on the binding of benzamide and oxadiazole PqsR ligands. $\Delta\Delta G$, $\Delta\Delta H$, and $-T\Delta\Delta S$ are $\Delta G_{8/2} - \Delta G_{C/9}$, $\Delta H_{8/2} - \Delta H_{C/9}$, and $-T(\Delta S_{8/2} - \Delta S_{C/9})$, respectively. Negative values indicate a loss; positive values, a gain. Errors indicate SD calculated via Gaussian error propagation. Significance: effect of exchanging CF_3 by *t*Bu on ligands binding to PqsR. ^{*} $p < 0.003$; [°] $p < 0.05$.

The above data provide a structural hint for the optimization of **2** and therefore it was investigated whether the introduction of *tert*-butyl (compound **9**) instead of CF₃ also increases the affinity of the oxadiazole derivative **2**. In contrast to what was observed in the benzamide class the *tert*-butyl substituted oxadiazole derivative (**9**, $K_D = 3.1 \mu\text{M}$) showed a slightly reduced affinity compared to the CF₃ substituted derivative (**2**, $K_D = 1.3 \mu\text{M}$) and no significant difference in ΔH was observed (Figure 6). Obviously, due to the absence of the H-bond with Gln194 the oxadiazole derivatives are able to adopt different binding conformations that allow compound **2** to interact via the CF₃ substituted phenyl ring and compound **9** via the *tert*-butyl group, respectively.

Conclusion

In summary, thermodynamic and functional data were used for hit characterization and as a guidepost for candidate selection. The evaluated hits **1-5** showed enthalpy driven binding, promising LEs and in addition to this the oxadiazole derivative **2** revealed an antagonistic activity comparable to that observed for the hydroxamic acid-derived PqsR antagonist **B**. Site-directed mutagenesis together with thermodynamic analysis disclosed that **2** and the former reported small-molecule PqsR ligands (**B**, **C**) bind competitively to PqsR but do not cover exactly the same space in the LBD thereby offering suggestions for optimization using fragment growing strategies. First structural modifications of **2** together with calorimetric evaluation were done to investigate the relative importance of the functional groups in order to guide fragment optimization. Future experiments will aim at merging the best features of the different fragment classes to develop druglike molecules that open the door for therapeutic agents with novel modes of action for the treatment of *P. aeruginosa* infections.

Methods

Protein Expression and Purification. Wild-type, Q194A mutant, and F221A mutant H₆SUMO-PqsR^{C87} were expressed in *E. coli* and purified using a single affinity chromatography step. Briefly, *E. coli* BL21 (DE3) cells containing the pSUMO3_ck4_pqsR^{C87}, the pSUMO3_ck4_Q194ApqsR^{C87} or the pSUMO3_ck4_F221ApqsR^{C87} plasmid²⁵ were grown in LB medium containing 50 $\mu\text{g ml}^{-1}$ kanamycin at 37 °C to an OD₆₀₀ of approximately 0.8 and induced with 0.2 mM IPTG for 16 h at 16 °C. The cells were harvested by centrifugation (5000 rpm, 10 min, 4 °C) and the cell pellet was resuspended in 100 ml binding buffer (50 mM Tris-HCl, pH 7.8, 150 mM NaCl, 20 mM imidazole, 10% glycerol (v/v)) and lysed by sonication for a total process time of 2.5 min. Cell debris were removed by centrifugation (13000 rpm, 30 min) and the supernatant was filtered through a syringe filter (0.2 μm). The clarified lysate was immediately applied to a Ni-NTA column (GE Healthcare), washed with 50 mM Tris-HCl, pH 7.8, 150 mM NaCl, 20 mM imidazole, 10% glycerol (v/v), and eluted with 500 mM imidazole.

The protein containing fractions were buffer-exchanged into 20 mM Tris, pH 7.4, 150 mM NaCl, 10% glycerol (v/v) for the wild-type and into 20 mM Tris, pH 7.8, 300 mM NaCl, 10% glycerol (v/v) for the Q194A and the F221A mutants, using a PD10 column (GE Healthcare) and judged pure by SDS-PAGE analysis. The H₆SUMO-tagged proteins were stored at -80 °C and used for biophysical studies.

Isothermal titration calorimetry. ITC experiments were carried out using an ITC₂₀₀ instrument (Microcal Inc., GE Healthcare). Concentrations of ligand stock solutions in DMSO were determined by the weight of the compound. Final ligand concentrations were achieved by diluting 1:20 (v/v) in the experimental buffer resulting in a final DMSO concentration of 5% (v/v). Protein concentration was determined by measuring the absorbance at 280 nm using a theoretical molarity extinction coefficient of 22,900 M⁻¹cm⁻¹. DMSO concentration in the protein solution was adjusted to 5% (v/v). ITC measurements were routinely performed at 25 °C in 20 mM Tris, pH 7.4, 150 mM NaCl, 10% glycerol (v/v), 5% DMSO (v/v) for the wild-type PqsR^{C87} and in 20 mM Tris, pH 7.4, 300 mM NaCl, 10% glycerol (v/v), 5% DMSO (v/v) for the Q194A and the F221A mutants, respectively. The titrations were performed on 43-190 μM H₆SUMO-PqsR^{C87}, H₆SUMO-Q194APqsR^{C87} or H₆SUMO-F221APqsR^{C87} in the 200 μl sample cell using 2-2.6 μl injections of 0.7-2.0 mM ligand solution every 180 s. The competition experiment was performed on 43 μM H₆SUMO-PqsR^{C87}, which was incubated with 0.5 mM compound C for 30 min at 25 °C. Raw data were collected and the area under each peak was integrated. To correct for heats of dilution and mixing the final base line consisting of small peaks of the same size at the end of the experiment was subtracted. The experimental data were fitted to a theoretical titration curve (one site binding model) using MicroCal Origin 7 software, with ΔH (enthalpy change in kcal/mol), K_A (association constant in M⁻¹), and N (number of binding sites) as adjustable parameters. Thermodynamic parameters were calculated from Eq. (3),

$$\Delta G = \Delta H - T\Delta S = RT\ln K_A = -RT\ln K_D \quad (3)$$

where ΔG , ΔH , and ΔS are the changes in free energy, enthalpy, and entropy of binding, respectively, T is the absolute temperature, and $R = 1.98$ cal/mol/K. The LE for each compound was calculated from Eq. (4),

$$LE = -\Delta G / (\text{heavy atom count}) \quad (4)$$

where ΔG is the change in free energy and heavy atom count is the number of non-hydrogen atoms of the compound. For each ligand at least two independent experiments were performed.

Representative ITC titrations of **1** and **2** against H₆SUMO-PqsR^{C87}, H₆SUMO-Q194APqsR^{C87}, and H₆SUMO-F221APqsR^{C87} are shown in Figure 7.

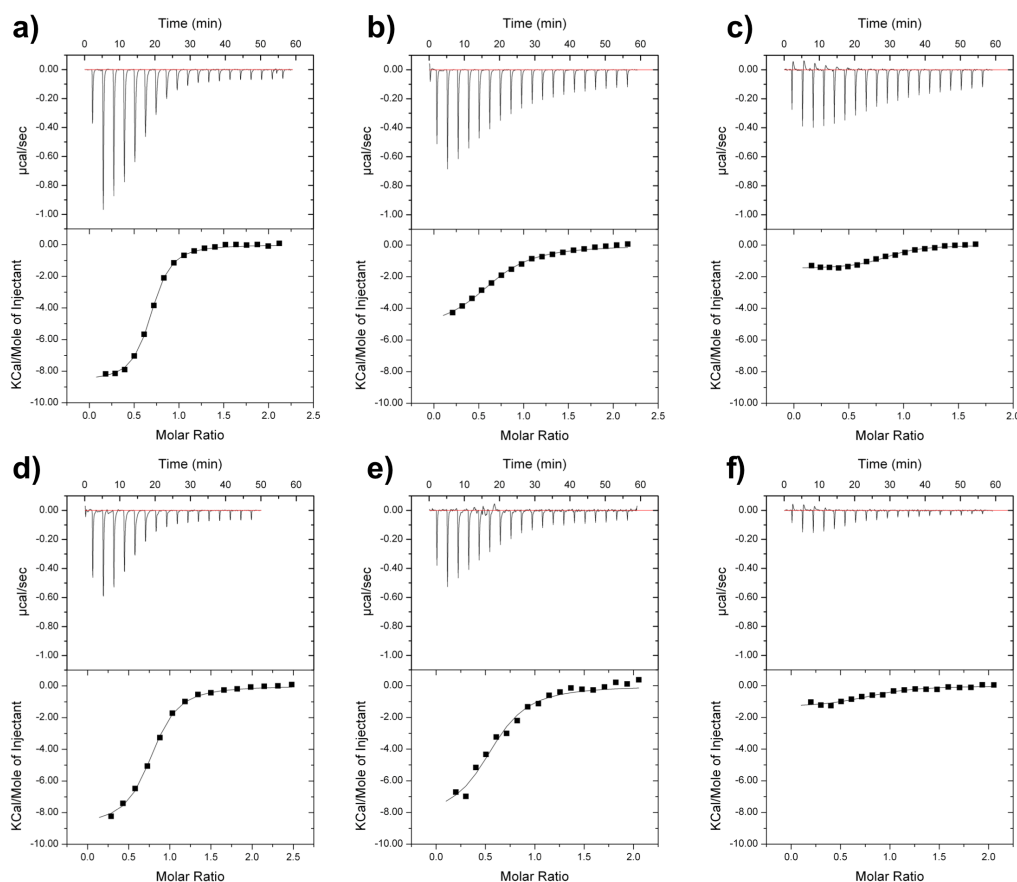


Figure 7. Representative ITC titrations. **a)** ITC titration of **1** (900 μ M) against H₆SUMO-PqsR^{C87} (86 μ M). **b)** ITC titration of **1** (1 mM) against H₆SUMO-Q194APqsR^{C87} (95 μ M). **c)** ITC titration of **1** (1 mM) against H₆SUMO-F221APqsR^{C87} (124 μ M). **d)** ITC titration of **2** (500 μ M) against H₆SUMO-PqsR^{C87} (43 μ M). **e)** ITC titration of **2** (500 μ M) against H₆SUMO-Q194APqsR^{C87} (50 μ M). **f)** ITC titration of **2** (500 μ M) against H₆SUMO-F221APqsR^{C87} (50 μ M). The recorded change in heat is shown in units of μ cal/sec as a function of time for successive injections of the ligand (upper row). Integrated heats (black squares) plotted against the molar ratio of the binding reaction. The continuous line represents the results of the non-linear least squares fitting of the data to a binding model (lower row).

Reporter Gene Assay in *E. coli*. The ability of the compounds to either stimulate or antagonize the PqsR-dependent transcription was performed as previously described using a β -galactosidase reporter gene assay³⁴ in *E. coli* expressing PqsR with some modifications to enable a higher throughput.⁴¹ PQS and PqsR ligands were diluted in ethyl acetate, added to the wells of a 96 deep well plate and the solvent was evaporated. Overnight cultures of *E. coli* DH5 α cells containing the plasmid pEAL08-2 which encodes PqsR under the control of the *tac* promoter and the β -galactosidase reporter gene *lacZ* controlled by the *pqsA* promoter, were diluted 1:100 in Luria-Bertani medium with ampicillin (50 μ g/ml). The culture was incubated at

37 °C with shaking until it reached an OD₆₀₀ of 0.2. For the determination of agonistic activities, 1 ml aliquots were supplemented with either PQS (50 nM) or the test compound (100 μM). Ethyl acetate was used as control. Antagonistic effects of the compounds (100 μM) were evaluated in the presence of 50 nM PQS. The β-galactosidase activity was determined after a 2.5 h incubation period at 37 °C with shaking (150 rpm). OD₆₀₀, OD₄₂₀ and OD₅₅₀ were measured and the activity is expressed as ratio of the ethyl acetate control relative to the cultures that received either PQS, a test compound or both. For the determination of IC₅₀ value, compound **2** was tested at least at six different concentrations. The given data represent mean of two experiments with n = 4. The log (inhibitor) vs. response model (Prism 5.0) was applied for nonlinear regression and determination of IC₅₀-values; the Hill slope was constrained equal to 1.0.

Chemical and Analytical Methods. ¹H and ¹³C NMR spectra were recorded on a Bruker DRX-500 instrument. Chemical shifts are given in parts per million (ppm), and tetramethylsilane (TMS) was used as internal standard for spectra obtained in CDCl₃, MeOH-*d*₄ and DMSO-*d*₆. Coupling constants (*J*) are given in hertz. Mass spectrometry (LC/MS) was performed on a MSQ[®] electro spray mass spectrometer (Thermo Fisher). The system was operated by the standard software Xcalibur[®]. A RP C18 NUCLEODUR[®] 100-5 (125 × 3 mm) column (Macherey-Nagel GmbH) was used as stationary phase with water/acetonitrile mixtures as eluents. All solvents were HPLC grade. Reagents were used as obtained from commercial suppliers without further purification. The reaction progress was determined by thin-layer chromatography (TLC) analyzes on silica gel 60, F₂₅₄ (Merck). Visualization was accomplished with UV light.

General procedure for the synthesis of benzoylthiosemicarbazids. Hydrazinecarbothioamide (3 eq.) and THF were filled into a three necked flask. Benzoyl chloride (1 eq, 0,2 molar) was added through a dropping funnel while cooling on an ice-bath. The mixture was aged at RT under a nitrogen atmosphere for 24 h. The mixture was quenched by addition of water and alkalinized using NaHCO₃ saturated. Afterwards THF was evaporated under reduced pressure till a white solid precipitated. The suspension was filtered and the resulting cake was washed with water. The white solid was dried in an exsiccator to afford the expected benzoylthiosemicarbazids.

General procedure for the synthesis of Oxadiazole-2-amines. Benzoylthiosemicarbazid (1 eq, 0,25 molar) was filled into a three necked flask and IPA was added to give a white suspension. A solution of potassium iodid (0,3 eq.) in water (2 ml) and were added. The reaction mixture was chilled on an ice-bath and NaOH (1,5 eq) 5 M solution was added to give a yellow solution. Dibromodimethylhydantoin (0,75 eq.) dissolved in ACN was added through a dropping funnel over 1 h while maintaining the temperature under 10°C. Afterwards the reaction was aged for 1 h below 10 °C. The reaction mixture was quenched using NaHSO₃ sat.

(1 ml) and water was added. The pH was adjusted over 12 using NaHCO₃ saturated solution. Volatiles were removed under reduced pressure to give a yellow precipitate. The suspension was filtered and the cake rinsed with water and IPA to give the respective 5-pheny-[1,3,4]-oxadiazole-2-amines .

5-(3-(trifluoromethyl)phenyl)-1,3,4-oxadiazol-2-amine (2) was prepared according to the general procedure and additionally purified by silica gel chromatography using DCM:MeOH 98:2 to 97:3. ¹H-NMR (500 MHz, DMSO-*d*₆): δ 8.08 (d, *J* = 7.88 Hz, 1H), 8.01 (s, 1H), 7.85 - 7.90 (m, 1H), 7.75 - 7.81 (m, 1H), 7.39 (s, 2H). ¹³C NMR (126 MHz, DMSO-*d*₆) d ppm 121.16 (m, 1 C), 123.70 (d, ¹*J*(C,F)=270.4 Hz, 1 C), 125.35, 126.73 (q, ³*J*(C,F)=3.7 Hz, 1 C), 128.80, 129.79 (q, ²*J*(C,F)=31.2 Hz, 1 C), 130.67, 156.17, 164.19. Rt: 8.30; M+ACN+H: 270.83.

5-(*m*-tolyl)-1,3,4-oxadiazol-2-amine (6) was prepared according to the general procedure.

¹H NMR (500 MHz, DMSO-*d*₆) δ ppm 2.37 (s, 3 H) 7.21 (s, 2 H) 7.27 - 7.34 (m, 1 H) 7.41 (t, *J*=7.57 Hz, 1 H) 7.56 - 7.60 (m, 1 H) 7.60 - 7.62 (m, 1 H). ¹³C NMR (126 MHz, DMSO-*d*₆) δ ppm 20.87, 122.19, 124.31, 125.39, 129.11, 130.99, 138.54, 157.37, 163.78. Rt: 7,81 M+ACN+H: 217,00

2-(3-(trifluoromethyl)phenyl)-1,3,4-oxadiazole (7) A sealed reaction vial was charged with 3-(trifluoromethyl)benzohydrazide (400 mg, 1,959 mmol) and triethylorthoformiate (4 ml, 24,02 mmol). The mixture was heated under an argon atmosphere for 2 h at 160°C. The reaction mixture was poured into an saturated Na₂CO₃ solution on an ice bath while stirring vigourously. The aqueous phase was extracted with EtOAc (2 times) and the combined organic phases were washed with brine (2 times). The EtOAc phase was dried with MgSO₄ and concentrated to dryness to yield a yellow oil. The resulting oil was adsorbed to silica gel and purified by flash chromatography Hex:EtOAc 95:5 to 80:20 to give a colourless oil. The oil crystallized in the fridge as the expected pure product. ¹H NMR (300 MHz, DMSO-*d*₆) δ ppm 7.86 (t, *J*=8.75 Hz, 1 H) 8.02 (d, *J*=7.82 Hz, 1 H) 8.25 (s, 1 H) 8.32 (d, *J*=7.64 Hz, 1 H) 9.43 (s, 1 H). ¹³C NMR (126 MHz, DMSO-*d*₆) δ ppm 123.6 (q, ¹*J*(C,F)=272.2 Hz, 1 C), 123.0 (q, ³*J*(C,F)=3.7 Hz, 1 C), 124.3, 128.5 (q, ³*J*(C,F)=3.7 Hz, 1 C) 130.1 (q, ²*J*(C,F)=32.1 Hz, 1 C), 130.7, 130.9, 155.0, 162.6. Rt: 10.03 [M+ACN+H] 255.91.

5-(3-(tert-butyl)phenyl)-1,3,4-oxadiazol-2-amine (9) was prepared starting from (3-(tert-butyl)benzoyl)thiosemiamidecarbazine and following the general procedure for the preparation of oxadiazole-2-amines. ¹H NMR (500 MHz, DMSO-*d*₆) d ppm 1.31 (s, 9 H), 7.23 (s, 2 H), 7.45 (t, *J*=7.7 Hz, 1 H), 7.55 (d, *J*=7.9 Hz, 1 H), 7.61 (d, *J*=7.6 Hz, 1 H), 7.79 (s, 1 H). ¹³C NMR (126 MHz, DMSO-*d*₆) d ppm 30.90 (3 C), 34.48, 121.49, 122.36, 124.15, 127.48, 129.04, 151.60, 157.59, 163.80. LC-MS: Rt: 9,65 [M+H] 218,12 [M+ACN+H] 259,09

References

- (1) Robinson, V. L.; Buckler, D. R.; Stock, A. M. *Nat. Struct. Biol.* **2000**, *7*, 626–633.
- (2) Karavolos, M. H.; Williams, P.; Khan, C. M. A. *Virulence* **2011**, *2*, 371–374.
- (3) Stock, A. M.; Robinson, V. L.; Goudreau, P. N. *Annu. Rev. Biochem.* **2000**, *69*, 183–215.
- (4) Fuqua, W. C.; Winans, S. C.; Greenberg, E. P. *J. Bacteriol.* **1994**, *176*, 269–275.
- (5) Waters, C. M.; Bassler, B. L. *Annu. Rev. Cell. Dev. Biol.* **2005**, *21*, 319–346.
- (6) Rahme, L. G.; Stevens, E. J.; Wolfort, S. F.; Shao, J.; Tompkins, R. G.; Ausubel, F. M. *Science* **1995**, *268*, 1899–1902.
- (7) Blanc, D. S.; Petignat, C.; Janin, B.; Bille, J.; Francioli, P. *Clin. Microbiol. Infect.* **1998**, *4*, 242–247.
- (8) Koch, C.; Høiby, N. *Lancet* **1993**, *341*, 1065–1069.
- (9) Gambello, M. J.; Iglewski, B. H. *J. Bacteriol.* **1991**, *173*, 3000–3009.
- (10) Passador, L.; Cook, J. M.; Gambello, M. J.; Rust, L.; Iglewski, B. H. *Science* **1993**, *260*, 1127–1130.
- (11) Ochsner, U. A.; Reiser, J. *Proc. Natl. Acad. Sci. USA* **1995**, *92*, 6424–6428.
- (12) Ochsner, U. A.; Koch, A. K.; Fiechter, A.; Reiser, J. *J. Bacteriol.* **1994**, *176*, 2044–2054.
- (13) Pesci, E. C.; Milbank, J. B.; Pearson, J. P.; McKnight, S.; Kende, A. S.; Greenberg, E. P.; Iglewski, B. H. *Proc. Natl. Acad. Sci. USA* **1999**, *96*, 11229–11234.
- (14) Diggle, S. P.; Lumjiaktase, P.; Dipilato, F.; Winzer, K.; Kunakorn, M.; Barrett, D. A.; Chhabra, S. R.; Cámara, M.; Williams, P. *Chem. Biol.* **2006**, *13*, 701–710.
- (15) Xiao, G.; Déziel, E.; He, J.; Lépine, F.; Lesic, B.; Castonguay, M.-H.; Milot, S.; Tampakaki, A. P.; Stachel, S. E.; Rahme, L. G. *Mol. Microbiol.* **2006**, *62*, 1689–1699.
- (16) Cao, H.; Krishnan, G.; Goumnerov, B.; Tsongalis, J.; Tompkins, R.; Rahme, L. G. *Proc. Natl. Acad. Sci. USA* **2001**, *98*, 14613–14618.
- (17) Dubern, J.-F.; Diggle, S. P. *Mol. Biosyst.* **2008**, *4*, 882–888.
- (18) Déziel, E.; Gopalan, S.; Tampakaki, A. P.; Lépine, F.; Padfield, K. E.; Saucier, M.; Xiao, G.; Rahme, L. G. *Mol. Microbiol.* **2005**, *55*, 998–1014.
- (19) Allesen-Holm, M.; Barken, K. B.; Yang, L.; Klausen, M.; Webb, J. S.; Kjelleberg, S.; Molin, S.; Givskov, M.; Tolker-Nielsen, T. *Mol. Microbiol.* **2006**, *59*, 1114–1128.
- (20) Maddocks, S. E.; Oyston, P. C. F. *Microbiology* **2008**, *154*, 3609–3623.
- (21) Breidenstein, E. B. M.; la Fuente-Núñez, de, C.; Hancock, R. E. W. *Trends Microbiol.* **2011**, *19*, 419–426.
- (22) Ma, D.; Cook, D. N.; Hearst, J. E.; Nikaido, H. *Trends Microbiol.* **1994**, *2*, 489–493.
- (23) Lu, C.; Kirsch, B.; Zimmer, C.; de Jong, J. C.; Henn, C.; Maurer, C. K.; Müsken, M.; Häussler, S.; Steinbach, A.; Hartmann, R. W. *Chem. Biol.* **2012**, *19*, 381–390.
- (24) Lu, C.; Kirsch, B.; Maurer, C. K.; Zimmer, C.; de Jong, J. C.; Steinbach, A.; Hartmann, R. W. *in preparation*.
- (25) Klein, T.; Henn, C.; de Jong, J. C.; Zimmer, C.; Kirsch, B.; Maurer, C. K.; Pistorius, D.; Müller, R.; Steinbach, A.; Hartmann, R. W. *ACS Chem. Biol.* **2012**, accepted.
- (26) Mochalkin, I.; Miller, J. R.; Narasimhan, L.; Thanabal, V.; Erdman, P.; Cox, P. B.; Prasad, J. V. N. V.; Lightle, S.; Huband, M. D.; Stover, C. K. *ACS Chem. Biol.* **2009**, *4*, 473–483.
- (27) Waldrop, G. L. *ACS Chem. Biol.* **2009**, *4*, 397–399.
- (28) Schulz, M. N.; Hubbard, R. E. *Curr. Opin. Pharmacol.* **2009**, *9*, 615–621.
- (29) Henn, C.; Dolezal, O.; Steinbach, A.; Hartmann, R. W. *in preparation*.
- (30) Ladbury, J. E. *Biochem. Soc. Trans.* **2010**, *38*, 888–893.
- (31) Ladbury, J. E.; Klebe, G.; Freire, E. *Nat. Rev. Drug Discov.* **2010**, *9*, 23–27.
- (32) Wyatt, P. G.; Woodhead, A. J.; Berdini, V.; Boulstridge, J. A.; Carr, M. G.; Cross, D. M.; Davis, D. J.; Devine, L. A.; Early, T. R.; Feltell, R. E.; Lewis, E. J.; McMenamin, R. L.; Navarro, E. F.; O'Brien, M. A.;

- O'Reilly, M.; Reule, M.; Saxty, G.; Seavers, L. C. A.; Smith, D.-M.; Squires, M. S.; Trewartha, G.; Walker, M. T.; Woolford, A. J.-A. *J. Med. Chem.* **2008**, *51*, 4986–4999.
- (33) Hopkins, A. L.; Groom, C. R.; Alex, A. *Drug Discov. Today* **2004**, *9*, 430–431.
- (34) Cugini, C.; Calfee, M. W.; Farrow, J. M.; Morales, D. K.; Pesci, E. C.; Hogan, D. A. *Mol. Microbiol.* **2007**, *65*, 896–906.
- (35) Fletcher, M. P.; Diggle, S. P.; Crusz, S. A.; Chhabra, S. R.; Cámara, M.; Williams, P. *Environ. Microbiol.* **2007**, *9*, 2683–2693.
- (36) Rubes, M.; Bludský, O.; Nachtigall, P. *ChemPhysChem* **2008**, *9*, 1702–1708.
- (37) Lewis, M.; Bagwill, C.; Hardebeck, L. K. E.; Wireduaah, S. *Comput. Struct. Biotechnol. J.* **2012**, *1*, e201204004
- (38) Sinnokrot, M. O.; Valeev, E. F.; Sherrill, C. D. *J. Am. Chem. Soc.* **2002**, *124*, 10887–10893.
- (39) de Bentzmann, S.; Plésiat, P. *Environ. Microbiol.* **2011**, *13*, 1655–1665.
- (40) Böhm, H.-J.; Klebe, G.; Kubinyi, H. *Wirkstoffdesign*; Spektrum Akademischer Verlag Heidelberg, 2002.
- (41) Griffith, K. L.; Wolf, R. E. *Biochem. Biophys. Res. Co.* **2002**, *290*, 397–402.

3.3 Structural Basis for Species Specific Inhibition of 17 β -HSD1: Computational Study and Biological Validation

Tobias Klein, Claudia Henn, Matthias Negri, Martin Frotscher

Reprinted from *PLoS ONE* **2011**, *6*, e22990.

Copyright: © 2011 Klein et al. This article is distributed under the terms of the Creative Commons Attribution License.

Publication III

Abstract: 17 β -Hydroxysteroid dehydrogenase type 1 (17 β -HSD1) catalyzes the reduction of estrone to estradiol, which is the most potent estrogen in humans. Inhibition of 17 β -HSD1 and thereby reducing the intracellular estradiol concentration is thus a promising approach for the treatment of estrogen dependent diseases. In the past, several steroidal and non-steroidal inhibitors of 17 β -HSD1 have been described but so far there is no cocrystal structure of the latter in complex with 17 β -HSD1. However, a distinct knowledge of active site topologies and protein-ligand interactions is a prerequisite for structure-based drug design and optimization. An elegant strategy to enhance this knowledge is to compare inhibition values obtained for one compound toward ortholog proteins from various species, which are highly conserved in sequence and differ only in few residues. In this study the inhibitory potencies of selected members of different non-steroidal inhibitor classes toward marmoset 17 β -HSD1 were determined and the data were compared with the values obtained for the human enzyme. A species specific inhibition profile was observed in the class of the (hydroxyphenyl)naphthols. Using a combination of computational methods, including homology modelling, molecular docking, MD simulation, and binding energy calculation, a reasonable model of the three-dimensional structure of marmoset 17 β -HSD1 was developed and inhibition data were rationalized on the structural basis. In marmoset 17 β -HSD1, residues 190 to 196 form a small α -helix, which induces conformational changes compared to the human enzyme. The docking poses suggest these conformational changes as determinants for species specificity and energy decomposition analysis highlighted the outstanding role of Asn152 as interaction partner for inhibitor binding. In summary, this strategy of comparing the biological activities of inhibitors toward highly conserved ortholog proteins might be an alternative to laborious x-ray or site-directed mutagenesis experiments in certain cases. Additionally, it facilitates inhibitor design and optimization by offering new information on protein-ligand interactions.

Introduction

Human 17β -hydroxysteroid dehydrogenase type 1 (17β -HSD1) catalyzes the NAD(P)H dependent reduction of the weak estrogen estrone (E1) to the biologically most active estrogen estradiol (E2; Fig. 1) [1].

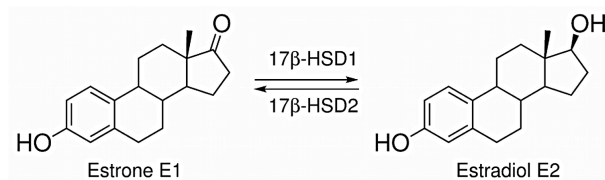


Figure 1. Interconversion of estrone (E1) and estradiol (E2).

This reaction, which represents the last step in E2 biosynthesis, takes place in target cells where the estrogens exert their effects via the estrogen receptors α and β . Besides their physiological effects, estrogens are involved in the development and the progression of estrogen dependent diseases (EDDs) like breast cancer, endometriosis and endometrial hyperplasia [2-4]. In the past few years, aromatase inhibitors have been intensively investigated for the treatment of EDDs [5-7] but they lead to unwanted side effects due to their strong reduction of estrogen levels in the whole body. Therefore reducing local E2 levels by inhibition of 17β -HSD1 is a promising therapeutic approach for the treatment of EDDs. An analogous intracrine concept has already been proved successful for the treatment of androgen dependent diseases such as benign prostatic hyperplasia and alopecia by using 5α -reductase inhibitors [8-11]. 17β -HSD2 catalyzes the reverse reaction (oxidation of E2 to E1; Fig. 1) and inhibition of this enzyme must be avoided for the therapeutic concept to work. However, specific inhibition of 17β -HSD2 in bone cells may provide a novel approach to prevent osteoporosis [12].

17β -HSD1 is a cytosolic enzyme that belongs to the superfamily of short-chain dehydrogenases/reductases (SDRs) [13]. It consists of 327 amino acid residues (34.9 kDa) and the active form exists as homodimer [14]. 17β -HSD1 comprises a Rossmann fold, associated with cofactor binding, and a steroid-binding cleft [15]. The latter is described as a hydrophobic tunnel with polar residues at each end: His221/Glu282 on the C-terminal side, and Ser142/Tyr155, belonging to the catalytic tetrad, which is present in the majority of characterized SDRs [16], on the other side [17]. To date 22 crystal structures of 17β -HSD1 are available as apoform, binary or ternary complexes [18-20]. All crystal structures show an overall identical tertiary structure, while major differences have been identified only for the highly flexible β FaG'-loop. It is not resolved in ten crystal structures, while the remaining twelve showed high b-factor values for this area, which is an additional hint for the flexibility of the β FaG'-loop. In some crystal structures a short α -helix was observed in the loop region but its occurrence seems not to be dependent on the presence of steroidal ligands, cofactor or

inhibitor. However, the position and length of the α -helix changes: in the apoform (PDB entry 1bhs) the helix is limited to the beginning of the loop while in presence of steroidal ligands and/or cofactor it is shifted to the end (PDB entries 1dht, 1equ, and 1iol). Further, dependent on the presence of cofactor and ligands, the β F α G'-loop can occupy three possible orientations: an opened, semi-opened, and closed enzyme conformation [21].

Several steroidal and non-steroidal inhibitors of 17 β -HSD1 have been described [18,22-37], but only for the former cocrystal structures exist. While several computational studies have been performed in order to elucidate the interactions of non-steroidal inhibitors with 17 β -HSD1 [26,27,33,37,38], structural data confirming the results are still missing.

However, a distinct knowledge of active site topologies and protein-ligand interactions is a prerequisite for structure-based drug design and optimization. To further increase this knowledge, inhibition values obtained for one compound toward proteins, differing only in few residues might be advantageous. For this purpose, wild type proteins and their mutants carrying a set of point mutations can be used. As alternative, proteins from various species, which are highly conserved in sequence and differ only in few residues, might be considered.

This latter approach was applied in the present study employing human and marmoset monkey (*callithrix jacchus*) 17 β -HSD1. Selected human 17 β -HSD1 inhibitors, representative of our structurally diverse inhibitor classes, were tested toward the marmoset 17 β -HSD1. The resulting inhibitory potencies were compared with those obtained for the human enzyme and remarkable differences were only observed in the class of the (hydroxyphenyl)naphthols. In order to rationalize the species-specific inhibition profiles at the structural basis, a homology model of the marmoset enzyme was built using a human 17 β -HSD1 x-ray structure as template. Further, the docking poses of selected compounds into both the human crystal structure and the modelled marmoset 17 β -HSD1 were considered. Notably, the marmoset homology model and the docking poses of the inhibitors presented herein were validated by their ability to explain inhibition data. Subsequently, the complexes of two representative inhibitors, docked into the marmoset model and the human crystal structure, respectively, were subjected to MD simulations to investigate their conformational equilibrium. In addition, binding energy calculations as well as energy decomposition analysis were performed, with the aim to investigate the influence of the marmoset amino acid variations on the inhibitory potencies. The current work provides new insights into the marmoset 17 β -HSD1 active site topology, reveals probable inhibitor binding modes in human and marmoset 17 β -HSD1, and identifies amino acids responsible for species specificity in 17 β -HSD1 inhibition.

Results

Comparison of 17 β -HSD type 1 and type 2 sequences. To identify regions that are conserved through several species, the sequences of rodent, cynomolgus, marmoset and human 17 β -HSDs 1 were aligned (Fig. 2A). The N-terminal region (residues 1-190), which constitutes the common Rossmann fold as well as the catalytic tetrad, is highly conserved for the analyzed species. Remarkable differences were observed in the F/G segment (residues 191-230), which is lining the steroid-binding site, and the C-terminal region (residues 231-285). Sequence alignment of human and marmoset 17 β -HSD1 revealed that they share 80 % sequence identity and 85 % similarity (Fig. 2A). Focusing on the steroid-binding site (residues 94 to 196 and 214 to 284), the identity increases to 87 %, with five major amino acid variations observed in the marmoset enzyme: A191P, E194Q, S222N, V225I and E282N. In contrast, comparing cynomolgus and human 17 β -HSD1, which show even 91% identity, only one of the aforementioned amino acid variations can be found (E282H; Fig. 2A). With the exception of marmoset 17 β -HSD1, Ala191 and Glu194 are conserved through the analyzed species (Fig. 2A) indicating the significance of the observed variations between human and marmoset. 17 β -HSDs 1 of mouse and rat are 83 % similar to the human enzyme in the first 287 amino acids. In both analyzed rodent enzymes His221, which is involved in steroid binding [17], is mutated into a glycine (H221G). Moreover, several other amino acids of the substrate-binding site are replaced by more bulky residues (L96F, N152H, M193Y/H, S222Y). Interestingly, rat and mouse 17 β -HSDs 1 are significantly less sensitive to inhibition by steroidal inhibitors compared to the human ortholog [39] and different classes of non-steroidal potent human 17 β -HSD1 inhibitors turned out to be only weak inhibitors of E2 formation in rat liver preparations [40]. This might be partially explained by the absence of His221 as interaction partner as well as by the reduced volume of the active site (M193Y/H, S222Y). Sequence identities between human 17 β -HSD2 and 17 β -HSD2 of the selected species range from 61 % (mouse) to 93 % (cynomolgus) while the F/G segment and the C-terminal region show the most pronounced variability (Fig. 2B). The comparison of 17 β -HSD1 with the correspondent type 2 enzymes of the analyzed species revealed, that the type 2 enzymes have about 80 additional N-terminal residues relative to the type 1 enzymes. Sequence comparison showed that they share a very low overall sequence identity (≤ 25 %) with major differences in the F/G segment and the C-terminal domain, which constitute the active site. However, some amino acid motifs, characteristic for SDR enzymes [18], are highly conserved: the T-G-xxx-G-x-G motif, the Y-xxx-K sequence and the N-A-G motif (Fig. 2B). For marmoset 17 β -HSD2 only a fragment of the primary sequence is available, which is 143 amino acids in length and constitutes the Rossmann fold whereas the F/G segment and the C-terminal region are missing (Fig. 2B). This segment is 29 % identical to marmoset 17 β -HSD1.

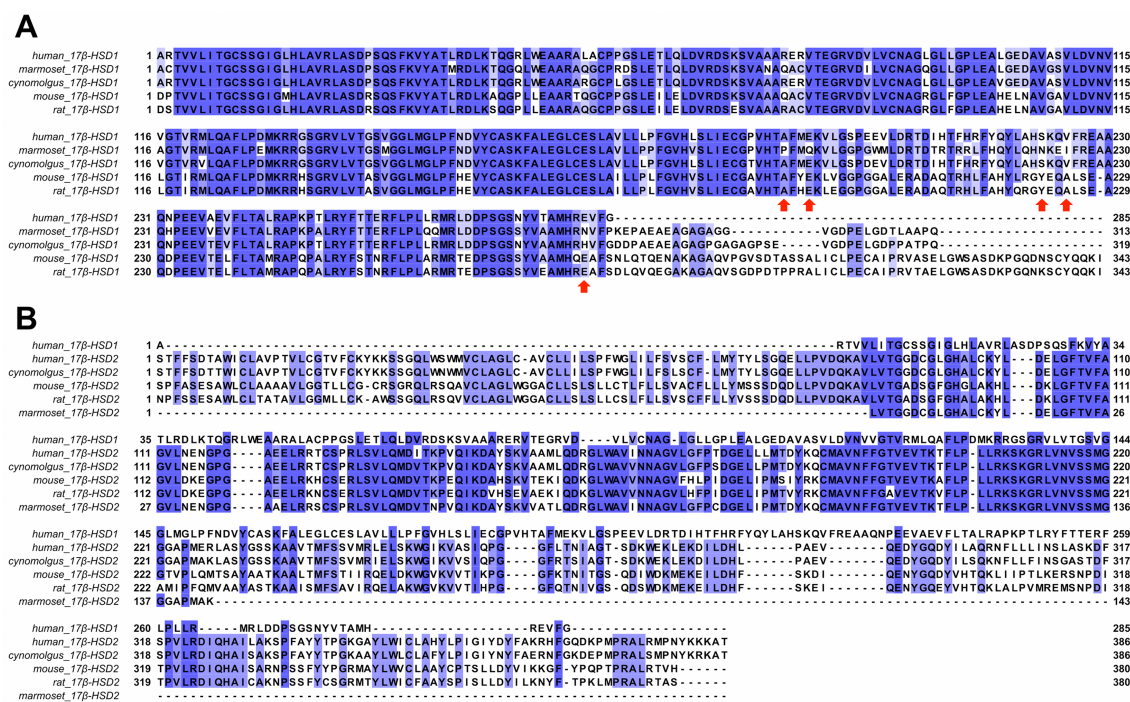


Figure 2. Multiple sequence alignment of 17 β -HSD type 1 and type 2 from selected species. Species and subtype are indicated on the left, followed by residue numbering. Residues are colored by percentage identity and red arrows indicate major amino acid variations in marmoset compared to the other species. A) Multiple sequence alignment of 17 β -HSD1 from selected species. B) Multiple sequence alignment of human 17 β -HSD1 with 17 β -HSD2 from selected species.

As human and marmoset 17 β -HSD1 differ in a few residues of the activesite, comparison of the inhibitory potencies of selected inhibitors, observed toward both enzymes, is suitable to further increase the knowledge of active site topologies and protein-ligand interactions. In particular, the amino acid variations in the flexible β FAG'-loop, which is suggested to play a crucial role in ligand binding, will be used to elucidate the function of the loop in more detail.

Inhibition of marmoset 17 β -HSD1 and 17 β -HSD2. Marmoset placental tissue was used as enzyme source and the proteins were partially purified following a described procedure [41]. Tritiated E1 was incubated with 17 β -HSD1, cofactor and inhibitor. The separation of substrate and product was performed by HPLC. In an assay similar to the 17 β -HSD1 test, marmoset placental microsomes containing 17 β -HSD2 were incubated with tritiated E2 in the presence of NAD^+ and inhibitor. Labelled product was quantified after HPLC separation.

The inhibition values of compounds **1-20** (Fig. 3) are shown in Table 1. The bis(hydroxyphenyl) substituted arenes **1-11** showed comparable or even higher inhibitory potencies toward marmoset 17 β -HSD1 compared to the human enzyme. For example, compound **8**, which is a potent inhibitor of human 17 β -HSD1 (IC_{50} = 151 nM), showed a stronger inhibitory potency toward marmoset 17 β -HSD1 (IC_{50} = 4 nM).

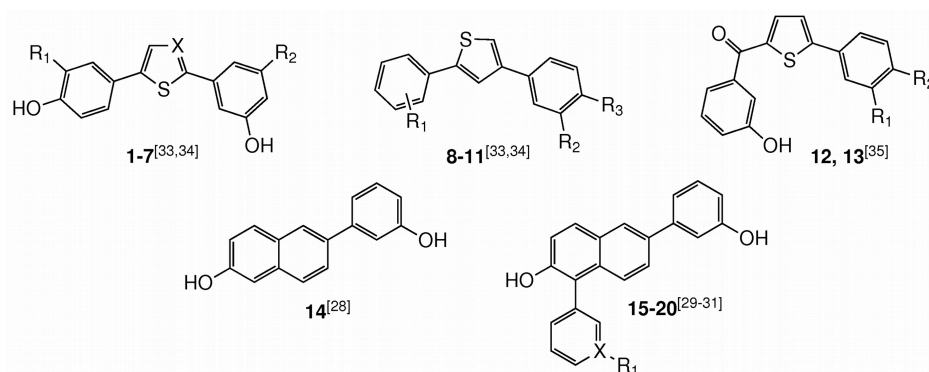


Figure 3. Chemical structures of selected human 17 β -HSD1 inhibitors. Representative structures of our three inhibitor classes: the bis(hydroxyphenyl) substituted arenes (**1-11**), the bicyclic substituted hydroxyphenylmethanones (**12, 13**) and the (hydroxyphenyl)naphthols (**14-20**).

Table 1. Inhibition of human and marmoset 17 β -HSD1 and 17 β -HSD2 by compounds **1-20**.

compd	X	R ₁	R ₂	R ₃	Human IC ₅₀ [nM]		Marmoset IC ₅₀ [nM] ^c	
					17 β -HSD1 ^a	17 β -HSD2 ^b	17 β -HSD1 ^d	17 β -HSD2 ^e
1	CH	F	H		8	940	< 5 ^f	> 50
2	N	H	H		50	4004	102	> 50
3	CH	H	H		69	1953	31	> 50
4	CH	CH ₃	H		46	1971	< 50	> 50
5	N	CH ₃	H		143	2023	< 50	> 50
6	CH	H	F		42	463	< 5 ^f	85
7	CH	F	F		17	218	< 5 ^f	43
8		4-OH	OH	H	151	1690	4 ^f	> 50
9		3-OH	H	OH	77	1271	2 ^f	> 50
10		3-OH	CH ₃	OH	64	869	3 ^f	> 50
11		3-OH	F	OH	64	510	< 50	72
12		H	OH		33	478	< 50	43
13		OC ₂ H ₅			78	502	< 50	59
14					116	5641	> 50	> 50
15	C	OH			36	959	32	> 50
16	N				26	1157	> 50	> 50
17	C	H			20	540	52	> 50
18	C	NH ₂			53	1757	n.i.	> 50
19	C	NHSO ₂ CH ₃			15	403	> 50	> 50
20	C	NHCOCH ₃			83	1239	> 50	n.i.

^aHuman placental, cytosolic fraction, substrate E1, 500 nM, cofactor NADH, 500 μ M; ^bHuman placental, microsomal fraction, substrate E2, 500 nM, cofactor NAD⁺, 1500 μ M; ^cLogit transformed values calculated from % inhibition at 50 nM inhibitor concentration, for inhibition values < 30% or > 70%, a trend is given; ^dMarmoset monkey placental, cytosolic fraction, substrate E1, 500 nM, cofactor NADH, 500 μ M; ^eMarmoset monkey placental, microsomal fraction, substrate E2, 500 nM, cofactor NAD⁺, 1500 μ M; ^fInhibitor concentration: 5nM; n.i.: no inhibition; Human IC₅₀ values were retrieved from literature (corresponding references are indicated with the structural formulas in Fig. 3).

Comparable inhibition data for human and marmoset 17 β -HSD1 were also measured for the bicyclic substituted hydroxyphenylmethanones **12** and **13**. This indicates that the binding of the two aforementioned inhibitor classes is reinforced or at least not affected by the amino acid variations in marmoset 17 β -HSD1. In the class of the (hydroxyphenyl)naphthols, the human 17 β -HSD1 inhibitor **14** (IC_{50} = 116 nM) showed also a good inhibitory potency toward marmoset 17 β -HSD1 (IC_{50} > 50 nM). The introduction of space filling substituents in position 1 of the naphthol core of **14** is beneficial for the inhibition of the human enzyme (**16**, IC_{50} = 26 nM), but for marmoset 17 β -HSD1 no increase in inhibitory potency was observed (**16**, IC_{50} > 50 nM) compared to the unsubstituted **14**. Interestingly, further enlargement of the substituents in 1-position of **14** led to highly active human 17 β -HSD1 inhibitors (**19**, IC_{50} = 15 nM) while a reduced potency toward marmoset 17 β -HSD1 (**19**, IC_{50} > 50 nM) was found.

The inhibitory potencies of compounds **1-20** toward marmoset 17 β -HSD2 were also determined to prove whether marmoset monkey is a suitable species for *in vivo* evaluation of 17 β -HSD1 inhibitors (Table 1). Remarkably, lower selectivity of compounds toward non-target marmoset 17 β -HSD2 was observed, when comparing to human 17 β -HSD2.

Homology modelling and MD simulations of marmoset 17 β -HSD1. In order to obtain a more precise picture of the three-dimensional structure of the marmoset 17 β -HSD1, a homology model was generated. A set of 100 models was built with MODELLER 9v7 [42] using the ternary complex E1-NADPH-human 17 β -HSD1 as template. This complex was obtained by docking E1 into human 17 β -HSD1 employing the Protein Data Bank (PDB) entry 1fdt with conformation B for residues 187-200 (in the following determined as 1fdtB). This 3D structure was chosen as it represents a ternary complex with NADP⁺ and E2 in the closed enzyme conformation, as the β F α G'-loop is resolved, and as this protein structure was already successfully used in previous docking studies with the investigated compound classes [30,36]. The best model was chosen according to internal DOPE-score [43] and PROCHECK [44] tests. Notably, it presents a short α -helix (residues 190-196) in the region between the β F-sheet (residues 178-186) and the α G'-helix (residues 209-227), with Pro191 in the first turn of the helix (N1 position; Fig. 4), thus differing from the secondary structure of the template.

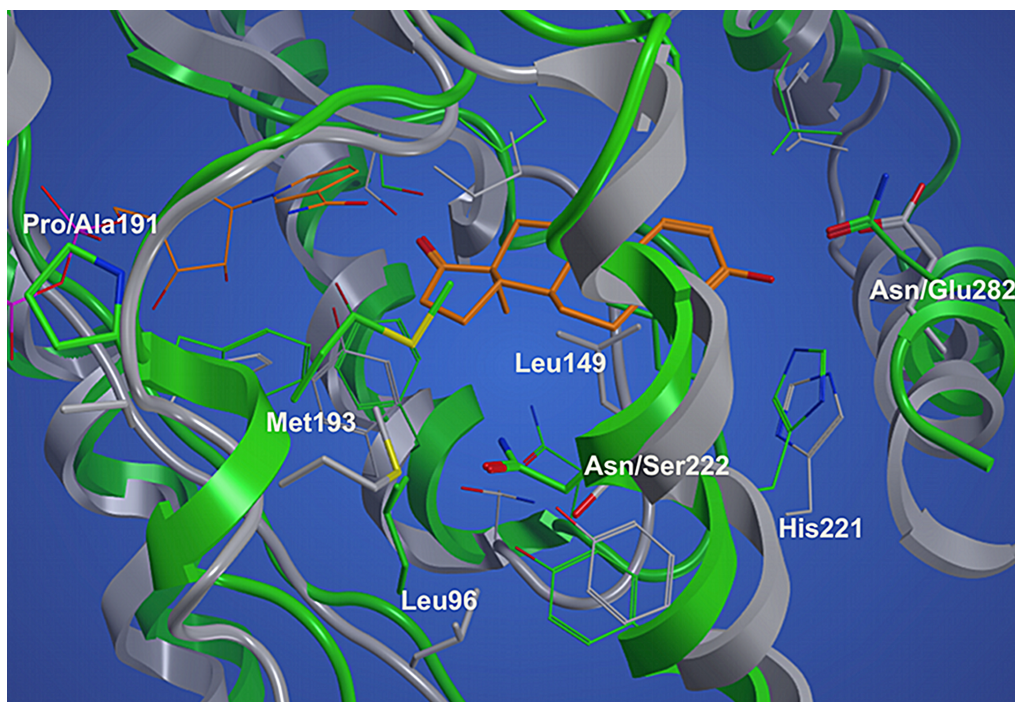


Figure 4. Three-dimensional structure superimposition of marmoset and human 17 β -HSD1. Low energy structure of marmoset 17 β -HSD1 (green) in complex with E1 and NADPH (orange) from MD simulation superimposed onto the x-ray structure of human 17 β -HSD1 (grey, PDB code: 1fdtB). When two residues are indicated, the first corresponds to marmoset 17 β -HSD1 and the second to human 17 β -HSD1.

The selected model was further refined both as holoenzyme with NADPH and as ternary complex with NADPH and E1 by MD simulations. The trajectories of the two MD simulations were stable with a α -carbon root-mean-square deviation (RMSD) to the starting structure below 3.0 Å (Fig. 5). No major structural differences were observed when comparing the simulated holoenzyme and the ternary complex. Therefore, the following results, based on analysis of the ternary complex, also apply to the holoform.

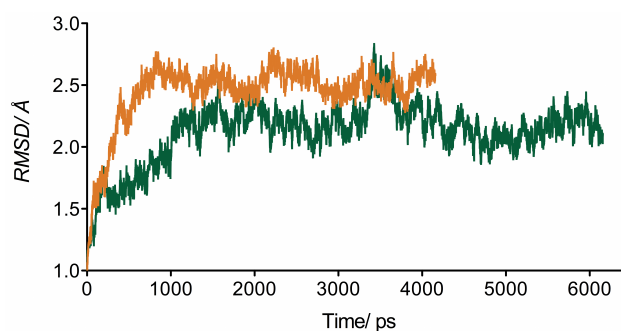


Figure 5. RMSD analysis of the MD simulations of the marmoset 17 β -HSD1 model. Time-dependent C_{α} -RMSD for all residues of the secondary (orange) and ternary (green) complex.

After an initial inward rotation in the MD simulation, the short α -helix (residues 190-196) remained stable for the last 5 ns of the MD simulation, with an average backbone RMSD to the final conformation of 1.03 Å. Remarkably, a similar behaviour cannot be expected for the region between the β F-sheet and the α G'-helix in the human enzyme. The differences in the crystal structures suggest a high flexibility for the β F α G'-loop: it is not resolved in ten crystal structures and the remaining twelve show high b-factor values for this area. Some crystal structures present a short α -helix in the loop region whose position and length varies dependent on the presence of steroidal ligands, cofactor or inhibitor. In the apoform (PDB entry 1bhs) the helix is limited to the beginning of the loop, whereas in presence of steroidal ligands and/or cofactor it is shifted to the end (PDB entries 1dht, 1equ, and 1iol). Further, in the human enzyme, the β F α G'-loop axis occupies different orientations dependent on the presence of cofactor and ligands. In the marmoset however, both the holoform and the ternary complex show a helix starting already at the beginning of the β F α G'-loop with its axis in only one conformation.

The presence of the newly formed α -helix (residues 190-196) induced a different orientation of the side chain of Met193. Compared to the template structure, Met193 protrudes deeper into the substrate-binding site and stabilizes E1 by hydrophobic interactions (Fig. 4). Furthermore, during MD simulation a kink in the loop between the β D-sheet and the α E-helix was observed. Thereby the side chain of Leu96 was brought closer to E1 allowing Van der Waals contacts (Fig. 4). Summarizing, in the final part of the MD simulation E1 was stabilized by both lipophilic interactions and hydrogen bonds: Leu96, Leu149, Met193, and Phe259 constrained the steroidal scaffold while Ser142/Tyr155 and His221/Asn282 interacted with the carbonyl oxygen in 17-position and the 3 OH-group, respectively. The latter residue took over the H-bond acceptor abilities of Glu282, which is involved in forming an H-bond with the 3 OH-group of E1 in the human enzyme.

Employing CASTp [45], the active site volumes of human and marmoset 17 β -HSD1 were calculated. The above-described conformational changes of Leu96 and Met193 as well as the S222N and V225I mutations resulted in a reduced volume of the marmoset 17 β -HSD1 active site (478 Å³) compared to that of the human ortholog (627 Å³).

The stereochemical quality of the holoenzyme and the ternary complex models obtained from MD simulations was checked with PROCHECK [44]. The majority of the residues of the investigated structures were found to occupy the most favoured regions of the Ramachandran plots, while the other residues occupied the additional allowed regions. In detail, in the ternary complex 78.1 % of the residues were placed in the most favoured region, 20.2 % in the additional allowed region, 1.2 % in the generously allowed region, and only 0.4 % in the disallowed region (for the holoform: 81.8 %, 17.4 %, 0.8 % and 0 %).

Molecular docking. As the potent inhibitors of human 17 β -HSD1 **12** and **19** are structurally diverse and exhibit different potencies toward marmoset 17 β -HSD1 they were chosen as representatives to rationalize the observed species-specific inhibition profiles. Employing AutoDock 4 [46], both compounds were docked into the active sites of marmoset and human 17 β -HSD1 using the equilibrated, ternary complex after 5537 ps and the x-ray structure 1fdtB (see experimental part), respectively. The inhibitor poses used for further investigation were selected considering binding energy and statistical representativity (cluster population; Table S1) and are shown in Figure 6.

Table S1. Cluster analysis of molecular docking results.

Comp	No of clusters	Cluster	No of conformations	Best binding energy (ΔG_{bind})
Human x-ray structure (1fdtB)				
12	3	1	2	-4.77
		2	45	-4.65
		3	3	-4.58
19	5	1	24	-5.94
		2	1	-5.44
		3	19	-4.98
		4	1	-4.92
		5	5	-4.87
Marmoset monkey homology model				
12	3	1	21	-5.60
		2	27	-5.41
		3	1	-5.0
		4	1	-4.59
19	5	1	7	-5.79
		2	33	-5.74
		3	3	-5.11
		4	5	-4.41
		5	2	-4.10

All energies are expressed in kcal mol⁻¹. The lowest energy conformation of each cluster, which is marked in bold was used for further investigation.

In the human enzyme both inhibitors are placed in the substrate-binding site and they occupy an apolar subpocket consisting of the following amino acids: Gly94, Leu95, Leu96, Asn152, Tyr155, and Phe192 (Fig. 6A). While the carbonyl group of compound **12** mimics the D-ring keto function of E1, forming H-bonds with Ser142 and Tyr155, its para-OH group resembles the 3-OH of E1, which interacts with His221 via an H-bond. The meta-hydroxyphenyl moiety is projecting into the subpocket, where it forms an additional H-bond with Asn152 and is stabilized by π - π -interactions with Tyr155 and Phe192.

The (hydroxyphenyl)naphthol-core of compound **19** occupies the substrate-binding site and is stabilized by three H-bonds: the 2-OH group interacts with Ser142 as well as with Tyr155 and

the OH group in meta position of the phenyl ring in 6-position interacts with His221. In this case, the sulfonamide substituted phenyl ring in 1-position of the naphthol core protrudes into the subpocket, where it is stabilized by H-bonds with Asn152 and with the -NH- of the backbone of Leu95 (Fig. 6A).

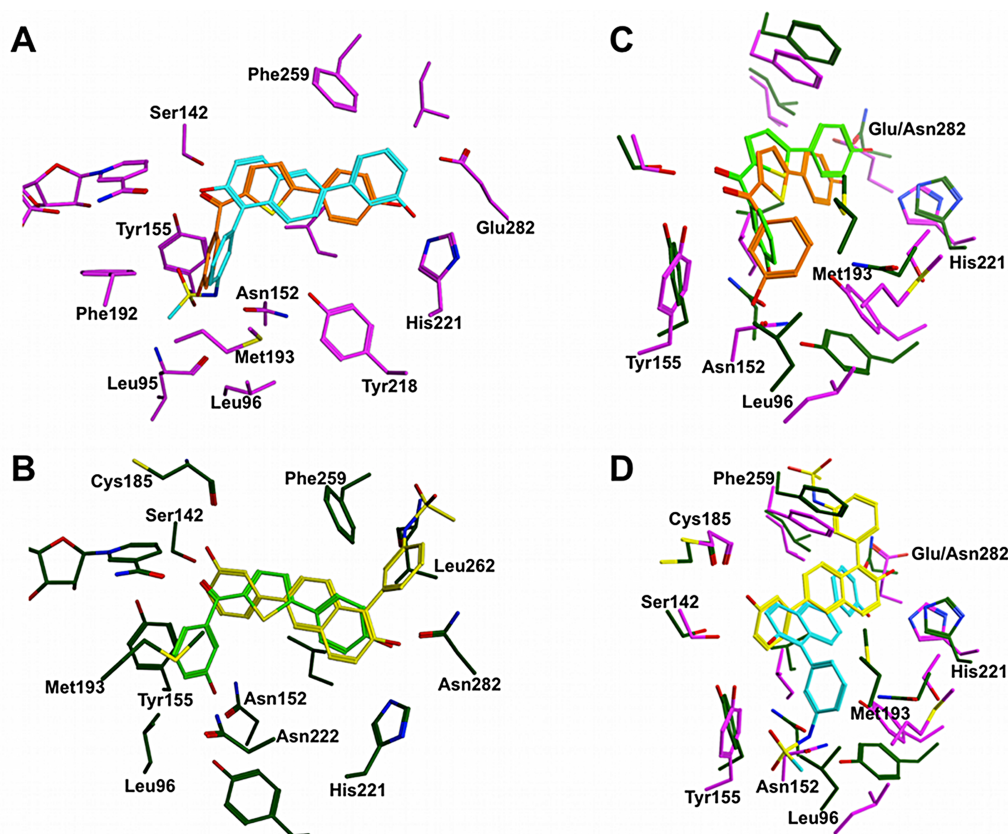


Figure 6. Hypothetical binding modes of compounds **12** and **19**. **A)** Superimposition of lowest energy structures of **12** (orange) and **19** (cyan) obtained by docking into the x-ray structure of human 17 β -HSD1 (magenta, PDB code: 1fdtB). **B)** Superimposition of lowest energy structures of **12** (light green) and **19** (yellow) obtained by docking into the marmoset 17 β -HSD1 homology model (green). **C)** Superimposition of lowest energy structures of **12** (light green) docked into the marmoset 17 β -HSD1 model (green) and of **12** (orange) docked into the x-ray structure of human 17 β -HSD1 (magenta, PDB code: 1fdtB). **D)** Superimposition of lowest energy structures of **19** (yellow) docked into the marmoset 17 β -HSD1 model (green) and of **19** (cyan) docked into the x-ray structure of human 17 β -HSD1 (magenta, PDB code: 1fdtB).

Also in the marmoset enzyme both compounds occupy the substrate-binding site, but only **12** protrudes into the apolar subpocket (Fig. 6B). Due to the altered side chain conformation of Leu96 in the marmoset enzyme, compound **12** is slightly displaced toward the C-terminus (Fig. 6C). Regarding the interaction pattern, only minor changes were observed: the carbonyl group forms only an H-bond with Ser142 but for the para-OH group a second H-bond with Asn282 was observed (Fig. 6C).

Interestingly, compound **19** resulted in a completely different binding mode when docked into the homology model of marmoset 17 β -HSD1 with respect to its position in the human

crystal structure 1fdtB (Fig. 6D). The OH-group in meta position of the phenyl ring makes an H-bond with the backbone carbonyl oxygen of Cys185 and the 2-OH function forms H-bonds with His221 and Asn282 in a bifurcated fashion. The sulfonamide substituted phenyl ring is located in the C-terminal gate and might be stabilized by π - π -interactions with Phe259 and an H-bond with the backbone -NH- of Leu262.

Validation of the docking complexes by means of MD simulations and free energy calculations (MM/PBSA). With the aim to validate the docking results and to unravel possible induced-fit mechanisms, different MD simulations were run in explicit aqueous solution. Distance restraints were applied to inhibitors only in the first ns of the MD simulations with the aim of maintaining their proper orientation. For the rest of the MD simulation no restraints were used and the whole complexes were left free to move. This was done in order to avoid trapping the inhibitor in an unstable conformation, which could bias the results. The RMSD values of the heavy atoms of the inhibitors and of the C α -atoms of the enzymes were analyzed as a function of time to assess the degree of conformational drift, as shown in Figure 7.

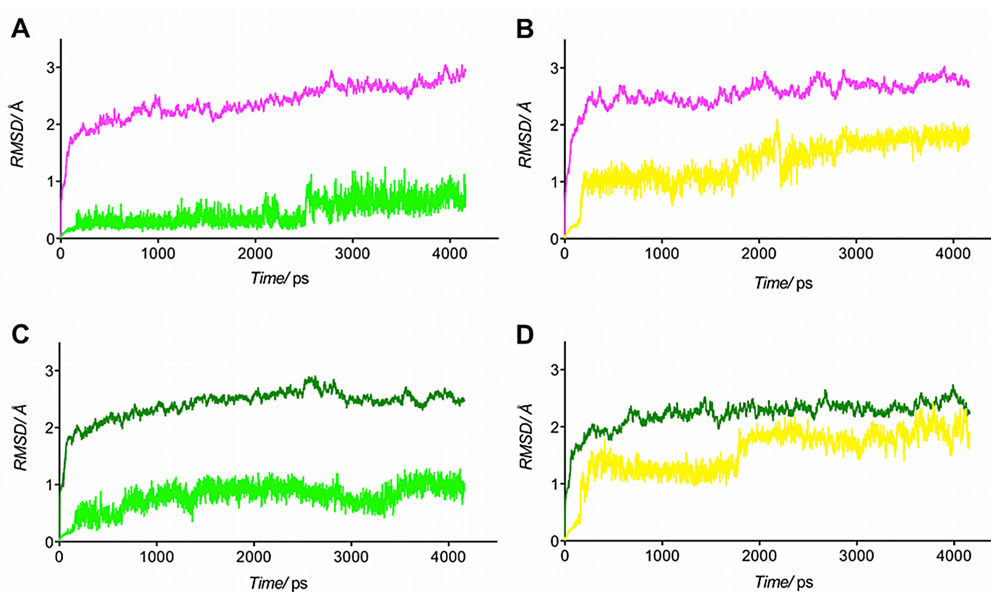


Figure 7. Time dependent RMSD analysis of C α of 17 β -HSD1 and of the heavy atoms in the ligands. **A)** C α -RMSD of human 17 β -HSD1 is colored in magenta and the heavy atoms RMSD of compound **12** in light green. **B)** C α -RMSD of human 17 β -HSD1 is colored in magenta and the heavy atoms RMSD of compound **19** in yellow. **C)** C α -RMSD of marmoset 17 β -HSD1 is colored in green and the heavy atoms RMSD of compound **12** in light green. **D)** C α -RMSD of marmoset 17 β -HSD1 is colored green and the heavy atoms RMSD of compound **19** in yellow.

In the simulation of **12** bound to human 17 β -HSD1 the C α -RMSD of the protein as well as the RMSD of the heavy atoms of **12** showed a stable plateau (~ 2.2 Å) from 1.0 to 2.5 ns (Fig. 7A). After 2.5 ns the C α -RMSD of the protein increased and a minor fluctuation of the heavy atom

RMSD of **12** was observed. The latter finding could be related to a slight shift of the inhibitor toward the C-terminal end of the enzyme. Notably, the hydrogen bonds between **12** and 17 β -HSD1, which were observed in the initial structure, were conserved during the 4 ns simulation suggesting that both protein and **12** fluctuations do not impact the inhibitor binding.

Both human 17 β -HSD1 and compound **19** were stable in the simulation of their complex (Fig 7B). During the simulation (after 1.5 ns) the hydrogen bond of the *meta*-OH group with His221 is replaced by an H-bond with Glu282. However, after 2.1 ns, this hydrogen bond is interrupted for 0.2 ns allowing the hydroxyphenyl ring to rotate freely around the axis of the bond to the naphthol core thereby inducing a minor fluctuation of the heavy atom RMSD of **19**. After this short interruption the H-bond interaction with Glu282 is re-established. On the other side, the hydrogen bonds between the 2-OH group and Ser142/Tyr155 as well as between the sulfonamide moiety and Asn152/Leu95 endured constant.

During the MD simulation of **12** in complex with marmoset 17 β -HSD1, the *meta*-hydroxyphenyl moiety of **12** moved further out of the subpocket. This was reflected by the minor fluctuation of the RMSD of the heavy atoms of **12** after 1.4 ns (Fig. 7C). While this motion caused the break of the H-bond with Asn152, it also placed the *meta*-OH group in an appropriate distance to Asn222, thus allowing a new H-bond formation.

The analysis of the MD simulation of the marmoset 17 β -HSD1-**19** complex revealed an overall stable C α -RMSD of the protein. However, after 1.8 ns, a ~ 0.5 Å fluctuation of the heavy atom RMSD of **19** was observed (Fig. 7D) corresponding to the rotation around the axis of the bond between the hydroxyphenyl ring and the naphthol core. Thereby the H-bond with the backbone amino group of Leu262 was lost.

Furthermore, for each of the four MD trajectories absolute free energy (ΔG) and relative binding affinity (ΔG_{bind}) were calculated applying MM/PBSA methods and NMODE analysis (Table 2).

Table 2. Free energy calculations for the MD simulations of the four docking complexes.

comp	ELEC	VDW mean	GAS mean	PBSOL mean	PBTOT (ΔG_{bind}) mean (\pm SE)	TSTOT mean (\pm SE)	ΔG mean (\pm SE)
Human x-ray structure (1fdtB)							
12	-15.4	-40.4	-55.7	35.1	-20.6 \pm 3.8	-15.9 \pm 6.6	-4.7 \pm 7.6
19	-36.7	-50.1	-86.8	64.2	-22.6 \pm 5.0	-15.3 \pm 6.8	-7.3 \pm 8.4
Marmoset monkey homology model							
12	-24.5	-38.1	-61.3	40.0	-21.3 \pm 4.9	-15.4 \pm 5.3	-5.8 \pm 7.2
19	-42.2	-34.4	-76.5	50.3	-26.3 \pm 4.4	-23.1 \pm 4.3	-3.2 \pm 6.1

ΔG and ΔG_{bind} values correspond to the longest stable plateau for each MD. (ΔG) free binding energy; (PBTOT) (ΔG_{bind}) relative binding energy; (ELEC) electrostatic contribution in gas phase; (VDW) Van der Waals contribution in gas phase; (GAS) free energy in vacuum; (PBSOL) solvation energy; (TSTOT) ($T\Delta S$) entropic contribution; (mean) mean value; (SE) standard error of the mean; all energies expressed in kcal mol⁻¹.

This was done for the following stable sectors: 1000 to 2500 ps for **12** in complex with human 17 β -HSD1 (Fig. 7A), 2300 to 4160 ps for **19** in complex with human 17 β -HSD1 (Fig. 7B), 1500 to 4160 ps for **12** in complex with marmoset 17 β -HSD1 (Fig. 7C) and 1800 to 4160 ps for **19** in complex with marmoset 17 β -HSD1 (Fig 7D). All four complexes showed favorable ΔG values, ranging from -7.3 kcal mol⁻¹ to -3.2 kcal mol⁻¹. The free energies observed for compound **12** in complex with human ($\Delta G = -4.7$ kcal mol⁻¹) and marmoset 17 β -HSD1 ($\Delta G = -5.8$ kcal mol⁻¹) are in the same range. This is in accordance with the inhibitory activities of **12**, which are comparable for both species (see Table 1). Regarding compound **19**, the complex with human 17 β -HSD1 shows a more favorable free energy ($\Delta G = -7.3$ kcal mol⁻¹) than the one with marmoset 17 β -HSD1 ($\Delta G = -3.2$ kcal mol⁻¹). This is mainly due to poor entropic contributions in the latter case. Remarkably, this finding is in concert with the experimentally determined inhibition data: compound **19** is a highly potent human 17 β -HSD1 inhibitor ($IC_{50} = 15$ nM) with reduced activity toward the marmoset enzyme ($IC_{50} > 50$ nM).

Analysis of the binding interactions using MM/GBSA methods. Focusing on the specific interactions, which mediate the binding of **12** and **19** to human and marmoset 17 β -HSD1, we have analyzed the interaction energies of both inhibitors with the residues of the binding sites, employing a pairwise per-residue energy decomposition analysis.

Table 3. Interaction energies between the inhibitors **12** and **19** and the proximal (4.0 Å) binding site residues of human 17 β -HSD1.

comp	Gly94	Leu95	Leu96	Ser142	Leu149	Asn152	Tyr155	Cys185	Gly186	Pro187
12	-1.8	-0.3	-1.2	-1.3	-2.2	-4.1	-1.5	-0.2	-0.4	-1.3
19	-0.7	-0.7	-1.7	-1.3	-2.0	-5.7	-2.6	-0.3	-0.8	-2.0
comp	Phe192	Met193	Tyr218	His221	Ser222	Val225	Arg258	Phe259	Leu262	Glu282
12	-1.2	-1.0	-0.7	-1.8	-0.8	-1.7	-0.1	-1.2	-0.4	-0.1
19	-1.8	-1.9	-0.1	-0.2	-0.4	-1.9	-0.5	-0.9	-0.3	-4.3

All energies are expressed in kcal mol⁻¹.

Inspection of the interaction energies with human 17 β -HSD1 (Table 3) showed that the hydrogen bonds of **12** (-4.1 kcal mol⁻¹) and **19** (-5.7 kcal mol⁻¹) with Asn152 contributed most to the interaction energies. Besides Asn152, further residues of the subpocket (Gly94, Leu95, Leu96) interact with both inhibitors revealing energies from -0.3 kcal mol⁻¹ to -1.8 kcal mol⁻¹. The energies of the hydrogen bonds between **12** and the catalytic residues Ser142 as well as Tyr155 are -1.3 kcal mol⁻¹ and -1.5 kcal mol⁻¹, respectively. In case of compound **19** the interaction energies are -1.3 kcal mol⁻¹ for the H-bond with Ser142 and -1.3 kcal mol⁻¹ for the H-bond with Tyr155. Further binding site residues, which significantly contribute to the binding of compounds **12** and **19** (Leu149, Pro187, Phe192, Met193, Val225, and Phe259) show interaction energies from -0.9 kcal mol⁻¹ to -2.2 kcal mol⁻¹. Regarding the polar amino acids at

the C-terminal end of the binding site, His221 takes primarily part in the binding of **12** (-1.8 kcal mol⁻¹ for **12** vs. -0.2 kcal mol⁻¹ for **19**) while Glu282 is mainly involved in binding compound **19** (-0.1 kcal mol⁻¹ for **12** vs. -4.3 kcal mol⁻¹ for **19**).

The interaction energies of **12** and **19** with marmoset 17 β -HSD1 are listed in Table 4. Remarkably, for inhibitor **12**, the energy contribution of the H-bond with the marmoset Asn152 (-1.6 kcal mol⁻¹) is 2.6 fold reduced compared to the human enzyme, while for compound **19** it is almost lost (-0.2 kcal mol⁻¹). Both for **12** and **19** reduced energies were also observed for interactions with Gly94, Leu95, and Leu96. Interestingly, inhibitor **12** showed an interaction with Asn222 in the marmoset enzyme (-3.3 kcal mol⁻¹), which was not observed for Ser222 in human 17 β -HSD1 (-0.8 kcal mol⁻¹). This is not the case for **19**, as the interaction with Asn222 (-0.3 kcal mol⁻¹) does not contribute significantly to the interaction energy. In addition to Leu149, Pro187, Met193, Ile225, and Phe259, which interact with both compounds in the human enzyme, Gly186, His221, and Asn282 significantly contribute to the binding of **12** and **19** to marmoset 17 β -HSD1 with interaction energies in the range from -0.4 kcal mol⁻¹ to -3.6 kcal mol⁻¹. Interestingly, in marmoset 17 β -HSD1 the interaction energy between **12** and Asn282 (-3.2 kcal mol⁻¹) is 32 fold increased compared to that with Glu282 in the human enzyme (-0.1 kcal mol⁻¹). In marmoset 17 β -HSD1 an increased energy is also observed for the interaction of compound **19** with His221 (-2.6 kcal mol⁻¹) compared to the human enzyme (-0.2 kcal mol⁻¹).

Table 4. Interaction energies between the inhibitors **12** and **19** and the proximal (4.0 Å) binding site residues of marmoset monkey 17 β -HSD1.

comp	Gly94	Leu95	Leu96	Ser142	Leu149	Asn152	Tyr155	Cys185	Gly186	Pro187
12	-0.0	-0.1	-0.8	-2.1	-2.0	-1.6	-0.8	-0.3	-0.7	-2.0
19	-0.0	-0.1	-0.2	-0.9	-1.1	-0.2	-0.3	-3.5	-2.0	-2.0
comp	Phe192	Met193	Tyr218	His221	Asn222	Ile225	Arg258	Phe259	Leu262	Asn282
12	-0.4	-1.3	-1.4	-0.8	-3.3	-1.9	-0.1	-1.3	-0.9	-3.2
19	-0.0	-0.4	-0.0	-2.6	-0.3	-2.6	-3.7	-1.9	-1.0	-3.6

All energies are expressed in kcal mol⁻¹.

Discussion

When the three-dimensional structures of marmoset and human 17 β -HSD1 are compared, one of the most striking features is the small α -helix including the residues 190 to 196. It is formed in the segment between the β F-sheet and the α G'-helix starting from the interface residue Thr190, which is half in and half out of the helix (N-cap position). In contrast to the human enzyme, where this region is highly flexible, as suggested by the different crystal structures, the α -helix stayed stable during the MD simulation in both the holoform and the ternary complex. The observed conformational stability might be explained by the presence of a proline in position 191 instead of an alanine. Proline is a favorable candidate for N1 position because of its own conformational properties: with only one rotatable angle it loses less entropy than other

amino acids in forming an α -helix and thereby it should have some stabilizing influence [47]. Furthermore, in an analysis of sequence-structural characteristics in protein crystal structures, proline was found to be a favoured residue at N1 position. Especially the residue pair involving threonine at N-cap and proline at N1 position, which is observed for marmoset 17 β -HSD1, has a high prevalence [48].

In order to analyze the influence of the conformational changes in marmoset 17 β -HSD1 on ligand binding, docking studies with subsequent MD simulations, free energy calculations, and energy decomposition analyzes were carried out. While the conformational differences between the marmoset and the human enzyme did not affect the binding mode of **12** remarkably, the suggested binding mode of **19** differed strongly in 17 β -HSD1 of both species. One possible explanation for that might be the lower sterical demand of **12** compared to **19**. However, the energy contribution of the interaction between **12** and the marmoset Asn152 is reduced, whereas it was outstanding in complex with the human enzyme. Due to the minimal shift of **12** in the marmoset binding pocket, the geometric parameters for the H-bond with Asn152 are no longer optimal. Interestingly, in the marmoset enzyme an additional interaction of **12** with Asn222 is observed, which seems to compensate the deficit in interaction energy due to the absent interaction with Asn152 resulting in comparable binding energies for **12** in complex with human and marmoset 17 β -HSD1. The latter finding is in accordance with the inhibition data observed for compound **12** and validates the marmoset 17 β -HSD1 model.

Considering compound **19**, no particular interactions with the subpocket residues of the marmoset enzyme exist. Although weak interactions between **19** and the C-terminal region of marmoset 17 β -HSD1 are observed, the binding free energy is less favorable compared to that calculated for the human 17 β -HSD1-**19** complex. As the C-terminal part of the enzyme has already been discussed as a potential product exit gate of the enzyme [21], inhibitor **19** might be solvent exposed. This is consistent with the unfavorable entropy term of this complex resulting in the least favorable free energy.

Obviously, the presence of a proline in the flexible loop region and the thereby induced conformational changes in marmoset 17 β -HSD1 are decisive for the species specific inhibition of **19**. On one hand interactions with subpocket residues like Asn152, recently discussed as relevant interaction partner [49], are prevented and on the other hand the inhibitor is forced in an unfavorable solvent exposed conformation.

The bis(hydroxyphenyl) substituted arenes (compounds **1-11**) show similar or increased inhibitory potencies toward marmoset 17 β -HSD1 when comparing to human 17 β -HSD1. Recently performed docking experiments proposed a steroidal binding mode when the human crystal structure 1fdtB was used [33]. The high inhibitory potencies toward marmoset 17 β -HSD1 are in concert with the modelled structure of marmoset 17 β -HSD1 as steroid-like binding is not affected by the proposed conformational changes. Obviously, they even stabilize the

bis(hydroxyphenyl) substituted arenes in the marmoset 17 β -HSD1 binding pocket as indicated by the observed inhibitory potencies.

Differing inhibitory potencies toward human 17 β -HSD1 and 17 β -HSD2 may arise from sequence variations in the regions 94-196 and 214-284 (numbering according to 17 β -HSD1), which might lead to differences in the active sites of the two human subtypes. A lower selectivity of compounds toward non-target marmoset 17 β -HSD2 was observed, when comparing to human 17 β -HSD2. Obviously, the differences in the active sites of marmoset 17 β -HSD1 and 17 β -HSD2 are less pronounced compared to the human orthologs. However, as the available marmoset 17 β -HSD2 sequence is missing the F/G segment and the C-terminal part this hypothesis cannot be proved.

The validity of the presented homology model is further substantiated by its ability to explain the reduced inhibitory potency of C-15 substituted estrone derivatives toward marmoset 17 β -HSD1 [39]. The substituents in 15-position of the steroid were designed to occupy the hole between the flexible β F α G'-loop and the α G'-helix in the human enzyme [50]. Together with the helix formation and the conformational changes in the β D/ α E-segment, the S222N mutation limits the size of the hole in marmoset 17 β -HSD1 and thereby might reduce the inhibitory potency toward the marmoset enzyme.

Conclusion

An elegant strategy to gain more knowledge of active site topologies and, in particular, of protein-ligand interactions is to compare inhibition values obtained for one compound toward ortholog proteins from various species, which are highly conserved in sequence and differ only in few residues. Thereby, such an approach can be a valid alternative to site-directed mutagenesis. As human and marmoset 17 β -HSD1 enzymes meet these criteria, selected human 17 β -HSD1 inhibitors were assessed for their inhibitory potencies toward marmoset 17 β -HSD1. While a species specific inhibition profile was observed in the class of the (hydroxyphenyl)naphthols, representatives of the other evaluated compound classes showed similar or even higher inhibition compared to those observed for the human enzyme. Using a combination of computational methods, including homology modeling, molecular docking, MD simulation, and binding energy calculation, a reasonable model of the three-dimensional structure of marmoset 17 β -HSD1 was developed and inhibition data were rationalized on the structural basis. In the marmoset 17 β -HSD1, residues 190 to 196 form a small α -helix, which is obviously stabilized by the presence of a proline in N-cap position (residue 191) and induces conformational changes that affect ligand binding. Furthermore energy decomposition analysis highlighted the important role of Asn152 as interaction partner for inhibitor binding.

This work could not only offer a better understanding of the active site topologies and of the protein-ligand interactions, but also provides novel structural clues that will help to design and

optimize potent human 17 β -HSD1 inhibitors with improved inhibitory potency toward marmoset 17 β -HSD1. This is an important step to turn compounds, which show a promising pharmaceutical profile, into candidates for *in vivo* evaluation. Thus, our combined computational approach could also be considered as a valuable tool to achieve this goal.

Methods

Sequence Alignment and Model Building. The amino acid sequences of rat (accession number P51657), mouse (P51656) cynomolgus (Q4JK77) and marmoset 17 β -HSD1 (Q9GME2) as well as human (P37059), cynomolgus (Q4JK76), marmoset (Q9GME5), mouse (P51658) and rat (Q62730) 17 β -HSD2 were obtained from the uniprot webpage. These sequences were pairwise aligned with human 17 β -HSD1 (PDB code: 1fdt) using MAFFT version 5 [51]. Using this alignment, a set of 100 comparative models of marmoset 17 β -HSD1 was built employing Modeller9v7 [42], with the ternary complex E1-NADPH-human 17 β -HSD1 as template. This complex resulted from docking of E1 to human 17 β -HSD1 (PDB code: 1fdtB) (see below). The best homology model was then selected according to the Modeller energy score, DOPE score [43] and PROCHECK [44] tests. The reliability of the built homology models was checked by Prosa2003 [52] (Fig. S1), ERRAT [53], and Verify3D [54] (Fig. S2).

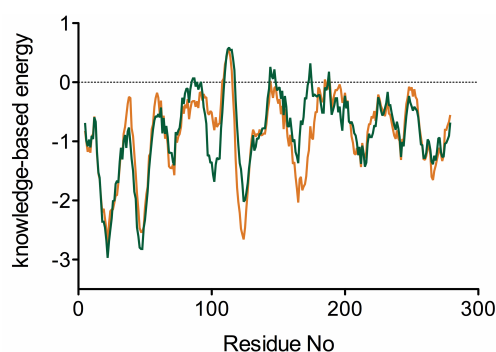


Figure S1. Energy profile drawn for the marmoset 17 β -HSD1 model using PROSA. Energy profiles of marmoset 17 β -HSD1 in complex with NADPH (orange) and of marmoset 17 β -HSD1 in complex with NADPH and E1 (green).

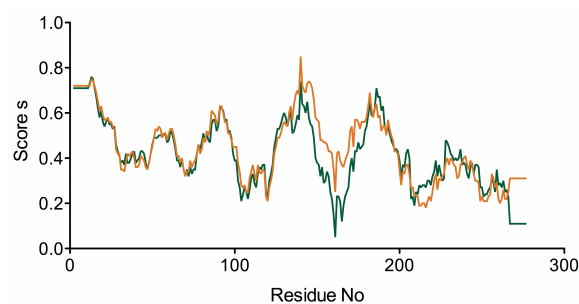


Figure S2. Verify3D results for the marmoset 17 β -HSD1 model.. Verify-3D results are shown for the secondary complex of marmoset 17 β -HSD1 (orange) with NADPH and for ternary complex (green) with NADPH and E1; residues with positive score are reasonably folded.

MD Simulations. MD simulations were performed using the AMBER 9.0 suite program [55]. The partial atomic charges for E1 and the inhibitors were derived from the molecular electrostatic potential (MEP) previously calculated using GAMESS [56], according to the RESP methodology [57]. For the protein, partial atomic charges were read from the AMBER 9.0 libraries. The AMBER99SB force field [58] was employed to define atom types and potentials for the protein, while the general AMBER force field (gaff) [59] was used to define all needed atom types and parameters for E1 and the inhibitors. For NADPH (charge -4), the parameters previously reported by Ulf Ryde were applied ().

The input files for the MD simulation were prepared with the xLEaP module of AMBER. Each system was solvated with an octahedral box of TIP3P water molecules of 10Å radius and neutralized by the addition of Na⁺ ions. Finally, for each complex the topology and the coordinate files were written and used in the MD simulations.

Before starting the production-run phase, the following equilibration protocol was applied to all systems. At the beginning the system was energy-minimized in two stages: firstly, the solvent was relaxed while all the solute atoms were harmonically restrained to their original positions with a force constant of 100 kcal mol⁻¹ Å⁻² for 1000 steps; and secondly, the whole molecular system was minimized for 2500 steps by conjugate gradient. Subsequently, the system was heated during 60 ps from 0 to 300 K at constant volume conditions (NTV, PBC conditions), and then equilibrated keeping both temperature and pressure constant (NTP, PBC conditions, 300 K, 1 atm) during 100 ps. Electrostatic interactions were computed using the Particle Mesh Ewald method [60], and the SHAKE [61] algorithm was employed to keep all bonds involving hydrogen atoms rigid. NADPH, E1 and the inhibitors were constrained during the equilibration with a force constant of 20 kcal mol⁻¹ Å⁻². After equilibration, a MD production stage (NTP, PBC conditions, 300 K, 1 atm) was performed. The total simulation length differed for the various complexes ranging from 4 to 6 ns. Distance restraints were applied to substrate/inhibitor with the aim of maintaining their proper orientation at the beginning (first ns) of production stage.

For the ternary complex of marmoset 17 β -HSD1 with E1 and NADPH, two additional distance restraints were used: between the keto-oxygen of E1 and the side chain oxygen of Ser142 (d=2.40-3.00 Å; force constant: 10 kcal mol⁻¹ Å⁻²) and between the oxygen of the OH-group in 17-position of E1 and the NE2 nitrogen of the His221 side chain (d=2.70-3.40 Å; force constant: 10 kcal mol⁻¹ Å⁻²).

For the ternary complex of human 17 β -HSD1 with 12 and NADPH, three additional distance restraints were used: between the keto-oxygen of 12 and the side chain oxygen of Tyr155 (d=2.80-3.40 Å; force constant: 10 kcal mol⁻¹ Å⁻²), between the oxygen of the OH-group in *meta*-position of 12 and the OD1 oxygen of the Asn152 side chain (d=2.70-3.30 Å; force

constant: $10 \text{ kcal mol}^{-1} \text{ \AA}^{-2}$), and between the oxygen of the *para* OH-group of 12 and the NE2 nitrogen of the His221 side chain ($d=2.70\text{-}3.30 \text{ \AA}$; force constant: $10 \text{ kcal mol}^{-1} \text{ \AA}^{-2}$).

For the ternary complex of marmoset 17 β -HSD1 with 12 and NADPH three additional distance restraints were used: between the keto-oxygen of 12 and the side chain oxygen of Ser142 ($d=2.50\text{-}3.10 \text{ \AA}$; force constant: $10 \text{ kcal mol}^{-1} \text{ \AA}^{-2}$), between the oxygen of the OH-group in *meta*-position of 1 and the OD1 oxygen of the Asn152 side chain ($d=2.40\text{-}3.00 \text{ \AA}$; force constant: $10 \text{ kcal mol}^{-1} \text{ \AA}^{-2}$), and between the oxygen of the *para* OH-group of 12 and the OD1 oxygen of the Asn282 side chain ($d=2.50\text{-}3.10 \text{ \AA}$; force constant: $10 \text{ kcal mol}^{-1} \text{ \AA}^{-2}$).

For the ternary complex of human 17 β -HSD1 with 19 and NADPH three additional distance restraints were used: between the oxygen of the OH-group in 2-position of the naphthol core and the side chain oxygen of Tyr155 ($d=2.80\text{-}3.40 \text{ \AA}$; force constant: $10 \text{ kcal mol}^{-1} \text{ \AA}^{-2}$), between the oxygen of the OH-group in *meta*-position of the phenyl ring and the NE2 nitrogen of the His221 side chain ($d=3.00\text{-}4.20 \text{ \AA}$; force constant: $10 \text{ kcal mol}^{-1} \text{ \AA}^{-2}$), and between the nitrogen of the sulfonamide moiety of 19 and the OD1 oxygen of the Asn152 side chain ($d=2.70\text{-}3.40 \text{ \AA}$; force constant: $10 \text{ kcal mol}^{-1} \text{ \AA}^{-2}$).

For the ternary complex of marmoset 17 β -HSD1 with 19 and NADPH two additional distance restraints were used: between the oxygen of the OH-group in 2-position of the naphthol core and the NE2 nitrogen of the His221 side chain ($d=2.70\text{-}3.40 \text{ \AA}$; force constant: $10 \text{ kcal mol}^{-1} \text{ \AA}^{-2}$) and between the oxygen of the OH-group in *meta*-position of the phenyl ring of 19 and the backbone carbonyl oxygen of Cys185 ($d=2.40\text{-}3.00 \text{ \AA}$; force constant: $10 \text{ kcal mol}^{-1} \text{ \AA}^{-2}$).

Trajectories were analyzed using the AMBER ptraj module, the MMTSB toolset [62] and the molecular visualization program VMD (Visual Molecular Dynamics) [63]. The resulting low energy structures were extracted for the homology model (apoforn and ternary complex) and subjected to a subsequent minimization of 1000 steps (500 steps of steepest descent followed by 500 steps of conjugate gradient), using the sander module of AMBER. The modified generalized Born solvation model (IGB=2) [64] was used. Active site volumes of low energy structures were calculated using the CASTp [45].

Molecular docking. The three-dimensional structures used for docking studies were either retrieved from the PDB (1fdt, conformation B for residues 187-200) or from the homology modelling with subsequent MD simulation (equilibrated ternary complex after 5537 ps). The cocrystallized E2 and water molecules were removed from the PDB file. Hydrogen atoms and neutral end groups were added, NADP⁺ was turned into NADPH and correct atom types were set. Ionization states and hydrogen positions were assigned using the Protonate 3D utility of MOE2009.10 (Chemical Computing Group Inc., Montreal, Canada). Ligand structures were built in MOE and RESP charges were assigned as described above. The 17 β -HSD1 three-dimensional structures and ligand structures were prepared for docking studies through the graphical user interface AutoDockTools4 [46]. For the ligands, non-polar hydrogen atoms were

deleted, rotatable bonds were defined and RESP charges were kept. For the protein, non-polar hydrogen atoms were deleted and charges were added to the structure. Autodock4.2 [46] was used to dock the ligands in the steroidal binding site of the processed protein structures. A box, centered on the steroid-binding site, was set to define the docking area. Grid points of 90 x 90 x 90 with 0.250 Å spacing were calculated around the docking area for all the ligand atom types using AutoGrid4.2. For each inhibitor, 50 separate docking calculations were performed. Each docking calculation consisted of 25×10^5 energy evaluations using the Lamarckian genetic algorithm local search (GALS) method. Each docking run was performed with a population size of 250. A mutation rate of 0.02 and a crossover rate of 0.8 were used to generate new docking trials for subsequent generations. The docking results from each of the 50 calculations were clustered on the basis of root-mean-square deviation (RMSD = 2.0 Å) between the Cartesian coordinates of the ligand atoms and were ranked on the basis of the free binding energy.

Free energy calculations using the MM/PBSA method. The calculation of binding free energy was evaluated using the MM/PBSA (Molecular Mechanics/ Poisson Boltzmann Surface Area) method as implemented in AMBER11 [65]. The electronic and Van der Waals energies were calculated using the sander module in AMBER11. The solvation free energy contributions may be further decomposed into an electrostatic and hydrophobic contribution. The electrostatic portion is calculated using the linearized PB equation. The hydrophobic contribution is approximated by the LCPO method [66] implemented within sander. The changes in entropy upon ligand association ΔS are estimated by normal mode analysis. For stable plateaus of the MD trajectories, snapshots were collected every 20th frame (every 20 ps) and used to calculate relative binding affinity (ΔG_{bind}) and absolute free energy (ΔG).

Energy decomposition using the MM/GBSA method. A free energy decomposition of the protein ligand complexes was performed on a pairwise per-residue basis using the MM/GBSA (Molecular Mechanics/ Generalized Born Surface Area) method as implemented in AMBER11. The GBSA implicit-solvent solvation model was used in order to avoid the retarding effect of the PBSA method.

Inhibition assay. [2, 4, 6, 7-³H]-E1 and [2, 4, 6, 7-³H]-E2 were bought from Perkin Elmer, Boston. Quickszint Flow 302 scintillator fluid was bought from Zinsser Analytic, Frankfurt. Marmoset 17 β -HSD1 and 17 β -HSD2 were obtained from marmoset placenta according to previously described procedures [41]. Fresh marmoset placenta was homogenized and cytosolic and microsomal fractions were separated by centrifugation. For the partial purification of 17 β -HSD1, the cytosolic fraction was precipitated with ammonium sulfate. 17 β -HSD2 was obtained from the microsomal fraction.

Inhibition of 17 β -HSD1: Inhibitory activities were evaluated by an established method with minor modifications [41]. Briefly, the enzyme preparation was incubated with NADH [500 μ M] in the presence of potential inhibitors at 37 °C in a phosphate buffer (50 mM)

supplemented with 20 % of glycerol and EDTA (1 mM). Inhibitor stock solutions were prepared in DMSO. The final concentration of DMSO was adjusted to 1 % in all samples. The enzymatic reaction was started by addition of a mixture of unlabelled- and [2, 4, 6, 7-³H]-E1 (final concentration: 500 nM, 0.15 μ Ci). After 10 min, the reaction was stopped by the addition of HgCl₂ (10 mM) and the mixture was extracted with diethylether. After evaporation, the steroids were dissolved in acetonitrile. E1 and E2 were separated using acetonitrile/water (45:55) as mobile phase in a C18 reverse phase chromatography column (Nucleodur C18 Gravity, 3 μ m, Macherey-Nagel, Düren) connected to an HPLC-system (Agilent 1200 Series, Agilent Technologies, Waldbronn). Detection and quantification of the steroids were performed using a radioflow detector (Agilent 1200 Series, Agilent Technologies, Waldbronn). The conversion rate was calculated after analysis of the resulting chromatograms according to the following equation: $\%conversion = \frac{\%E2}{\%E2 + \%E1} \times 100$. Each value was calculated from at least three independent experiments.

Inhibition of 17 β -HSD2: The 17 β -HSD2 inhibition assay was performed similarly to the 17 β -HSD1 procedure. The microsomal fraction was incubated with NAD⁺ [1500 μ M], test compound and a mixture of unlabelled- and [2, 4, 6, 7-³H]-E2 (final concentration: 500 nM, 0.11 μ Ci) for 20 min at 37 °C. Further treatment of the samples and HPLC separation was carried out as mentioned above. The conversion rate was calculated after analysis of the resulting chromatograms according to the following equation: $\%conversion = \frac{\%E1}{\%E1 + \%E2} \times 100$.

Acknowledgement

We thank Prof. Dr. Rolf W. Hartmann for helpful discussion and Prof. Dr. Almuth Einspanier for providing marmoset placenta

References

1. Poutanen M, Isomaa V, Peltoketo H, Vihko R (1995) Role of 17 beta-hydroxysteroid dehydrogenase type 1 in endocrine and intracrine estradiol biosynthesis. *J Steroid Biochem Mol Biol* 55: 525-532.
2. Travis RC, Key TJ (2003) Oestrogen exposure and breast cancer risk. *Breast Cancer Res* 5: 239-247.
3. Dizerega GS, Barber DL, Hodgen GD (1980) Endometriosis: role of ovarian steroids in initiation, maintenance and suppression. *Fertil Steril* 33: 649-653.
4. Saloniemi T, Jarvensivu P, Koskimies P, Jokela H, Lamminen T, et al. (2010) Novel Hydroxysteroid (17 β) Dehydrogenase 1 Inhibitors Reverse Estrogen-Induced Endometrial Hyperplasia in Transgenic Mice. *Am J Pathol* 176: 1443-1451.
5. Gobbi S, Cavalli A, Rampa A, Belluti F, Piazzzi L, et al. (2006) Lead optimization providing a series of flavone derivatives as potent nonsteroidal inhibitors of the cytochrome P450 aromatase enzyme. *J Med Chem* 49: 4777-4780.
6. Cavalli A, Bisi A, Bertucci C, Rosini C, Paluszczak A, et al. (2005) Enantioselective nonsteroidal aromatase inhibitors identified through a multidisciplinary medicinal chemistry approach. *J Med Chem* 48: 7282-7289.

7. Leonetti F, Favia A, Rao A, Aliano R, Paluszczak A, et al. (2004) Design, synthesis, and 3D QSAR of novel potent and selective aromatase inhibitors. *J Med Chem* 47: 6792-6803.
8. Aggarwal S, Thareja S, Verma A, Bhardwaj T, Kumar M (2010) An overview on 5 α -reductase inhibitors. *Steroids* 75: 109-153.
9. Picard F, Schulz T, Hartmann RW (2002) 5-Phenyl substituted 1-methyl-2-pyridones and 4'-substituted biphenyl-4-carboxylic acids. synthesis and evaluation as inhibitors of steroid-5 α -reductase type 1 and 2. *Bioorg Med Chem* 10: 437-448.
10. Baston E, Hartmann RW (1999) N-substituted 4-(5-indolyl)benzoic acids. Synthesis and evaluation of steroid 5 α -reductase type I and II inhibitory activity. *Bioorg Med Chem Lett* 9: 1601-1606.
11. Baston E, Paluszczak A, Hartmann RW (2000) 6-Substituted 1H-quinolin-2-ones and 2-methoxy-quinolines: synthesis and evaluation as inhibitors of steroid 5 α reductases types 1 and 2. *Eur J Med Chem* 35: 931-940.
12. Wetzel M, Marchais-Oberwinkler S, Hartmann RW (2011) 17 β -HSD2 inhibitors for the treatment of osteoporosis: Identification of a promising scaffold. *Bioorg Med Chem* 19: 807-815.
13. Jörnvall H, Persson B, Krook M, Atrian S, Gonzalez-Duarte R, et al. (1995) Short-chain dehydrogenases/reductases (SDR). *Biochemistry* 34: 6003-6013.
14. Peltoketo H, Isomaa V, Mäentausta O, Viiko R (1988) Complete amino acid sequence of human placental 17 beta-hydroxysteroid dehydrogenase deduced from cDNA. *FEBS Lett* 239: 73-77.
15. Ghosh D, Pletnev VZ, Zhu DW, Wawrzak Z, Duax WL, et al. (1995) Structure of human estrogenic 17beta-hydroxysteroid dehydrogenase at 2.20 Å resolution. *Structure* 3: 503-513.
16. Filling C, Berndt KD, Benach J, Knapp S, Prozorovski T, et al. (2002) Critical residues for structure and catalysis in short-chain dehydrogenase/reductase. *J Biol Chem* 277: 25677-25684.
17. Azzi A, Rehse PH, Zhu DW, Campbell RL, Labrie F, et al. (1996) Crystal structure of human estrogenic 17beta-hydroxysteroid dehydrogenase complexed with 17 beta-estradiol. *Nat Struct Biol* 3: 665-668.
18. Marchais-Oberwinkler S, Henn C, Möller G, Klein T, Negri M, et al. (2010) 17 β -Hydroxysteroid dehydrogenases (17 β -HSDs) as therapeutic targets: Protein structures, functions and recent progress in inhibitor development. *J Steroid Biochem Mol Biol* 125: 66-82 and references therein cited.
19. Mazumdar M, Chen J, Lin SX Molecular basis of sex-steroid translation. PDB ID: 3km0.
20. Mazumdar M, Chen J, Lin SX Molecular basis of sex-steroids: thier translational activity. PDB ID: 3klp.
21. Negri M, Recanatini M, Hartmann RW (2010) Insights in 17 β -HSD1 Enzyme Kinetics and Ligand Binding by Dynamic Motion Investigation. *PLoS ONE* 5: e12026.
22. Brožić P, Lanišnik Rižner T, Gobec S (2008) Inhibitors of 17beta-hydroxysteroid dehydrogenase type 1. *Curr Med Chem* 15: 137-150 and references therein cited.
23. Poirier D (2009) Advances in development of inhibitors of 17beta hydroxysteroid dehydrogenases. *Anticancer Agents Med Chem* 9: 642-660.
24. Day JM, Tutill HJ, Purohit A (2010) 17 β -Hydroxysteroid dehydrogenase inhibitors. *Minerva Endocrinol* 35: 87-108.
25. Day JM, Tutill HJ, Purohit A, Reed MJ (2008) Design and validation of specific inhibitors of 17beta-hydroxysteroid dehydrogenases for therapeutic application in breast and prostate cancer, and in endometriosis. *Endocr Relat Cancer* 15: 665-692.
26. Messinger J, Hirvelä L, Husen B, Kangas L, Koskimies P, et al. (2006) New inhibitors of 17beta-hydroxysteroid dehydrogenase type 1. *Mol Cell Endocrinol* 248: 192-198.
27. Karkola S, Lilienkamp A, Wähälä K (2008) A 3D QSAR model of 17beta-HSD1 inhibitors based on a thieno[2,3-d]pyrimidin-4(3H)-one core applying molecular dynamics simulations and ligand-protein docking. *ChemMedChem* 3: 461-472.

28. Frotscher M, Ziegler E, Marchais-Oberwinkler S, Kruchten P, Neugebauer A, et al. (2008) Design, synthesis, and biological evaluation of (hydroxyphenyl)naphthalene and -quinoline derivatives: potent and selective nonsteroidal inhibitors of 17 β -hydroxysteroid dehydrogenase type 1 (17 β -HSD1) for the treatment of estrogen-dependent diseases. *J Med Chem* 51: 2158-2169.
29. Marchais-Oberwinkler S, Frotscher M, Ziegler E, Werth R, Kruchten P, et al. (2009) Structure-activity study in the class of 6-(3'-hydroxyphenyl)naphthalenes leading to an optimization of a pharmacophore model for 17 β -hydroxysteroid dehydrogenase type 1 (17 β -HSD1) inhibitors. *Mol Cell Endocrinol* 301: 205-211.
30. Marchais-Oberwinkler S, Kruchten P, Frotscher M, Ziegler E, Neugebauer A, et al. (2008) Substituted 6-phenyl-2-naphthols. Potent and selective nonsteroidal inhibitors of 17 β -hydroxysteroid dehydrogenase type 1 (17 β -HSD1): design, synthesis, biological evaluation, and pharmacokinetics. *J Med Chem* 51: 4685-4698.
31. Marchais-Oberwinkler S, Wetzel M, Ziegler E, Kruchten P, Werth R, et al. (2011) New Drug-Like Hydroxyphenylnaphthol Steroidomimetics As Potent and Selective 17 β -Hydroxysteroid Dehydrogenase Type 1 Inhibitors for the Treatment of Estrogen-Dependent Diseases. *J Med Chem* 54: 534-547.
32. Bey E, Marchais-Oberwinkler S, Kruchten P, Frotscher M, Werth R, et al. (2008) Design, synthesis and biological evaluation of bis (hydroxyphenyl) azoles as potent and selective non-steroidal inhibitors of 17 β -hydroxysteroid dehydrogenase type 1 (17 β -HSD1) for the treatment of estrogen-dependent diseases. *Bioorg Med Chem* 16: 6423-6435.
33. Bey E, Marchais-Oberwinkler S, Negri M, Kruchten P, Oster A, et al. (2009) New Insights into the SAR and Binding Modes of Bis(hydroxyphenyl)thiophenes and -benzenes: Influence of Additional Substituents on 17 β -Hydroxysteroid Dehydrogenase Type 1 (17 β -HSD1) Inhibitory Activity and Selectivity. *J Med Chem* 52: 6724-6743.
34. Bey E, Marchais-Oberwinkler S, Werth R, Negri M, Al-Soud YA, et al. (2008) Design, synthesis, biological evaluation and pharmacokinetics of bis(hydroxyphenyl) substituted azoles, thiophenes, benzenes, and aza-benzenes as potent and selective nonsteroidal inhibitors of 17 β -hydroxysteroid dehydrogenase type 1 (17 β -HSD1). *J Med Chem* 51: 6725-6739.
35. Oster A, Hinsberger S, Werth R, Marchais-Oberwinkler S, Frotscher M, et al. (2010) Bicyclic Substituted Hydroxyphenylmethanones as Novel Inhibitors of 17 β -Hydroxysteroid Dehydrogenase Type 1 (17 β -HSD1) for the Treatment of Estrogen-Dependent Diseases. *J Med Chem* 53: 8176-8186.
36. Oster A, Klein T, Henn C, Werth R, Marchais-Oberwinkler S, et al. (2011) Bicyclic Substituted Hydroxyphenylmethanone Type Inhibitors of 17 β -Hydroxysteroid Dehydrogenase Type 1 (17 β -HSD1): The Role of the Bicyclic Moiety. *ChemMedChem* 6: 476-487.
37. Oster A, Klein T, Werth R, Kruchten P, Bey E, et al. (2010) Novel estrone mimetics with high 17 β -HSD1 inhibitory activity. *Bioorg Med Chem* 18: 3494-3505.
38. Negri M, Recanatini M, Hartmann RW (2011) Computational investigation of the binding mode of bis(hydroxyphenyl)arenes in 17 β -HSD1: molecular dynamics simulations, free energy calculations, and molecular electrostatic potential maps. *J Comput Aided Mol Des*: submitted.
39. Möller G, Husen B, Kowalik D, Hirvelä L, Plewczynski D, et al. (2010) Species Used for Drug Testing Reveal Different Inhibition Susceptibility for 17 β -Hydroxysteroid Dehydrogenase Type 1. *PLoS ONE* 5: e10969.
40. Kruchten P, Werth R, Marchais-Oberwinkler S, Bey E, Ziegler E, et al. (2009) Development of biological assays for the identification of selective inhibitors of estradiol formation from estrone in rat liver preparations. *C R Chim* 12: 1110-1116.
41. Kruchten P, Werth R, Marchais-Oberwinkler S, Frotscher M, Hartmann RW (2009) Development of a biological screening system for the evaluation of highly active and selective 17 β -HSD1-inhibitors as potential therapeutic agents. *Mol Cell Endocrinol* 301: 154-157.

42. Sali A, Blundell TL (1993) Comparative protein modelling by satisfaction of spatial restraints. *J Mol Biol* 234: 779-815.
43. Shen M-Y, Sali A (2006) Statistical potential for assessment and prediction of protein structures. *Protein Sci* 15: 2507-2524.
44. Laskowski RA, MacArthur MW, Moss DS, Thornton JM (1993) PROCHECK: a program to check the stereochemical quality of protein structures. *J App Cryst* 26: 283-291.
45. Dundas J, Ouyang Z, Tseng J, Binkowski A, Turpaz Y, et al. (2006) CASTp: computed atlas of surface topography of proteins with structural and topographical mapping of functionally annotated residues. *Nucleic Acids Res* 34: W116-118.
46. Morris GM, Huey R, Lindstrom W, Sanner MF, Belew RK, et al. (2009) AutoDock4 and AutoDockTools4: Automated Docking with Selective Receptor Flexibility. *J Comput Chem* 30: 2785-2791.
47. Richardson JS, Richardson DC (1988) Amino acid preferences for specific locations at the ends of alpha helices. *Science* 240: 1648-1652.
48. Kumar S, Bansal M (1998) Dissecting alpha-helices: position-specific analysis of alpha-helices in globular proteins. *Proteins* 31: 460-476.
49. Lilienkamp A, Karkola S, Alho-Richmond S, Koskimies P, Johansson N, et al. (2009) Synthesis and biological evaluation of 17 β -hydroxysteroid dehydrogenase type 1 (17 β -HSD1) inhibitors based on a thieno[2,3-d]pyrimidin-4(3H)-one core. *J Med Chem* 52: 6660-6671.
50. Messinger J, Husen B, Koskimies P, Hirvelä L, Kallio L, et al. (2009) Estrone C15 derivatives--a new class of 17 β -hydroxysteroid dehydrogenase type 1 inhibitors. *Mol Cell Endocrinol* 301: 216-224.
51. Katoh K, Kuma K, Toh H, Miyata T (2005) MAFFT version 5: improvement in accuracy of multiple sequence alignment. *Nucleic Acids Res* 33: 511-518.
52. Sippl MJ (1993) Recognition of errors in three-dimensional structures of proteins. *Proteins* 17: 355-362.
53. Colovos C, Yeates TO (1993) Verification of protein structures: patterns of nonbonded atomic interactions. *Protein Sci* 2: 1511-1519.
54. Lüthy R, Bowie JU, Eisenberg D (1992) Assessment of protein models with three-dimensional profiles. *Nature* 356: 83-85.
55. Case D, Darden T, Cheatham T, III, Simmerling C, et al. (2006) AMBER 9. University of California, San Francisco.
56. Schmidt M, Baldrige K, Boatz J, Elbert S, Gordon M, et al. (1993) General atomic and molecular electronic structure system. *J Comput Chem* 14: 1347-1363.
57. Bayly CI, Cieplak P, Cornell WD, Kollman PA (1993) A well behaved electrostatic potential based method using charge restraints for determining atom-centered charges: the RESP model. *J Phys Chem* 97: 10269-10280.
58. Hornak V, Abel R, Okur A, Strockbine B, Roitberg A, et al. (2006) Comparison of multiple Amber force fields and development of improved protein backbone parameters. *Proteins* 65: 712-725.
59. Wang J, Wolf RM, Caldwell JW, Kollman PA, Case DA (2004) Development and testing of a general amber force field. *J Comput Chem* 25: 1157-1174.
60. Darden T, Perera L, Li L, Pedersen L (1999) New tricks for modelers from the crystallography toolkit: the particle mesh Ewald algorithm and its use in nucleic acid simulations. *Structure* 7: R55-60.
61. Ryckaert J-P, Ciccotti G, Berendsen HJC (1977) Numerical integration of the cartesian equations of motion of a system with constraints: molecular dynamics of n-alkanes. *J Comput Phys* 23: 327-341.
62. Feig M, Karanicolas J, Brooks CL (2004) MMTSB Tool Set: enhanced sampling and multiscale modeling methods for applications in structural biology. *J Mol Graph Model* 22: 377-395.
63. Humphrey W, Dalke A, Schulten K (1996) VMD: visual molecular dynamics. *J Mol Graph* 14: 33-38.

64. Onufriev A, Bashford D, Case DA (2004) Exploring protein native states and large-scale conformational changes with a modified generalized born model. *Proteins* 55: 383-394.
65. Kollman PA, Massova I, Reyes C, Kuhn B, Huo S, et al. (2000) Calculating structures and free energies of complex molecules: combining molecular mechanics and continuum models. *Acc Chem Res* 33: 889-897.
66. Weiser J, Shenkin PS, Still WC (1999) Approximate solvent-accessible surface areas from tetrahedrally directed neighbor densities. *Biopolymers* 50: 373-380.

3.4 Bicyclic Substituted Hydroxyphenylmethanone Type Inhibitors of 17 β -Hydroxysteroid Dehydrogenase Type 1 (17 β -HSD1): The Role of the Bicyclic Moiety

Alexander Oster, **Tobias Klein**, Claudia Henn, Ruth Werth, Sandrine Marchais-Oberwinkler, Martin Frotscher, Rolf W. Hartmann

Reprinted with permission from *ChemMedChem* **2011**, 6, 476-487.

Copyright: © 2011 Wiley.

Publication IV

Abstract: An attractive target, that has still to be explored for the treatment of estrogen-dependent diseases, such as breast cancer and endometriosis, is the enzyme responsible for the last step in the biosynthesis of estradiol (E2): 17 β -hydroxysteroid dehydrogenase type 1 (17 β -HSD1). It catalyzes the reduction of the weakly active estrone (E1) into E2, which is the most potent estrogen in humans. Inhibition of 17 β -HSD1 lowers intracellular E2 concentrations and thus presents a therapy option for estrogen-dependent pathologies. Recently, we have reported on a new class of highly active and selective 17 β -HSD1 inhibitors: bicyclic substituted hydroxyphenylmethanones. Here, further structural variations on the bicyclic moiety were performed, especially focusing on the exchange of its OH-function. Twenty-nine novel inhibitors were synthesized and evaluated for 17 β -HSD1 inhibition in a cell-free and cellular assay, for selectivity toward 17 β -HSD2 and estrogen receptors (ER) α and β as well as for metabolic stability. Compound **23** turned out to be the best compound of this study with excellent IC₅₀-values of 12 nM in the cell-free assay and 78 nM in the cellular assay, a high selectivity, and a reasonable stability. A molecular docking study provided insight into the protein-ligand interactions of **23**.

Introduction

17 β -Hydroxysteroid dehydrogenases (17 β -HSDs) are responsible for the oxido-reduction reactions of steroid hormones at the 17 position, especially for estrogens and androgens, and use subtype-specifically NADPH (in case of 17 β -HSD1) or NAD⁺ (17 β -HSD2) as cofactors. Although these are reversible reactions, under in vivo conditions the catalysis is unidirectional due to the fact that NADP⁺ is abundant in its reduced form, whereas NAD⁺ is mainly present in its oxidized form.^[1] 17 β -HSDs catalyze the conversion of hormones with high receptor affinity to the corresponding low affinity forms and *vice versa*. They are expressed in the gonads and show characteristic expression patterns in peripheral tissues.^[2] Therefore 17 β -HSDs play a pivotal role in the local regulation of hormone levels.^[2] In addition to their individual tissue and subcellular distributions, they also differ in their substrate specificities.^[3,4]

17 β -HSD1 is the most extensively characterized 17 β -HSD subtype. It catalyzes the last step in the biosynthesis of the highly active estrogen 17 β -estradiol (E2): the reduction of the weakly active estrone (E1; Figure 1).

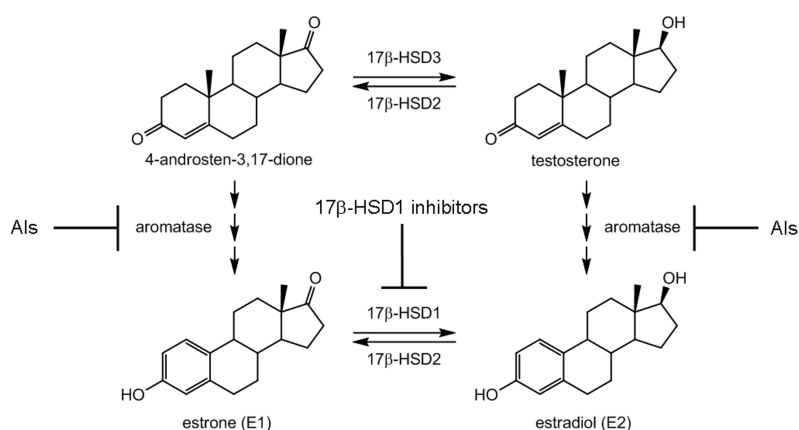


Figure 1. Intervention of AIs and 17 β -HSD1 inhibitors in the estrogen synthesis.

It is well known that E2, the natural ligand of the estrogen receptors α and β (ER α and ER β), has a high impact on the development and progression of estrogen-dependent diseases, such as breast cancer, endometriosis, and endometrial hyperplasia.^[5-7] Reduction of estrogen levels by interference with E2 biosynthesis has been used as a treatment of ER-positive postmenopausal breast cancer for almost thirty years. Up to now, aromatase inhibitors (AIs) are the first-line therapeutics for these patients.^[8,9] In the past few years, AIs have been intensively investigated.^[10-15] However, inhibition of E2 synthesis by AIs does not affect the last but only the penultimate step. It results in a strong reduction of estrogen levels in the whole body leading to unwanted side effects. Therefore, intracellular regulation of estrogen levels in the diseased tissues by 17 β -HSD1 is a promising therapeutic approach for the treatment of estrogen-dependent diseases. An analogous concept has already been proved successful for the treatment

of androgen-dependent diseases, such as benign prostatic hyperplasia and alopecia, by using 5 α -reductase inhibitors.^[16–19] Proof-of-concept for the treatment of breast cancer was performed in different mouse models.^[20–22] However, no 17 β -HSD1 inhibitor has reached clinical trials so far. Furthermore, inhibition of 17 β -HSD1 could have an additional antitumor effect, because it is also involved in the metabolism of retinoic acid,^[23,24] a natural compound known to have tumor inhibiting activity.^[25] As the therapeutic efficacy of 17 β -HSD1 inhibitors should not be counteracted, selectivity towards 17 β -hydroxysteroid dehydrogenase type 2 (17 β -HSD2) is required. This enzyme catalyzes the reverse reaction - oxidation of E2 into E1. Additionally, for reducing the risk of intrinsic estrogenic effects, affinity of the inhibitors to the ERs should be avoided.

In recent years, the structural architecture of 17 β -HSD1 has been investigated and numerous crystallographic data have been determined^[24] and assigned to the different steps of the catalytic cycle.^[26] Several, mostly steroidal, compounds have already been published as 17 β -HSD1 inhibitors,^[24,27–30] using this information. With regards to nonsteroidal inhibitors, there are three compound classes with IC₅₀ values in the low nanomolar range described: thiophenepyrimidinones,^[31,32] hydroxyphenyl-naphthols,^[33–36] and bis(hydroxyphenyl)heterocycles.^[37–41] Recently, we reported bicyclic substituted hydroxyphenylmethanones as a new class of 17 β -HSD1 inhibitors (Figure 2A).^[42]

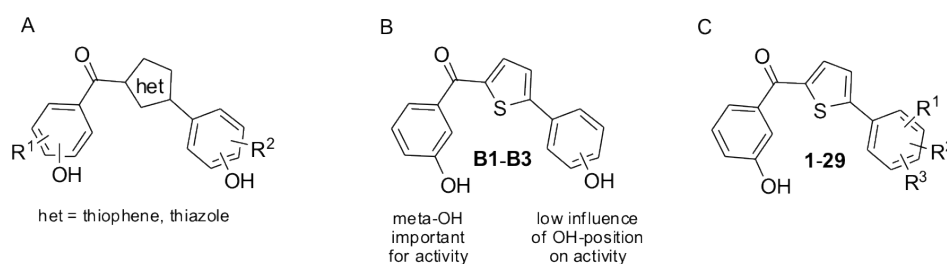


Figure 2. Bicyclic substituted hydroxyphenylmethanones as inhibitors of 17 β -HSD1

These inhibitors also show a very promising biological profile. As the hydroxy function on the benzoyl part is more important for inhibitory activity (Figure 2B), replacement of the phenyl OH group was regarded as an appropriate modification to gain further interactions and to avoid possible phase II metabolism in this position.^[43]

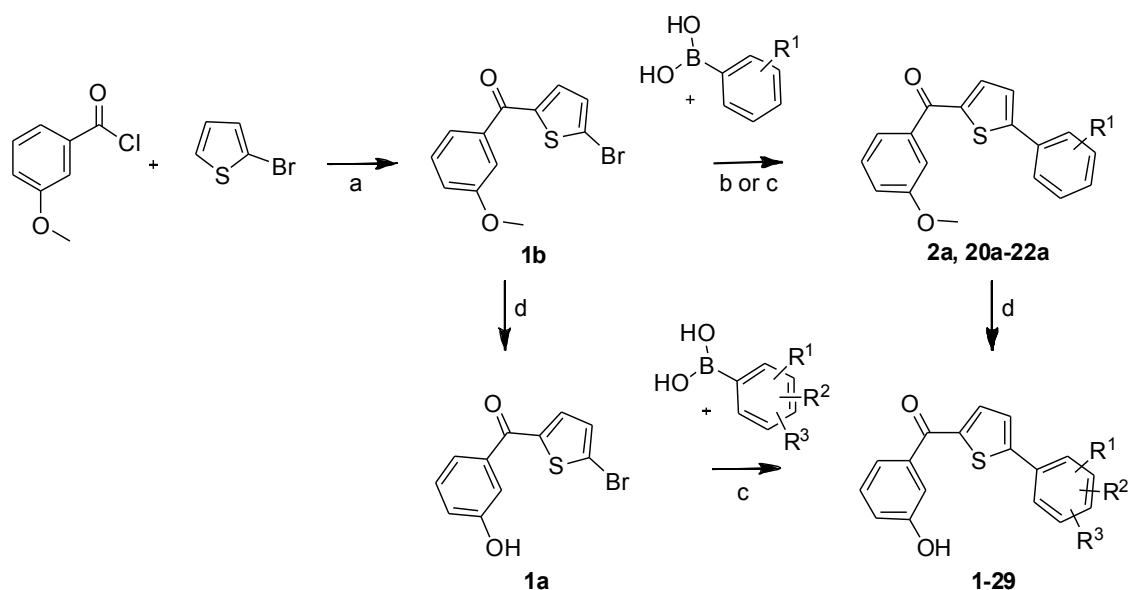
Herein, we report the replacement of the hydroxy group of the phenyl ring adjacent to the thiophene in bicyclic substituted hydroxyphenyl methanones. In order to evaluate whether it is possible to achieve additional interactions in the C-terminal region of the target enzyme, various substituents were introduced. Synthesis, biological evaluation and structure–activity relationships (SAR) of new highly potent and selective 17 β -HSD1 inhibitors are described. Furthermore, the probable binding mode of the most potent compound was investigated by molecular docking studies to explain the SAR obtained.

Design

Binding mode investigations of three potent compounds of this class (**B1–B3**) revealed a steroid-like binding mode with the benzoyl moiety occupying an apolar subpocket, previously described to have an impact on ligand binding.^[44,45] The phenyl ring adjacent to the thiophene was found to mimic the steroidal A ring binding in the C-terminal region of the protein. It is known that there is space for additional substituents in this region since several highly active steroidal inhibitors have extensions in position 2.^[46] The most potent inhibitors of these derivatives bear an additional phenyl ring connected by a C2 linker.^[46] Thus, the expected steroid-like binding mode of **B1–B3** prompted us to further investigate this C-terminal region by exchanging the phenyl hydroxy group.

Results

Chemistry. The synthesis of compounds **1–29** is depicted in Scheme 1. The methoxylated intermediate **1b** was synthesized via Friedel-Crafts-acylation of 2-bromothiophene with 3-methoxybenzoyl chloride using aluminium chloride. The methoxy function was cleaved according to method B (BBr_3 , CH_2Cl_2 , $-78\text{ }^\circ\text{C}$ to rt, 18 h)^[47] to yield compound **1a** in quantitative yields.



Scheme 1. Synthesis of compounds **1–29**. Reagents and conditions: a) AlCl_3 , anhydrous CH_2Cl_2 , $0\text{ }^\circ\text{C}$, 0.5 h followed by rt, 1 h for compound **1b**; b) Cs_2CO_3 , $\text{Pd}(\text{PPh}_3)_4$, $\text{DME}/\text{EtOH}/\text{water}$ (1:1:1), microwave conditions (150 W, 15 bar, $150\text{ }^\circ\text{C}$, 15 min) for compound **2a**; c) Cs_2CO_3 , $\text{Pd}(\text{PPh}_3)_4$, DME/water (1:1) reflux, 4 h for compounds **20a–22a** and **29** (Method A2) and 2 h for compounds **1**, **3–19** and **23–28** (Method A1); d) Method B: BBr_3 , CH_2Cl_2 , $-78\text{ }^\circ\text{C}$, 18 h for compounds **1a**, **2** and **20–22**.

Starting from these brominated key intermediates **1a** and **1b** and the appropriate commercially available boronic acids, Suzuki cross coupling reactions^[48] were carried out using two different

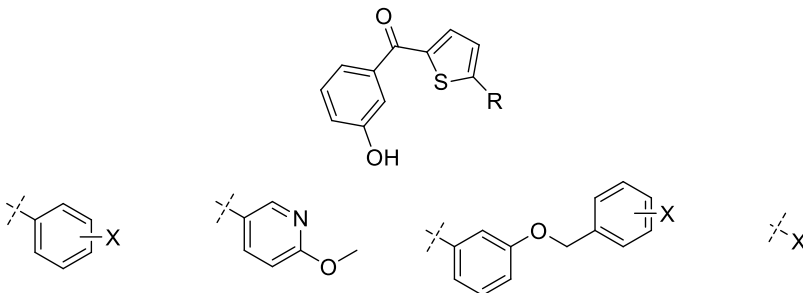
methods. Compound **2a** was prepared in a one-pot synthesis by means of microwave assisted Suzuki reaction (Cs₂CO₃, DME/EtOH/water (1:1:1), Pd(PPh₃)₄, MW (150 W, 150 °C, 15 bar 15 min)).^[38] All other compounds were prepared following method A. Using DME/water (1:1) as solvent, caesium carbonate and Pd(PPh₃)₄ as catalyst, the reaction mixtures were stirred under reflux either for 2 h (method A1; **1**, **3-19** and **23-28**) or for 4 h (method A2; **20a-22a** and **29**). Demethylation of **2a**, sulfonamide derivatives **21** and **22** and nitrile **20** was performed using method B (BBr₃, CH₂Cl₂, -78 °C to rt, 18 h).

Activity: Inhibition of human 17 β -HSD1. Human placenta was used as enzyme source and partially purified following a described procedure.^[49] Tritiated E1 was incubated with 17 β -HSD1, cofactor and inhibitor. The separation of substrate and product was performed by HPLC. The inhibition values of compounds **1-29** are shown in Table 1.

Compound **1**, lacking the OH-function on the phenyl ring, showed an inhibitory activity, which is slightly weaker than the activities of the hydroxylated compounds **B1-B3**. As compound **2** (*ortho*-methoxy) and **3** (*meta*-methoxy) revealed remarkable IC₅₀ values around 90 nM, it became apparent that a hydrogen-bond donor is beneficial (**B1-B3**)^[42] but not necessarily needed in this region for inhibitory potency. The *ortho*- and *meta*-ethoxy-compounds **9** and **10**, respectively, exhibited similar 17 β -HSD1 inhibition as their corresponding methoxy-derivatives **2** and **3** indicating that there is some space for further substituents. The good inhibitory activity of **12** (IC₅₀ = 62 nM) indicates the presence of additional space, which was further investigated by the introduction of substituents on each position of the benzyloxy-moiety (**13-19**).

While the introduction of a carbonitrile in the *meta* position adjacent to the thiophene (**20**, IC₅₀ = 225 nM) or methanesulfonamide group (**21**, IC₅₀ = 150 nM; **22**, IC₅₀ = 125 nM) did not induce significant changes in enzyme inhibition compared to the unsubstituted compound **1** (IC₅₀ = 155 nM), the methylbenzenesulfonamide **23** was clearly more potent and exhibited the highest 17 β -HSD1 inhibitory activity (IC₅₀ = 12 nM) in this study similar to those obtained in the previous study **B1-B3**.^[42]

Compared to compound **1** (IC₅₀ = 155 nM), the naphthalene-substituted derivative **24** showed a slight drop of activity (IC₅₀ = 300 nM). Introduction of a dihydrobenzofuran moiety (**25**), which represents a rigidification of the ethoxy-substituent of compound **11** (IC₅₀ = 498 nM), led to increased inhibition values (IC₅₀ = 55 nM). Obviously, rigidified systems are more appropriate for inhibitory activity in this position of the molecule indicating a sterical hindrance for larger substituents in *para*-position. This observation was confirmed by comparing compounds **6** and **26**; by replacing the two methoxy-functions (**6**) with an acetale (**26**), the weak inhibition (44 % at 1 μ M) could be increased to an IC₅₀-value of 66 nM.

Table 1. Inhibition of human 17 β -HSD1 and 17 β -HSD2 by compounds 1-29


Compd.	X	IC ₅₀ [nM] ^[a]		selectivity factor ^[d]
		17 β -HSD1 ^[b]	17 β -HSD2 ^[c]	
B1	2-hydroxy	95	18	0.2
B2	3-hydroxy	22	109	5
B3	4-hydroxy	33	478	14
1	H	155	128	0.8
2	2-methoxy	86	196	2
3	3-methoxy	95	342	4
4	4-methoxy	220	507	2
5		510	1036	2
6	3,4-dimethoxy	44 % ^[e]	44 % ^[e]	
7	3,4,5-trimethoxy	54 % ^[e]	26 % ^[e]	
8	2,3,4-trimethoxy	515	915	2
9	2-ethoxy	94	195	2
10	3-ethoxy	78	502	6
11	4-ethoxy	498	586	1
12	H	62	797	13
13	2-methoxy	35	1065	30
14	3-methoxy	47	768	16
15	4-methoxy	60	702	12
16	3,5-dimethoxy	31	789	26
17	2-chloro	54	1197	22
18	3-chloro	40	1034	26
19	4-chloro	36	1003	28
20	3-nitrile	225	354	2
21	3-methanesulfonamide	150	563	4
22	<i>N</i> -methylmethanesulfonamide	125	559	4
23	3-(4-methylbenzenesulfonamide)	12	169	14
24	2-naphthalene	300	253	0.8
25	5-(2,3-dihydrobenzofurane)	55	319	6
26	5-(1,3-benzodioxol)	66	299	5
27	5-indole	151	173	1
28	6-indole	192	283	2
29	6-indazole	107	410	4

[a] Mean value of three determinations, standard deviation less than 26 %; [b] Human placenta, cytosolic fraction, substrate E1, 500 nM, cofactor NADH, 500 μ M; [c] Human placenta, microsomal fraction, substrate E2, 500 nM, cofactor NAD⁺, 1500 μ M; [d] IC₅₀ (17 β -HSD2) / IC₅₀ (17 β -HSD1); [e] inhibition at 1 μ M (inhibitor concentration).

Selectivity: Inhibition of human 17 β -HSD2 and affinities for ER α and ER β . 17 β -HSD2 acts as a biological counterpart of the type 1 enzyme by catalyzing the reverse reaction. Therefore, inhibition of this enzyme must be avoided. In an assay similar to the 17 β -HSD1 test, human placental microsomes were incubated with tritiated E2 in the presence of NAD⁺ and inhibitor to evaluate inhibition of 17 β -HSD2. Labeled product was quantified after HPLC separation. Inhibition values of all compounds are depicted in Table 1. In vitro selectivity toward 17 β -HSD2 is expressed as selectivity factor (SF), describing the ratio of the concentrations required to inhibit the isoenzymes by 50 % (IC₅₀ 17 β -HSD2/IC₅₀ 17 β -HSD1).

SFs of methoxy- and ethoxy-compounds **1-2**, **4-9** and **11** do not exceed 2. Higher SFs were observed for compounds bearing substituents in *meta* position. However, SFs up to 50, as achieved in the previous study,^[42] were not obtained.

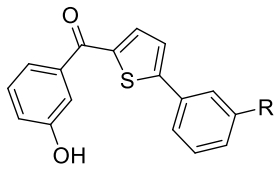
Interestingly, enlargement of the ether resulted in a slight increase of selectivity: compound **3** (SF = 4) versus **10** (SF = 6). Remarkably, the benzyloxy-derivative **12** showed a 13-fold higher inhibition of 17 β -HSD1 compared to the type 2 enzyme indicating that the space within this area of the latter enzyme might be more restricted than in 17 β -HSD1. Accordingly, introduction of substituents into the benzyloxy moiety might lead to further enhancement of selectivity. While this hypothesis was confirmed by the *meta*-methoxy- (**13**), dimethoxy- (**16**) and the chloro-derivatives (**17-19**), the monomethoxy-compounds (**14-15**) showed different results. Compounds **14** (*meta*-methoxy, SF = 16) and **15** (*para*-methoxy, SF = 12) revealed similar selectivity toward 17 β -HSD2 as the nonsubstituted benzyloxy compound **12** (SF = 13).

Considering the sulfonamides **21-23**, it is striking that the introduction of a phenyl ring also increases selectivity (for **21** and **22**, SF = 4 versus **23** SF = 14). These results attract increasing notice to a phenyl ring within this area of the protein with regard to its influence on activity and selectivity.

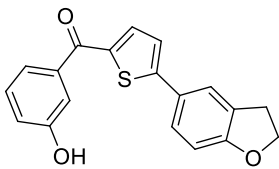
As estrogens function via activation of ERs, the affinity of 17 β -HSD1 inhibitors toward ER α and ER β should be as low as possible in order to avoid stimulatory effects. Since E1 shows tenfold lower affinity toward ER α ^[50] and 50-fold lower affinity toward ER β ^[50] compared with E2 (relative binding affinity (RBA) = 100 % for E2), inhibitors having an RBA below 0.1 % were considered to possess too little affinity to exert estrogenic effects. As E1 is the only active estrogen present during 17 β -HSD1 inhibition, inhibitors with much lower receptor affinity than E1 are negligible for receptor activation. All compounds having a SF value higher than 10 were evaluated in this competition assay. None of them showed higher RBA values than 0.1 % (data not shown) confirming our design concept focusing on nonsteroidal inhibitors.

Further biological evaluations. Using T47D cells expressing both 17 β -HSD1 and 17 β -HSD2, the intracellular potencies of selected compounds were evaluated (Table 2).

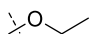
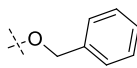
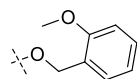
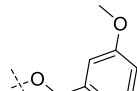
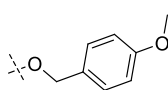
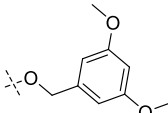
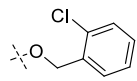
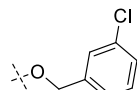
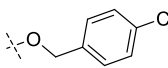
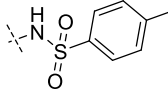
Table 2. Inhibition of 17 β -HSD1 in cell-free and cellular assay by selected compounds.



10, 12-19, 23



25

Compd.	R	IC ₅₀ [nM] ^[a]	
		cell-free assay ^[b]	cellular assay ^[c]
10		78	154
12		62	53 % ^[d]
13		35	441
14		47	565
15		60	526
16		31	40 % ^[d]
17		54	34 % ^[d]
18		40	49 % ^[d]
19		36	47 % ^[d]
23		12	78
25		55	357

^{a]} Mean value of three determinations, standard deviation less than 24 %; ^[b] Human placenta, cytosolic fraction, substrate E1, 500 nM, cofactor NADH, 500 μ M; ^[c] T47D cells, substrate E1, 50 nM; ^[d] inhibition at 1 μ M (inhibitor concentration)

Regarding the benzyloxy-substituted compounds **12-19**, only the monomethoxy-substituted benzyloxy-derivatives **13-15** showed moderate inhibition of E2 formation (IC₅₀ = 526, 441 and 565 nM, respectively). However, the dimethoxy (**16**) and chloro substituents (**17-19**) have a negative impact on cellular activity, which might be explained by insufficient cell penetration or

increased intracellular metabolism. Interestingly, the ethoxy derivative **10**, without bearing an additional phenyl ring, exhibited a three- to fourfold higher intracellular inhibitory activity ($IC_{50} = 154$ nM) than compounds **13-15**.

Methylbenzenesulfonamide **23** turned out to be the most potent 17 β -HSD1 inhibitor of this study both in the cell-free ($IC_{50} = 12$ nM) and in the cellular assay ($IC_{50} = 78$ nM).

In order to find an appropriate species for demonstrating *in vivo* efficacy in a disease-oriented animal model, compounds **1**, **13** and **23** were tested in a cell-free assay using the cytosolic fraction of mouse liver preparation and under conditions similar to our standard cell-free assay. However, no mentionable inhibition of 17 β -HSD1 or 17 β -HSD2 could be detected (data not shown). Therefore, the search for an optimal species pertaining to *in vivo* proof-of-concept for this class of compounds is ongoing.

Furthermore, metabolic stability of the most active compound **23** ($IC_{50} = 12$ nM) and the most selective compound **13** (SF = 30) of this study were evaluated using human liver microsomes (Table 3). The data of both compounds and the references dextrometorphan and verapamil are given in Table 3. Compounds **13** and **23** showed intrinsic clearances (CL_{int}) of 81.2 and 109 $\mu\text{L min}^{-1} \text{mg}^{-1}$ protein, respectively, and therefore can be considered to be in the high clearance category. Regarding the reference drugs, dextrometorphan and verapamil, the commonly used calcium channel blocker verapamil revealed a very similar CL_{int} of 105 $\mu\text{L min}^{-1} \text{mg}^{-1}$ protein defining a high but not too high liability to metabolic degradation.

Table 3. Metabolic stability of compounds **13**, **23** and control compounds using human liver microsomes

Compd.	$CL_{int}^{[a]}$ [$\mu\text{L}/\text{min}/\text{mg}$ protein]	t $_{1/2}$ [min]
dextrometorphan	10.7	129
verapamil	105	13.2
13	81.2	17.1
23	109	12.8

^[a] Intrinsic metabolic clearance (CL_{int}); test concentration = 3 μM .

Molecular Modeling. A docking study was performed in order to gain deeper insight into the molecular interactions between the most potent inhibitor **23** and 17 β -HSD1 and to understand the SAR. In Figure 3, the binding mode of compound **23** is shown, indicating hydrogen-bonding interactions between the OH functionality and Asn152, as well as between the keto oxygen atom and Tyr155. The second hydrogen bond of the ketone with Ser142, which was proposed for **B1-B3**, was not predicted by modeling studies to be present for **23**. The methylbenzenesulfonamide substituent is predicted to interact with two amino acids, which are located in the C-terminal region. His221 is suggested to form a hydrogen bond with one sulfonamide-oxygen atom, while Phe259 might be involved in π - π -interactions with the benzene moiety.

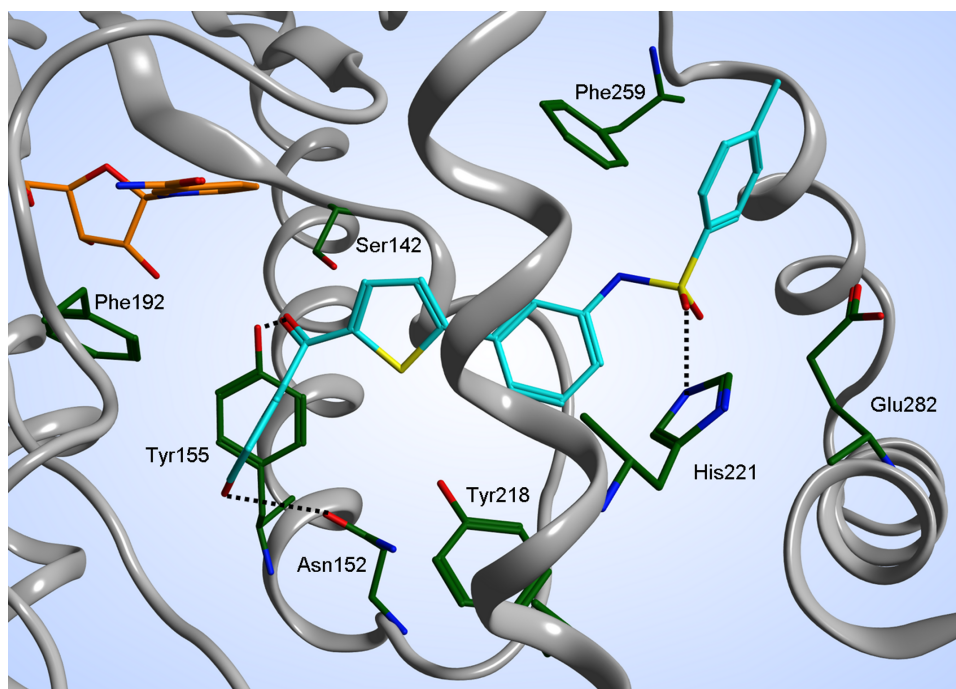


Figure 3. Hypothetical binding mode of compound **23** (cyan) obtained by docking into 17 β -HSD1 (PDB-ID: 1FDT-B). Cofactor NADPH (orange), interacting residues (green) and cartoon rendered tertiary structure (grey) of the active site are shown. Hydrogen bonds are drawn in black dashed lines. Figure generated with MOE (Chemical Computing Group Inc., Montreal, Canada).

Discussion and Conclusions

From our previous work in this class of compounds,^[42] it was demonstrated that variation of the OH position on the phenyl ring do not result in marked differences in the inhibitory activity of evaluated compounds **B1-B3**. In this paper, we have reported on the replacement of the hydroxy group on the phenyl ring in the class of the bicyclic substituted hydroxyphenyl methanones. Various substituents were introduced in order to evaluate whether additional interactions in the C-terminal region are beneficial for inhibitory activity. The biological data show that 17 β -HSD1 inhibition can also be achieved without the OH functionality on the phenyl ring. Considering the design concept of the previous study, this hydroxyl group was expected to form hydrogen bonds with His221 and Glu282 in the C-terminal region of the steroid binding pocket. Obviously, the hydrogen-bond donor property is not necessary for strong inhibitory activity with regard to the methoxy derivatives. Glu282, which is expected to accept a hydrogen bond from this OH group, does not seem to be involved in inhibitor binding at all. In general, its relevance for ligand binding is discussed controversially. While site-directed mutagenesis studies indicated no significant interaction between Glu282 and the 3-OH group of the substrate,^[51] hydrogen bonding between both was found in several independent crystal structures.^[52,53] The hydrogen-bond acceptor property of the phenol might play a more important role since compound **1**,

without hydroxyl functionality on the phenyl ring, showed a slightly reduced 17 β -HSD1 inhibition. However, the potential hydrogen-bond donor His221 is already known as an important factor for substrate interaction.^[54] Although this amino acid is described to be implicated in enzyme stabilisation^[44] by interacting with Glu282, it appears to be also involved in the binding of our inhibitors.

Regarding the mono-methoxy- and ethoxy derivatives (**2-5** and **9-11**, respectively), it becomes apparent that the *para*-position seems to be less favorable than *meta* and *ortho*. Moreover, di- and trimethoxy-derivatives (**6-8**) showed a strong decrease in activity as well, indicating that the space around this phenyl ring is sterically restricted. This finding is in accordance with our docking results. According to the orientation of the phenyl ring, the disubstitution of **6** compels the methoxy groups to adopt a conformation leading to steric clashes with either Tyr218 or Phe259. Indeed, taking into account that the 1,3-benzodioxol compound **26** showed a much higher affinity than the corresponding dimethoxy compound **6**, it can be concluded that the binding pocket is very restricted.

Concerning flexible substituents, 17 β -HSD1 inhibitory activity as well as selectivity toward the type 2 enzyme revealed the *meta* position to be the most favorable. Starting with compound **3**, it is striking that an enlargement of the *meta* substituents resulted in increased selectivity (SF of **3** < **10** < **12** < **13/16-19**). Interestingly, the IC₅₀ values for 17 β -HSD1 inhibition of all benzyloxy-derivatives are in the same range and similar to that of the ethoxy compound **10**. Therefore, although influencing the selectivity toward 17 β -HSD2, the phenyl ring of the benzyloxy substituent does not seem to specifically interact with 17 β -HSD1. Further investigation is still warranted as to whether the phenyl ring is pointing out of the 17 β -HSD1 active site.

Sulfonamide **23** turned out to be the most potent inhibitor of this study. Compared to its methanesulfonamide analog **21**, the introduction of the phenyl led to 12-fold higher 17 β -HSD1 inhibition. The docking study revealed the benzene ring of **23** to be implicated in a π - π interaction with Phe259. Comparing **B2** (*meta*-OH) and **23**, both compounds interact with Asn152. The relevance of this amino acid for ligand binding was already confirmed by a co-crystal structure of a highly potent, steroidal 17 β -HSD1 inhibitor.^[44] **B2** and **23** showed similar IC₅₀ values although the hydrogen-bonding interaction of **23** with Ser142 was not present in the observed binding mode. The π - π interactions found for compound **23** might be able to compensate the loss of the hydrogen bond between the ketone and Ser142.

In summary, we have reported on further developments in the class of bicyclic substituted hydroxyphenylmethanones. The high inhibitory activities of inhibitors bearing large substituents like benzyloxysulfonamide or benzyloxy revealed that these groups take advantage of the additional space in the C-terminal region. Although comparable inhibitory potencies were achieved, they have to be considered critically in terms of ligand efficiency. However, further bioisosteric

replacements of the phenolic hydroxyl group might lead to compounds combining high potency with good selectivity and intracellular activity. The most promising compound of this study, methylbenzenesulfonamide **23**, shows strong inhibitory activity in both cellular and cell-free assays as well as no affinity toward estrogen receptors α and β . It might be a candidate for further lead optimization, especially regarding its selectivity and cellular activity.

Experimental Section

Chemistry. Chemical names follow IUPAC nomenclature. Starting materials were purchased from Aldrich, Acros, Lancaster, Combi Blocks, Merck or Fluka and were used without purification. Column chromatography (CC) was performed on silica gel (70-200 μ m). Preparative thin layer chromatography (TLC) was performed on 1 mm SIL G-100 UV₂₅₄ glass plates (Macherey-Nagel). Reactions were monitored using Alugram SIL G UV₂₅₄ TLC plates (Macherey-Nagel). All microwave irradiation experiments were carried out in a CEM-Discover monomode microwave apparatus.

¹H-NMR and ¹³C-NMR spectra were measured on a Bruker AM 500 spectrometer (500 MHz) at 300 K. Chemical shifts (δ) are reported in parts per million (ppm), with the residual solvent as the internal standard (CDCl₃: δ = 7.24 ppm (¹H-NMR) and δ = 77 ppm (¹³C-NMR) and CD₃COCD₃: δ = 2.05 ppm (¹H-NMR) and δ = 30.8 ppm (¹³C-NMR)). Signals are described as singlet (s), doublet (d), triplet (t), doublet of doublets (dd), doublet of doublets of doublets (ddd), multiplet (m), doublet of triplets (dt), triplet of doublets (td), and quadruplet (q). All coupling constants (J) are given in hertz (Hz). Mass spectra were recorded on a TSQ Quantum (Thermo Finnigan) instrument using electrospray ionization (ESI).

Tested compounds possessed >98% chemical purity as measured by HPLC. The methods for HPLC analysis and a table of data for all tested compounds are provided in the Supporting Information.

General procedure for Suzuki coupling (Method A): A mixture of 2-bromothiophene derivative (1 eq), boronic acid derivative (1.2 eq), caesium carbonate (4 eq) and tetrakis(triphenylphosphine) palladium (0.01 eq) in an oxygen free DME/water (1:1) solution was refluxed under nitrogen atmosphere for 2 h (method A1) or 4 h (method A2), respectively. The reaction mixture was cooled to rt. The aqueous layer was extracted with ethyl acetate. The combined organic layers were washed with brine, dried over magnesium sulfate, filtered and concentrated to dryness. The product was purified by column chromatography (CC), CC followed by preparative TLC or CC followed by preparative HPLC, respectively.

General procedure for ether cleavage (Method B): To a solution of methoxybenzene derivative (1 eq) in dry dichloromethane at -78 °C (dry ice/acetone bath), boron tribromide in dichloromethane (1 M, 3 eq per methoxy function) was added dropwise. The reaction mixture

was stirred for 20 h at rt under nitrogen atmosphere. Water was added to quench the reaction, and the aqueous layer was extracted with ethyl acetate. The combined organic layers were washed with brine, dried over sodium sulfate, filtered and concentrated to dryness. The product was purified by CC, CC followed by preparative HPLC or recrystallization, respectively.

General procedure for purification using preparative HPLC: Compounds were purified via an Agilent Technologies Series 1200–preparative HPLC using a RP C18 Nucleodur 100-5 column (30 x 100 mm / 50 μ M from Macherey Nagel GmbH) as the stationary phase with a linear gradient (solvents: acetonitrile, water) starting from 20 % acetonitrile up to 100 % over 36 min.

(5-Bromo-2-thienyl)(3-methoxyphenyl)methanone (1b). A mixture of 2-bromothiophene (145 mg, 0.89 mmol), 3-methoxybenzoyl chloride (152 mg, 0.89 mmol) and aluminium chloride (119 mg, 0.89 mmol) in anhydrous dichloromethane was stirred at 0 °C for 0.5 h. The reaction mixture was warmed to rt and stirred for 1 h. HCl 1M was used to quench the reaction. The aqueous layer was extracted with ethyl acetate. The combined organic layers were washed with brine, dried over magnesium sulfate, filtered and concentrated to dryness. The product was purified by CC (hexane/ethyl acetate 97:3); yield: 77 % (204 mg, white powder). ^1H NMR (CD_3COCD_3): 7.55 (d, $J = 4.1$ Hz, 1H), 7.47 (t, $J = 7.9$ Hz, 1H), 7.42 (td, $J = 1.5$ Hz and $J = 7.9$ Hz, 1H), 7.35-7.34 (m, 1H), 7.33 (d, $J = 4.1$ Hz, 1H), 7.22 (ddd, $J = 0.9$ Hz and $J = 2.5$ Hz and $J = 8.2$ Hz, 1H), 3.88 (s, 3H); ^{13}C NMR (CD_3COCD_3): 187.90, 161.75, 140.45, 137.40, 133.85, 131.60, 123.95, 123.05, 120.45, 115.45, 56.85.

(5-Bromo-2-thienyl)(3-hydroxyphenyl)methanone (1a). The title compound was prepared by reaction of **1b** (650 mg, 2.19 mmol) and boron tribromide (6.57 mmol) according to method B. The product was used in the next step without further purification; quantitative yield (620 mg, white powder). ^1H NMR (CD_3COCD_3): 8.76 (s, 1H), 7.54 (d, $J = 4.1$ Hz, 1H), 7.39 (t, $J = 7.8$ Hz, 1H), 7.34-7.32 (m, 2H), 7.30 (t, $J = 2.1$ Hz, 1H), 7.13 (ddd, $J = 1.3$ Hz and $J = 2.5$ Hz and $J = 8.2$ Hz, 1H); ^{13}C NMR (CD_3COCD_3): 187.90, 159.45, 147.25, 140.45, 137.25, 133.80, 131.70, 123.80, 122.10, 121.60, 117.25.

(3-Hydroxyphenyl)(5-phenyl-2-thienyl)methanone (1). The title compound was prepared by reaction of **1a** (150 mg, 0.53 mmol), benzene boronic acid (78 mg, 0.64 mmol), caesium carbonate (691 mg, 2.12 mmol) and tetrakis(triphenylphosphine) palladium (6 mg, 5 mmol) according to method A1. The product was purified by CC (hexane/ethyl acetate 8:2); yield: 28 % (42 mg, beige powder); ^1H NMR (CD_3COCD_3): 8.81 (s, 1H), 7.81-7.80 (m, 2H), 7.72 (d, $J = 4.1$ Hz, 1H), 7.60 (d, $J = 4.1$ Hz, 1H), 7.49 (t, $J = 7.9$ Hz, 2H), 7.44-7.39 (m, 2H), 7.37 (dt, $J = 1.5$ Hz and $J = 7.6$ Hz, 1H), 7.34-7.33 (m, 1H), 7.13 (ddd, $J = 1.5$ Hz and $J = 2.5$ Hz and $J = 7.9$ Hz, 1H); ^{13}C NMR (CD_3COCD_3): 188.75, 159.40, 154.30, 144.20, 141.30, 137.85, 135.15, 131.55, 131.15, 131.05, 128.05, 126.30, 122.05, 121.25, 117.30; MS (ESI): 281 (M+H) $^+$.

(3-Methoxyphenyl)[5-(2-methoxyphenyl)-2-thienyl]methanone (2a). A mixture of **1b** (200 mg, 0.67 mmol), 2-methoxybenzene boronic acid (122 mg, 0.80 mmol), caesium carbonate (873 mg, 2.68 mmol) and tetrakis(triphenylphosphine) palladium (8 mg, 7 mmol) was suspended in an oxygen free DME/EtOH/water (1:1:1) solution. The reaction mixture was exposed to microwave irradiation (15 min, 150 W, 150 °C, 15 bar). After reaching rt, water was added and the aqueous layer was extracted with ethyl acetate. The combined organic layers were washed with brine, dried over magnesium sulfate, filtered and concentrated to dryness. The product was purified by CC (hexane/ethyl acetate 9:1); yield: 67 % (145 mg, yellow powder). ¹H NMR (CD₃COCD₃): 7.85 (dd, *J* = 1.9 Hz and *J* = 7.9 Hz, 2H), 7.69 (d, *J* = 1.3 Hz, 1H), 7.49-7.44 (m, 2H), 7.42-7.38 (m, 2H), 7.21-7.18 (m, 2H), 7.07 (dt, *J* = 0.9 Hz and *J* = 7.9 Hz, 1H), 4.01 (s, 3H), 3.89 (s, 3H); ¹³C NMR (CD₃COCD₃): 189.10, 161.70, 158.10, 149.85, 144.05, 141.70, 136.50, 132.15, 131.45, 130.15, 127.80, 123.75, 123.10, 122.95, 119.90, 115.50, 114.05, 57.10, 56.80.

(3-Hydroxyphenyl)[5-(2-methoxyphenyl)-2-thienyl]methanone (2). The title compound was obtained by reaction of **2a** (145 mg, 0.45 mmol) and boron tribromide (2.70 mmol) according to method B. The product was purified by CC (hexane/ethyl acetate 8:2) followed by preparative HPLC; yield: 55 % (76 mg, yellow oil); ¹H NMR (CD₃COCD₃): 7.83 (dd, *J* = 1.6 Hz and *J* = 7.9 Hz, 1H), 7.69 (d, *J* = 4.1 Hz, 1H), 7.67 (d, *J* = 4.1 Hz, 1H), 7.41-7.35 (m, 4H), 7.18 (d, *J* = 7.9 Hz, 1H), 7.14-7.12 (m, 1H), 7.07-7.04 (m, 1H), 4.00 (s, 3H); ¹³C NMR (CD₃COCD₃): 189.20, 159.30, 158.05, 149.70, 144.10, 141.70, 136.40, 132.10, 131.45, 130.10, 127.70, 123.75, 122.90, 122.05, 120.95, 117.25, 114.00, 57.10; MS (ESI): 311 (M+H)⁺.

(3-Hydroxyphenyl)[5-(3-methoxyphenyl)-2-thienyl]methanone (3). The title compound was prepared by reaction of (5-bromo-2-thienyl)(3-hydroxyphenyl)methanone (**1a**) (150 mg, 0.53 mmol), 3-methoxybenzene boronic acid (97 mg, 0.64 mmol), caesium carbonate (691 mg, 2.12 mmol) and tetrakis(triphenylphosphine) palladium (6 mg, 5 mmol) according to method A1. The product was purified by CC (hexane/ethyl acetate 9:1); yield: 94 % (154 mg, beige powder); ¹H NMR (CD₃COCD₃): 7.71 (d, *J* = 4.1 Hz, 1H), 7.60 (d, *J* = 4.1 Hz, 1H), 7.42-7.35 (m, 4H), 7.34 (t, *J* = 1.9 Hz, 1H), 7.32 (t, *J* = 1.9 Hz, 1H), 7.13 (ddd, *J* = 1.3 Hz and *J* = 2.2 Hz and *J* = 7.6 Hz, 1H), 7.00 (ddd, *J* = 1.3 Hz and *J* = 2.2 Hz and *J* = 7.6 Hz, 1H), 3.89 (s, 3H); ¹³C NMR (CD₃COCD₃): 188.75, 162.35, 159.45, 154.20, 144.25, 141.30, 137.75, 136.45, 132.25, 131.60, 126.55, 122.10, 121.25, 120.45, 117.30, 116.75, 113.35, 56.80; MS (ESI): 311 (M+H)⁺.

(3-Hydroxyphenyl)[5-(4-methoxyphenyl)-2-thienyl]methanone (4). The title compound was prepared by reaction of **1a** (150 mg, 0.53 mmol), 4-methoxybenzene boronic acid (97 mg, 0.64 mmol), caesium carbonate (691 mg, 2.12 mmol) and tetrakis(triphenylphosphine) palladium (6 mg, 5 mmol) according to method A1. The product was purified by CC (hexane/ethyl acetate 8:2) followed by preparative TLC (hexane/ethyl acetate 7:3); yield: 96 % (158 mg, yellow powder); ¹H NMR (CD₃COCD₃): 8.72 (s, 1H), 7.72 (d, *J* = 8.8 Hz, 2H), 7.66

(d, $J = 4.1$ Hz, 1H), 7.45 (d, $J = 4.1$ Hz, 1H), 7.39 (t, $J = 7.8$ Hz, 1H), 7.35 (dt, $J = 1.3$ Hz and $J = 7.8$ Hz, 1H), 7.34 (t, $J = 2.1$ Hz, 1H), 7.12 (ddd, $J = 1.3$ Hz and $J = 2.5$ Hz and $J = 7.9$ Hz, 1H), 7.02 (d, $J = 8.8$ Hz, 2H), 3.85 (s, 3H); ^{13}C NMR (CD_3COCD_3): 188.60, 162.65, 159.35, 154.65, 143.15, 141.45, 138.00, 131.50, 129.45, 127.75, 125.05, 122.05, 121.05, 117.25, 116.50, 56.80; MS (ESI): 311 (M+H) $^+$.

(3-Hydroxyphenyl)[5-(6-methoxypyridin-3-yl)-2-thienyl]methanone (5). The title compound was prepared by reaction of **1a** (150 mg, 0.53 mmol), 6-methoxypyridine-3-boronic acid (98 mg, 0.64 mmol), caesium carbonate (691 mg, 2.12 mmol) and tetrakis(triphenylphosphine) palladium (6 mg, 5 mmol) according to method A1. The product was purified by CC (hexane/ethyl acetate 85:15); yield: 63 % (104 mg, beige powder); ^1H NMR (CD_3COCD_3): 8.86 (s, 1H), 8.60 (dd, $J = 0.6$ Hz and $J = 2.4$ Hz, 1H), 8.06 (dd, $J = 2.5$ Hz and $J = 8.5$ Hz, 1H), 7.71 (d, $J = 4.1$ Hz, 1H), 7.55 (d, $J = 4.1$ Hz, 1H), 7.40 (t, $J = 7.8$ Hz, 1H), 7.36 (dt, $J = 1.3$ Hz and $J = 7.6$ Hz, 1H), 7.33-7.32 (m, 1H), 7.12 (ddd, $J = 1.3$ Hz and $J = 2.5$ Hz and $J = 7.8$ Hz, 1H), 6.88 (dd, $J = 0.6$ Hz and $J = 8.5$ Hz, 1H), 3.94 (s, 3H); ^{13}C NMR (CD_3COCD_3): 188.65, 166.40, 159.45, 150.95, 146.40, 141.25, 138.55, 137.90, 131.55, 126.10, 122.05, 121.25, 117.25, 113.05, 54.95; MS (ESI): 312 (M+H) $^+$.

[5-(3,4-Dimethoxyphenyl)-2-thienyl](3-hydroxyphenyl)methanone (6). The title compound was prepared by reaction of **1a** (150 mg, 0.53 mmol), 3,4-dimethoxybenzene boronic acid (117 mg, 0.64 mmol), caesium carbonate (691 mg, 2.12 mmol) and tetrakis(triphenylphosphine) palladium (6 mg, 5 mmol) according to method A1. The product was purified by CC (hexane/ethyl acetate 8:2); yield: 73 % (132 mg, yellow powder); ^1H NMR (CD_3COCD_3): 8.78 (s, 1H), 7.68 (d, $J = 4.1$ Hz, 1H), 7.51 (d, $J = 4.1$ Hz, 1H), 7.39 (t, $J = 7.8$ Hz, 1H), 7.38-7.34 (m, 3H), 7.32-7.31 (m, 1H), 7.12 (ddd, $J = 1.3$ Hz and $J = 2.5$ Hz and $J = 7.9$ Hz, 1H), 7.06-7.04 (m, 1H), 3.92 (s, 3H), 3.87 (s, 3H); ^{13}C NMR (CD_3COCD_3): 189.65, 159.40, 152.60, 151.80, 141.50, 137.95, 131.55, 128.05, 125.35, 122.00, 121.10, 120.95, 117.25, 114.05, 111.70, 57.25, 57.20; MS (ESI): 341 (M+H) $^+$.

(3-Hydroxyphenyl)[5-(3,4,5-trimethoxyphenyl)-2-thienyl]methanone (7). The title compound was prepared by reaction of **1a** (150 mg, 0.53 mmol), 3,4,5-trimethoxybenzene boronic acid (136 mg, 0.64 mmol), caesium carbonate (691 mg, 2.12 mmol) and tetrakis(triphenylphosphine) palladium (6 mg, 5 mmol) according to method A1. The product was purified by CC (hexane/ethyl acetate 8:2); yield: 71 % (140 mg, yellow powder); ^1H NMR (CD_3COCD_3): 8.76 (s, 1H), 7.68 (d, $J = 4.1$ Hz, 1H), 7.56 (d, $J = 4.1$ Hz, 1H), 7.40 (t, $J = 7.8$ Hz, 1H), 7.35 (dt, $J = 1.3$ Hz and $J = 7.6$ Hz, 1H), 7.33-7.32 (m, 1H), 7.12 (ddd, $J = 1.3$ Hz and $J = 2.5$ Hz and $J = 7.9$ Hz, 1H), 7.07 (s, 2H), 3.93 (s, 6H), 3.78 (s, 3H); ^{13}C NMR (CD_3COCD_3): 188.70, 159.40, 155.95, 154.75, 143.80, 141.35, 137.75, 131.55, 130.70, 126.20, 122.05, 121.15, 117.25, 105.85, 61.70, 57.65; MS (ESI): 371 (M+H) $^+$.

(3-Hydroxyphenyl)[5-(2,3,4-trimethoxyphenyl)-2-thienyl]methanone (8). The title compound was prepared by reaction of **1a** (150 mg, 0.53 mmol), 2,3,4-trimethoxybenzene boronic acid (136 mg, 0.64 mmol), caesium carbonate (691 mg, 2.12 mmol) and tetrakis(triphenylphosphine) palladium (6 mg, 5 mmol) according to method A1. The product was purified by CC (hexane/ethyl acetate 8:2); yield: 62 % (122 mg, yellow powder); ^1H NMR (CD_3COCD_3): 8.80 (s, 1H), 7.66 (d, $J = 4.1$ Hz, 1H), 7.59-7.56 (m, 2H) 7.39 (t, $J = 7.8$ Hz, 1H), 7.35 (dt, $J = 1.3$ Hz and $J = 7.6$ Hz, 1H), 7.33-7.32 (m, 1H), 7.11 (ddd, $J = 1.3$ Hz and $J = 2.5$ Hz and $J = 7.9$ Hz, 1H), 6.92 (d, $J = 9.1$ Hz, 1H), 3.95 (s, 3H), 3.91 (s, 3H), 3.87 (s, 3H); ^{13}C NMR (CD_3COCD_3): 189.10, 159.40, 156.60, 152.85, 149.65, 143.70, 141.80, 136.60, 131.45, 126.65, 124.40, 122.00, 121.65, 121.00, 117.25, 110.35, 62.05, 62.00, 57.50; MS (ESI): 371 (M+H) $^+$.

5-(2-Ethoxyphenyl)-2-thienyl(3-hydroxyphenyl)methanone (9). The title compound was prepared by reaction of **1a** (150 mg, 0.53 mmol), 2-ethoxybenzene boronic acid (106 mg, 0.64 mmol), caesium carbonate (691 mg, 2.12 mmol) and tetrakis(triphenylphosphine) palladium (6 mg, 5 mmol) according to method A1. The product was purified by CC (hexane/ethyl acetate 85:15); yield: 88 % (151 mg, yellow oil); ^1H NMR (CD_3COCD_3): 7.87 (dd, $J = 1.5$ Hz and $J = 7.9$ Hz, 1H), 7.74 (d, $J = 4.1$ Hz, 1H), 7.69 (d, $J = 4.1$ Hz, 1H), 7.41-7.35 (m, 3H), 7.34 (t, $J = 2.1$ Hz, 1H), 7.18-7.16 (m, 1H), 7.12 (ddd, $J = 1.3$ Hz and $J = 2.5$ Hz and $J = 7.6$ Hz, 1H), 7.06 (td, $J = 1.3$ Hz and $J = 7.6$ Hz, 1H), 4.28 (q, $J = 6.9$ Hz, 2H), 1.55 (t, $J = 6.9$ Hz, 3H); ^{13}C NMR (CD_3COCD_3): 189.15, 157.30, 144.00, 141.75, 138.40, 136.30, 132.05, 131.45, 130.05, 127.55, 123.80, 122.80, 122.10, 121.00, 117.30, 114.75, 113.00, 66.35, 16.10; MS (ESI): 325 (M+H) $^+$.

[5-(3-Ethoxyphenyl)-2-thienyl](3-hydroxyphenyl)methanone (10). The title compound was prepared by reaction of **1a** (150 mg, 0.53 mmol), 3-ethoxybenzene boronic acid (106 mg, 0.64 mmol), caesium carbonate (691 mg, 2.12 mmol) and tetrakis(triphenylphosphine) palladium (6 mg, 5 mmol) according to method A1. The product was purified by CC (hexane/ethyl acetate 8:2) followed by preparative TLC (hexane/ethyl acetate 7:3); yield: 91 % (157 mg, beige powder); ^1H NMR (CD_3COCD_3): 8.80 (s, 1H), 7.69 (d, $J = 4.1$ Hz, 1H), 7.56 (d, $J = 4.1$ Hz, 1H), 7.41-7.34 (m, 4H), 7.32 (dt, $J = 1.3$ Hz and $J = 7.6$ Hz, 1H), 7.28 (t, $J = 2.1$ Hz, 1H), 7.13 (ddd, $J = 1.3$ Hz and $J = 2.5$ Hz and $J = 7.6$ Hz, 1H), 6.96 (ddd, $J = 1.3$ Hz and $J = 2.5$ Hz and $J = 7.9$ Hz, 1H), 4.11 (q, $J = 6.9$ Hz, 2H), 1.38 (t, $J = 6.9$ Hz, 3H); ^{13}C NMR (CD_3COCD_3): 188.70, 161.55, 159.35, 154.20, 144.10, 141.25, 137.70, 136.35, 132.20, 131.55, 126.40, 122.05, 121.20, 120.25, 117.25, 117.15, 113.90, 65.25, 16.05; MS (ESI): 325 (M+H) $^+$.

[5-(4-Ethoxyphenyl)-2-thienyl](3-hydroxyphenyl)methanone (11). The title compound was prepared by reaction of **1a** (150 mg, 0.53 mmol), 4-ethoxybenzene boronic acid (106 mg, 0.64 mmol), caesium carbonate (691 mg, 2.12 mmol) and tetrakis(triphenylphosphine) palladium (6 mg, 5 mmol) according to method A1. The product was purified by CC (hexane/ethyl acetate 8:2); yield: 71 % (122 mg, beige powder); ^1H NMR (CD_3COCD_3): 8.76 (s,

1H), 7.72 (d, $J = 8.8$ Hz, 2H), 7.67 (d, $J = 4.1$ Hz, 1H), 7.45 (d, $J = 4.1$ Hz, 1H), 7.39 (t, $J = 7.8$ Hz, 1H), 7.35 (dt, $J = 1.3$ Hz and $J = 7.8$ Hz, 1H), 7.33-7.32 (m, 1H), 7.11 (ddd, $J = 0.9$ Hz and $J = 2.5$ Hz and $J = 7.8$ Hz, 1H), 7.01 (d, $J = 8.8$ Hz, 2H), 4.11 (q, $J = 6.9$ Hz, 2H), 1.38 (t, $J = 6.9$ Hz, 3H); ^{13}C NMR (CD_3COCD_3): 188.60, 162.00, 159.40, 154.75, 143.10, 141.45, 138.05, 131.50, 129.45, 127.60, 125.00, 122.00, 121.05, 117.25, 117.00, 65.30, 16.00; MS (ESI): 325 (M+H) $^+$.

{5-[3-(Benzyloxy)phenyl]-2-thienyl}(3-hydroxyphenyl)methanone (12). The title compound was prepared by reaction of **1a** (150 mg, 0.53 mmol), 3-(benzyloxy)benzene boronic acid (146 mg, 0.64 mmol), caesium carbonate (691 mg, 2.12 mmol) and tetrakis(triphenylphosphine) palladium (6 mg, 5 mmol) according to method A1. The product was purified by CC (hexane/ethyl acetate 8:2); yield: 71 % (146 mg, beige powder); ^1H NMR (CD_3COCD_3): 8.76 (s, 1H), 7.70 (d, $J = 4.1$ Hz, 1H), 7.58 (d, $J = 4.1$ Hz, 1H), 7.52-7.51 (m, 2H), 7.43-7.32 (m, 9H), 7.13 (ddd, $J = 1.3$ Hz and $J = 2.5$ Hz and $J = 7.6$ Hz, 1H), 7.08 (ddd, $J = 1.3$ Hz and $J = 2.5$ Hz and $J = 7.6$ Hz, 1H), 5.22 (s, 2H); ^{13}C NMR (CD_3COCD_3): 188.70, 161.40, 159.40, 154.10, 144.20, 141.25, 139.10, 137.75, 136.45, 132.30, 131.55, 130.30, 129.70, 129.50, 126.50, 122.10, 121.25, 120.65, 117.65, 117.30, 114.35, 71.65; MS (ESI): 387 (M+H) $^+$.

(3-Hydroxyphenyl)(5-{3-[(2-methoxybenzyl)oxy]phenyl}-2-thienyl)methanone (13). The title compound was prepared by reaction of **1a** (150 mg, 0.53 mmol), 3-[(2-methoxybenzyl)oxy]benzene boronic acid (165 mg, 0.64 mmol), caesium carbonate (691 mg, 2.12 mmol) and tetrakis(triphenylphosphine) palladium (6 mg, 5 mmol) according to method A1. The product was purified by CC (hexane/ethyl acetate 7:3); yield: 64 % (142 mg, beige powder); ^1H NMR (CD_3COCD_3): 8.74 (s, 1H), 7.71 (d, $J = 4.1$ Hz, 1H), 7.60 (d, $J = 4.1$ Hz, 1H), 7.48 (m, 1H), 7.42-7.36 (m, 5H), 7.34-7.31 (m, 2H), 7.13 (ddd, $J = 1.3$ Hz and $J = 2.5$ Hz and $J = 7.9$ Hz, 1H), 7.08-7.04 (m, 2H), 6.97 (td, $J = 1.3$ Hz and $J = 7.6$ Hz, 1H), 5.21 (s, 2H), 3.90 (s, 3H); ^{13}C NMR (CD_3COCD_3): 188.75, 161.55, 159.40, 159.15, 154.20, 144.20, 141.30, 137.75, 136.45, 132.30, 131.60, 131.15, 130.85, 126.95, 126.50, 122.30, 122.10, 121.25, 120.55, 117.60, 117.30, 114.25, 112.55, 66.70, 56.95; MS (ESI): 417 (M+H) $^+$.

(3-Hydroxyphenyl)(5-{3-[(3-methoxybenzyl)oxy]phenyl}-2-thienyl)methanone (14). The title compound was prepared by reaction of **1a** (150 mg, 0.53 mmol), 3-[(3-methoxybenzyl)oxy]benzene boronic acid (165 mg, 0.64 mmol), caesium carbonate (691 mg, 2.12 mmol) and tetrakis(triphenylphosphine) palladium (6 mg, 5 mmol) according to method A1. The product was purified by CC (hexane/ethyl acetate 8:2); yield: 74 % (163 mg, beige powder); ^1H NMR (CD_3COCD_3): 8.75 (s, 1H), 7.71 (d, $J = 4.1$ Hz, 1H), 7.60 (d, $J = 4.1$ Hz, 1H), 7.44-7.36 (m, 5H), 7.34-7.30 (m, 2H), 7.13 (ddd, $J = 1.3$ Hz and $J = 2.5$ Hz and $J = 7.9$ Hz, 1H), 7.10-7.08 (m, 3H), 6.91-6.89 (m, 1H), 5.21 (s, 2H), 3.81 (s, 3H); ^{13}C NMR (CD_3COCD_3): 188.75, 161.95, 161.40, 159.45, 154.10, 141.30, 140.70, 137.75, 136.50, 132.30, 131.60,

131.40, 126.55, 122.10, 121.55, 121.25, 120.70, 117.70, 117.30, 115.15, 115.00, 114.40, 71.55, 56.55; MS (ESI): 417 (M+H)⁺.

(3-Hydroxyphenyl)(5-{3-[(4-methoxybenzyl)oxy]phenyl}-2-thienyl)methanone (15). The title compound was prepared by reaction of **1a** (150 mg, 0.53 mmol), 3-[(4-methoxybenzyl)oxy]benzene boronic acid (165 mg, 0.64 mmol), caesium carbonate (691 mg, 2.12 mmol) and tetrakis(triphenylphosphine) palladium (6 mg, 5 mmol) according to method A1. The product was purified by CC (hexane/ethyl acetate 8:2); yield: 59 % (131 mg, beige powder); ¹H NMR (CD₃COCD₃): 8.83 (s, 1H), 7.71 (d, *J* = 4.1 Hz, 1H), 7.60 (d, *J* = 4.1 Hz, 1H), 7.44 (d, *J* = 8.5 Hz, 2H), 7.41-7.36 (m, 5H), 7.34-7.33 (m, 1H), 7.13 (ddd, *J* = 1.3 Hz and *J* = 2.5 Hz and *J* = 7.9 Hz, 1H), 7.07 (ddd, *J* = 1.3 Hz and *J* = 2.5 Hz and *J* = 7.9 Hz, 1H), 6.96 (d, *J* = 8.5 Hz, 2H), 5.14 (s, 2H), 3.80 (s, 3H); ¹³C NMR (CD₃COCD₃): 186.90, 181.65, 161.60, 161.50, 159.40, 144.25, 141.30, 137.75, 136.45, 132.30, 131.60, 131.30, 131.00, 126.50, 122.10, 121.25, 120.55, 117.75, 117.30, 115.75, 114.35, 71.50, 56.55; MS (ESI): 417 (M+H)⁺.

(3-Hydroxyphenyl)(5-{3-[(3,5-dimethoxybenzyl)oxy]phenyl}-2-thienyl)methanone (16). The title compound was prepared by reaction of **1a** (150 mg, 0.53 mmol), 3-[(3,5-dimethoxybenzyl)oxy]benzene boronic acid (184 mg, 0.64 mmol), caesium carbonate (691 mg, 2.12 mmol) and tetrakis(triphenylphosphine) palladium (6 mg, 5 mmol) according to method A1. The product was purified by CC (hexane/ethyl acetate 8:2) followed by preparative HPLC; yield: 47 % (112 mg, beige powder); ¹H NMR (CD₃COCD₃): 7.71 (d, *J* = 4.1 Hz, 1H), 7.59 (d, *J* = 4.1 Hz, 1H), 7.42-7.35 (m, 5H), 7.33-7.32 (m, 1H), 7.12 (ddd, *J* = 1.3 Hz and *J* = 2.5 Hz and *J* = 7.9 Hz, 1H), 7.09-7.06 (m, 1H), 6.68 (d, *J* = 2.2 Hz, 2H), 6.44 (t, *J* = 2.2 Hz, 1H), 5.17 (s, 2H), 3.79 (s, 6H); ¹³C NMR (CD₃COCD₃): 188.80, 163.10, 161.35, 159.50, 154.10, 144.25, 141.50, 141.25, 137.75, 136.45, 132.30, 131.55, 126.55, 122.00, 121.25, 120.65, 117.70, 117.30, 114.40, 107.20, 101.35, 71.55, 56.65; MS (ESI): 447 (M+H)⁺.

(3-Hydroxyphenyl)(5-{3-[(2-chlorobenzyl)oxy]phenyl}-2-thienyl)methanone (17). The title compound was prepared by reaction of **1a** (150 mg, 0.53 mmol), 3-[(2-chlorobenzyl)oxy]benzene boronic acid (168 mg, 0.64 mmol), caesium carbonate (691 mg, 2.12 mmol) and tetrakis(triphenylphosphine) palladium (6 mg, 5 mmol) according to method A1. The product was purified by CC (hexane/ethyl acetate 8:2); yield: 51 % (113 mg, beige powder); ¹H NMR (CD₃COCD₃): 8.78 (s, 1H), 7.71 (d, *J* = 4.1 Hz, 1H), 7.68-7.66 (m, 1H), 7.61 (d, *J* = 4.1 Hz, 1H), 7.50-7.48 (m, 1H), 7.46-7.45 (m, 1H), 7.43-7.36 (m, 6H), 7.34-7.33 (m, 1H), 7.14-7.10 (m, 2H), 5.31 (s, 2H); ¹³C NMR (CD₃COCD₃): 188.75, 161.20, 159.40, 153.95, 144.30, 141.25, 137.75, 136.60, 136.55, 134.80, 132.40, 131.70, 131.55, 131.50, 131.30, 129.15, 126.65, 122.10, 121.25, 121.00, 117.55, 117.30, 114.40, 69.10; MS (ESI): 421 (M+H)⁺.

(3-Hydroxyphenyl)(5-{3-[(3-chlorobenzyl)oxy]phenyl}-2-thienyl)methanone (18). The title compound was prepared by reaction of (5-bromo-2-thienyl)(3-hydroxyphenyl)methanone (**1a**) (150 mg, 0.53 mmol), 3-[(3-chlorobenzyl)oxy]benzene boronic acid (168 mg, 0.64 mmol),

caesium carbonate (691 mg, 2.12 mmol) and tetrakis(triphenylphosphine) palladium (6 mg, 5 mmol) according to method A1. The product was purified by CC (hexane/ethyl acetate 8:2); yield: 55 % (122 mg, beige powder); ^1H NMR (CD_3COCD_3): 8.80 (s, 1H), 7.70 (d, $J = 4.1$ Hz, 1H), 7.58 (d, $J = 4.1$ Hz, 1H), 7.57-7.56 (m, 1H), 7.48-7.46 (m, 1H), 7.43-7.34 (m, 8H), 7.13 (ddd, $J = 1.3$ Hz and $J = 2.5$ Hz and $J = 7.9$ Hz, 1H), 7.10-7.08 (m, 1H), 5.24 (s, 2H); ^{13}C NMR (CD_3COCD_3): 188.75, 161.10, 159.40, 153.95, 144.25, 141.65, 141.25, 137.70, 136.50, 135.75, 132.35, 132.05, 131.55, 129.70, 129.25, 127.75, 126.55, 122.05, 121.25, 120.85, 117.60, 117.30, 114.35, 70.70; MS (ESI): 421 (M+H) $^+$.

(3-Hydroxyphenyl)(5-{3-[(4-chlorobenzoyl)oxy]phenyl}-2-thienyl)methanone (19). The title compound was prepared by reaction of **1a** (150 mg, 0.53 mmol), 3-[(4-chlorobenzoyl)oxy]benzene boronic acid (168 mg, 0.64 mmol), caesium carbonate (691 mg, 2.12 mmol) and tetrakis(triphenylphosphine) palladium (6 mg, 5 mmol) according to method A1. The product was purified by CC (hexane/ethyl acetate 8:2); yield: 63 % (141 mg, beige powder); ^1H NMR (CD_3COCD_3): 8.76 (s, 1H), 7.71 (d, $J = 4.1$ Hz, 1H), 7.60 (d, $J = 4.1$ Hz, 1H), 7.54 (d, $J = 8.8$ Hz, 2H), 7.45-7.38 (m, 6H), 7.37 (dt, $J = 1.3$ Hz and $J = 7.6$ Hz, 1H), 7.34-7.33 (m, 1H), 7.13 (ddd, $J = 1.3$ Hz and $J = 2.5$ Hz and $J = 7.9$ Hz, 1H), 7.09-7.08 (m, 1H), 5.24 (s, 2H); ^{13}C NMR (CD_3COCD_3): 188.75, 161.20, 159.40, 154.00, 144.30, 141.25, 138.15, 137.75, 136.50, 135.05, 132.35, 131.55, 131.20, 130.40, 126.55, 122.10, 121.25, 120.85, 117.65, 117.30, 114.35, 70.85; MS (ESI): 421 (M+H) $^+$.

3-[5-(3-Methoxybenzoyl)-2-thienyl]benzotrile (20a). The title compound was prepared by reaction of **1b** (300 mg, 1.01 mmol), 3-cyanobenzene boronic acid (178 mg, 1.21 mmol), caesium carbonate (1.32 g, 4.04 mmol) and tetrakis(triphenylphosphine) palladium (12 mg, 10 mmol) according to method A2. The product was purified by CC (hexane/ethyl acetate 9:1); yield: 88 % (282 mg, beige powder); ^1H NMR (CDCl_3): 7.95 (t, $J = 1.6$ Hz, 1H), 7.90-7.88 (m, 1H), 7.67-7.64 (m, 2H), 7.55 (t, $J = 7.9$ Hz, 1H), 7.47 (dt, $J = 1.3$ Hz and $J = 7.6$ Hz, 1H), 7.42 (t, $J = 7.9$ Hz, 1H), 7.40-7.39 (m, 2H), 7.15 (ddd, $J = 1.3$ Hz and $J = 2.8$ Hz and $J = 8.2$ Hz, 1H), 3.88 (s, 3H); ^{13}C NMR (CDCl_3): 187.50, 159.70, 149.70, 138.95, 135.65, 134.70, 132.05, 130.45, 130.10, 129.55, 129.50, 125.00, 121.65, 118.80, 118.15, 113.80, 113.60, 55.50.

3-[5-(3-Hydroxybenzoyl)-2-thienyl]benzotrile (20). The title compound was prepared by reaction of **20a** (282 mg, 0.88 mmol) and boron tribromide (2.64 mmol) according to method B. The product was purified by recrystallization (EtOH/acetonitrile); yield: 66 % (176 mg, beige powder); ^1H NMR (CD_3COCD_3): 8.78 (s, 1H), 8.23 (t, $J = 1.6$ Hz, 1H), 8.12 (ddd, $J = 0.9$ Hz and $J = 1.9$ Hz and $J = 7.9$ Hz, 1H), 7.83-7.81 (m, 1H), 7.78-7.76 (m, 2H), 7.72 (td, $J = 0.7$ Hz and $J = 7.9$ Hz, 1H), 7.41 (t, $J = 7.6$ Hz, 1H), 7.40-7.38 (m, 1H), 7.36-7.35 (m, 1H), 7.14 (ddd, $J = 1.6$ Hz and $J = 2.5$ Hz and $J = 7.6$ Hz, 1H); ^{13}C NMR (CD_3COCD_3): 188.75, 151.25, 145.50, 141.00, 140.70, 137.75, 136.45, 134.15, 132.40, 131.65, 131.30, 127.85, 122.15, 121.45, 117.30, 115.35, 110.30; MS (ESI): 306 (M+H) $^+$.

***N*-{3-[5-(3-Methoxybenzoyl)-2-thienyl]phenyl}methanesulfonamide (21a).** The title compound was prepared by reaction of **1b** (300 mg, 1.01 mmol), 3-[(methylsulfonyl)amino]benzene boronic acid (178 mg, 1.21 mmol), caesium carbonate (1.32 g, 4.04 mmol) and tetrakis(triphenylphosphine) palladium (12 mg, 10 mmol) according to method A2. The product was used in the next step without further purification; yield: 96 % (376 mg, beige powder); ^1H NMR (CD_3COCD_3): 7.76 (t, $J = 1.9$ Hz, 1H), 7.70 (d, $J = 4.1$ Hz, 1H), 7.55-7.52 (m, 2H), 7.48-7.43 (m, 3H), 7.41 (ddd, $J = 0.9$ Hz and $J = 1.9$ Hz and $J = 7.9$ Hz, 1H), 7.38-7.37 (m, 1H), 7.21-7.19 (m, 1H), 3.87 (s, 3H), 3.07 (s, 3H); ^{13}C NMR (CD_3COCD_3): 188.60, 161.60, 153.60, 144.30, 141.40, 141.05, 137.90, 136.15, 131.45, 126.70, 123.70, 123.05, 122.35, 120.05, 119.30, 115.50, 59.70, 40.65.

***N*-{3-[5-(3-Hydroxybenzoyl)-2-thienyl]phenyl}methanesulfonamide (21).** The title compound was prepared by reaction of **21a** (200 mg, 0.52 mmol) and boron tribromide (1.56 mmol) according to method B. The crude mixture was washed with MeOH. The resulted suspension was filtered and the precipitated product was evaporated to dryness; yield: 87 % (168 mg, beige powder); ^1H NMR (CD_3COCD_3): 8.79 (s, 1H), 8.76 (s, 1H), 7.76 (t, $J = 1.9$ Hz, 1H), 7.73 (d, $J = 4.1$ Hz, 1H), 7.60-7.57 (m, 2H), 7.48 (t, $J = 7.9$ Hz, 1H), 7.42-7.36 (m, 3H), 7.34 (t, $J = 1.9$ Hz, 1H), 7.13 (ddd, $J = 1.2$ Hz and $J = 2.5$ Hz and $J = 7.6$ Hz, 1H), 3.07 (s, 3H); ^{13}C NMR (CD_3COCD_3): 188.75, 159.45, 153.50, 144.50, 141.45, 137.80, 132.30, 131.65, 126.70, 122.35, 122.10, 121.30, 119.30, 117.30, 40.65; MS (ESI): 374 (M+H) $^+$.

***N*-{3-[5-(3-Methoxyphenyl)-2-thienyl]benzyl}methanesulfonamide (22a).** The title compound was prepared by reaction of **1b** (200 mg, 0.67 mmol), 3-[[[(methylsulfonyl)amino]methyl]benzene boronic acid (183 mg, 0.80 mmol), caesium carbonate (1.32 g, 4.04 mmol) and tetrakis(triphenylphosphine) palladium (12 mg, 10 mmol) according to method A2. The product was purified by CC (hexane/ethyl acetate 9:1); yield: 94 % (253 mg, beige powder); ^1H NMR (CD_3COCD_3): 7.87-7.86 (m, 1H), 7.75-7.72 (m, 1H), 7.61 (d, $J = 4.1$ Hz, 1H), 7.51-7.45 (m, 4H), 7.39-7.38 (m, 1H), 7.22 (ddd, $J = 1.6$ Hz and $J = 2.5$ Hz and $J = 7.6$ Hz, 1H), 7.42 (s, 1H), 7.41 (s, 1H), 3.90 (s, 3H), 2.92 (s, 3H); ^{13}C NMR (CD_3COCD_3): 188.70, 161.75, 154.15, 144.20, 141.65, 138.00, 135.35, 131.55, 131.40, 130.55, 127.45, 127.05, 126.55, 123.05, 120.10, 115.50, 56.85, 48.30, 41.60.

***N*-{3-[5-(3-Hydroxybenzoyl)-2-thienyl]benzyl}methanesulfonamide (22).** The title compound was prepared by reaction of **22a** (253 mg, 0.63 mmol) and boron tribromide (1.89 mmol) according to method B. The crude mixture was washed with MeOH. The resulted suspension was filtered and the precipitated product was evaporated to dryness; yield: 81 % (197 mg, beige powder); ^1H NMR (CD_3COCD_3): 8.76 (s, 1H), 7.86 (s, 1H), 7.75-7.72 (m, 2H), 7.62 (d, $J = 4.0$ Hz, 4H), 7.50-7.48 (m, 2H), 7.41 (t, $J = 7.8$ Hz, 1H), 7.37 (dt, $J = 1.4$ Hz and $J = 7.6$ Hz, 1H), 7.34-7.33 (m, 1H), 7.13 (ddd, $J = 1.2$ Hz and $J = 2.4$ Hz and $J = 7.6$ Hz, 1H), 6.61 (s, 1H), 4.41 (s, 1H), 4.40 (s, 1H), 2.92 (s, 3H); ^{13}C NMR (CD_3COCD_3): 188.75, 159.45,

154.00, 144.30, 141.65, 141.25, 137.85, 135.35, 131.60, 131.40, 130.50, 127.45, 127.05, 126.50, 122.10, 121.25, 117.25, 48.30, 41.55; MS (ESI): 388 (M+H)⁺.

N-{3-[5-(3-Hydroxybenzoyl)-2-thienyl]phenyl}-4-methylbenzenesulfonamide (23). The title compound was prepared by reaction of **1a** (150 mg, 0.53 mmol), 3-[(4-methylphenyl)sulfonyl]amino}benzene boronic acid (239 mg, 0.64 mmol), caesium carbonate (691 mg, 2.12 mmol) and tetrakis(triphenylphosphine) palladium (6 mg, 5 mmol) according to method A1. The crude mixture was washed with MeOH. The resulted suspension was filtered and the precipitated product was evaporated to dryness.; yield: 53 % (126 mg, beige powder); ¹H NMR (CD₃COCD₃): 7.75 (d, *J* = 8.2 Hz, 2H), 7.70 (d, *J* = 4.1 Hz, 1H), 7.62 (t, *J* = 1.8 Hz, 1H), 7.50-7.48 (m, 2H), 7.40 (t, *J* = 7.6 Hz, 1H), 7.38-7.32 (m, 5H), 7.27 (ddd, *J* = 0.9 Hz and *J* = 2.2 Hz and *J* = 8.2 Hz, 1H), 7.13 (ddd, *J* = 1.3 Hz and *J* = 2.5 Hz and *J* = 7.9 Hz, 1H), 2.35 (s, 3H); ¹³C NMR (CD₃COCD₃): 188.70, 159.45, 153.40, 145.75, 144.45, 141.20, 140.95, 138.85, 137.80, 136.05, 132.10, 131.60, 131.55, 129.05, 126.60, 123.80, 122.70, 122.05, 121.30, 119.55, 117.30, 22.35; MS (ESI): 450 (M+H)⁺.

(3-Hydroxyphenyl)[5-(2-naphthyl)-2-thienyl]methanone (24). The title compound was prepared by reaction of **1a** (150 mg, 0.53 mmol), 2-naphthaleneboronic acid (110 mg, 0.64 mmol), caesium carbonate (691 mg, 2.12 mmol) and tetrakis(triphenylphosphine) palladium (6 mg, 5 mmol) according to method A1. The product was purified by CC (hexane/ethyl acetate 8:2); yield: 57 % (100 mg, yellow powder); ¹H NMR (CD₃COCD₃): 8.86 (s, 1H), 8.36 (s, 1H), 8.03-8.00 (m, 2H), 7.95-7.91 (m, 2H), 7.76 (d, *J* = 4.1 Hz, 1H), 7.74 (d, *J* = 4.1 Hz, 1H), 7.59-7.54 (m, 2H), 7.42 (t, *J* = 7.6 Hz, 1H), 7.39 (dt, *J* = 1.5 Hz and *J* = 7.6 Hz, 1H), 7.37-7.36 (m, 1H), 7.15-7.13 (m, 1H); ¹³C NMR (CD₃COCD₃): 188.75, 159.45, 154.30, 144.35, 141.30, 137.95, 135.55, 131.60, 130.90, 130.30, 129.65, 128.85, 128.80, 127.05, 126.70, 125.80, 122.05, 121.25, 117.30; MS (ESI): 331 (M+H)⁺.

[5-(2,3-Dihydro-1-benzofuran-5-yl)-2-thienyl](3-hydroxyphenyl)methanone (25). The title compound was prepared by reaction of **1a** (150 mg, 0.53 mmol), 2,3-dihydro-1-benzofuran-5-boronic acid (105 mg, 0.64 mmol), caesium carbonate (691 mg, 2.12 mmol) and tetrakis(triphenylphosphine) palladium (6 mg, 5 mmol) according to method A1. The product was purified by CC (hexane/ethyl acetate 7:3); yield: 65 % (111 mg, yellow powder); ¹H NMR (CD₃COCD₃): 7.67-7.66 (m, 2H), 7.57-7.55 (m, 1H), 7.44 (d, *J* = 4.1 Hz, 1H), 7.39 (t, *J* = 7.8 Hz, 1H), 7.35 (dt, *J* = 1.3 Hz and *J* = 7.6 Hz, 1H), 7.32-7.31 (m, 1H), 7.11 (ddd, *J* = 1.3 Hz and *J* = 2.5 Hz and *J* = 7.9 Hz, 1H), 6.82 (d, *J* = 8.5 Hz, 1H), 4.63 (t, *J* = 8.8 Hz, 2H), 3.29 (t, *J* = 8.8 Hz, 2H); ¹³C NMR (CD₃COCD₃): 188.55, 159.35, 141.55, 138.05, 131.50, 130.85, 128.40, 127.80, 125.05, 124.80, 122.00, 121.00, 117.20, 111.45, 73.55, 73.50; MS (ESI): 323 (M+H)⁺.

[5-(1,3-Benzodioxol-5-yl)-2-thienyl](3-hydroxyphenyl)methanone (26). The title compound was prepared by reaction of **1a** (150 mg, 0.53 mmol), 1,3-benzodioxole-5-boronic acid (106 mg, 0.64 mmol), caesium carbonate (691 mg, 2.12 mmol) and

tetrakis(triphenylphosphine) palladium (6 mg, 5 mmol) according to method A1. The product was purified by CC (hexane/ethyl acetate 8:2); yield: 70 % (120 mg, yellow powder); ^1H NMR (CD_3COCD_3): 8.76 (s, 1H), 7.66 (d, $J = 4.1$ Hz, 1H), 7.46 (d, $J = 4.1$ Hz, 1H), 7.39 (t, $J = 7.8$ Hz, 1H), 7.35 (dt, $J = 1.3$ Hz and $J = 7.6$ Hz, 1H), 7.33-7.32 (m, 1H), 7.30 (ddd, $J = 0.6$ Hz and $J = 1.9$ Hz and $J = 8.2$ Hz, 1H), 7.28-7.27 (m, 1H), 7.12 (ddd, $J = 1.3$ Hz and $J = 2.5$ Hz and $J = 7.9$ Hz, 1H), 6.93 (d, $J = 7.9$ Hz, 1H), 6.08 (s, 2H); ^{13}C NMR (CD_3COCD_3): 188.60, 159.40, 154.40, 150.55, 143.35, 141.35, 137.90, 131.55, 129.35, 125.60, 122.35, 122.05, 121.15, 117.25, 110.65, 108.15, 103.70; MS (ESI): 325 (M+H) $^+$.

(3-Hydroxyphenyl)[5-(1*H*-indol-5-yl)-2-thienyl]methanone (27). The title compound was prepared by reaction of **1a** (150 mg, 0.53 mmol), indol-5-boronic acid (103 mg, 0.64 mmol), caesium carbonate (691 mg, 2.12 mmol) and tetrakis(triphenylphosphine) palladium (6 mg, 5 mmol) according to method A1. The product was purified by CC (hexane/ethyl acetate 7:3); yield: 47 % (80 mg, yellow powder); ^1H NMR (CD_3COCD_3): 10.46 (s, 1H), 8.70 (s, 1H), 7.90-7.89 (m, 1H), 7.69 (d, $J = 4.1$ Hz, 1H), 7.67 (d, $J = 8.2$ Hz, 1H), 7.53 (d, $J = 4.1$ Hz, 1H), 7.49 (dd, $J = 1.5$ Hz and $J = 8.2$ Hz, 1H), 7.46-7.45 (m, 1H), 7.40 (t, $J = 7.6$ Hz, 1H), 7.36 (dt, $J = 1.5$ Hz and $J = 7.6$ Hz, 1H), 7.34-7.33 (m, 1H), 7.12 (ddd, $J = 1.3$ Hz and $J = 2.5$ Hz and $J = 7.9$ Hz, 1H), 6.54-6.53 (m, 1H); ^{13}C NMR (CD_3COCD_3): 186.40, 159.40, 138.10, 137.50, 131.50, 128.95, 125.05, 122.85, 122.00, 121.00, 119.80, 117.25, 111.10, 103.85; MS (ESI): 320 (M+H) $^+$.

(3-Hydroxyphenyl)[5-(1*H*-indol-6-yl)-2-thienyl]methanone (28). The title compound was prepared by reaction of **1a** (150 mg, 0.53 mmol), indol-6-boronic acid (103 mg, 0.64 mmol), caesium carbonate (691 mg, 2.12 mmol) and tetrakis(triphenylphosphine) palladium (6 mg, 5 mmol) according to method A1. The product was purified by CC (hexane/ethyl acetate 7:3); yield: 49 % (83 mg, yellow powder); ^1H NMR (CD_3COCD_3): 10.48 (s, 1H), 8.77 (s, 1H), 7.90-7.89 (m, 1H), 7.69 (d, $J = 4.1$ Hz, 1H), 7.66 (d, $J = 8.2$ Hz, 1H), 7.53 (d, $J = 4.1$ Hz, 1H), 7.49 (dd, $J = 1.5$ Hz and $J = 8.2$ Hz, 1H), 7.45-7.44 (m, 1H), 7.40 (td, $J = 0.6$ Hz and $J = 7.6$ Hz, 1H), 7.36 (dt, $J = 1.5$ Hz and $J = 7.6$ Hz, 1H), 7.34-7.33 (m, 1H), 7.12 (ddd, $J = 1.3$ Hz and $J = 2.5$ Hz and $J = 7.9$ Hz, 1H), 6.54-6.53 (m, 1H); ^{13}C NMR (CD_3COCD_3): 188.60, 159.40, 156.90, 142.85, 141.60, 138.50, 138.10, 131.50, 131.15, 128.95, 128.45, 125.05, 122.85, 122.00, 121.00, 119.80, 117.25, 111.10, 103.80; MS (ESI): 320 (M+H) $^+$.

(3-Hydroxyphenyl)[5-(2*H*-indazol-5-yl)-2-thienyl]methanone (29). The title compound was prepared by reaction of **1a** (150 mg, 0.53 mmol), 2*H*-indazole-5-boronic acid (104 mg, 0.64 mmol), caesium carbonate (691 mg, 2.12 mmol) and tetrakis(triphenylphosphine) palladium (6 mg, 5 mmol) according to method A2 refluxing the mixture for 14 h instead of 4 h. The product was purified by CC (hexane/ethyl acetate 6:4); yield: 75 % (127 mg, yellow powder); ^1H NMR (CD_3SOCD_3): 13.27 (s, 1H), 9.87 (s, 1H), 8.24 (s, 1H), 8.17 (s, 1H), 7.79 (dd, $J = 1.5$ Hz and $J = 8.5$ Hz, 1H), 7.71 (d, $J = 4.1$ Hz, 1H), 7.66-7.63 (m, 2H), 7.38 (t, $J = 7.9$ Hz, 1H), 7.28 (dt, $J =$

1.3 Hz and $J = 7.9$ Hz, 1H), 7.22-7.21 (m, 1H), 7.06 (ddd, $J = 0.9$ Hz and $J = 2.5$ Hz and $J = 7.9$ Hz, 1H); ^{13}C NMR (CD_3SOCD_3): 186.60, 179.45, 157.35, 153.20, 140.45, 139.85, 138.65, 136.65, 134.35, 129.70, 125.10, 124.65, 124.15, 123.25, 119.50, 118.35, 115.05, 111.05; MS (ESI): 321 (M+H) $^+$.

Biology. [2, 4, 6, 7- ^3H]-E2 and [2, 4, 6, 7- ^3H]-E1 were bought from Perkin Elmer (Boston, USA). Quickszint Flow 302 scintillator fluid was bought from Zinsser Analytic (Frankfurt, Germany). 17 β -HSD1 and 17 β -HSD2 were obtained from human placenta according to previously described procedures.^[49] Fresh human placenta was homogenized and cytosolic fraction and microsomes were separated by centrifugation. For the partial purification of 17 β -HSD1, the cytosolic fraction was precipitated with ammonium sulfate. 17 β -HSD2 was obtained from the microsomal fraction. For the use of human placenta, informed consent was obtained from the parturient.

Inhibition of 17 β -HSD1: Inhibitory activities were evaluated by an established method with minor modifications. Briefly, the enzyme preparation was incubated with NADH [500 μM] in the presence of potential inhibitors at 37 $^\circ\text{C}$ in a phosphate buffer (50 mM) supplemented with 20 % of glycerol and EDTA (1mM). Inhibitor stock solutions were prepared in DMSO. The final concentration of DMSO was adjusted to 1 % in all samples. The enzymatic reaction was started by addition of a mixture of unlabelled- and [2, 4, 6, 7- ^3H]-E1 (final concentration: 500 nM, 0.15 mCi). After 10 min, the incubation was stopped with HgCl_2 and the mixture was extracted with diethylether. After evaporation, the steroids were dissolved in acetonitrile. E1 and E2 were separated using acetonitrile/water (45:55) as mobile phase in a C18 reverse phase chromatography column (Nucleodur C18 Gravity, 3 μm , Macherey-Nagel, Düren, Germany) connected to a HPLC-system (Agilent 1100 Series, Agilent Technologies, Waldbronn, Germany). Detection and quantification of the steroids were performed using a radioflow detector (Berthold Technologies, Bad Wildbad, Germany). The conversion rate was calculated after analysis of the resulting chromatograms according to the following equation:

$\%conversion = \frac{\%E2}{\%E2 + \%E1} \times 100$. Each value was calculated from at least three independent experiments.

Inhibition of 17 β -HSD2: The 17 β -HSD2 inhibition assay was performed similarly to the 17 β -HSD1 procedure. The microsomal fraction was incubated with NAD^+ [1500 μM], test compound and a mixture of unlabelled- and [2, 4, 6, 7- ^3H]-E2 (final concentration: 500 nM, 0.11 mCi) for 20 min at 37 $^\circ\text{C}$. Further treatment of the samples and HPLC separation was carried out as mentioned above. The conversion rate was calculated after analysis of the

resulting chromatograms according to the following equation: $\%conversion = \frac{\%E1}{\%E1 + \%E2} \times 100$.

ER-affinity: The binding affinity of selected compounds to the ER α and ER β was determined according to Zimmermann et al. Briefly, 0.25 pmol of ER α or ER β , respectively, were incubated with [2, 4, 6, 7- 3 H]-E2 (10 nM) and test compound for 1 h at room temperature. The potential inhibitors were dissolved in DMSO (5 % final concentration). Evaluation of non-specific-binding was performed with diethylstilbestrol (10 μ M). After incubation, ligand-receptor complexes were selectively bound to hydroxyapatite (5 g/ 60 mL TE-buffer). The complex formed was separated, washed and resuspended in ethanol. For radiodetection, scintillator cocktail (Quickszint 212, Zinsser Analytic, Frankfurt, Germany) was added and samples were measured in a liquid scintillation counter (Rack Beta Primo 1209, Wallac, Turku, Finland). For determination of the relative binding affinity (RBA), inhibitor and E2 concentrations required to displace 50 % of the receptor bound labeled E2 were determined.

RBA values were calculated according to the following equation:

$$RBA[\%] = \frac{IC_{50}(E2)}{IC_{50}(compound)} \times 100$$

The RBA value for E2 was set at 100 %.

Inhibition of 17 β -HSD1 in T47D cells: A stock culture of T47D cells was grown in RPMI 1640 medium supplemented with 10 % FCS, L-glutamine (2 mM), penicillin (100 IU/mL), streptomycin (100 μ g/mL), insulin-zinc-salt (10 μ g/mL) and sodium pyruvate (1 mM) at 37 $^{\circ}$ C under 5 % CO $_2$ humidified atmosphere. The cells were seeded into a 24-well plate at 1x10 6 cells/well in DMEM medium with FCS, L-glutamine and the antibiotics added in the same concentrations as mentioned above. After 24 h the medium was changed for fresh serum free DMEM and a solution of test compound in DMSO was added. Final concentration of DMSO was adjusted to 1 % in all samples. After a pre-incubation of 30 min at 37 $^{\circ}$ C with 5 % CO $_2$, the incubation was started by addition of a mixture of unlabelled- and [2, 4, 6, 7- 3 H]- E1 (final concentration : 50 nM, 0.15 mCi). After 0.5 h incubation, the enzymatic reaction was stopped by removing of the supernatant medium. The steroids were extracted with diethylether. Further treatment of the samples was carried out as mentioned for the 17 β -HSD1 assay.

Metabolic stability: Human liver microsomes (final protein concentration 0.5 mg/mL), 0.1 M phosphate buffer pH 7.4 and test compound (final substrate concentration = 3 μ M; final DMSO concentration = 0.25 %) were preincubated at 37 $^{\circ}$ C prior to the addition of NADPH (final concentration = 1 mM) to initiate the reaction. Dextrometorphan and verapamil were used as references. All incubations were performed singularly for each test compound. Each compound was incubated for 0, 5, 15, 30 and 45 min (control: 45 min). The reactions were stopped by the addition of 50 μ L methanol containing internal standard at the appropriate time points. The incubation plates were centrifuged at 2,000 rpm for 20 min at 4 $^{\circ}$ C to precipitate the protein. The sample supernatants were combined in cassettes of up to 4 compounds and analyzed using LC-MS/MS.

Molecular Modeling: Docking studies were performed using the AutoDock4.2^[56] program. Atomic coordinates of 17 β -HSD1 were derived from the structure of the ternary complex 17 β -HSD1, NADP⁺ and E2 (PDB-ID: 1FDT (conformation B for residues 187-200)). The crystal structure was energy minimized with MOE2009.10 (Chemical Computing Group Inc., Montreal, Canada) applying the AMBER99 force field and generalized Born model, keeping the coordinates of backbone atoms fixed. Ligand structures were built, assigned AM1-BCC charges, and minimized in MOE with the MMFF94x force field. The 17 β -HSD1 x-ray structure and ligand structures were prepared for docking studies through the graphical user interface AutoDockTools1.5.4.^[56] For the ligands, nonpolar hydrogen atoms were deleted, rotatable bonds were defined and AM1-BCC charges kept. For the protein, non-polar hydrogen atoms were deleted and charges were added to the structure. The docking area has been defined by a box, centered on the steroid binding site. Grid points of 90 x 90 x 90 with 0.250 Å spacing were calculated around the docking area for all the ligand atom types using AutoGrid4.2. For each inhibitor, 50 separate docking calculations were performed. Each docking calculation consisted of 25x10⁵ energy evaluations using the Lamarckian genetic algorithm local search (GALS) method. Each docking run was performed with a population size of 250. A mutation rate of 0.02 and a crossover rate of 0.8 were used to generate new docking trials for subsequent generations. The docking results from each of the 50 calculations were clustered on the basis of root-mean-square deviation (RMSD = 2.0 Å) between the Cartesian coordinates of the ligand atoms and were ranked on the basis of the free binding energy.

Acknowledgement

We are grateful to the Deutsche Forschungsgemeinschaft (HA1315/8-1) for financial support of this work. We thank Dr. Jörg Hauptenthal for coordinating the biological tests and Jannine Ludwig for her help in performing the in vitro tests (17 β -HSD1, 17 β -HSD2, cellular inhibition assay).

References

- [1] M. M. Miettinen, M. V. Mustonen, M. H. Poutanen, V. V. Isomaa, R. K. Vihko, *Biochem. J.* **1996**, *314*, 839-845.
- [2] S. Nobel, L. Abrahmsen, U. Oppermann, *Eur. J. Biochem.* **2001**, *268*, 4113-4125.
- [3] J. Adamski, F. J. Jakob, *Mol. Cell. Endocrinol.* **2001**, *171*, 1-4.
- [4] F. Labrie, V. Luu-The, S. X. Lin, J. Simard, C. Labrie, M. El-Alfy, G. Pelletier, A. Belanger, *J. Mol. Endocrinol.* **2000**, *25*, 1-16.
- [5] R. C. Travis, T. J. Key, *Breast Cancer Res.* **2003**, *5*, 239-247.
- [6] G. S. Dizerega, D. L. Barber, G. D. Hodgen, *Fertil. Steril.* **1980**, *33*, 649-653.
- [7] T. Saloniemi, P. Jarvensivu, P. Koskimies, H. Jokela, T. Lamminen, S. Ghaem-Maghani, R. Dina, P. Damdimopoulou, S. Makela, A. Perheentupa, H. Kujari, J. Brosens, M. Poutanen, *Am. J. Pathol.* **2010**, *176*, 1443-1451.
- [8] J. Geisler, *Breast Cancer* **2008**, *15*, 17-26.
- [9] J. Geisler, P. E. Lonning, *Clin. Cancer Res.* **2005**, *11*, 2809-2821.
- [10] F. Leonetti, A. Favia, A. Rao, R. Aliano, A. Paluszczak, R. W. Hartmann, A. Carotti, *J. Med. Chem.* **2004**, *47*, 6792-6803.
- [11] M. Le Borgne, P. Marchand, M. Duflos, B. Delevoye-Seiller, S. Piessard-Robert, G. Le Baut, R. W. Hartmann, M. Palzer, *Arch. Pharm. (Weinheim)* **1997**, *330*, 141-145.
- [12] C. I. Herold, K. L. Blackwell, *Clin. Breast Cancer* **2008**, *8*, 50-64.
- [13] S. Gobbi, C. Zimmer, F. Belluti, A. Rampa, R. W. Hartmann, M. Recanatini, A. Bisi, *J. Med. Chem.* **2010**, *53*, 5347-5351.
- [14] M. Le Borgne, P. Marchand, B. Delevoye-Seiller, J. M. Robert, G. Le Baut, R. W. Hartmann, M. Palzer, *Bioorg. Med. Chem. Lett.* **1999**, *9*, 333-336.
- [15] S. Gobbi, A. Cavalli, A. Rampa, F. Belluti, L. Piazza, A. Paluszczak, R. W. Hartmann, M. Recanatini, A. Bisi, *J. Med. Chem.* **2006**, *49*, 4777-4780.
- [16] S. Chen, S. Masri, Y. Hong, X. Wang, S. Phung, Y. C. Yuan, X. Wu, *J. Steroid Biochem. Mol. Biol.* **2007**, *106*, 8-15.
- [17] F. Picard, T. Schulz, R. W. Hartmann, *Bioorg. Med. Chem.* **2002**, *10*, 437-448.
- [18] E. Baston, R. W. Hartmann, *Bioorg. Med. Chem. Lett.* **1999**, *9*, 1601-1606.
- [19] E. Baston, A. Paluszczak, R. W. Hartmann, *Eur. J. Med. Chem.* **2000**, *35*, 931-940.
- [20] J. M. Day, P. A. Foster, H. J. Tutill, M. F. Parsons, S. P. Newman, S. K. Chander, G. M. Allan, H. R. Lawrence, N. Vicker, B. V. Potter, M. J. Reed, A. Purohit, *Int. J. Cancer* **2008**, *122*, 1931-1940.
- [21] B. Husen, K. Huhtinen, M. Poutanen, L. Kangas, J. Messinger, H. Thole, *Mol. Cell. Endocrinol.* **2006**, *248*, 109-113.
- [22] B. Husen, K. Huhtinen, T. Saloniemi, J. Messinger, H. H. Thole, M. Poutanen, *Endocrinology* **2006**, *147*, 5333-5339.
- [23] F. Haller, E. Moman, R. W. Hartmann, J. Adamski, R. Mindnich, *J. Mol. Biol.* **2010**, *399*, 255-267.
- [24] S. Marchais-Oberwinkler, C. Henn, G. Möller, T. Klein, M. Lordon, M. Negri, A. Oster, A. Spadaro, R. Werth, K. Xu, M. Frotscher, R. W. Hartmann, J. Adamski, *J. Steroid Biochem. Mol. Biol.* **2010**, *125*, 66-82.
- [25] D. M. Moore, D. V. Kalvakolanu, S. M. Lippman, J. J. Kavanagh, W. K. Hong, E. C. Borden, M. Paredes-Espinoza, I. H. Krakoff, *Semin. Hematol.* **1994**, *31*, 31-37.
- [26] M. Negri, M. Recanatini, R. W. Hartmann, *PLoS ONE* **2010**, *5*, e12026.
- [27] D. Poirier, *Anticancer Agents Med. Chem.* **2009**, *9*, 642-660 and references therein cited.
- [28] P. Brožić, T. Lanišnik Rižner, S. Gobec, *Curr. Med. Chem.* **2008**, *15*, 137-150 and references therein cited.

- [29] J. M. Day, H. J. Tutill, A. Purohit, M. J. Reed, *Endocr.-Relat. Cancer* **2008**, *15*, 665-692 and references therein cited.
- [30] J. M. Day, H. J. Tutill, A. Purohit, *Minerva Endocrinol.* **2010**, *35*, 87-108 and references therein cited.
- [31] J. Messinger, L. Hirvelä, B. Husen, L. Kangas, P. Koskimies, O. Pentikäinen, P. Saarenketo, H. Thole, *Mol. Cell. Endocrinol.* **2006**, *248*, 192-198.
- [32] S. Karkola, A. Lilienkampf, K. Wähälä, *Chemmedchem* **2008**, *3*, 461-472.
- [33] M. Frotscher, E. Ziegler, S. Marchais-Oberwinkler, P. Kruchten, A. Neugebauer, L. Fetzer, C. Scherer, U. Müller-Vieira, J. Messinger, H. Thole, R. W. Hartmann, *J. Med. Chem.* **2008**, *51*, 2158-2169.
- [34] S. Marchais-Oberwinkler, P. Kruchten, M. Frotscher, E. Ziegler, A. Neugebauer, U. D. Bhoga, E. Bey, U. Müller-Vieira, J. Messinger, H. Thole, R. W. Hartmann, *J. Med. Chem.* **2008**, *51*, 4685-4698.
- [35] S. Marchais-Oberwinkler, M. Frotscher, E. Ziegler, R. Werth, P. Kruchten, J. Messinger, H. Thole, R. W. Hartmann, *Mol. Cell. Endocrinol.* **2009**, *301*, 205-211.
- [36] S. Marchais-Oberwinkler, M. Wetzel, E. Ziegler, P. Kruchten, R. Werth, C. Henn, R. W. Hartmann, M. Frotscher, *J. Med. Chem.* **2011**, *54*, 534-547.
- [37] E. Bey, S. Marchais-Oberwinkler, P. Kruchten, M. Frotscher, R. Werth, A. Oster, O. Algul, A. Neugebauer, R. W. Hartmann, *Bioorg. Med. Chem.* **2008**, *16*, 6423-6435.
- [38] E. Bey, S. Marchais-Oberwinkler, R. Werth, M. Negri, Y. A. Al-Soud, P. Kruchten, A. Oster, M. Frotscher, B. Birk, R. W. Hartmann, *J. Med. Chem.* **2008**, *51*, 6725-6739.
- [39] Y. A. Al-Soud, E. Bey, A. Oster, S. Marchais-Oberwinkler, R. Werth, P. Kruchten, M. Frotscher, R. W. Hartmann, *Mol. Cell. Endocrinol.* **2009**, *301*, 212-215.
- [40] E. Bey, S. Marchais-Oberwinkler, M. Negri, P. Kruchten, A. Oster, R. Werth, M. Frotscher, B. Birk, R. W. Hartmann, *J. Med. Chem.* **2009**, *52*, 6724-6743.
- [41] P. Kruchten, R. Werth, E. Bey, A. Oster, S. Marchais-Oberwinkler, M. Frotscher, R. W. Hartmann, *J. Steroid Biochem. Mol. Biol.* **2009**, *114*, 200-206.
- [42] A. Oster, S. Hinsberger, R. Werth, S. Marchais-Oberwinkler, M. Frotscher, R. W. Hartmann, *J. Med. Chem.* **2010**, *53*, 8176-8186.
- [43] E. J. Jeong, X. Liu, X. Jia, J. Chen, M. Hu, *Curr. Drug Metab.* **2005**, *6*, 455-468.
- [44] M. Mazumdar, D. Fournier, D. W. Zhu, C. Cadot, D. Poirier, S. X. Lin, *Biochem. J.* **2009**, *424*, 357-366.
- [45] A. Oster, T. Klein, R. Werth, P. Kruchten, E. Bey, M. Negri, S. Marchais-Oberwinkler, M. Frotscher, R. W. Hartmann, *Bioorg. Med. Chem.* **2010**, *18*, 3494-3505.
- [46] C. Gege, W. Regenhardt, O. Peters, A. Hillisch, J. Adamski, G. Mçller, D. Deluca, W. Elger, B. Schneider, (Schering AG; Berlin, Germany), WO/ 2006/003012, **2006** ; [Chem. Abstr. **2006**, *144*, 129148] .
- [47] B. E. Fink, D. S. Mortensen, S. R. Stauffer, Z. D. Aron, J. A. Katzenellenbogen, *Chem. Biol.* **1999**, *6*, 205-219.
- [48] N. Miyaura, A. Suzuki, *Synth. Commun.* **1995**, *11*, 513-519.
- [49] P. Kruchten, R. Werth, S. Marchais-Oberwinkler, M. Frotscher, R. W. Hartmann, *Mol. Cell. Endocrinol.* **2009**, *301*, 154-157.
- [50] B. T. Zhu, G. Z. Han, J. Y. Shim, Y. Wen, X. R. Jiang, *Endocrinology* **2006**, *147*, 4132-4150.
- [51] T. Puranen, M. Poutanen, D. Ghosh, P. Vihko, R. Vihko, *Mol. Endocrinol.* **1997**, *11*, 77-86.
- [52] A. Azzi, P. H. Rehse, D. W. Zhu, R. L. Campbell, F. Labrie, S.-X. Lin, *Nat. Struct. Biol.* **1996**, *3*, 665-668.
- [53] M. W. Sawicki, M. Eрман, T. Puranen, P. Vihko, D. Ghosh, *Proc. Natl. Acad. Sci. U.S.A.* **1999**, *96*, 840-845.
- [54] C. Mazza, R. Breton, D. Housset, J. C. Fontecilla-Camps, *J. Biol. Chem.* **1998**, *273*, 8145-8152.
- [55] J. Zimmermann, R. Liebl, E. von Angerer, *J. Steroid Biochem. Mol. Biol.* **2005**, *94*, 57-66.
- [56] G. M. Morris, R. Huey, W. Lindstrom, M. F. Sanner, R. K. Belew, D. S. Goodsell, A. J. Olson, *J. Comput. Chem.* **2009**, *30*, 2785-2791.

4 Final Discussion

Exploiting all the available information on the system under study is characteristic for a rational drug design approach that is able to organize drug discovery more successful. Thus, the aim of the present study was to increase the body of knowledge of protein-ligand interactions and active site topologies to advance drug discovery at different stages: (1) hit identification, characterization and optimization in case of PqsR and (2) lead optimization in case of 17 β -HSD1.

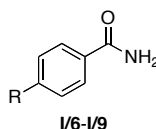
One major goal of this work was to discover low molecular weight compounds targeting the *P. aeruginosa* transcriptional regulator PqsR. In doing so, we followed a rational design strategy, which was based on the κ -opioid receptor agonist **I/1**[†] and is described in chapter 3.1. The latter was subjected to fragmentation into smaller pieces and analogs and the resulting library was screened for affinity toward PqsR in a SPR biosensor assay to map out different pharmacophoric elements required for high-affinity binding. Fragment-based drug discovery is considered as a promising strategy to address antibacterial discovery issues that are namely: (1) the lack of chemical diversity compatible with novel anti-bacterial targets (Mochalkin et al., 2009) and (2) the fact that the physicochemical properties, which are required to penetrate into the bacterial cytoplasm are considerably different from those needed for eukaryotic drug discovery (O'Shea and Moser, 2008). These are also two possible explanations why the high expectations of discovering novel antibacterial drugs employing high-throughput screening strategies with very large synthetic or natural product compound libraries have not met with success (Mochalkin et al., 2009). Some antibiotic natural products may have been naturally selected to possess desirable antibacterial properties, however, the absence of desirable drug-like properties and the low tractability for medicinal chemistry lead optimization efforts makes it difficult to use them as drugs. Another advantage of fragment-based design compared to conventional screening attempts is the number of screened compounds. In a fragment screening typically several thousand compounds are evaluated while a conventional screening assesses a million or more compounds (Hajduk and Greer, 2007). Besides the mentioned pros of screening small molecules an important issue is the usually low binding affinity (Waldrop, 2009). But LE, which is the ratio of free binding affinity to the number of heavy atoms, normalizes affinity and molecular size of a compound and therefore it is a valuable tool for effective hit selection. In the present study, it was successfully applied and led among other candidates to the identification of the most promising hit **I/4** (LE=0.63 kcal/mol). The latter also showed antagonistic activity in a heterologous reporter gene assay in *E. coli* highlighting its potential for further optimization.

[†] For the sake of clarity, all compounds that are referred to in chapter 4 are characterized by a Roman numeral I–IV to identify the paper in which they are published, and an Arabic numeral that is identical with the corresponding compound number of the particular publication (e.g., **I/1** is compound **1** from paper I)

Using *E. coli* for initial investigation of functionality allows to evaluate agonistic and antagonistic activities independent of the entire *pqs* system present in *P. aeruginosa* (Fletcher et al., 2007). Further, *P. aeruginosa* is characterized by a synergy between drug efflux pumps with broad substrate specificity and low outer membrane permeability (Ma et al., 1994) that would impede the analysis of structure-functional activity relationships for compounds, which have insufficient physicochemical properties to penetrate into the *P. aeruginosa* cytoplasm. However, especially due to the higher bar for getting small molecules into *P. aeruginosa* it is crucial to investigate, at least for the most active compounds, whether they also work in a *P. aeruginosa* background.

During the optimization of compound **I/4**, it has been observed that the introduction of an alkyl chain in the *para*-position of the benzamide core and its stepwise enlargement led to a gradual increase in affinity (compounds **I/6-I/9**). Interestingly, the rising affinity in this series is due to incremental more favorable enthalpic contributions. This finding is an indication that the alkyl chain contributes to ligand binding via specific non-covalent interactions and that the enlarged affinity is not just because of hydrophobic effects. Otherwise, increasing entropic contributions would have reflected it. As shown in Table 1, the latter is clearly not the case and the entropic contribution becomes rather more unfavorable in the course of expanding the alkyl residue.

Table 1. Thermodynamic parameters of ligands **I/6-I/9** binding to PqsR.



Ligand	R	K_D [μM]	ΔG [kcal mol ⁻¹]	ΔH [kcal mol ⁻¹]	$-T\Delta S$ [kcal mol ⁻¹]
6	Me	31.2±3.4	-6.1±0.1	-2.2±0.1	-3.9±0.1
7	Et	7.3±0.6	-7.0±0.1	-4.6±0.3	-2.4±0.3
8	<i>i</i> Pr	3.0±0.4	-7.5±0.1	-6.3±0.3	-1.3±0.4
9	<i>t</i> Bu	0.9±0	-8.3±0	-9.7±0.3	1.5±0.3

ITC titrations were performed at 298 K. Data represent mean \pm SD from at least three independent experiments.

Negatively correlated ΔH and $-T\Delta S$ changes are often observed in protein ligand interactions. This ubiquitous phenomenon is termed as enthalpy-entropy compensation and it arises from the structuring of protein regions by newly formed hydrogen bonds or other polar interactions, resulting in a loss in conformational entropy (Ladbury et al., 2010). This trend becomes particularly evident when plotting the ΔH value versus the $-T\Delta S$ values (Figure 15) revealing a reasonable linear correlation ($r^2 = 0.9573$, $n = 9$). In this context, ITC is a powerful method that allows improving our understanding of the enthalpic and entropic contributions to binding.

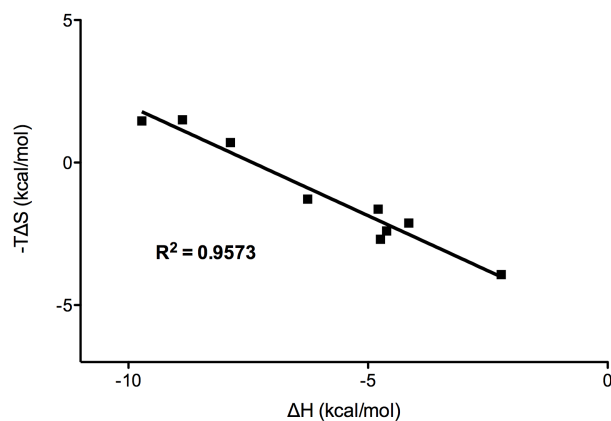


Figure 15. Plot of enthalpy (ΔH) vs entropy ($-T\Delta S$) for the investigated compounds **I/1**, **I/4**, and **I/6-I/12**.

To understand these interesting results on the molecular basis, site-directed mutagenesis was employed in combination with ITC. Compared to the wild-type, **I/9** binds to F221A mutant PqsR with a significant loss in ΔH (7.6 kcal/mol; Figure 16a) demonstrating that this amino acid is involved in a specific interaction, such as a CH/ π hydrogen bond. The latter has its origin in dispersion forces, which have an impact on the enthalpic term of free energy (Ramírez-Gualito et al., 2009). A salient feature of the CH/ π hydrogen bond is that it works cooperatively and for cases involving aliphatic CH groups as the hydrogen donor, the energy of a CH/ π hydrogen bond is between -1.5 and -2.5 kcal/mol (Nishio, 2011). This indicates that Phe221 might form three CH/ π bonds with the *t*Bu-moiety of **I/9** (Figure 16b) as described for the interaction of benzene with isobutane (Ran and Wong, 2006).

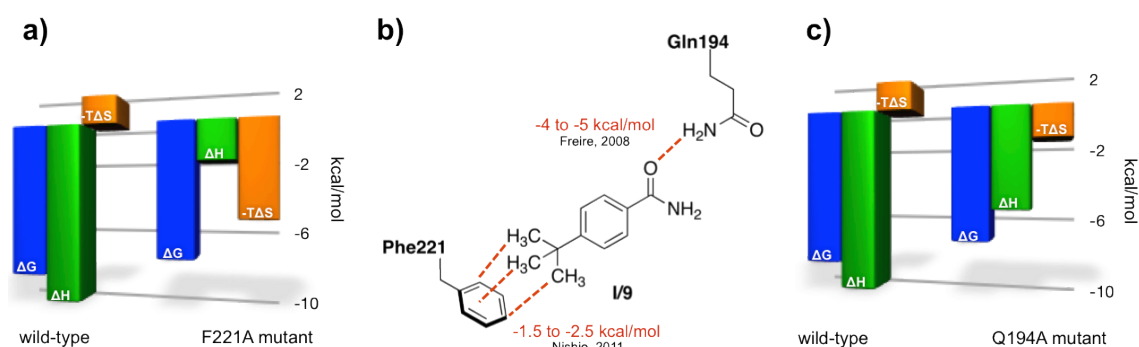


Figure 16. **a)** Thermodynamic profiles determined by ITC for the binding of ligand **I/9** to wild-type and F221A mutant PqsR. **b)** Proposed interactions between **I/9** and PqsR. **c)** Thermodynamic profiles determined by ITC for the binding of ligand **I/9** to wild-type and Q194A mutant PqsR. Hydrogen bonds are represented in red dashed lines.

Interestingly, for the interaction of **I/9** with the Q194A mutant also a loss in ΔH (4.4 kcal/mol; Figure 16c) was observed. Considering that a well-placed H-bond can make a favorable enthalpic contribution in the order of -4 to -5 kcal/mol (Freire, 2008), the results suggest that

Gln194 forms a H-bond with the amide function of **I/9** as shown in Figure 16b. Hence, thermodynamic analysis particularly in combination with site-directed mutagenesis provides a valuable tool to investigate protein-ligand interactions.

A further interesting observation made during this study was that the replacement of the amide in **I/9** and **I/7**, which showed agonistic and antagonistic activity, by a hydroxamic acid (compounds **I/11** and **I/12**) led to pure antagonists. Probably, the introduced OH group makes additional interactions that favour antagonism or it leads to a slight shift of the hydroxamic acid-derived ligands in the effector binding site. The latter could result in the formation of new interactions that promote antagonistic activity or in the loss of interactions that are essential for agonistic activity. However, the presence of a H-bond between the hydroxamic acid **I/11** and Gln194 is substantiated by the thermodynamic data. This finding led us to the conclusion that Gln194 is no key player in determining between agonistic and antagonistic activity.

Despite the higher bar for getting small molecules into *P. aeruginosa* the antagonistic activity of **I/11** could be confirmed (IC_{50} in *E. coli* = 12.5 μ M vs. IC_{50} in *P. aeruginosa* = 23.6 μ M). Additionally, **I/11** was able to reduce the production of the virulence factor pyocyanin in *P. aeruginosa* (IC_{50} = 87.2 μ M). These encouraging findings confirmed that fragment-based design is a proper strategy to handle physicochemical property issues. Probably, the penetration of the small hydrophilic hydroxamic acid **I/11** (MW=193.11 g/mol; logP = 2.1) across the outer membrane exceeds its efflux or the antagonist **I/11** is no substrate of the efflux pumps.

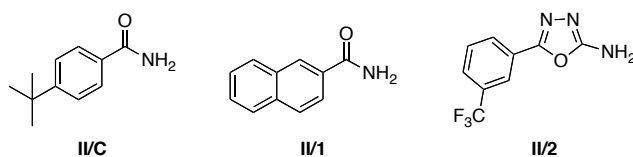
In summary, through application of rational design and biophysical methods, we developed to the best of our knowledge the first small-molecule PqsR ligands. LEs and functional properties were used to guide the elaboration process that resulted in the potent hydroxamic acid-derived PqsR antagonist **I/11**. Compared to the recently described HHQ analogues (Lu et al., 2012) compound **I/11** is a less potent antagonist but, as a consequence of its low molecular weight and its activity in *P. aeruginosa*, it has a high potential for further optimization. However, due to its ability to chelate metal ions the hydroxamic acids could impede bacterial iron utilization causing bacteriostasis. As this would counterwork the concept of *quorum sensing* inhibition, hit to lead optimization should address the replacement of this functional group. Site-directed mutagenesis together with thermodynamic analysis disclosed that Gln194 and Phe221 are involved in ligand binding, probably by making hydrogen bonds and CH/ π interactions, respectively. Though, the molecular basis of agonism and antagonism is still not understood and future experiments should tackle these questions.

Structural information and thermodynamic parameters or their accordant efficiency indices can be used to guide fragment progressing that includes three main strategies: linking, growing, and merging (Schulz and Hubbard, 2009). Besides the thermodynamic and functional characterization of the screening hits **II/1-II/5** towards PqsR chapter 3.2 describes the

application of site-directed mutagenesis, structure modifications, and calorimetric analysis to study PqsR-ligand interactions and to estimate the covered space in the binding pocket.

The efficiency index that includes affinity is LE. The latter plays an important role in selecting candidates that will undergo hit-to-lead optimization but it can also be used as a quantitative measure of effective fragment elaboration. LE values > 0.33 kcal/mol are desirable (Hopkins et al., 2004) and it is important to begin with a fragment above this threshold, regardless of absolute potency or molecular weight. Because efficiency remains constant throughout lead optimization, beginning with a suboptimal fragment lead can frustrate subsequent optimization efforts, especially when trying to balance multiple properties such as solubility, permeability, and stability. A drop in LE of more than 10% during fragment elaboration is likely an indication that either the site or the nature of the modification is not ideal, even if modest gains in potency are achieved (Hajduk, 2006). The enthalpic contribution is also often used for decision-making in hit selection and enthalpy driven binders are rather taken on the next optimization level than entropy driven binders for three major reasons: (1) it is harder to improve the ΔH contribution than to improve the ΔS contribution; (2) enthalpy steered interactions such as hydrogen bonds are more specific than entropy driven hydrophobic contacts, thus the optimization of enthalpic binders will reduce the risk of unspecific binding to off-target proteins, which is often associated with unwanted side-effects; (3) increasing the entropic contribution is accompanied by increasing hydrophobicity and therefore the improvement is limited by the compounds solubility (Ladbury et al., 2010). Based on these criteria the screening hits **II/1-II/5** are appropriate candidates for optimization: LEs range from 0.35 to 0.85 kcal/mol and all compounds show enthalpy driven binding.

Table 2. Effect of point mutations on the thermodynamic parameters of ligands **II/C**, **II/1**, **II/2**.



Ligand	Q194A			F221A		
	$\Delta\Delta G$ [kcal mol ⁻¹]	$\Delta\Delta H$ [kcal mol ⁻¹]	$-T\Delta\Delta S$ [kcal mol ⁻¹]	$\Delta\Delta G$ [kcal mol ⁻¹]	$\Delta\Delta H$ [kcal mol ⁻¹]	$-T\Delta\Delta S$ [kcal mol ⁻¹]
II/C	$-1.3 \pm 0.1^*$	$-4.4 \pm 0.3^*$	$3.1 \pm 0.3^*$	$-1.0 \pm 0.1^*$	$-7.6 \pm 0.3^*$	$6.6 \pm 0.4^*$
II/1	$-1.1 \pm 0.1^*$	$-3.2 \pm 0.2^*$	$2.1 \pm 0.2^*$	$-0.4 \pm 0.1^*$	$-7.1 \pm 0.2^*$	$6.7 \pm 0.2^*$
II/2	$-0.6 \pm 0.1^*$	-0.3 ± 0.6	-0.3 ± 0.7	$-0.6 \pm 0.1^*$	$-7.1 \pm 0.5^*$	$6.5 \pm 0.6^*$

$\Delta\Delta G$, $\Delta\Delta H$, and $-T\Delta\Delta S$ are $\Delta G_{WT} - \Delta G_{mutant}$, $\Delta H_{WT} - \Delta H_{mutant}$, and $-T(\Delta S_{WT} - \Delta S_{mutant})$, respectively. Negative values indicate a loss; positive values, a gain compared to wild-type. Errors indicate SD calculated via Gaussian error propagation. Significance: effect of the point mutation on the thermodynamic parameters of ligand binding compared to the wild-type. * $p < 0.003$; * $p < 0.05$.

Structural information has successfully been applied in numerous fragment-based lead discovery campaigns to guide optimization (Schulz and Hubbard, 2009). In this subproject, site-directed mutagenesis in combination with thermodynamic analysis was applied to investigate the space in the binding pocket that is covered by the ligands **II/1** and **II/2** (Table 2). Of the identified hits, the latter looked the most promising with respect to the above described criteria as well as functionality that is a further key feature in decision-making. Just like observed for compound **II/C**, Phe221 and Gln194 are also involved in the binding of **II/1**. Due to the structural similarity between these two compounds this finding is not wondrous and it can be assumed that **II/1** binds in a similar orientation: the naphthalene core takes part in a π - π interaction with Phe221 and the amide makes an H-bond with Gln194 (Figure 17a).

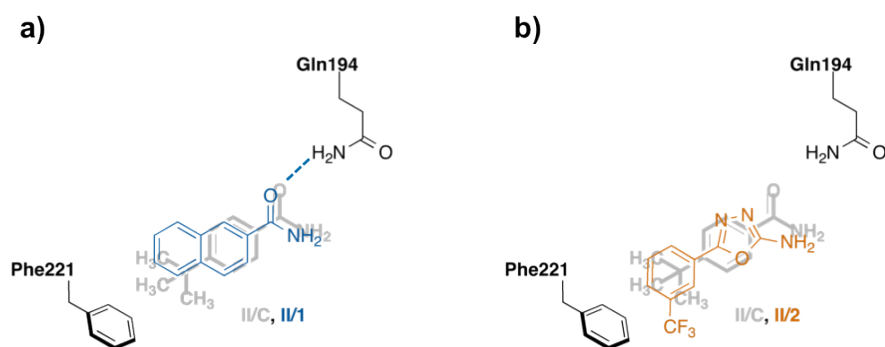


Figure 17. Hypothetical binding modes of compounds **II/1** and **II/2**. **a)** Overlay of the proposed binding modes of **II/C** (grey) and **II/1** (blue) in the PqsR effector binding site. **b)** Overlay of the proposed binding modes of **II/C** (grey) and **II/2** (orange) in the PqsR effector binding site. Hydrogen bonds are represented in red dashed lines. For the sake of clarity π - π -interactions are not depicted.

Thermodynamic analysis revealed that only Phe221 is involved in the binding of the oxadiazole **II/2** but competition experiments confirmed that it occupies the same site as **II/C**. These interesting findings can be rationalized on the proposed binding mode of **II/2**, which is depicted in Figure 17b. Possibly, the phenyl moiety of **2** makes a π - π interaction with F221 that is favored by the presence of the electron withdrawing CF_3 -substituent (Lewis et al., 2012). Oxadiazoles are often used as replacements for carbonyl containing compounds such as esters, amides, and hydroxamic acids and the two nitrogen atoms in the 1,3,4-isomers are described to be very favorable hydrogen bond acceptors (Boström et al., 2012). However, in this case the oxadiazole ring of **II/2** is not able to take over the H-bond acceptor ability of the carbonyl oxygen of **II/C** to interact with Gln194, as shown by the thermodynamic data (Table 2). Most likely, this is caused by an inappropriate geometrical orientation (distance, angle) of **II/2** in the binding site. The fact that **II/2** is a pure and potent PqsR antagonist, which does not interact with Gln194 underpins the above stated hypothesis that Gln194 is not important for antagonism.

The combination of site-directed mutagenesis with thermodynamic analysis has led to the identification of fragments with different scaffolds (**II/C** and **II/2**) that bind to the same site but

do not occupy exactly the same space. Thus, the gained structural information can be used to elaborate them by growing or merging while an attempt to link both fragments can be excluded. Accordingly, the here-applied approach to preserve structural information is a valuable strategy to direct fragment progressing. However, it is limited to the ability of identifying binding sites and interacting amino acids but it does not deliver a detailed structure of the protein-fragment complex including the targetable amino acids, which can be used to identify how and where to grow or modify the fragment. Crystallization of the complexes is a reliable method to obtain such information.

In the present study, ITC was also employed to derive and understand SAR. It was found that the CF_3 moiety plays an important role for the binding of **II/2**. Replacing it by a methyl group (compound **II/6**) reduced the affinity toward PqsR (**II/6**, $K_D = 12.4 \mu\text{M}$ vs. **II/2**, $K_D = 1.3 \mu\text{M}$) as result of a significant loss in ΔH of 4.4 kcal/mol (Figure 18).

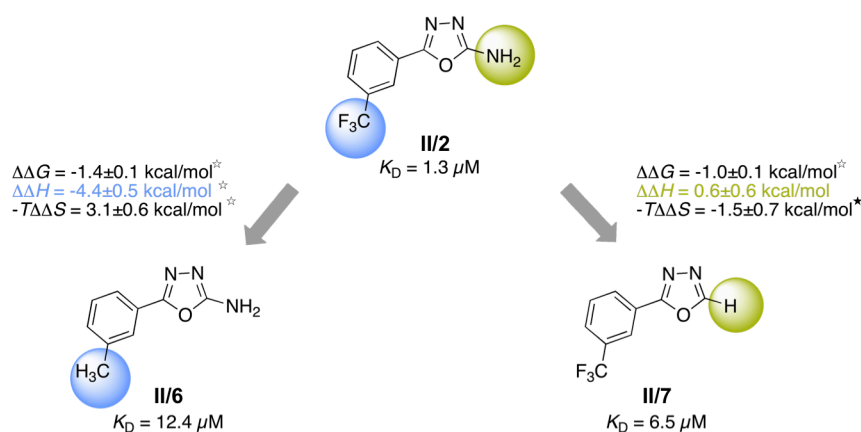


Figure 18. Relative thermodynamic contributions of functional groups to PqsR binding. $\Delta\Delta G$, $\Delta\Delta H$, and $-T\Delta\Delta S$ are $\Delta G_{\text{II/2}} - \Delta G_{\text{II/6; II/7}}$, $\Delta H_{\text{II/2}} - \Delta H_{\text{II/6; II/7}}$, and $-T(\Delta S_2 - \Delta S_{6/7})$, respectively. Negative values indicate a loss; positive values, a gain compared to compound **2**. Errors indicate SD calculated via Gaussian error propagation. Significance: thermodynamic contribution of the functional group on the binding of **2** to PqsR. ^{*} $p < 0.003$; ^{*} $p < 0.05$.

This finding is in accordance with the hypothetical binding mode of **II/2** proposing a π - π interaction between the phenyl ring of **II/2** and Phe221 (Figure 17a). Electron withdrawing substituents such as CF_3 promote π - π interactions while the introduction of electron-donating groups such as alkyl moieties are predicted to induce ever more unfavorable effects on π - π interactions. The latter can be attributed to repulsion of the increasingly negative electron densities forming on the aromatic centre (Lewis et al., 2012).

In comparison to **II/2** ($K_D = 1.3 \mu\text{M}$) compound **II/7** ($K_D = 6.5 \mu\text{M}$), which does not have an amino group in 2-position of the oxadiazole ring, shows a lower binding affinity. But what is even more important is the fact, that the enthalpic contribution is rather constant for both ligands (Figure 18). Thus, it can be assumed that the amino group of **II/2** is not involved in a specific interaction like an H-bond. This interesting observation would not have been made using

different technologies or assay formats monitoring only affinity. In view of that, ITC, which allows dissecting free energy of binding into its enthalpic and entropic contributions, is a helpful tool to analyze and understand SAR. The low throughput and the high amounts of protein, which are required, though, prevent thermodynamic profiling from being performed routinely.

In summary, thermodynamic analysis together with site-directed mutagenesis were used for hit characterization, as guidepost for candidate selection, and to understand SAR. The structural information obtained by this strategy led to the identification of fragments (**II/C** and **II/2**) that have the potential to be optimized by the application of fragment growing or merging. The relative importances of functional groups of **II/2** were investigated by ITC. The obtained results are of great relevance for the imminent optimization steps. Besides synthetic modifications future experiments should address the crystallization of PqsR-fragment complexes to get detailed information how and where to grow or modify the fragments. As alternative NMR spectroscopy could be used that also is a standard method for macromolecular three-dimensional structure determination (Pellecchia et al., 2002).

In the chapters 3.1 and 3.2 the comparison of thermodynamic signatures obtained for PqsR ligands towards the wild-type protein and site-directed mutants was successfully applied to increase the knowledge of protein–ligand interactions. As alternative to this laborious site-directed mutagenesis experiments, proteins from various species, which are highly conserved in sequence and differ only in few residues, might be considered. This latter approach was applied in subproject 3.3 employing human and marmoset monkey 17 β -HSD1. The present study aimed at increasing the information of active site topologies and protein-ligand interactions to facilitate structure-based design and optimization of 17 β -HSD1 inhibitors. The inhibitory potencies of selected members of different non-steroidal inhibitor classes toward marmoset 17 β -HSD1 were determined and the data were compared with the values obtained for the human enzyme. While among other inhibitor classes the bicyclic substituted hydroxyphenylmethanones (representative structure: **III/12**) showed comparable inhibition data for both enzymes, a species specific inhibition profile was observed in the class of the (hydroxyphenyl)naphthols (representative structure: **III/19**; Figure 19). A combination of computational methods, including homology modelling, molecular docking, MD simulation, and binding energy calculation, was used to develop a reasonable model of the three-dimensional structure of marmoset 17 β -HSD1 and inhibition data of compounds **III/12** and **III/19** were rationalized on the structural basis.

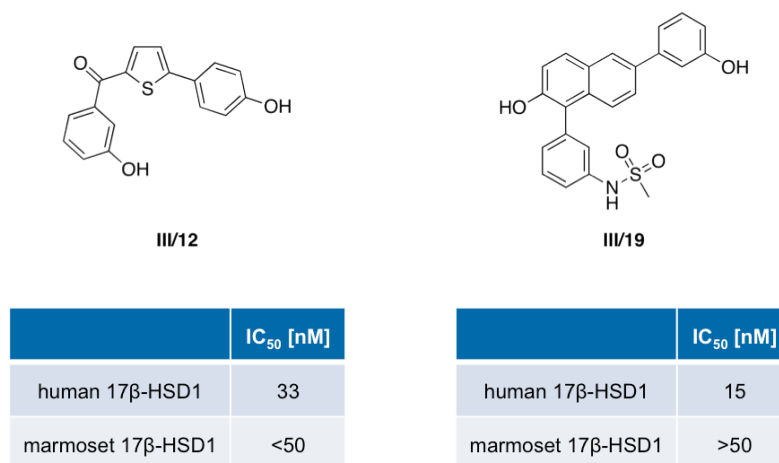


Figure 19. Inhibition of human and marmoset 17β-HSD1 by compounds III/12 and III/19. IC₅₀ values toward marmoset 17β-HSD1 are Logit transformed values calculated from % inhibition at 50 nM inhibitor concentration, for inhibition values <30% or >70%, a trend is given.

When the three-dimensional structures of marmoset and human 17β-HSD1 are compared, one of the most striking features is the small α-helix including the residues 190 to 196 (Figure 20a). It is formed in the segment between the βF-sheet and the αG'-helix starting from the interface residue Thr190, which is half in and half out of the helix (N-cap position). In contrast to the human enzyme, where this region is highly flexible, as suggested by the different crystal structures, the α-helix stayed stable during the MD simulation in both the holoform and the ternary complex (Figure 20b).

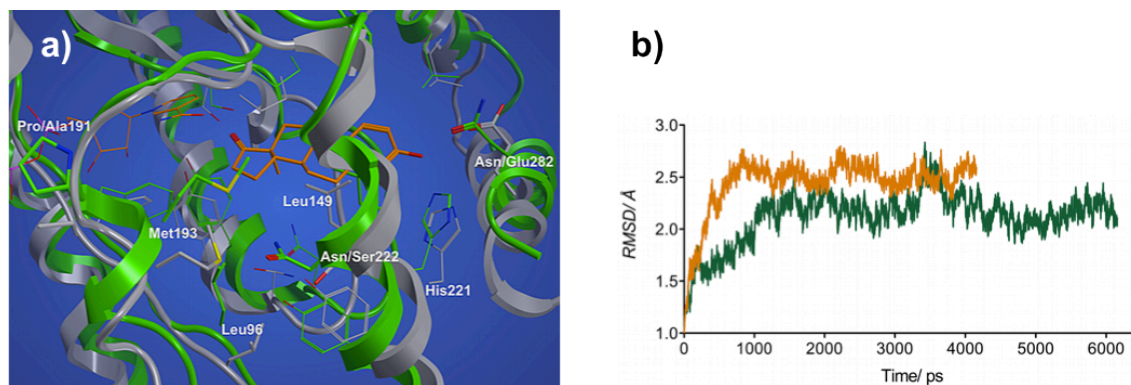


Figure 20. a) Three-dimensional structure superimposition of marmoset and human 17β-HSD1. Low energy structure of marmoset 17β-HSD1 (green) in complex with E1 and NADPH (orange) from MD simulation superimposed onto the x-ray structure of human 17β-HSD1 (grey, PDB code: 1fdtB). When two residues are indicated, the first corresponds to marmoset 17β-HSD1 and the second to human 17β-HSD1. **b)** RMSD analysis of the MD simulations of the marmoset 17β-HSD1 model. Time-dependent C_α-RMSD for all residues of the secondary (orange) and ternary (green) complex.

The observed conformational stability might be explained by the presence of a proline in position 191 instead of an alanine. Proline is a favorable candidate for N1 position because of its

own conformational properties: with only one rotatable angle it loses less entropy than other amino acids in forming an α -helix and thereby it should have some stabilizing influence (Richardson and Richardson, 1988). Furthermore, in an analysis of sequence-structural characteristics in protein crystal structures, proline was found to be a favoured residue at N1 position. Especially the residue pair involving threonine at N-cap and proline at N1 position, which is observed for marmoset 17 β -HSD1, has a high prevalence (Kumar and Bansal, 1998).

In order to analyze the influence of the conformational changes in marmoset 17 β -HSD1 on the binding of ligands **III/12** and **III/19**, docking studies with subsequent MD simulations, free energy calculations, and energy decomposition analyzes were carried out. While the conformational differences between the marmoset and the human enzyme did not affect the binding mode of **III/12** remarkably, the suggested binding mode of **III/19** differed strongly in 17 β -HSD1 of both species (Figure 21).

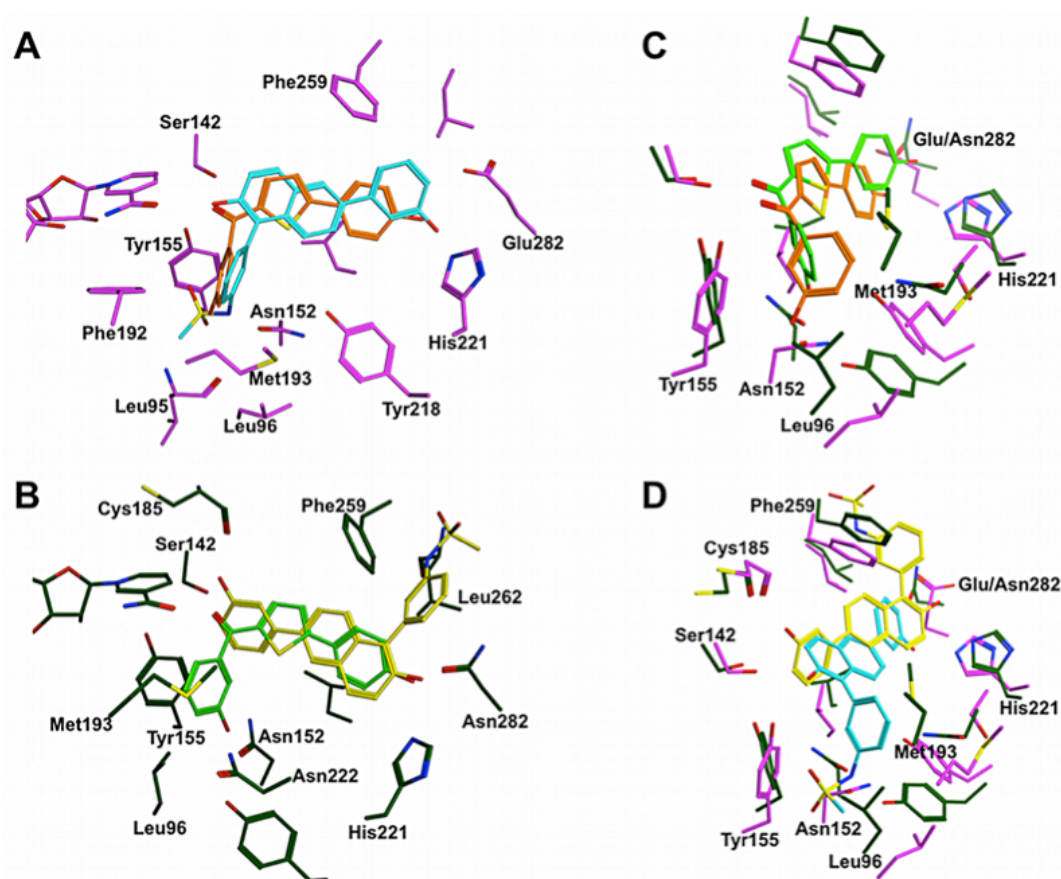


Figure 21. Hypothetical binding modes of compounds **III/12** and **III/19**. **A)** Superimposition of lowest energy structures of **III/12** (orange) and **III/19** (cyan) obtained by docking into the x-ray structure of human 17 β -HSD1 (magenta, PDB code: 1fdtB). **B)** Superimposition of lowest energy structures of **III/12** (light green) and **III/19** (yellow) obtained by docking into the marmoset 17 β -HSD1 homology model (green). **C)** Superimposition of lowest energy structures of **III/12** (light green) docked into the marmoset 17 β -HSD1 model (green) and of **III/12** (orange) docked into the x-ray structure of human 17 β -HSD1 (magenta, PDB code: 1fdtB). **D)** Superimposition of lowest energy structures of **III/19** (yellow) docked into the marmoset 17 β -HSD1 model (green) and of **III/19** (cyan) docked into the x-ray structure of human 17 β -HSD1 (magenta, PDB code: 1fdtB).

One possible explanation for that might be the lower sterical demand of **III/12** compared to **III/19**. However, the energy contribution of the interaction between **III/12** and the marmoset Asn152 (-1.6 kcal/mol) is reduced, whereas it was outstanding in complex with the human enzyme (-4.1 kcal/mol). Due to the minimal shift of **III/12** in the marmoset binding pocket, the geometric parameters for the H-bond with Asn152 are no longer optimal. Interestingly, in the marmoset enzyme an additional interaction of **III/12** with Asn222 is observed, which seems to compensate the deficit in interaction energy due to the absent interaction with Asn152 resulting in comparable binding energies for **III/12** in complex with human (-4.7 kcal/mol) and marmoset (-5.8 kcal/mol) 17 β -HSD1. The latter finding is in accordance with the inhibition data observed for compound **III/12** (Figure 19) and validates the marmoset 17 β -HSD1 model.

Considering compound **III/19**, no particular interactions with the subpocket residues of the marmoset enzyme exist. Although weak interactions between **III/19** and the C-terminal region of marmoset 17 β -HSD1 are observed, the binding free energy (-3.2 kcal/mol) is less favorable compared to that calculated for the human 17 β -HSD1-**III/19** complex (-7.3 kcal/mol). As the C-terminal part of the enzyme has already been discussed as a potential product exit gate of the enzyme (Negri et al., 2010), inhibitor **III/19** might be solvent exposed. This is consistent with the unfavorable entropy term of this complex resulting in the least favorable free energy.

Obviously, the presence of a proline in the flexible loop region and the thereby induced conformational changes in marmoset 17 β -HSD1 are decisive for the species specific inhibition of **III/19**. On one hand interactions with subpocket residues like Asn152, recently discussed as relevant interaction partner (Lilienkamp et al., 2009), are prevented and on the other hand the inhibitor is forced in an unfavorable solvent exposed conformation.

The validity of the presented homology model is further substantiated by its ability to explain the reduced inhibitory potency of C-15 substituted estrone derivatives toward marmoset 17 β -HSD1 (Möller et al., 2010). The substituents in 15-position of the steroid were designed to occupy the hole between the flexible β F α G'-loop and the α G'-helix in the human enzyme (Messinger et al., 2009). Together with the helix formation and the conformational changes in the β D/ α E- segment, the S222N mutation limits the size of the hole in marmoset 17 β -HSD1 and thereby might reduce the inhibitory potency toward the marmoset enzyme.

In summary, comparison of inhibitory potencies toward human and marmoset 17 β -HSD1 and their rationalization on the structural level increased the knowledge of active site topologies and protein-ligand interactions. Thus, the applied approach can be a valid alternative to site-directed mutagenesis. This work could not only offer a better understanding of the active site topologies and of the protein-ligand interactions, but also provides novel structural clues that will help to design and optimize potent human 17 β -HSD1 inhibitors with improved inhibitory potency toward marmoset 17 β -HSD1. This is an important step to turn compounds, which show

a promising pharmaceutical profile, into candidates for *in vivo* evaluation. Hence, our combined computational approach could also be considered as a valuable tool to achieve this goal. However, the explanatory power of the three-dimensional structure of marmoset 17 β -HSD1 and the proposed ligand binding modes should not be overestimated keeping in mind that they are models. But using these models in addition to complementary experimental methods such as *in vitro* enzyme assays or NMR spectroscopy that is a dynamic method to explore the structure of macromolecules, in particular of flexible proteins like 17 β -HSD1, can aid drug discovery.

The proposed binding mode of **III/12** (=IV/B3) was used to elaborate the bicyclic substituted hydroxyphenylmethanone type inhibitors of 17 β -HSD1. According to the suggested binding mode the bicyclic moiety of **IV/B3** occupies the C-terminal region of 17 β -HSD1. Given that several highly active steroidal inhibitors have extensions in position 2 with the most potent derivatives of them bearing an additional phenyl ring connected by a C2 linker (Gege et al., 2006) there is space for additional substituents in this region. Therefore this subproject aimed at investigating the role of the bicyclic moiety to gain further interactions and is described in chapter 3.4. The design concept of the bicyclic substituted hydroxyphenylmethanones that was reported in a preceding study (Oster et al., 2010a) expected the hydroxyl group of the phenyl ring to form hydrogen bonds with His221 and Glu282 in the C-terminal region of the steroid binding pocket. In the proposed binding mode compound **IV/B3** is stabilized by four H-bonds: the *meta*-hydroxyphenyl moiety forms an H-bond with Asn152, the carbonyl group interacts with Ser142 as well as with Tyr155 and the OH group in *para* position of the phenyl ring adjacent to the thiophene interacts with His221 (Figure 22).

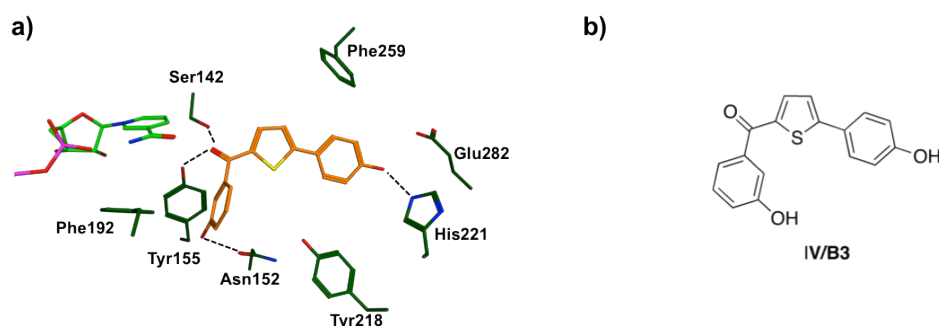
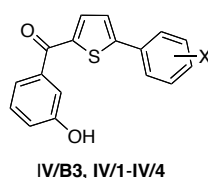


Figure 22. a) Hypothetical binding mode of compound **IV/B3** (orange) obtained by docking into 17 β -HSD1 (PDB-ID: 1FDT). Co-factor NADPH (light green) and interacting residues (dark green) of the active site are shown. Hydrogen bonds are represented in black dashed lines. b) Chemical structure of compound **IV/B3**.

However no interaction with Glu282 was observed. The proposed binding model is confirmed by the inhibitory potencies of the methoxy derivatives (**IV/2-IV/4**), which indicate that the hydrogen-bond donor property is not necessary for strong inhibitory activity (Table 3).

In general, the relevance of Glu282 for ligand binding is discussed controversially. While site-directed mutagenesis studies indicated no significant interaction between Glu282 and the 3-OH group of the substrate (Puranen et al., 1997), hydrogen bonding between both was found in several independent crystal structures (Azzi et al., 1996; Sawicki et al., 1999). The hydrogen-bond acceptor property of the phenol might play a more important role since compound **IV/1**, without hydroxy functionality on the phenyl ring, showed reduced 17 β -HSD1 inhibition (Table 3). Thus, the potential hydrogen-bond donor His221, which is known as an important factor for substrate interaction (Mazza et al., 1998), appears to be involved in the binding of our inhibitors although it is also described to be implicated in enzyme stabilization by interacting with Glu282 (Mazumdar et al., 2009).

Table 3. Inhibition of human 17 β -HSD1 and 17 β -HSD2 by compounds **IV/B3** and **IV/1-IV/4**



Compd.	X	IC ₅₀ [nM] ^[a]	
		17 β -HSD1 ^[b]	17 β -HSD2 ^[c]
IV/B3	4-hydroxy	33	478
IV/1	H	155	128
IV/2	2-methoxy	86	196
IV/3	3-methoxy	95	342
IV/4	4-methoxy	220	507

[a] Mean value of three determinations, standard deviation less than 26 %; [b] Human placenta, cytosolic fraction, substrate E1 (500 nM), cofactor NADH (500 μ M); [c] Human placenta, microsomal fraction, substrate E2 (500 nM), cofactor NAD⁺ (1500 μ M).

Regarding the mono-methoxy and ethoxy derivatives (**IV/2-IV/5** and **IV/9-IV/11**), respectively, it becomes apparent that the *para* position seems to be less favorable than *meta* and *ortho*. Moreover, di- and trimethoxy derivatives (**IV/6-IV/8**) showed a strong decrease in activity as well, indicating that the space around this phenyl ring is sterically restricted. This finding is in accordance with the docking results. According to the orientation of the phenyl ring, the disubstitution of **IV/6** compels the methoxy groups to adopt a conformation leading to steric clashes with either Tyr218 or Phe259. Indeed, taking into account that the 1,3-benzodioxol compound **IV/26** showed a much higher affinity than the corresponding dimethoxy compound **IV/6**, it can be concluded that the binding pocket is very restricted.

The sulfonamide **IV/23** (IC₅₀ = 12 nM) turned out to be the most potent inhibitor of this study. Compared to its methanesulfonamide analogue **IV/21**, the introduction of the phenyl led to 12-fold higher 17 β -HSD1 inhibition. The docking study revealed the benzene ring of **IV/23** to be implicated in a π - π interaction with Phe259 (Figure 23).

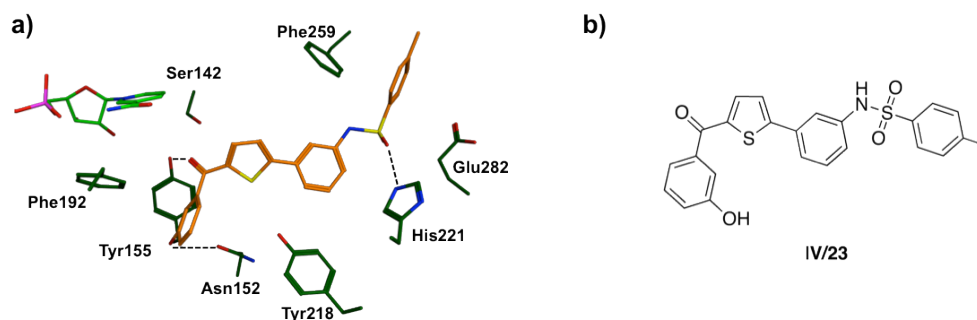


Figure 23. **a)** Hypothetical binding mode of compound **IV/23** (orange) obtained by docking into 17β-HSD1 (PDB-ID: 1FDT). Co-factor NADPH (light green) and interacting residues (dark green) of the active site are shown. Hydrogen bonds are represented in black dashed lines. For the sake of clarity π - π -interactions are not depicted. **b)** Chemical structure of compound **IV/23**.

Comparing **IV/B3** and **IV/23**, both compounds interact with Asn152. The relevance of this amino acid for ligand binding was already proposed in chapter 3.3 and is confirmed by a co-crystal structure of a highly potent, steroidal 17β-HSD1 inhibitor (Mazumdar et al., 2009). **IV/B3** and **IV/23** showed similar IC_{50} values although the hydrogen-bonding interaction of **IV/23** with Ser142 was not present in the observed binding mode. The π - π interactions found for compound **IV/23** might be able to compensate the loss of the hydrogen bond between the ketone and Ser142.

In summary, guided by *in silico* structural data further developments in the class of bicyclic substituted hydroxyphenylmethanones were achieved by organic synthesis and biological evaluation. The high inhibitory activities of compounds bearing large substituents like benzylsulfonamide or benzyloxy revealed that these groups take advantage of the additional space in the C-terminal region. Despite the good inhibitory potencies, they have to be considered critically in terms of ligand efficiency. However, further bio-isosteric replacements of the phenolic hydroxy group might lead to compounds combining high potency with good selectivity and intracellular activity. The most promising compound of this study, methylbenzenesulfonamide **IV/23**, shows strong inhibitory activity in both cellular and cell-free assays, as well as no affinity toward estrogen receptors α and β . It might be a candidate for further optimization, especially regarding its selectivity and cellular activity.

5 References

- Abad-Zapatero, C., and Metz, J.T. (2005). Ligand efficiency indices as guideposts for drug discovery. *Drug Discov. Today* 10, 464–469.
- Abdulhaq, H., and Geyer, C. (2008). Safety of adjuvant endocrine therapy in postmenopausal women with breast cancer. *Am. J. Clin. Oncol.* 31, 595–605.
- Aggarwal, S., Thareja, S., Verma, A., Bhardwaj, T., and Kumar, M. (2010). An overview on 5 α -reductase inhibitors. *Steroids* 75, 109–153.
- Aktories, K., Förstermann, U., Hofmann, F.B., and Starke, K. (2011). *Allgemeine und Spezielle Pharmakologie und Toxikologie* (Urban & Fischer).
- Allan, G., Vicker, N., Lawrence, H., Tutill, H., Day, J., Huchet, M., Ferrandis, E., Reed, M., Purohit, A., and Potter, B. (2008). Novel inhibitors of 17 β -hydroxysteroid dehydrogenase type 1: templates for design. *Bioorg. Med. Chem.* 16, 4438–4456.
- Allesen-Holm, M., Barken, K.B., Yang, L., Klausen, M., Webb, J.S., Kjelleberg, S., Molin, S., Givskov, M., and Tolker-Nielsen, T. (2006). A characterization of DNA release in *Pseudomonas aeruginosa* cultures and biofilms. *Mol. Microbiol.* 59, 1114–1128.
- Alonso, H., Bliznyuk, A.A., and Gready, J.E. (2006). Combining docking and molecular dynamic simulations in drug design. *Med. Res. Rev.* 26, 531–568.
- DeMichele, A., Troxel, A.B., Berlin, J.A., Weber, A.L., Bunin, G.R., Truzo, E., Schinnar, R., Burgh, D., Berlin, M., Rubin S.C., Rebbeck, T.R., Strom, B.L. (2008). Impact of Raloxifene or Tamoxifen Use on Endometrial Cancer Risk: A Population-Based Case-Control Study. *J. Clin. Oncol.* 26, 4151–4159.
- Azzi, A., Rehse, P., Zhu, D., Campbell, R., Labrie, F., and Lin, S.-X. (1996). Crystal structure of human estrogenic 17 β -hydroxysteroid dehydrogenase complexed with 17 β -estradiol. *Nat. Struct. Biol.* 3, 665–668.
- Bajorath, J. (2001). Rational drug discovery revisited: interfacing experimental programs with bio- and cheminformatics. *Drug Discov. Today* 6, 989–995.
- Bey, E., Marchais-Oberwinkler, S., Kruchten, P., Frotscher, M., Werth, R., Oster, A., Algül, O., Neugebauer, A., and Hartmann, R. (2008a). Design, synthesis and biological evaluation of bis (hydroxyphenyl) azoles as potent and selective non-steroidal inhibitors of 17 β -hydroxysteroid dehydrogenase type 1 (17 β -HSD1) for the treatment of estrogen-dependent diseases. *Bioorg. Med. Chem.* 16, 6423–6435.
- Bey, E., Marchais-Oberwinkler, S., Negri, M., Kruchten, P., Oster, A., Klein, T., Spadaro, A., Werth, R., Frotscher, M., Birk, B., et al. (2009). New insights into the SAR and binding modes of bis(hydroxyphenyl)thiophenes and -benzenes: influence of additional substituents on 17 β -hydroxysteroid dehydrogenase type 1 (17 β -HSD1) inhibitory activity and selectivity. *J. Med. Chem.* 52, 6724–6743.
- Bey, E., Marchais-Oberwinkler, S., Werth, R., Negri, M., Al-Soud, Y.A., Kruchten, P., Oster, A., Frotscher, M., Birk, B., and Hartmann, R.W. (2008b). Design, synthesis, biological evaluation and pharmacokinetics of bis(hydroxyphenyl) substituted azoles, thiophenes, benzenes, and aza-benzenes as potent and selective nonsteroidal inhibitors of 17 β -hydroxysteroid dehydrogenase type 1 (17 β -HSD1). *J. Med. Chem.* 51, 6725–6739.
- Bjarnsholt, T., and Givskov, M. (2007). Quorum-sensing blockade as a strategy for enhancing host defences against bacterial pathogens. *Philos. T. Roy. Soc. B* 362, 1213–1222.
- Bjarnsholt, T., Tolker-Nielsen, T., Høiby, N., and Givskov, M. (2010). Interference of *Pseudomonas aeruginosa* signaling and biofilm formation for infection control. *Expert Rev. Mol. Med.* 12, e11.
- Boström, J., Hogner, A., Llinàs, A., Wellner, E., and Plowright, A.T. (2012). Oxadiazoles in medicinal chemistry. *J. Med. Chem.* 55, 1817–1830.
- Bradbury, S.P. (1994). Predicting modes of toxic action from chemical structure: an overview. *SAR QSAR Environ. Res.* 2, 89–104.
- Breidenstein, E.B.M., la Fuente-Núñez, de, C., and Hancock, R.E.W. (2011). *Pseudomonas aeruginosa*: all roads lead to resistance. *Trends Microbiol.* 19, 419–426.

- Brown, W., Metzger, L., Barlow, J., Hunsaker, L., Deck, L., Royer, R., and Vander Jagt, D. (2003). 17 β -Hydroxysteroid dehydrogenase type 1: computational design of active site inhibitors targeted to the Rossmann fold. *Chem.-Biol. Interact.* 143-144, 481–491.
- Bulun, S., Zeitoun, K., Takayama, K., and Sasano, H. (2000). Estrogen biosynthesis in endometriosis: molecular basis and clinical relevance. *J. Mol. Endocrinol.* 25, 35–42.
- Bulun, S.E., Yang, S., Fang, Z., Gurates, B., Tamura, M., Zhou, J., and Sebastian, S. (2001). Role of aromatase in endometrial disease. *J. Steroid Biochem. Mol. Biol.* 79, 19–25.
- Cao, H., Krishnan, G., Goumnerov, B., Tsongalis, J., Tompkins, R., and Rahme, L.G. (2001). A quorum sensing-associated virulence gene of *Pseudomonas aeruginosa* encodes a LysR-like transcription regulator with a unique self-regulatory mechanism. *Proc. Natl. Acad. Sci. USA* 98, 14613–14618.
- Chia, Y.H., Ellis, M.J., and Ma, C.X. (2010). Neoadjuvant endocrine therapy in primary breast cancer: indications and use as a research tool. *Brit. J. Cancer* 103, 759–764.
- Chothia, C., and Lesk, A.M. (1986). The relation between the divergence of sequence and structure in proteins. *Embo J.* 5, 823–826.
- Christensen, L.D., van Gennip, M., Jakobsen, T.H., Alhede, M., Hougen, H.P., Høiby, N., Bjarnsholt, T., and Givskov, M. (2012). Synergistic antibacterial efficacy of early combination treatment with tobramycin and quorum-sensing inhibitors against *Pseudomonas aeruginosa* in an intraperitoneal foreign-body infection mouse model. *J. Antimicrob. Chemoth.* 67, 1198–1206.
- Clatworthy, A.E., Pierson, E., and Hung, D.T. (2007). Targeting virulence: a new paradigm for antimicrobial therapy. *Nat. Chem. Biol.* 3, 541–548.
- Cobellis, L., Razzi, S., De Simone, S., Sartini, A., Fava, A., Danero, S., Gioffrè, W., Mazzini, M., and Petraglia, F. (2004). The treatment with a COX-2 specific inhibitor is effective in the management of pain related to endometriosis. *Eur. J. Obstet. Gyn. R. B.* 116, 100–102.
- Coleman, J.P., Hudson, L.L., McKnight, S.L., Farrow, J.M., Calfee, M.W., Lindsey, C.A., and Pesci, E.C. (2008). *Pseudomonas aeruginosa* PqsA is an anthranilate-coenzyme A ligase. *J. Bacteriol.* 190, 1247–1255.
- Costerton, J.W., Stewart, P.S., and Greenberg, E.P. (1999). Bacterial biofilms: a common cause of persistent infections. *Science* 284, 1318.
- Cotterchio, M., Kreiger, N., Theis, B., Sloan, M., and Bahl, S. (2003). Hormonal factors and the risk of breast cancer according to estrogen- and progesterone-receptor subgroup. *Cancer Epidem. Biomar.* 12, 1053–1060.
- Cramer, R.D., Patterson, D.E., and Bunce, J.D. (1988). Comparative molecular field analysis (CoMFA). 1. Effect of shape on binding of steroids to carrier proteins. *J. Am. Chem. Soc.* 110, 5959–5967.
- Day, J., Foster, P., Tutill, H., Parsons, M., Newman, S., Chander, S., Allan, G., Lawrence, H., Vicker, N., Potter, B., et al. (2008). 17beta-hydroxysteroid dehydrogenase Type 1, and not Type 12, is a target for endocrine therapy of hormone-dependent breast cancer. *Int. J. Cancer* 122, 1931–1940.
- Day, J.M., Tutill, H.J., and Purohit, A. (2010). 17 β -Hydroxysteroid dehydrogenase inhibitors. *Minerva Endocrinol.* 35, 87–108.
- Defoirdt, T., Boon, N., and Bossier, P. (2010). Can bacteria evolve resistance to quorum sensing disruption? *PLoS Pathog.* 6, e1000989.
- Dehm, S.M., and Tindall, D.J. (2007). Androgen receptor structural and functional elements: role and regulation in prostate cancer. *Mol. Endocrinol.* 21, 2855–2863.
- Deroo, B.J., and Korach, K.S. (2006). Estrogen receptors and human disease. *J. Clin. Invest.* 116, 561.
- Déziel, E., Gopalan, S., Tampakaki, A.P., Lépine, F., Padfield, K.E., Saucier, M., Xiao, G., and Rahme, L.G. (2005). The contribution of MvfR to *Pseudomonas aeruginosa* pathogenesis and quorum sensing circuitry regulation: multiple quorum sensing-regulated genes are modulated without affecting lasRI, rhlRI or the production of N-acyl-L-homoserine lactones. *Mol. Microbiol.* 55, 998–1014.
- Diggle, S.P., Lumjiaktase, P., Dipilato, F., Winzer, K., Kunakorn, M., Barrett, D.A., Chhabra, S.R., Cámara, M., and Williams, P. (2006). Functional genetic analysis reveals a 2-Alkyl-4-quinolone signaling system in the human pathogen *Burkholderia pseudomallei* and related bacteria. *Chem. Biol.* 13, 701–710.

- Diggle, S.P., Winzer, K., Chhabra, S.R., Worrall, K.E., Cámara, M., and Williams, P. (2003). The *Pseudomonas aeruginosa* quinolone signal molecule overcomes the cell density-dependency of the quorum sensing hierarchy, regulates rhl-dependent genes at the onset of stationary phase and can be produced in the absence of LasR. *Mol. Microbiol.* *50*, 29–43.
- DiMasi, J.A., Hansen, R.W., and Grabowski, H.G. (2003). The price of innovation: new estimates of drug development costs. *J. Health Econ.* *22*, 151–185.
- Driffield, K., Miller, K., Bostock, J.M., O'Neill, A.J., and Chopra, I. (2008). Increased mutability of *Pseudomonas aeruginosa* in biofilms. *J. Antimicrob. Chemoth.* *61*, 1053–1056.
- Dubern, J.-F., and Diggle, S.P. (2008). Quorum sensing by 2-alkyl-4-quinolones in *Pseudomonas aeruginosa* and other bacterial species. *Mol. Biosyst.* *4*, 882–888.
- Ebert, A.D., Bartley, J., and David, M. (2005). Aromatase inhibitors and cyclooxygenase-2 (COX-2) inhibitors in endometriosis: new questions-old answers? *Eur. J. Obstet. Gyn. R. B.* *122*, 144–150.
- Emons, G., Grundker, C., Gunthert, A., Westphalen, S., Kavanagh, J., and Verschraegen, C. (2003). GnRH antagonists in the treatment of gynecological and breast cancers. *Endocr.-Relat. Cancer* *10*, 291–299.
- Engbrecht, J., and Silverman, M. (1984). Identification of genes and gene products necessary for bacterial bioluminescence. *Proc. Natl. Acad. Sci. USA* *81*, 4154–4158.
- Farrow, J.M., Sund, Z.M., Ellison, M.L., Wade, D.S., Coleman, J.P., and Pesci, E.C. (2008). PqsE functions independently of PqsR-*Pseudomonas* quinolone signal and enhances the rhl quorum-sensing system. *J. Bacteriol.* *190*, 7043–7051.
- Ferlay, J., Shin, H.-R., Bray, F., Forman, D., Mathers, C., and Parkin, D.M. (2010). Estimates of worldwide burden of cancer in 2008: GLOBOCAN 2008. *Int. J. Cancer* *127*, 2893–2917.
- Ferrero, S., Arena, E., Morando, A., and Remorgida, V. (2010). Prevalence of newly diagnosed endometriosis in women attending the general practitioner. *Int. J. Gynecol. Obstet.* *110*, 203–207.
- Filling, C., Berndt, K., Benach, J., Knapp, S., Prozorovski, T., Nordling, E., Ladenstein, R., Jornvall, H., and Oppermann, U. (2002). Critical residues for structure and catalysis in short-chain dehydrogenases/reductases. *J. Biol. Chem.* *277*, 25677–25684.
- Fletcher, M.P., Diggle, S.P., Crusz, S.A., Chhabra, S.R., Cámara, M., and Williams, P. (2007). A dual biosensor for 2-alkyl-4-quinolone quorum-sensing signal molecules. *Environ. Microbiol.* *9*, 2683–2693.
- Freire, E. (2004). Isothermal titration calorimetry: controlling binding forces in lead optimization. *Drug Discov. Today: Technologies* *1*, 295–299.
- Freire, E. (2008). Do enthalpy and entropy distinguish first in class from best in class? *Drug Discov. Today* *13*, 869–874.
- Frotscher, M., Ziegler, E., Marchais-Oberwinkler, S., Kruchten, P., Neugebauer, A., Fetzer, L., Scherer, C., Müller-Vieira, U., Messinger, J., Thole, H., et al. (2008). Design, synthesis, and biological evaluation of (hydroxyphenyl)naphthalene and -quinoline derivatives: potent and selective nonsteroidal inhibitors of 17 β -hydroxysteroid dehydrogenase type 1 (17 β -HSD1) for the treatment of estrogen-dependent diseases. *J. Med. Chem.* *51*, 2158–2169.
- Fuqua, C., Winans, S.C., and Greenberg, E.P. (1996). Census and consensus in bacterial ecosystems: the LuxR-LuxI family of quorum-sensing transcriptional regulators. *Annu. Rev. Microbiol.* *50*, 727–751.
- Fuqua, W.C., Winans, S.C., and Greenberg, E.P. (1994). Quorum sensing in bacteria: the LuxR-LuxI family of cell density-responsive transcriptional regulators. *J. Bacteriol.* *176*, 269–275.
- Gallagher, L.A., McKnight, S.L., Kuznetsova, M.S., Pesci, E.C., and Manoil, C. (2002). Functions required for extracellular quinolone signaling by *Pseudomonas aeruginosa*. *J. Bacteriol.* *184*, 6472–6480.
- Gambello, M.J., and Iglewski, B.H. (1991). Cloning and characterization of the *Pseudomonas aeruginosa* lasR gene, a transcriptional activator of elastase expression. *J. Bacteriol.* *173*, 3000–3009.
- Gangloff, A., Garneau, A., Huang, Y., Yang, F., and Lin, S.-X. (2001). Human oestrogenic 17 β -hydroxysteroid dehydrogenase specificity: enzyme regulation through an NADPH-dependent substrate inhibition towards the highly specific oestrone reduction. *Biochem. J.* *356*, 269–276.

- Gangloff, A., Shi, R., Nahoum, V., and Lin, S.-X. (2003). Pseudo-symmetry of C19 steroids, alternative binding orientations, and multispecificity in human estrogenic 17 β -hydroxysteroid dehydrogenase. *FASEB J.* *17*, 274–276.
- Gege, C., Regenhardt, W., Peters, O., Hillisch, A., Adamski, J., Möller, G., Deluca, D., Elger, W., and Schneider, B. (2006). Novel 2-Substituted D-Homo-Estra-1,3,5(10)-Triens as Inhibitors of 17 β -Hydroxysteroid Dehydrogenase Type 1. *Chem. Abstr.* *144*, 129148.
- Ghosh, D., and Vihko, P. (2001). Molecular mechanisms of estrogen recognition and 17-keto reduction by human 17 β -hydroxysteroid dehydrogenase 1. *Chem.-Biol. Interact.* *130-132*, 637–650.
- Ghosh, D., Pletnev, V., Zhu, D., Wawrzak, Z., Duax, W., Pangborn, W., Labrie, F., and Lin, S.-X. (1995). Structure of human estrogenic 17 β -hydroxysteroid dehydrogenase at 2.20 Å resolution. *Structure* *3*, 503–513.
- Ginalski, K. (2006). Comparative modeling for protein structure prediction. *Curr. Opin. Struc. Biol.* *16*, 172–177.
- Gordon, S.M., Serkey, J.M., Keys, T.F., Ryan, T., Fatica, C.A., Schmitt, S.K., Borsh, J.A., Cosgrove, D.M., and Yared, J.P. (1998). Secular trends in nosocomial bloodstream infections in a 55-bed cardiothoracic intensive care unit. *Ann. Thorac. Surg.* *65*, 95–100.
- Govan, J.R., and Deretic, V. (1996). Microbial pathogenesis in cystic fibrosis: mucoid *Pseudomonas aeruginosa* and *Burkholderia cepacia*. *Microbiol. Rev.* *60*, 539–574.
- Hajduk, P.J. (2006). Fragment-based drug design: how big is too big? *J. Med. Chem.* *49*, 6972–6976.
- Hajduk, P.J., and Greer, J. (2007). A decade of fragment-based drug design: strategic advances and lessons learned. *Nat. Rev. Drug Discov.* *6*, 211–219.
- Han, Q., Campbell, R., Gangloff, A., Huang, Y., and Lin, S.-X. (2000). Dehydroepiandrosterone and dihydrotestosterone recognition by human estrogenic 17 β -hydroxysteroid dehydrogenase. C-18/C-19 steroid discrimination and enzyme-induced strain. *J. Biol. Chem.* *275*, 1105–1111.
- Hansch, C. (1969). Quantitative approach to biochemical structure-activity relationships. *Acc. Chem. Res.* *2*, 232–239.
- Hart, C.A., and Winstanley, C. (2002). Persistent and aggressive bacteria in the lungs of cystic fibrosis children. *Brit. Med. Bull.* *61*, 81–96.
- Henderson, B.E., and Feigelson, H.S. (2000). Hormonal carcinogenesis. *Carcinogenesis* *21*, 427–433.
- Henn, C., Einspanier, A., Marchais-Oberwinkler, S., Frotscher, M., and Hartmann, R.W. (2012). Lead Optimization of 17 β -HSD1 Inhibitors of the (Hydroxyphenyl)naphthol Sulfonamide Type for the Treatment of Endometriosis. *J. Med. Chem.* *55*, 3307–3318.
- Hentzer, M., Riedel, K., Rasmussen, T.B., Heydorn, A., Andersen, J.B., Parsek, M.R., Rice, S.A., Eberl, L., Molin, S., Høiby, N., et al. (2002). Inhibition of quorum sensing in *Pseudomonas aeruginosa* biofilm bacteria by a halogenated furanone compound. *Microbiology* *148*, 87–102.
- Hentzer, M., Wu, H., Andersen, J.B., Riedel, K., Rasmussen, T.B., Bagge, N., Kumar, N., Schembri, M.A., Song, Z., Kristoffersen, P., et al. (2003). Attenuation of *Pseudomonas aeruginosa* virulence by quorum sensing inhibitors. *Embo J.* *22*, 3803–3815.
- Heurlier, K., Déneraud, V., Haenni, M., Guy, L., Krishnapillai, V., and Haas, D. (2005). Quorum-sensing-negative (lasR) mutants of *Pseudomonas aeruginosa* avoid cell lysis and death. *J. Bacteriol.* *187*, 4875–4883.
- Hopkins, A.L., Groom, C.R., and Alex, A. (2004). Ligand efficiency: a useful metric for lead selection. *Drug Discov. Today* *9*, 430–431.
- Huang, Y.W. (2001). Critical Residues for the Specificity of Cofactors and Substrates in Human Estrogenic 17-Hydroxysteroid Dehydrogenase 1: Variants Designed from the Three-Dimensional Structure of the Enzyme. *Mol. Endocrinol.* *15*, 2010–2020.
- Høiby, N., Bjarnsholt, T., Givskov, M., Molin, S., and Ciofu, O. (2010). Antibiotic resistance of bacterial biofilms. *Int. J. Antimicrob. Ag.* *35*, 322–332.
- Jansson, A. (2009). 17 β -hydroxysteroid dehydrogenase enzymes and breast cancer. *J. Steroid Biochem. Mol. Biol.* *114*, 64–67.

- Jornvall, H., Persson, B., Krook, M., Atrian, S., Gonzalez-Duarte, R., Jeffery, J., and Ghosh, D. (1995). Short-chain dehydrogenases/reductases (SDR). *Biochemistry* *34*, 6003–6013.
- Kalyaanamoorthy, S., and Chen, Y.-P.P. (2011). Structure-based drug design to augment hit discovery. *Drug Discov. Today* *16*, 831–839.
- Karkola, S., Lilienkampf, A., and Wähälä, K. (2008). A 3D QSAR model of 17 β -HSD1 inhibitors based on a thieno[2,3-d]pyrimidin-4(3H)-one core applying molecular dynamics simulations and ligand-protein docking. *ChemMedChem* *3*, 461–472.
- Kaul, P.N. (1998). Drug discovery: past, present and future. *Prog. Drug Res.* *50*, 9–105.
- Kim, H.J., Choi, M.Y., Kim, H.J., and Llinás, M. (2010). Conformational dynamics and ligand binding in the multi-domain protein PDC109. *PLoS ONE* *5*, e9180.
- Kitawaki, J., Kado, N., Ishihara, H., Koshiba, H., Kitaoka, Y., and Honjo, H. (2002). Endometriosis: the pathophysiology as an estrogen-dependent disease. *J. Steroid Biochem. Mol. Biol.* *83*, 149–155.
- Kitchen, D.B., Decornez, H., Furr, J.R., and Bajorath, J. (2004). Docking and scoring in virtual screening for drug discovery: methods and applications. *Nat. Rev. Drug Discov.* *3*, 935–949.
- Klein, T., Abgottspon, D., Wittwer, M., Rabbani, S., Herold, J., Jiang, X., Kleeb, S., Lüthi, C., Scharenberg, M., Bezençon, J., et al. (2010). FimH antagonists for the oral treatment of urinary tract infections: from design and synthesis to in vitro and in vivo evaluation. *J. Med. Chem.* *53*, 8627–8641.
- Kuiper, G.G., Enmark, E., Pelto-Huikko, M., Nilsson, S., and Gustafsson, J.A. (1996). Cloning of a novel receptor expressed in rat prostate and ovary. *Proc. Natl. Acad. Sci. USA* *93*, 5925–5930.
- Kulak, J., Fischer, C., Komm, B., and Taylor, H.S. (2011). Treatment with bazedoxifene, a selective estrogen receptor modulator, causes regression of endometriosis in a mouse model. *Endocrinology* *152*, 3226–3232.
- Kumar, S., and Bansal, M. (1998). Dissecting α -helices: position-specific analysis of α -helices in globular proteins. *Proteins* *31*, 460–476.
- Kurogi, Y., and Güner, O.F. (2001). Pharmacophore modeling and three-dimensional database searching for drug design using catalyst. *Curr. Med. Chem.* *8*, 1035–1055.
- Labrie, C., Belanger, A., and Labrie, F. (1988). Androgenic activity of dehydroepiandrosterone and androstenedione in the rat ventral prostate. *Endocrinology* *123*, 1412–1417.
- Labrie, F. (1991). Intracrinology. *Mol. Cell. Endocrinol.* *78*, C113–C118.
- Ladbury, J.E. (2010). Calorimetry as a tool for understanding biomolecular interactions and an aid to drug design. *Biochem. Soc. Trans.* *38*, 888–893.
- Ladbury, J.E., Klebe, G., and Freire, E. (2010). Adding calorimetric data to decision making in lead discovery: a hot tip. *Nat. Rev. Drug Discov.* *9*, 23–27.
- Latifi, A., Foglino, M., Tanaka, K., Williams, P., and Lazdunski, A. (1996). A hierarchical quorum-sensing cascade in *Pseudomonas aeruginosa* links the transcriptional activators LasR and RhIR (VsmR) to expression of the stationary-phase sigma factor RpoS. *Mol. Microbiol.* *21*, 1137–1146.
- Leach, A.R., Shoichet, B.K., and Peishoff, C.E. (2006). Prediction of protein-ligand interactions. Docking and scoring: successes and gaps. *J. Med. Chem.* *49*, 5851–5855.
- Lesic, B., Lépine, F., Déziel, E., Zhang, J., Zhang, Q., Padfield, K., Castonguay, M.-H., Milot, S., Stachel, S., Tzika, A.A., et al. (2007). Inhibitors of pathogen intercellular signals as selective anti-infective compounds. *PLoS Pathog.* *3*, 1229–1239.
- Lewis, M., Bagwill, C., Hardebeck, L.K.E., and Wireduaah, S. (2012). The Use of Hammett Constants to Understand the Non-Covalent Binding of Aromatics. *Comput. Struct. Biotechnol. J.* *1*, e201204004.
- Lépine, F., Milot, S., Déziel, E., He, J., and Rahme, L.G. (2004). Electrospray/mass spectrometric identification and analysis of 4-hydroxy-2-alkylquinolines (HAQs) produced by *Pseudomonas aeruginosa*. *J. Am. Soc. Mass Spectr.* *15*, 862–869.

- Lilienkamp, A., Karkola, S., Alho-Richmond, S., Koskimies, P., Johansson, N., Huhtinen, K., Vihko, K., and Wähälä, K. (2009). Synthesis and biological evaluation of 17 β -hydroxysteroid dehydrogenase type 1 (17 β -HSD1) inhibitors based on a thieno[2,3-d]pyrimidin-4(3H)-one core. *J. Med. Chem.* *52*, 6660–6671.
- Lipinski, C. (2000). Drug-like properties and the causes of poor solubility and poor permeability. *J. Pharmacol. Toxicol.* *44*, 235–249.
- Liu, S.V., Melstrom, L., Yao, K., Russell, C.A., and Sener, S.F. (2010). Neoadjuvant therapy for breast cancer. *J. Surg. Oncol.* *101*, 283–291.
- Lu, C., Kirsch, B., Zimmer, C., de Jong, J.C., Henn, C., Maurer, C.K., Müsken, M., Häussler, S., Steinbach, A., and Hartmann, R.W. (2012). Discovery of Antagonists of PqsR, a Key Player in 2-Alkyl-4-quinolone-Dependent Quorum Sensing in *Pseudomonas aeruginosa*. *Chem. Biol.* *19*, 381–390.
- Luu-The, V. (2001). Analysis and characteristics of multiple types of human 17 β -hydroxysteroid dehydrogenase. *J. Steroid Biochem. Mol. Biol.* *76*, 143–151.
- Ma, D., Cook, D.N., Hearst, J.E., and Nikaido, H. (1994). Efflux pumps and drug resistance in gram-negative bacteria. *Trends Microbiol.* *2*, 489–493.
- Marchais-Oberwinkler, S., Frotscher, M., Ziegler, E., Werth, R., Kruchten, P., Messinger, J., Thole, H., and Hartmann, R.W. (2009). Structure-activity study in the class of 6-(3'-hydroxyphenyl)naphthalenes leading to an optimization of a pharmacophore model for 17 β -hydroxysteroid dehydrogenase type 1 (17 β -HSD1) inhibitors. *Mol. Cell. Endocrinol.* *301*, 205–211.
- Marchais-Oberwinkler, S., Henn, C., Moller, G., Klein, T., Negri, M., Oster, A., Spadaro, A., Werth, R., Wetzel, M., and Xu, K. (2010). 17 β -Hydroxysteroid dehydrogenases (17 β -HSDs) as therapeutic targets: protein structures, functions, and recent progress in inhibitor development. *J. Steroid Biochem. Mol. Biol.* *125*, 66–82.
- Marchais-Oberwinkler, S., Kruchten, P., Frotscher, M., Ziegler, E., Neugebauer, A., Bhoga, U., Bey, E., Müller-Vieira, U., Messinger, J., Thole, H., et al. (2008). Substituted 6-phenyl-2-naphthols. Potent and selective nonsteroidal inhibitors of 17 β -hydroxysteroid dehydrogenase type 1 (17 β -HSD1): design, synthesis, biological evaluation, and pharmacokinetics. *J. Med. Chem.* *51*, 4685–4698.
- Marchais-Oberwinkler, S., Wetzel, M., Ziegler, E., Kruchten, P., Werth, R., Henn, C., Hartmann, R.W., and Frotscher, M. (2011). New drug-like hydroxyphenylnaphthol steroidomimetics as potent and selective 17 β -hydroxysteroid dehydrogenase type 1 inhibitors for the treatment of estrogen-dependent diseases. *J. Med. Chem.* *54*, 534–547.
- Martí-Renom, M.A., Stuart, A.C., Fiser, A., Sánchez, R., Melo, F., and Sali, A. (2000). Comparative protein structure modeling of genes and genomes. *Annu. Rev. Bioph. Biom. Struct.* *29*, 291–325.
- Maughan, K.L., Lutterbie, M.A., and Ham, P.S. (2010). Treatment of breast cancer. *Am. Fam. Physician* *81*, 1339–1346.
- Mavromoustakos, T., Durdagi, S., Koukoulitsa, C., Simeic, M., Papadopoulos, M.G., Hodoscek, M., and Grdadolnik, S.G. (2011). Strategies in the rational drug design. *Curr. Med. Chem.* *18*, 2517–2530.
- Mazumdar, M., Fournier, D., Zhu, D.-W., Cadot, C., Poirier, D., and Lin, S.-X. (2009). Binary and ternary crystal structure analyses of a novel inhibitor with 17 β -HSD type 1: a lead compound for breast cancer therapy. *Biochem. J.* *424*, 357–366.
- Mazza, C., Breton, R., Housset, D., and Fontecilla-Camps, J. (1998). Unusual charge stabilization of NADP⁺ in 17 β -hydroxysteroid dehydrogenase. *J. Biol. Chem.* *273*, 8145.
- McKnight, S.L., Iglewski, B.H., and Pesci, E.C. (2000). The *Pseudomonas* quinolone signal regulates rhl quorum sensing in *Pseudomonas aeruginosa*. *J. Bacteriol.* *182*, 2702–2708.
- Mendelsohn, M., and Karas, R. (1999). The protective effects of estrogen on the cardiovascular system. *New Engl. J. Med.* *340*, 1801–1811.
- Mendelson, M.H., Gurtman, A., Szabo, S., Neibart, E., Meyers, B.R., Policar, M., Cheung, T.W., Lillienfeld, D., Hammer, G., and Reddy, S. (1994). *Pseudomonas aeruginosa* bacteremia in patients with AIDS. *Clin. Infect. Dis.* *18*, 886–895.
- Messinger, J., Hirvelä, L., Husen, B., Kangas, L., Koskimies, P., Pentikäinen, O., Saarenketo, P., and Thole, H. (2006). New inhibitors of 17 β -hydroxysteroid dehydrogenase type 1. *Mol. Cell. Endocrinol.* *248*, 192–198.

- Messinger, J., Husen, B., Koskimies, P., Hirvelä, L., Kallio, L., Saarenketo, P., and Thole, H. (2009). Estrone C15 derivatives--a new class of 17 β -hydroxysteroid dehydrogenase type 1 inhibitors. *Mol. Cell. Endocrinol.* *301*, 216–224.
- Miller, M.B., and Bassler, B.L. (2001). Quorum sensing in bacteria. *Annu. Rev. Microbiol.* *55*, 165–199.
- Mochalkin, I., Miller, J.R., Narasimhan, L., Thanabal, V., Erdman, P., Cox, P.B., Prasad, J.V.N.V., Lightle, S., Huband, M.D., and Stover, C.K. (2009). Discovery of antibacterial biotin carboxylase inhibitors by virtual screening and fragment-based approaches. *ACS Chem. Biol.* *4*, 473–483.
- Moeller, G., and Adamski, J. (2009). Integrated view on 17 β -hydroxysteroid dehydrogenases. *Mol. Cell. Endocrinol.* *301*, 7–19.
- Molin, S., and Tolker-Nielsen, T. (2003). Gene transfer occurs with enhanced efficiency in biofilms and induces enhanced stabilisation of the biofilm structure. *Curr. Opin. Biotechnol.* *14*, 255–261.
- Möller, G., Husen, B., Kowalik, D., Hirvelä, L., Plewczynski, D., Rychlewski, L., Messinger, J., Thole, H., and Adamski, J. (2010). Species Used for Drug Testing Reveal Different Inhibition Susceptibility for 17 β -Hydroxysteroid Dehydrogenase Type 1. *PLoS ONE* *5*, e10969.
- Mutschler, E., Geisslinger, G., Kroemer, H.K., and Schäfer-Korting, M. (2001). *Mutschler Arzneimittelwirkungen* (Wissenschaftliche Verlagsgesellschaft mbH).
- Myers, S., and Baker, A. (2001). Drug discovery-an operating model for a new era. *Nat. Biotechnol.* *19*, 727–730.
- Nealson, K.H., and Hastings, J.W. (1979). Bacterial bioluminescence: its control and ecological significance. *Microbiol. Rev.* *43*, 496–518.
- Negri, M., Recanatini, M., and Hartmann, R.W. (2010). Insights in 17 β -HSD1 Enzyme Kinetics and Ligand Binding by Dynamic Motion Investigation. *PLoS ONE* *5*. e12026.
- Nishio, M. (2011). The CH/ π hydrogen bond in chemistry. Conformation, supramolecules, optical resolution and interactions involving carbohydrates. *Phys. Chem. Chem. Phys.* *13*, 13873–13900.
- Noble, L.S., Takayama, K., Zeitoun, K.M., Putman, J.M., Johns, D.A., Hinshelwood, M.M., Agarwal, V.R., Zhao, Y., Carr, B.R., and Bulun, S.E. (1997). Prostaglandin E2 stimulates aromatase expression in endometriosis-derived stromal cells. *J. Clin. Endocr. Metab.* *82*, 600–606.
- O'Shea, R., and Moser, H.E. (2008). Physicochemical properties of antibacterial compounds: implications for drug discovery. *J. Med. Chem.* *51*, 2871–2878.
- Ochsner, U.A., and Reiser, J. (1995). Autoinducer-mediated regulation of rhamnolipid biosurfactant synthesis in *Pseudomonas aeruginosa*. *Proc. Natl. Acad. Sci. USA* *92*, 6424–6428.
- Ochsner, U.A., Koch, A.K., Fiechter, A., and Reiser, J. (1994). Isolation and characterization of a regulatory gene affecting rhamnolipid biosurfactant synthesis in *Pseudomonas aeruginosa*. *J. Bacteriol.* *176*, 2044–2054.
- Olive, D.L., and Pritts, E.A. (2001). Treatment of endometriosis. *New Engl. J. Med.* *345*, 266–275.
- Ortmann, O., Cufer, T., Dixon, J.M., Maass, N., Marchetti, P., Pagani, O., Pronzato, P., Semiglazov, V., Spano, J.-P., Vrdoljak, E., et al. (2009). Adjuvant endocrine therapy for perimenopausal women with early breast cancer. *Breast* *18*, 2–7.
- Oster, A., Hinsberger, S., Werth, R., Marchais-Oberwinkler, S., Frotscher, M., and Hartmann, R.W. (2010a). Bicyclic substituted hydroxyphenylmethanones as novel inhibitors of 17 β -hydroxysteroid dehydrogenase type 1 (17 β -HSD1) for the treatment of estrogen-dependent diseases. *J. Med. Chem.* *53*, 8176–8186.
- Oster, A., Klein, T., Werth, R., Kruchten, P., and Bey, E. (2010b). Novel Estrone Mimetics with High 17 β -HSD1 Inhibitory Activity. *Bioorg. Med. Chem.* *18*, 3494–3505.
- Palmer, K.L., Mashburn, L.M., Singh, P.K., and Whiteley, M. (2005). Cystic fibrosis sputum supports growth and cues key aspects of *Pseudomonas aeruginosa* physiology. *J. Bacteriol.* *187*, 5267–5277.
- Palumbi, S.R. (2001). Humans as the world's greatest evolutionary force. *Science* *293*, 1786–1790.
- Passador, L., Cook, J.M., Gambello, M.J., Rust, L., and Iglewski, B.H. (1993). Expression of *Pseudomonas aeruginosa* virulence genes requires cell-to-cell communication. *Science* *260*, 1127–1130.

- Pellecchia, M., Sem, D.S., and Wüthrich, K. (2002). NMR in drug discovery. *Nat. Rev. Drug Discov.* *1*, 211–219.
- Peltoketo, H., Isomaa, V., Maentausta, O., and Vihko, R. (1988). Complete amino acid sequence of human placental 17 β -hydroxysteroid dehydrogenase deduced from cDNA. *FEBS Lett.* *239*, 73–77.
- Peng, J., Sengupta, S., and Jordan, V.C. (2009). Potential of selective estrogen receptor modulators as treatments and preventives of breast cancer. *Anti Canc. Agents Med. Chem.* *9*, 481–499.
- Penning, T.M. (1997). Molecular Endocrinology of Hydroxysteroid Dehydrogenases. *Endocr. Rev.* *18*, 281–305.
- Perkins, R., Fang, H., and Tong, W. (2003). Quantitative structure-activity relationship methods: Perspectives on drug discovery and toxicology. *Environ. Toxicol. Chem.* *8*, 1666–1679.
- Persson, B., Kallberg, Y., Bray, J.E., Bruford, E., Dellaporta, S.L., Favia, A.D., Duarte, R.G., Jörnvall, H., Kavanagh, K.L., Kedishvili, N., et al. (2009). The SDR (short-chain dehydrogenase/reductase and related enzymes) nomenclature initiative. *Chem.-Biol. Interact.* *178*, 94–98.
- Pesci, E.C., Milbank, J.B., Pearson, J.P., McKnight, S., Kende, A.S., Greenberg, E.P., and Iglewski, B.H. (1999). Quinolone signaling in the cell-to-cell communication system of *Pseudomonas aeruginosa*. *Proc. Natl. Acad. Sci. USA* *96*, 11229–11234.
- Picard, F., Schulz, T., and Hartmann, R. (2002). 5-Phenyl substituted 1-methyl-2-pyridones and 4'-substituted biphenyl-4-carboxylic acids. synthesis and evaluation as inhibitors of steroid-5 α -reductase type 1 and 2. *Bioorg. Med. Chem.* *10*, 437–448.
- Pistorius, D., Ullrich, A., Lucas, S., Hartmann, R.W., Kazmaier, U., and Müller, R. (2011). Biosynthesis of 2-Alkyl-4(1H)-Quinolones in *Pseudomonas aeruginosa*: Potential for Therapeutic Interference with Pathogenicity. *ChemBioChem* *12*, 850–853.
- Podlogar, B.L., and Ferguson, D.M. (2000). QSAR and CoMFA: a perspective on the practical application to drug discovery. *Drug Des. Discov.* *17*, 4–12.
- Poirier, D. (2003). Inhibitors of 17 β -hydroxysteroid dehydrogenases. *Curr. Med. Chem.* *10*, 453–477 and references therein cited.
- Poirier, D. (2009). Advances in development of inhibitors of 17 β -hydroxysteroid dehydrogenases. *Anti Canc. Agents Med. Chem.* *9*, 642–660.
- Prehn, C., Möller, G., and Adamski, J. (2009). Recent advances in 17 β -hydroxysteroid dehydrogenases. *J. Steroid Biochem. Mol. Biol.* *114*, 72–77.
- Puranen, T., Poutanen, M., Ghosh, D., Vihko, P., and Vihko, R. (1997). Characterization of structural and functional properties of human 17 β -hydroxysteroid dehydrogenase type 1 using recombinant enzymes and site-directed mutagenesis. *Mol. Endocrinol.* *11*, 77–86.
- Racine, A.-C., Legrand, E., Lefebvre-Lacoeuille, C., Hoppe, E., Catala, L., Sentilhes, L., and Descamps, P. (2010). Treatment of endometriosis by aromatase inhibitors: efficacy and side effects. *Gynecol. Obstet. Ferti.* *38*, 318–323.
- Rahme, L.G., Stevens, E.J., Wolfort, S.F., Shao, J., Tompkins, R.G., and Ausubel, F.M. (1995). Common virulence factors for bacterial pathogenicity in plants and animals. *Science* *268*, 1899–1902.
- Ramírez-Gualito, K., Alonso-Ríos, R., Quiroz-García, B., Rojas-Aguilar, A., Díaz, D., Jiménez-Barbero, J., and Cuevas, G. (2009). Enthalpic nature of the CH/ π interaction involved in the recognition of carbohydrates by aromatic compounds, confirmed by a novel interplay of NMR, calorimetry, and theoretical calculations. *J. Am. Chem. Soc.* *131*, 18129–18138.
- Rampioni, G., Pustelny, C., Fletcher, M.P., Wright, V.J., Bruce, M., Rumbaugh, K.P., Heeb, S., Cámara, M., and Williams, P. (2010). Transcriptomic analysis reveals a global alkyl-quinolone-independent regulatory role for PqsE in facilitating the environmental adaptation of *Pseudomonas aeruginosa* to plant and animal hosts. *Environ. Microbiol.* *12*, 1659–1673.
- Ran, J., and Wong, M.W. (2006). Saturated hydrocarbon-benzene complexes: theoretical study of cooperative CH/ π interactions. *J. Phys. Chem. A* *110*, 9702–9709.
- Rasmussen, T.B., and Givskov, M. (2006). Quorum-sensing inhibitors as anti-pathogenic drugs. *Int. J. Med. Microbiol.* *296*, 149–161.

- Rester, U. (2008). From virtuality to reality - Virtual screening in lead discovery and lead optimization: a medicinal chemistry perspective. *Curr. Opin. Drug Discov. Devel.* 11, 559–568.
- Richardson, J.S., and Richardson, D.C. (1988). Amino acid preferences for specific locations at the ends of α -helices. *Science* 240, 1648–1652.
- Riordan, J.R. (2008). CFTR function and prospects for therapy. *Annu. Rev. Biochem.* 77, 701–726.
- Ruth C Travis, T.J.K. (2003). Oestrogen exposure and breast cancer risk. *Breast Cancer Res.* 5, 239–247.
- Sainsbury, J.R., Anderson, T.J., and Morgan, D.A. (2000). ABC of breast diseases: breast cancer. *Brit. Med. J.* 321, 745–750.
- Saloniemi, T., Järvensivu, P., Koskimies, P., Jokela, H., Lamminen, T., Ghaem-Maghami, S., Dina, R., Damdimopoulou, P., Mäkelä, S., Perheentupa, A., et al. (2010). Novel Hydroxysteroid (17 β) Dehydrogenase 1 Inhibitors Reverse Estrogen-Induced Endometrial Hyperplasia in Transgenic Mice. *Am. J. Pathol.* 176, 1443–1451.
- Sampson, J. (1927). Metastatic or Embolic Endometriosis, due to the Menstrual Dissemination of Endometrial Tissue into the Venous Circulation. *Am. J. Pathol.* 3, 93–110.
- Sandoz, K.M., Mitzimberg, S.M., and Schuster, M. (2007). Social cheating in *Pseudomonas aeruginosa* quorum sensing. *Proc. Natl. Acad. Sci. USA* 104, 15876–15881.
- Sasano, H., Okamoto, M., Mason, J.I., Simpson, E.R., Mendelson, C.R., Sasano, N., and Silverberg, S.G. (1989). Immunolocalization of aromatase, 17 α -hydroxylase and side-chain-cleavage cytochromes P-450 in the human ovary. *J. Reprod. Fertil.* 85, 163–169.
- Sasano, H., Suzuki, T., Takeyama, J., Utsunomiya, H., Ito, K., Ariga, N., and Moriya, T. (2000). 17 β -hydroxysteroid dehydrogenase in human breast and endometrial carcinoma. A new development in intracrinology. *Oncology* 59 Suppl 1, 5–12.
- Sawicki, M., Erman, M., Puranen, T., Vihko, P., and Ghosh, D. (1999). Structure of the ternary complex of human 17 β -hydroxysteroid dehydrogenase type 1 with 3-hydroxyestra-1,3,5,7-tetraen-17-one (equilin) and NADP. *Proc. Natl. Acad. Sci. U S A* 96, 840–845.
- Schäcke, H., Döcke, W.D., and Asadullah, K. (2002). Mechanisms involved in the side effects of glucocorticoids. *Pharmacol. Therapeut.* 96, 23–43.
- Schulz, M.N., and Hubbard, R.E. (2009). Recent progress in fragment-based lead discovery. *Curr. Opin. Pharmacol.* 9, 615–621.
- Sherbet, D.P., Guryev, O.L., Papari-Zareei, M., Mizrahi, D., Rambally, S., Akbar, S., and Auchus, R.J. (2009). Biochemical Factors Governing the Steady-State Estrone/Estradiol Ratios Catalyzed by Human 17 β -Hydroxysteroid Dehydrogenases Types 1 and 2 in HEK-293 Cells. *Endocrinology* 150, 4154–4162.
- Sherbet, D.P., Papari-Zareei, M., Khan, N., Sharma, K.K., Brandmaier, A., Rambally, S., Chattopadhyay, A., Andersson, S., Agarwal, A.K., and Auchus, R.J. (2007). Cofactors, redox state, and directional preferences of hydroxysteroid dehydrogenases. *Mol. Cell. Endocrinol.* 265–266, 83–88.
- Smith, R.S., and Iglewski, B.H. (2003). *P. aeruginosa* quorum-sensing systems and virulence. *Curr. Opin. Microbiol.* 6, 56–60.
- Spadaro, A., Frotscher, M., and Hartmann, R.W. (2012a). Optimization of hydroxybenzothiazoles as novel potent and selective inhibitors of 17 β -HSD1. *J. Med. Chem.* 55, 2469–2473.
- Spadaro, A., Negri, M., Marchais-Oberwinkler, S., Bey, E., and Frotscher, M. (2012b). Hydroxybenzothiazoles as new nonsteroidal inhibitors of 17 β -hydroxysteroid dehydrogenase type 1 (17 β -HSD1). *PLoS ONE* 7, e29252.
- Stevens, A.M., Dolan, K.M., and Greenberg, E.P. (1994). Synergistic binding of the *Vibrio fischeri* LuxR transcriptional activator domain and RNA polymerase to the lux promoter region. *Proc. Natl. Acad. Sci. USA* 91, 12619–12623.
- Stuart-Harris, R., and Davis, A. (2010). Optimal adjuvant endocrine therapy for early breast cancer. *Women's Health* 6, 383–398.
- Swift, S., Downie, J.A., Whitehead, N.A., Barnard, A.M., Salmond, G.P., and Williams, P. (2001). Quorum sensing as a population-density-dependent determinant of bacterial physiology. *Adv. Microb. Physiol.* 45, 199–270.

- Taft, C.A., Da Silva, V.B., and Da Silva, C.H.T.D.P. (2008). Current topics in computer-aided drug design. *J. Pharm. Sci.* *97*, 1089–1098.
- Tsai, S., Wu, M., Lin, C., Sun, H., and Chen, H. (2001). Regulation of steroidogenic acute regulatory protein expression and progesterone production in endometriotic stromal cells. *J. Clin. Endocr. Metab.* *86*, 5765–5773.
- Turner, R.T., Riggs, B.L., and Spelsberg, T.C. (1994). Skeletal effects of estrogen. *Endocr. Rev.* *15*, 275–300.
- Urruticoechea, A. (2007). The oestrogen-dependent biology of breast cancer. Sensitivity and resistance to aromatase inhibitors revisited: a molecular perspective. *Clin. Transl. Oncol.* *9*, 752–759.
- van Delden, C., and Iglewski, B.H. (1998). Cell-to-cell signaling and *Pseudomonas aeruginosa* infections. *Emerg. Infect. Dis.* *4*, 551–560.
- Vasil, M.L. (1986). *Pseudomonas aeruginosa*: biology, mechanisms of virulence, epidemiology. *J. Pediatr.* *108*, 800–805.
- Verma, J., Khedkar, V.M., and Coutinho, E.C. (2010). 3D-QSAR in Drug Design - A Review. *Curr. Top. Med. Chem.* *10*, 95–115.
- Vihko, P., Härkönen, P., Soronen, P., Törn, S., Herrala, A., Kurkela, R., Pulkka, A., Oduwole, O., and Isomaa, V. (2004). 17 β -hydroxysteroid dehydrogenases- their role in pathophysiology. *Mol. Cell. Endocrinol.* *215*, 83–88.
- Voet, D., and Voet, J.G. (1994). *Biochemie* (Wiley-VCH).
- Wade, D.S., Calfee, M.W., Rocha, E.R., Ling, E.A., Engstrom, E., Coleman, J.P., and Pesci, E.C. (2005). Regulation of *Pseudomonas* quinolone signal synthesis in *Pseudomonas aeruginosa*. *J. Bacteriol.* *187*, 4372–4380.
- Waldrop, G.L. (2009). Smaller is better for antibiotic discovery. *ACS Chem. Biol.* *4*, 397–399.
- Walter, P., Green, S., Greene, G., Krust, A., Bornert, J.M., Jeltsch, J.M., Staub, A., Jensen, E., Scrace, G., and Waterfield, M. (1985). Cloning of the human estrogen receptor cDNA. *Proc. Natl. Acad. Sci. USA* *82*, 7889–7893.
- Waters, C.M., and Bassler, B.L. (2005). Quorum sensing: cell-to-cell communication in bacteria. *Annu. Rev. Cell. Dev. Biol.* *21*, 319–346.
- Wermuth, C.G., Ganellin, C.R., Lindberg, P., and Mitscher, L.A. (1998). Glossary of terms used in medicinal chemistry (IUPAC recommendations 1998). *Pure Appl. Chem.* *70*, 1129–1143.
- WHO (2008). *The Global Burden of Disease*. 1–160.
- Wilder, C.N., Allada, G., and Schuster, M. (2009). Instantaneous within-patient diversity of *Pseudomonas aeruginosa* quorum-sensing populations from cystic fibrosis lung infections. *Infect. Immun.* *77*, 5631–5639.
- Xiao, G., Déziel, E., He, J., Lépine, F., Lesic, B., Castonguay, M.-H., Milot, S., Tampakaki, A.P., Stachel, S.E., and Rahme, L.G. (2006). MvfR, a key *Pseudomonas aeruginosa* pathogenicity LTTR-class regulatory protein, has dual ligands. *Mol. Microbiol.* *62*, 1689–1699.
- Yang, S.-Y. (2010). Pharmacophore modeling and applications in drug discovery: challenges and recent advances. *Drug Discov. Today* *15*, 444–450.
- Yue, W., Wang, J.-P., Li, Y., Bocchinfuso, W.P., Korach, K.S., Devanesan, P.D., Rogan, E., Cavalieri, E., and Santen, R.J. (2005). Tamoxifen versus aromatase inhibitors for breast cancer prevention. *Clin. Cancer Res.* *11*, 925–930.
- Zhang, S. (2011). Computer-aided drug discovery and development. *Methods Mol. Biol.* *716*, 23–38.

6 Acknowledgements

Mein besonderer Dank gilt Prof. Dr. Rolf W. Hartmann, der mir durch die Überlassung der interessanten und herausfordernden Themen, sowie seine stete Unterstützung und Diskussionsbereitschaft in wissenschaftlichen Belangen die Möglichkeit gab diese Arbeit in einem außergewöhnlichen Umfeld anzufertigen. Vielen Dank für das mir entgegengebrachte Vertrauen und den Freiraum, den Sie mir gewährt haben um meine Ideen zu entfalten.

Herzlich bedanken möchte ich mich des Weiteren bei folgenden Personen, die maßgeblich zum Gelingen dieser Arbeit beigetragen haben:

Prof. Dr. Dr. h.c. Hans H. Maurer für die Übernahme des Koreferats.

Dr. Anke Steinbach und Dr. Christina Zimmer sowie Dr. Sandrine Marchais-Oberwinkler und Dr. Martin Frotscher für die Leitung der PQS- bzw. 17 β HSD1-Projektgruppe.

Claudia Henn für die tolle Büro- und Labornachbarschaft sowie die geniale Zusammenarbeit im PQS und 17 β HSD1 Projekt; die wissenschaftlichen Diskussionen beim Espresso und nicht zuletzt für ihre gute Freundschaft. Dr. Matthias Negri für die praktische Einführung in die computergestützten Methoden sowie seine stete Diskussionsbereitschaft. Christian Schmitt für die gute Zusammenarbeit im Labor, seine Freundschaft sowie die sportlichen Auszeiten. Dr. Alexander Oster für die gute Zusammenarbeit, seine ständige Diskussionsbereitschaft sowie seinen Humor, der für viel Spaß bei der Arbeit gesorgt hat. Dr. Martin Frotscher, Dr. Matthias Negri, Dr. Marie Wetzel, Christian Schmitt und Andreas Thomann für die gemeinsame Gestaltung, Planung und Durchführung des Praktikums Medizinische Chemie. Christian Ruge, der mit mir gemeinsam den Weg vom Pharmaziestudium bis zur Promotion gegangen ist, für die gute Freundschaft und die zahlreichen metawissenschaftlichen Diskussionen. Dr. Alexander Titz für die gute Freundschaft seit unserer gemeinsamen Zeit an der Universität Basel und seine ständige Diskussionsbereitschaft auch weit über naturwissenschaftliche Fragestellungen hinweg. Katrin Schmitt und Martina Schwarz für die tolle Organisation im Sekretariat.

Allen aktuellen und ehemaligen PhamMedChem und DDOP Mitarbeitern für die gute Atmosphäre und Zusammenarbeit im Labor sowie für viele schöne gemeinsam verbrachte Stunden, die die Zeit der Promotion einzigartig gemacht haben.

Meiner Familie und meinen Freunden dafür, dass Sie mich auch mal auf andere Gedanken gebracht haben und es nicht persönlich nahmen wenn ich viel Zeit im Labor verbrachte.

Meinen Eltern, die mir die Ausbildung ermöglicht haben um diese Arbeit in Angriff nehmen zu können und mich in meinem Tun in den letzten 29 Jahren gefördert und unterstützt haben.

Meiner Judith, die immer für mich da war und an mich geglaubt hat; für Ihre Geduld, Unterstützung und noch vieles mehr. Thank Ju!

7 Appendix

7.1 Curriculum Vitae

PERSÖNLICHE DATEN

Name Tobias Klein
Geburtsdaten 6. Januar 1983 in Wadern

WISSENSCHAFTLICHER WERDEGANG

Ab 09/2012 Postdoc-Aufenthalt in der Abteilung Discovery Sciences, AstraZeneca R&D, Alderley Edge, UK
Thema: *Understanding FGFR Kinase Inhibitor Isoform Selectivity and SAR by Thermodynamic, Kinetic and Structural Profiling*

01/2009 – 08/2012 Doktorarbeit unter Anleitung von Prof. Dr. Rolf W. Hartmann am Institut für Pharmazeutische & Medizinische Chemie, Universität des Saarlandes und am Helmholtz Institut für Pharmazeutische Forschung Saarland, Saarbrücken
Thema: *Characterization of Protein-Ligand Interactions: The Role of Thermodynamic and Structural Data in the Drug Discovery Process*

11/2007 – 04/2008 Forschungspraktikum unter Anleitung von Prof. Dr. Beat Ernst am Institut für Molekulare Pharmazie, Universität Basel, Basel
Thema: *FimH antagonists for oral treatment of urinary tract infections: from design and synthesis to in vitro and in vivo evaluation*

AUSBILDUNG

12/2008 Approbation als Apotheker

05/2008 – 10/2008 Pharmaziepraktikum, Markt Apotheke, Losheim am See

10/2003 – 10/2007 Studium der Pharmazie, Universität des Saarlandes, Saarbrücken
Abschluss: II. Staatsexamen Pharmazie

08/2002 – 05/2003 Zivildienst, Staatliche Schule für Gehörlose und Schwerhörige, Lebach

08/1993 – 06/2002 Allgemeine Hochschulreife, Hochwaldgymnasium, Wadern,
Abschluss: Abitur

MITGLIEDSCHAFTEN

Deutsche Pharmazeutische Gesellschaft DPhG e.V.
Alumni und Freunde der Fachrichtung Pharmazie an der Universität des Saarlandes e.V.

AUSZEICHNUNGEN

08/2012 Best Poster Award, 22nd International Symposium on Medicinal Chemistry 2012, Berlin, "Identification of Small-Molecule Antagonists of the *P. aeruginosa* Transcriptional Regulator PqsR: Biophysically Guided Hit Discovery and Optimization"

08/2012 HZI-Paper of the Month Award for an outstanding publication, Klein T. et al, *ACS Chem. Biol.* **2012**, DOI: 10.1021/cb300208g

06/2002 Volksbanken-Preis für das beste Abitur im Fach Chemie

7.2 Publications

- 8) Klein T, Henn C, de Jong JC, Zimmer C, Pistorius D, Müller R, Steinbach A, Hartmann RW. Identification of Small-Molecule Antagonists of the *Pseudomonas aeruginosa* Transcriptional Regulator PqsR: Biophysically Hit Discovery and Optimization. *ACS Chem. Biol.* **2012**, DOI: 10.1021/cb300208g.
- 7) Klein T, Henn C, Negri M, Frotscher M. Structural Basis for Species Specific Inhibition of 17 β -Hydroxysteroid Dehydrogenase Type 1 (17 β -HSD1): Computational Study and Biological Validation. *PLOS one* **2011**, *6*, e22990.
- 6) Oster A, Klein T, Henn C, Werth R, Marchais-Oberwinkler S, Frotscher M, Hartmann RW. Bicyclic Substituted Hydroxyphenylmethanone Type Inhibitors of 17 β -Hydroxysteroid Dehydrogenase Type 1 (17 β -HSD1): The Role of the Bicyclic Moiety. *ChemMedChem* **2011**, *6*, 476-487.
- 5) Marchais-Oberwinkler S, Henn C, Möller G, Klein T, Negri M, Oster A, Spadaro A, Werth R, Wetzel M, Xu K, Frotscher M, Hartmann RW, Adamski J. 17 β -Hydroxysteroid Dehydrogenases (17 β -HSDs) as therapeutic targets: protein structures, functions, and recent progress in inhibitor development. *J. Steroid Biochem. Mol. Biol.* **2011**, *125*, 66-82.
- 4) Klein T, Abgottspon D, Wittwer M, Rabbani S, Herold J, Jiang X, Kleeb S, Lüthi C, Scharenberg M, Bezencon J, Gubler E, Pang L, Smiesko M, Cutting B, Schwaradt O, Ernst B. FimH antagonists for oral treatment of urinary tract infections: from design and synthesis to in vitro and in vivo evaluation. *J. Med. Chem.* **2010**, *53*, 8627-8641.
- 3) Oster A, Klein T, Werth R, Kruchten P, Bey E, Negri M, Marchais-Oberwinkler S, Frotscher M, Hartmann RW. Novel estrone mimetics with high 17 β -HSD1 inhibitory activity. *Bioorg. Med. Chem.* **2010**, *18*, 3494-3505.
- 2) Reum N, Fink-Straube C, Klein T, Hartmann RW, Lehr CM, Schneider M. Multilayer coating of gold nanoparticles with drug-polymer coadsorbates. *Langmuir* **2010**, *26*, 16901-16908.
- 1) Bey E, Marchais-Oberwinkler S, Negri M, Kruchten P, Oster A, Klein T, Spadaro A, Werth R, Frotscher M, Birk B, Hertmann RW. New insights into the SAR and binding modes of bis(hydroxyphenyl)thiophenes and -benzenes: influence of additional substituents on 17 β -hydroxysteroid dehydrogenase type 1 (17 β -HSD1) inhibitory activity and selectivity. *J. Med. Chem.* **2009**, *52*, 6724-6743.

7.3 Oral Presentations

- 1) Klein T, Henn C, de Jong, JC, Zimmer C, Pistorius D, Müller R, Steinbach A, Hartmann RW. Identification of Small-Molecule Antagonists of the *Pseudomonas aeruginosa* Transcriptional Regulator PqsR: Biophysically Guided Hit Discovery and Optimization. *2nd International HIPS Symposium* June **2012** Saarbrücken, Germany.

7.4 Poster Presentations

- 4) Klein T, Henn C, de Jong, JC, Zimmer C, Pistorius D, Müller R, Steinbach A, Hartmann RW. Identification of Small-Molecule Antagonists of the *Pseudomonas aeruginosa* Transcriptional Regulator PqsR: Biophysically Guided Hit Discovery and Optimization. *22nd International Symposium on Medicinal Chemistry* September **2012** Berlin, Germany.
- 2) Klein T, Henn C, de Jong, JC, Kirsch B, Amann S, Zimmer C, Pistorius D, Müller R, Ritter C, Hartmann RW. Identification of PqsR Ligands: Rational Design and Fragment Screening. *1st International HIPS Symposium* June **2011** Saarbrücken, Germany.
- 2) Klein T, Oster A, Werth R, Negri M, Marchais-Oberwinkler S, Frotscher M, Hartmann RW. Novel Estrone Mimetics with High 17 β -HSD1 Inhibitory Activity. *21st International Symposium on Medicinal Chemistry* September **2010** Brussels, Belgium. Abstract published in *Drugs Fut* **2010**, 35 (Suppl A) 119.
- 1) Klein T, Negri M, Spadaro A, Henn C, Marchais-Oberwinkler S, Frotscher M, Hartmann RW. Development and Validation of a Ligand-Steered 17 β -Hydroxysteroid Dehydrogenase Type 1 (17 β HSD1) Homology Model: A Predictive Tool for the Identification of New Nonsteroidal 17 β HSD1 Inhibitors. Internationale DPhG-Doktorandentagung November **2009** Pichlarn, Austria.